NEURAL MECHANISMS OF PERCEPTUAL DECISION MAKING

By

Braden A. Purcell

Dissertation

Submitted to the Faculty of the

Graduate School of Vanderbilt University

in partial fulfillment of the requirements

for the degree of

DOCTOR OF PHILOSOPHY

in

Psychology

May, 2013

Nashville, Tennessee

Approved:

Professor Thomas J. Palmeri

Professor Jeffrey D. Schall

Professor Gordon, D. Logan

Professor Mark T. Wallace

ACKNOWLEDGEMENTS

I thank my family for their constant love and support, for emphasizing the importance of education, and for teaching me the joy of learning. I thank Tom Palmeri for taking me on as a graduate student, teaching me cognitive modeling, and supporting me through every step in my graduate career. I thank Jeff Schall for taking me into his lab, teaching me to question everything, and always pushing me to be a better scientist. I thank Gordon Logan for his excellent guidance and for reminding me to always do work that I love. I thank Mark Wallace for serving on my committee and asking stimulating questions. I thank everyone in Jeff Schall's laboratory for countless valuable discussions. In particular, I thank Rich Heitz and Jeremiah Cohen for training me in neurophysiology and for immeasurable intellectual contributions to our projects. I thank Geoff Woodman for teaching me to record and interpret event-related potentials in non-human primates. I thank Polly Weigand for long hours spent on data collection and histology. I thank David Godlove for constant constructive criticism. I thank everyone in the Division of Animal Care, Vanderbilt Vision Research Center, Center for Integrative and Cognitive Neuroscience, Advanced Computing Center for Research and Education, and the Psychology Department staff for exceptional support throughout graduate school. I thank all of my colleagues in Department of Psychology and Vanderbilt Neuroscience Program for so many useful discussions, great feedback, and fascinating talks. I cannot imagine a better environment to have completed my doctorate. Finally, I thank Jonathan Hooper for helping me maintain the work-life balance that is necessary for a successful career.

This work was supported by National Institutes of Health Grants T32-EY07135, NEI RO1-EY08890, NEI P30-EY008126, P30-HD015052, NEI R01-EY21833, NEI R01-EY019882, National Science Foundation Grants SBE-0542013 and BCS0957074, and by Robin and Richard Patton through the E. Bronson Ingram Chair in Neuroscience at Vanderbilt University.

TABLE OF CONTENTS

Page

LIST OF TABLES

LIST OF FIGURES

CHAPTER I

INTRODUCTION

1.1 Introduction

Perceptual decisions guide responses based on sensory information. For example, upon encountering a new object, we must decide what it is that we're seeing before we decide how to respond. Perceptual decisions are among the most simple and frequent types of decisions exhibited by humans (e.g., Palmeri, 1997), monkeys (e.g., Schall, 2003), rats (e.g., Kepecs et al., 2008), mice (e.g., Harvey et al., 2012), and fruit flies (e.g., Zhang et al., 2007). Therefore, if we want to understand the neural mechanisms underlying complex goal-directed behavior, then perceptual decision making is a good place to start.

Recent advances in methods for monitoring neural activity from awake, behaving animals and humans have opened the door to rich descriptions of neurophysiological signals occurring during perceptual decisions. However, understanding how this underlying neural activity ultimately leads to behavior is not trivial. Even the simplest behaviors depend on coordinated activity across a number of different brain areas. Different brain areas might implement different computations, or the same computation might be distributed across different areas. Moreover, even within a small region of cortex, different neurons have distinct morphologies, patterns of connectivity, and response properties depending on their position within the local microcircuit. Thus, even within a single brain area, different neuronal populations might implement different computations. Given this complexity, how can we begin to meaningfully relate the growing body of neurophysiological observations to complex behavior like decision-making?

The field of cognitive psychology provides an alternative perspective for understanding behavior. A fundamental concept in cognitive psychology is that mental operations can be divided into a series of basic processes (Donders, 1969; Marr, 1982; Sternberg, 2001). These

theories explain behavior in terms of simple processes that often fit with our subjective experience of what it means to think and act. For example, I first perceive an object, and then categorize it, and then act. Mathematical psychologists have made this approach more rigorous by implementing these processes in computational models (Townsend and Ashby, 1984; Luce, 1991; Busemeyer and Diederich, 2009; Farrell and Lewandowsky, 2010). Cognitive models make the processes explicit by establishing how information is quantitatively represented and the algorithms by which it is transformed to drive behavior.

Cognitive and mathematical psychology have more-or-less converged on a general framework to explain the processes underlying perceptual decisions. *Stochastic accumulator models* (also termed *sequential-sampling models*, *accumulator models*, or *rise-to-threshold models*) explain perceptual decision-making by assuming that perceptual information accumulates to a response threshold (Nosofsky and Palmeri, 1997; Ratcliff and Rouder, 1998; Smith and Van Zandt, 2000; Usher and McClelland, 2001; Ratcliff and Smith, 2004; Bogacz et al., 2006). These models propose that perceptual decision-making entails at least two distinct processes: (1) a stimulus must be encoded with respect to the current task, and (2) some mechanism must accumulate that evidence to reach a decision. This family of models currently provides the best account of decision-making behavior across a broad range of behavioral paradigms. Ultimately, however, these models were not developed to explain how these representations and algorithms could be implemented by the biological processes in the brain.

This overall goal of this work is to evaluate whether specific neuronal populations can be identified with the stages of processing proposed by stochastic accumulator models. If so, then these models might provide a framework to understand how observed neural activity leads to choice behavior. One advantage of the accumulator model framework is that it makes clear predictions for how specific model elements should change under certain conditions. By recording neurophysiological signals from macaque monkeys performing perceptual decision-making tasks, we can test whether the responses of different neuronal populations change in ways

that are consistent with model predictions. In this way, the models can provide a way to understand how basic computations underlying perceptual decisions might be distributed across different brain areas, or even across different neuronal populations within the same region.

The remainder of this chapter will review evidence that specific neuronal populations can be identified with the processes proposed by stochastic accumulator models. I will focus on perceptual decisions about where and when to move the eyes because the basic anatomy and physiology of the oculomotor system are relatively well understood. Likewise, I will focus mainly on decisions about visual information because the visual system is better understood than other sensory modalities. I will first review the stochastic accumulator model framework and its key assumptions. I will then review anatomy of visually-guided saccades. Finally, I will review the neurophysiology of sensorimotor areas thought to be involved in perceptual decisions. This literature review raises open questions regarding potential links between accumulator models and distinct neural states that will motivate the studies described in subsequent chapters.

1.2 Stochastic accumulator models of perceptual decision making

Stochastic accumulator models divide response time into two basic processes. First, sensory information must be encoded with respect to the current task and potential responses to reflect perceptual evidence for a response (Figure 1.1A). Sensory information is noisy due to external noise in the stimulus or internal noise in the brain; thus, a single stimulus is associated with a distribution of evidence. In a standard signal detection theory framework, a perceptual decision would be explained by taking a single sample from the appropriate distribution, comparing it to some criterion, and basing the decision on whether the sample was greater than or less than some criterion (Green and Swets, 1966). Stimuli that are more easily discriminated will more often result in correct classification, whereas stimuli that are more similar will more often produce errors. While this approach provides a good account of choice data across a broad range of tasks (e.g., Murdock Jr, 1965; Ashby and Townsend, 1986; Verghese, 2001), it does not explain how

the decision unfolds over time.

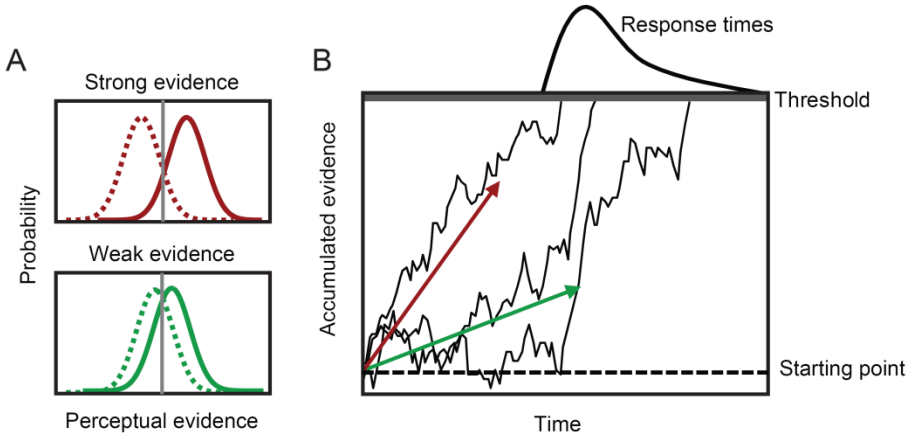

Figure 1.1 Illustrations of perceptual evidence (**A**) and evidence accumulation (**B**). **A**: Representation of perceptual evidence for target (solid lines) and non-target (dashed lines) stimuli when the discrimination is easy (top, red) or difficult (bottom, green). Signal detection theory predicts that choices are made by comparing a single sample of evidence to some criterion (e.g., vertical gray line). **B:** Evidence accumulation dynamics. Samples of perceptual evidence are repeatedly sampled (black lines) until some threshold is reached (gray line). Only one accumulator is illustrated, but decisions typically include multiple racing accumulators representing alternative responses. The quality of perceptual evidence determines the mean rate at which evidence accumulates. Stronger evidence causes faster rates of rise (red arrow) and weaker evidence causes slower rates of rise (green arrow).

Stochastic accumulator models extend signal-detection theory by providing a theory for how samples of evidence are read-out over time. Rather than basing decisions on a single sample of evidence, the distribution of perceptual evidence is repeatedly sampled and accumulated over time (Figure 1.1B). Alternative responses may be represented by bounds in different directions (e.g., Ratcliff, 1978) or by multiple accumulators (e.g., Brown and Heathcote, 2005). A response is selected when the first accumulator bound, or *threshold*, is reached. The strength of sensory evidence for a particular response increases the rate at which evidence for that response accumulates (termed the *drift* or *drift rate).* Stimuli that are more easily discriminate will result in faster drift rates for the correct response accumulator. Responses with the greatest drift rate are more likely to be selected, but other responses will occasionally win because of *noise* in the evidence distributions. Often, the drift rate is a free parameter whose value is selected to optimize the match between predicted and observed behavior (e.g., Ratcliff and Smith, 2004), but more recent models have been developed to explain the computations by which the stimulus

representation and drift rate are generated (e.g., Nosofsky and Palmeri, 1997; Palmeri, 1997; Ashby, 2000; Lamberts, 2000; Palmeri and Tarr, 2008; Smith and Ratcliff, 2009).

Several additional parameters govern the nature of the accumulation process (see Ratcliff and McKoon, 2008, for review). First, the total time necessary for processes outside the accumulation of evidence is referred to as the *non-decision time*. The non-decision time includes time preceding the decision that is necessary to encode the stimulus and compute the distribution of perceptual evidence, as well as motor delay after a response threshold is reached. Second, adjustments in the *starting point* of the accumulation can bias the process in favor of particular responses. Accumulators that start closer to the threshold are more likely to win the race for selection. Third, varying the threshold across all accumulators can adjust the emphasis on speed relative to accuracy. Higher thresholds lead to slower decisions, but allow more time for evidence to accumulate. This increases the probability that the accumulator with the highest drift rate will win the race (i.e., the correct response). Thus, changes in non-decision time, starting point, and threshold predict very different patterns of behavior.

Alternative models also propose different mechanisms for whether and how accumulators representing alternative responses interact. *Independent race* models assume that evidence for each response accumulates independently; the first accumulator to reach threshold determines which response is made (Vickers, 1970; Smith and Van Zandt, 2000). Other models assume that alternative responses compete through inhibitory interactions. Models that assume *feed-forward inhibition* propose that model inputs supporting one response simultaneously reflect evidence against alternative responses (Mazurek et al., 2003; Ditterich, 2006). *Drift diffusion* (Ratcliff, 1978; Ratcliff and Rouder, 1998) and their discrete analogue *random walk* models (Laming, 1968; Link and Heath, 1975; Nosofsky and Palmeri, 1997) represent a form of feed-forward inhibition because they assume response boundaries in opposite directions (Bogacz et al., 2006). In contrast, models that assume *lateral inhibition* propose that alternative responses inhibit one another. As evidence in favor of one response grows, it inhibits alternative responses more

strongly in a winner-take-all fashion (Grossberg, 1976; Usher and McClelland, 2001). These alternative models can vary in other respects such as whether integration of evidence is perfect or leaky. However, it has been very difficult to discriminate these models based on behavioral data alone (Smith and Ratcliff, 2004).

The accumulator model framework parses a single decision into a series of interacting processes that determine behavior. The model makes predictions about how processes should change under specific conditions. For example, drift rate should decline with the difficulty of a perceptual decision and the threshold should increase when accuracy is emphasized. These predictions establish a foundation to begin asking whether the proposed processes map onto specific neuronal populations. Importantly, the neuronal population must also have appropriate anatomical connectivity to mediate the proposed function. For example, a neuron that is said to represent evidence must be anatomically positioned to provide input to a neuron proposed to accumulate evidence. Thus, anatomical considerations provide a basis to begin exploring the potential links between model components and neuronal populations.

1.3 Neuroanatomy of eye movement decisions

The outcome of a decision is a choice expressed through action. A neuron that is involved in decisions about eye movements must therefore be capable of influencing neurons that initiate a shift of gaze. Eye movements are initiated by a network of nuclei in the brainstem (Scudder et al., 2002; Sparks, 2002). Briefly, saccades are produced by a pulse of force that rotates the eyes followed by a step of force that maintains eccentric gaze by opposing the elastic forces of the orbit (Robinson, 1964). The pulse of force is generated by motor neurons that are directly innervated by burst neurons that discharge for saccades of a particular direction, amplitude, and velocity (Fuchs and Luschei, 1970). The step of force is generated by tonic neurons that integrate the velocity to provide a tonic position signal to motor neurons (Cannon and Robinson, 1987). Burst neurons and motor neurons are tonically inhibited by omnipause neurons (OPNs) that fire

tonically, but cease immediately before saccades (Luschei and Fuchs, 1972). OPNs are thought to be inhibited by long-lead burst neurons via inhibitory interneurons (Kamogawa et al., 1996). Thus, excitation of burst neurons and inhibition of OPNs is necessary for saccade generation.

Three sensorimotor areas are well anatomically positioned to initiate saccades when a response threshold is reached: Superior colliculus (SC), frontal eye field (FEF), and supplementary eye field (SEF). SC is the main source of subcortical input to the oculomotor brainstem nuclei (Moschovakis et al., 1988). There are also projections from cerebellar nuclei, but they will not be discussed here (see Scudder et al., 2002 for review). FEF, located in the anterior bank of the arcuate sulcus, and SEF, located on the dorsal bank of medial frontal cortex, are the main source of cortical input to the oculomotor brainstem nuclei (Huerta et al., 1987; Stanton et al., 1988; Huerta and Kaas, 1990; Shook et al., 1990). Of these structures, SC and FEF appear to be most critical for control of saccade initiation. Lesions of either SC or FEF alone result in minimal deficits whereas lesions of both FEF and SC result in an inability to generate voluntary saccades (Schiller et al., 1979). In contrast, lesions of SEF result in temporary increases in saccade latency, but no major deficits (Schiller and Chou, 2000). Thus, an intact FEF or SC is sufficient for saccade generation, whereas SEF is neither necessary nor sufficient.

To be identified with a representation of perceptual evidence, a neuronal population must be innervated by cortical areas that encode sensory information. Neurons in primary and extrastriate visual cortex encode stimulus features (see Orban, 2008, for review). FEF neurons receive topographic input from many extrastriate visual areas V2, V3, V4, MT, TE and TEO (Schall et al., 1995a; Bullier et al., 1996). The intermediate layers of SC also receive converging inputs from diverse posterior visual areas (Leichnetz et al., 1981; Sparks, 1986; Leichnetz and Gonzalo-Ruiz, 1996; Fries, 2004). Thus, FEF and SC seem to be well positioned to integrate diverse sources of visual information. In contrast, SEF receives inputs from far fewer visual areas (Huerta and Kaas, 1990). However, FEF and SEF are densely connected, and SC receives direct projections from and sends indirect projections to FEF and SEF via the medial dorsal nucleus

(MD) of the thalamus (Sommer and Wurtz, 2004b, a; Tanaka, 2007). Therefore, SEF could receive indirect visual information from other sensorimotor areas.

FEF, SEF, and SC are also interconnected with posterior parietal cortex. In particular, the lateral intraparietal area (LIP) in posterior parietal cortex is densely and reciprocally interconnected with FEF and SC (Andersen et al., 1990; Blatt et al., 1990), and also SEF to a somewhat lesser degree (Schall et al., 1995a). LIP also receives input from numerous visual areas including V3, V3A, V4, MT, MST, and TEO (Blatt et al., 1990), although the topography of these connections is far rougher than those connecting to FEF. Feedback from SC is also relayed to LIP via the MD nucleus of the thalamus and the medial pulvinar (Hardy and Lynch, 1992; Asanuma et al., 2004; Schmahmann and Pandya, 2004). Unlike FEF and SC, however, LIP is not directly connected to oculomotor nuclei in the brainstem (May and Andersen, 1986; Schmahmann and Pandya, 1989). Thus, while LIP has inputs appropriate to represent perceptual evidence, only FEF, SC, and SEF can directly influence saccade production.

T o summarize, FEF, SC, LIP, and SEF are all at the junction between perceptual and motor processing, but the anatomical connectivity for each region places limits on proposed functions. First, neurons in FEF, SC, and LIP receive diverse inputs from visual cortex and could integrate different sources of sensory information to represent perceptual evidence. SEF is embedded within this network, although it receives inputs from far fewer early visual areas. Second, FEF, SC, and SEF are directly connected to the brainstem saccade generating nuclei and could initiate saccades when a fixed threshold is reached. Neurons in LIP and other extrastriate visual areas are not directly connected to the saccade generating nuclei of the brainstem and therefore their outputs may undergo further processing prior to saccade initiation. Given these anatomical constraints, we can next ask how neurons within these areas respond while the organism is engaged in perceptual decisions and whether the form of modulation is consistent with predictions of stochastic accumulator models.

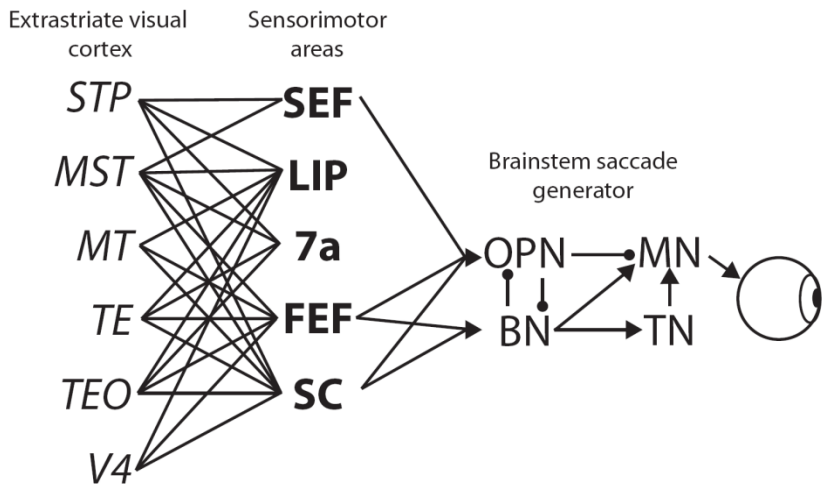

Figure 1.2 Schematic of brain areas and pathways involved in visually-guided saccade generation. Lines indicate reciprocal connections. Arrows indicate one-way projections. SEF, LIP, 7a, and FEF are interconnected. SC is connected to other sensorimotor areas via the mediodorsal nucleus of the thalamus (not pictured). **OPN**: omnipause neurons. **BN**: burst neurons. **MN**: motor neurons. **TN**: tonic neurons. See text for more details.

1.4 Neurophysiology of eye movement decisions

Neurons in FEF, SC, SEF, and LIP have highly heterogeneous response properties. At the most basic level, these neurons can be classified according to their sensorimotor response properties (e.g., Bruce and Goldberg, 1985). *Visual neurons* respond briskly when a stimulus is flashed in their receptive field and may sustain an elevated firing rate when the stimulus must be remembered (Figure 1.3, top). These neurons may also show some pre-saccadic discharge (termed *visuomovement neurons*[1]). Another class of *movement neurons* responds primarily when saccades of a particular direction and amplitude are initiated (Figure 1.3, bottom). Visual and visuomovement neurons are found in FEF, SC, LIP, and SEF (Bruce and Goldberg, 1985; Gnadt and Andersen, 1988; Stuphorn et al., 2010). However, saccade-related neurons are found primarily in FEF, SC, and SEF and much less frequently in LIP (Gottlieb and Goldberg, 1999).

The diversity of response properties must be dictated by differences in the local

[1] In subsequent chapters, I will use the term *visually-responsive* neurons to refer to visual and visuomovement neurons that may also have weaker saccade-related discharge, and I will use the term *saccade-related* neurons to refer to movement and visuomovement neurons that may also have a weak visual response.

microcircuity. In particular, converging evidence suggests that movement neurons in SEF and FEF can be identified with deeper layer 5 pyramidal neurons that distinguish these areas from adjacent cortex (Stanton et al., 1989; Matelli et al., 1991) and are the likely origin of projections to downstream subcortical oculomotor areas (Stanton et al., 1988; Shook et al., 1990, 1991; Pouget et al., 2009). In SEF, the distribution of movement neurons was found to be significantly deeper than visually-responsive neurons (Russo and Bruce, 2000). In FEF, neurons anti-dromically stimulated from OPN regions in the brainstem show primarily saccade-related or fixation-related responses (Segraves, 1992). Also, the current threshold for electrically evoked eye movements in FEF is lowest at sites in which saccade-related activity has been recorded (Bruce and Goldberg, 1985). In contrast, histological reconstructions suggest that visually-responsive neurons are distributed throughout the layers (Thompson et al., 1996). Note that some layer 5 projection neurons can also be identified as visually-responsive (Everling and Munoz, 2000; Sommer and Wurtz, 2000), so the division by layer is not perfect. Altogether, however, these observations suggest that visually-responsive and movement-related neurons may represent functionally distinct subpopulations of neurons within sensorimotor areas.

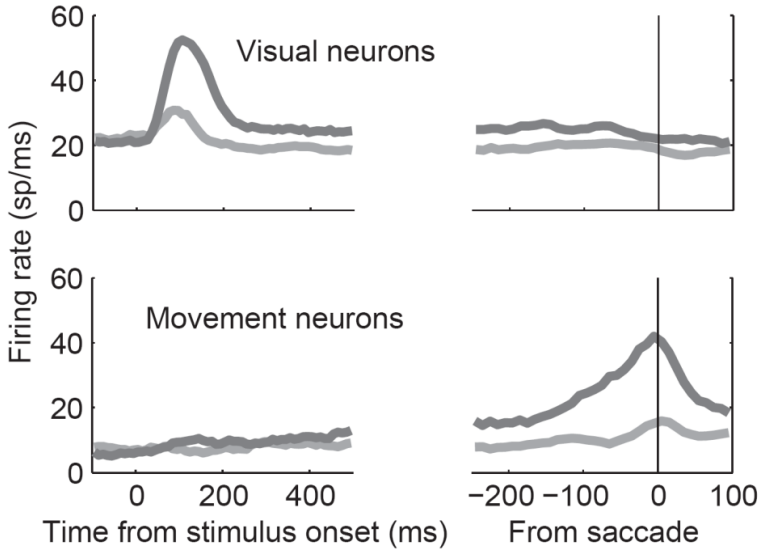

Figure 1.3 Population averages from 33 visual and 21 movement neurons recorded from FEF during a memory-guided saccade task in which the target appeared inside (dark gray) or opposite (light gray) the RF of the neurons.

In order to understand how visual and movement neurons might correspond to accumulator-model processes, their properties must be recorded while monkeys perform perceptual decision-making tasks. The visual search paradigm is a perceptual decision-making task that requires subjects to discriminate a target object among a number of distractors in order to select a response (see Wolfe, 2007, for review). Different models have been developed to explain how subjects can discriminate the relevant target from the irrelevant distractors. Many models of search propose that a *salience map* combines both the physical conspicuousness (i.e., bottom-up information) and the behavioral relevance (i.e., top-down information) of items in the visual field in order to guide both covert attention and eye movements (Treisman and Sato, 1990; Wolfe, 1994; Itti and Koch, 2001; Bundesen et al., 2005; Wolfe, 2007). Eye movements and covert attention are assumed to be guided to peaks on the salience map.

I will first consider the role of visual neurons during the visual search task. Converging evidence suggests that visual neurons in FEF, SC, and LIP can be identified with the salience map proposed by models of visual attention (Findlay and Walker, 1999; Thompson and Bichot, 2005; Gottlieb, 2007; Bisley and Goldberg, 2010). During search, the firing rate of these neurons initially elevates regardless of the stimulus in the receptive field. Over time, however, firing rates evolve to select the location of behaviorally-relevant stimuli by maintaining an increased firing rate if the relevant target is in the neuron's receptive field and reducing firing rate if an irrelevant distractor is in a neuron's receptive field. This target selection process takes place across a distributed network of visuomotor areas including FEF (Schall and Hanes, 1993; Thompson et al., 1996; Bichot and Schall, 1999a), SC (McPeek and Keller, 2002; Shen and Paré, 2007), LIP (Ipata et al., 2006; Thomas and Pare, 2007; Ogawa and Komatsu, 2009), substantia nigra pars reticulata (Basso and Wurtz, 2002), parietal area 7a, (Constantinidis and Steinmetz, 2001; Katsuki and Constantinidis, 2012), PFC (Hasegawa et al., 2000; Constantinidis and Steinmetz, 2001; Buschman and Miller, 2007; Katsuki and Constantinidis, 2012), and medial dorsal nucleus of the

thalamus (Schall and Thompson, 1994; Wyder et al., 2004). However, it is not known whether SEF neurons represent visual salience.

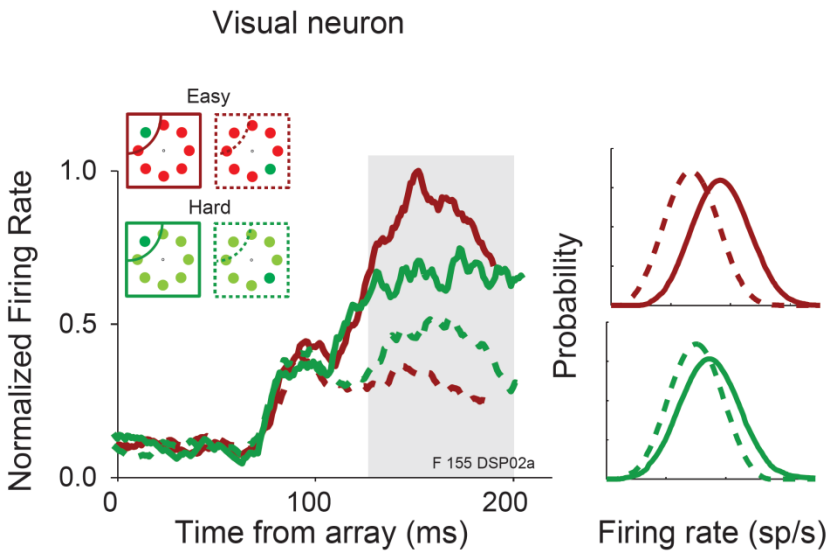

Figure 1.4 Visual neuron recorded from the FEF of a macaque monkey performing the visual search task. The left panel shows the average normalized firing rate when the target (solid lines) or a distractor (dashed lines) were inside the receptive field of the neuron during an easy (red) and hard (green) color search task. The right panels show the distribution of mean firing rates in the time window 125-200 ms after the array onset (gray box in left panel). Conventions as in left panel. Firing rate distributions were convolved with a Gaussian distribution for smoothing.

The pattern of firing rate modulation during target selection is consistent with the properties of the hypothetical salience map in several ways. First, the selection process is influence by bottom-up properties of the stimulus. When the target and distractor are easily discriminated, the target is selected earlier and the post-selection firing rate difference (i.e., the *magnitude of selection*) is larger (Figure 1.4; Basso and Wurtz, 1998; Bichot and Schall, 1999a; Sato et al., 2001; Balan et al., 2008; Cohen et al., 2009b). Note that the evolution of salience is dynamic and these dynamics must be taken into account when explaining decision-making. Second, the selection process is influenced by top-down factors including trial history and expected reward. When the target identity is fixed for several consecutive trials, the magnitude of selection is greater than if target identity has recently changed (Bichot and Schall, 2002). Firing rates are also modulated by the probability and magnitude of expected reward (Platt and Glimcher, 1999; Roesch and Olson, 2003; Ding and Hikosaka, 2006). Third, the representation of visual salience

by visual neurons is independent of movement production. Search targets are selected even if the animal is instructed to withhold a saccade (Thompson et al., 1997), if the animal responds manually (Thompson et al., 2005a), or if the location of the target unexpectedly changes (Murthy et al., 2001; Murthy et al., 2009). Importantly, these are the same properties that would be expected of a population of neurons that represented perceptual evidence that a target is present within their receptive field. However, the connection between the neurophysiological representation of salience and accumulator models has not been established.

Recall that the connections between posterior visual areas and sensorimotor areas that encode visual salience are reciprocal (Figure 1.2). Neurons in the superficial layers of FEF and LIP send feed-back projections to many visual areas (Blatt et al., 1990; Pouget et al., 2009) and SC can relay signals to visual cortex via the pulvinar (Benevento and Standage, 2004; Lyon et al., 2010). Although, the firing rates of neurons in posterior visual areas are primarily driven by their preference for object features, these responses can also be modulated to some degree by the object's behavioral relevance (i.e., visual attention; Moran and Desimone, 1985; Luck et al., 1997b; Ogawa and Komatsu, 2004). The effect of microstimulation and pharmacological manipulation of FEF on extrastriate neurons suggests that feedback from frontal areas like FEF might be one source driving these modulations (Moore and Armstrong, 2003; Monosov et al., 2011; Noudoost and Moore, 2011; but note that the role of SC has recently been called into question; Zenon and Krauzlis, 2012). If so, then the representation of salience in sensorimotor areas may be detectable at a population level in regions of posterior visual cortex, although this connection has not been conclusively established.

Next, consider the response properties of FEF and SC movement neurons (Figure 1.5). During search, movement neuron responses differ from visual neuron responses in two key ways. First, unlike visual neurons, movement neuron firing rates are not independent of saccade production. Movement neurons respond only before saccades of a particular direction and amplitude (Schiller and Koerner, 1971; Bruce and Goldberg, 1985; Schall, 1991b; Munoz and

Wurtz, 1995). These neurons fire before saccades when no stimuli are visible (Bruce and Goldberg, 1985) and when the saccade is directed away from a visual target (Everling et al., 1999; Everling and Munoz, 2000). During search, the onset time of movement neuron firing increases with response time if the target location is indicated via saccade (Figure 1.5, right; Woodman et al., 2008), but firing rates are suppressed if the location is indicated by hand (Thompson et al., 2005a). When a monkey is instructed to withhold a pre-cued saccade, movement neurons, but not visual neurons, modulate their firing rate sufficiently early to predict whether or not the saccade was withheld or initiated (Hanes et al., 1998; Brown et al., 2008; Murthy et al., 2009). The lack of independence from saccade production indicates that these neurons cannot be identified with a covert representation of salience or perceptual evidence.

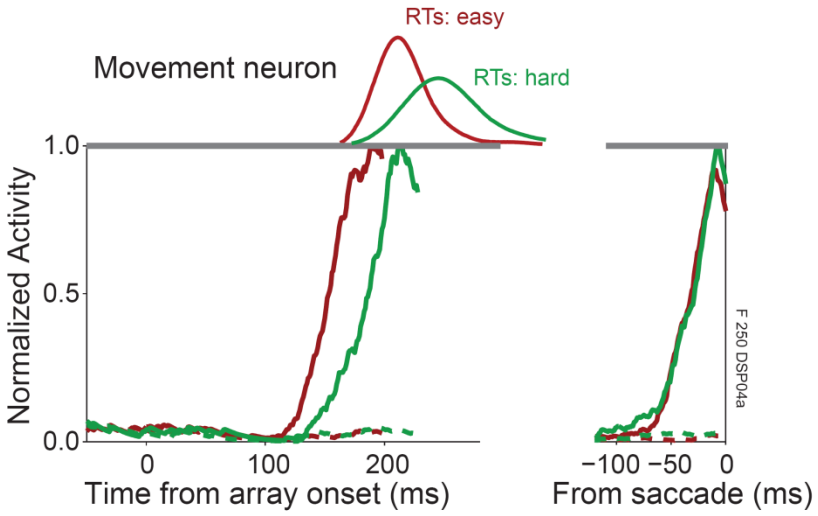

Figure 1.5 Movement neuron recorded from the FEF of a macaque monkey performing a color search task. Conventions as in Figure 1.4. Left panel is aligned on array onset and right panel is aligned on saccade.

The second key difference between movement and visually-responsive neurons is that movement neurons reach a fixed firing rate threshold immediately prior to saccades (Hanes and Schall, 1996; Dorris and Munoz, 1998; Ratcliff et al., 2003; Brown et al., 2008). This threshold may be identified with the trigger that initiates a saccade by tipping the balance of excitation and inhibition between burst neurons and OPNs (Figure 1.5). The time when movement neuron, but

not visual neuron, firing rates reach a fixed level accounts for random variability in response time (Hanes and Schall, 1996; Brown et al., 2008). If a task is made perceptually more difficult, then response times are longer, but movement neurons still reach the same firing rate immediately prior to a saccade (Ratcliff et al., 2003; Ratcliff et al., 2007; Woodman et al., 2008). Note that the value of the threshold is not fixed across all conditions; it may vary during non-visually-guided antisaccades (Everling et al., 1999; Everling and Munoz, 2000), when errors are made (Thompson et al., 2005b), or when deadlines are employed (Heitz and Schall, 2012). Critically, however, it always appears to be constant within a single condition. Altogether, these observations indicate that movement neurons exhibit dynamics that seem qualitatively consistent with the predictions of stochastic accumulator models.

1.5 Linking propositions

Linking propositions are statements that map unobservable cognitive states onto observable neural states, and the population of neurons that instantiate the process are referred to as a *bridge locus* (Teller, 1984; Schall, 2004). Accumulator models make predictions about how the bridge locus for the perceptual evidence and evidence accumulation should change under certain conditions. Given what we now know about the anatomy and physiology of perceptual decision-making, what are the potential bridge loci for perceptual evidence and evidence accumulation? In this section, I summarize four potential neuronal populations to be evaluated (Figure 1.6).

One potential link between model and brain are visual neurons in FEF, LIP, and SC that seem to represent the salience of objects in the visual field. Existing models of visual salience propose that eye movements are targeted to locations at the peak of the salience map, but the neural mechanisms by which a peak on the map are transformed into a command to move the eyes are generally not clear. One possibility is that the representation of salience can be identified with the representation of perceptual evidence that drives a stochastic accumulation to threshold, but this proposal has not been rigorously evaluated.

A second potential link between model and brain are FEF and SC movement neurons. The observation that these neurons reach a fixed firing rate threshold seems consistent with the temporal dynamics predicted by accumulator models. Therefore, one possibility is that these neurons might instantiate the accumulation process. Several existing models have shown that movement neuron dynamics can be explained by stochastic accumulation (Ratcliff et al., 2003; Boucher et al., 2007; Ratcliff et al., 2007), but these models do not explain the source of perceptual evidence. A complete theory of perceptual decision-making will need to explain both where the accumulation takes place, and the source of evidence being accumulated.

A third potential link between the model and brain are neurons in posterior visual cortex. Existing models have focused on the role of feature-selective neurons as a source of feed-forward inputs to FEF, LIP, and SC (Shadlen and Newsome, 2001; Mazurek et al., 2003). However, feed-back from FEF and possible also LIP are thought to modulate feature-selective neurons according to behavioral relevance (Ogawa and Komatsu, 2004). One hypothesis is that visual neurons that represent perceptual evidence in FEF are the source of top down inputs. If so, then simultaneous recordings from FEF and posterior visual cortex should reveal very similar patterns of modulation in FEF visual neurons and posterior visual cortex.

A fourth potential link between model and brain are SEF neurons in medial frontal cortex. SEF is interconnected with FEF, SC, and LIP (Huerta and Kaas, 1990). SEF has both visual and movement neurons (Schall, 1991a). SEF movement neurons, unlike FEF and SC movement neurons, do not reach a fixed response threshold and therefore seem inconsistent with evidence accumulation (Stuphorn et al., 2010). However, the role of SEF visual neurons in representing perceptual evidence is not known. To address this question, SEF neurons must be recorded during the same visual search task as FEF, SC, and LIP. If SEF neurons represent perceptual evidence, then they should be modulated by physical conspicuousness and behavioral relevance similar to other areas known to represent visual salience.

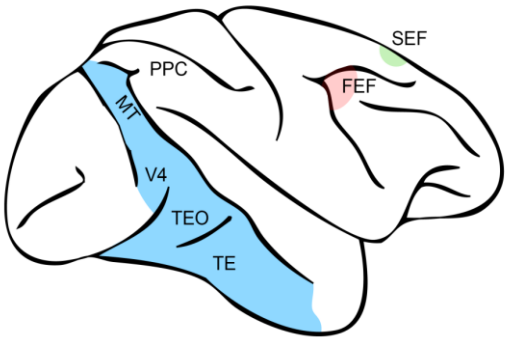

Figure 1.6. Potential bridge loci of stochastic accumulator model processes. The following chapters will address whether different regions of macaque cortex represent different components of stochastic accumulator models. Chapters III and IV will investigate visual and movement neurons in FEF (red). Chapter V will investigate the relationship between FEF and event-related potentials recorded over posterior visual cortex (blue). Chapter VI will investigate the role SEF (green).

1.6 Overview of studies

In the following chapters describe a series of experiments that test whether the neuronal populations described above could serve as the bridge loci for accumulator model processes. Each of the following chapters are published papers or in preparation for publication, and therefore each one is written as an independent entity. However, all papers are connected by a common theme in that they provide evidence for the identification of different neuronal populations with either a representation of perceptual evidence or evidence accumulation.

Chapter II does not directly evaluate potential bridge loci of accumulator model processes, but instead evaluates methods for comparing accumulator models to neural activity. The purpose of this study was to characterize accumulator model predictions for neural dynamics under a range of parameterizations. This is important preliminary step to identify neurons that implement evidence accumulation because noise can cause counterintuitive patterns of dynamics. This study will show that the mapping between model parameters and standard measures of neural dynamics is not one-to-one in the face of noise. In particular, with noise, patterns of predicted dynamics based on intuitions about noiseless accumulators can mislead interpretations of patterns of neurophysiology. These results suggest that model dynamics should be directly compared to

neural dynamics, which is the methodology followed in Chapters III and IV. This work is currently in preparation for publication.

Chapter III evaluates whether FEF visual neurons can be identified with a representation of perceptual evidence and whether FEF movement neurons can be identified evidence accumulation. Following the methodology established in (Purcell et al., 2010), I will use visual neuron firing rates as input to a multiple accumulator model of search behavior. I found that a model that uses visual neuron firing rates as input can predict detailed search behavior. Next, following the methodology established in Chapter II, I will compare predicted model dynamics with observed movement neuron dynamics. I found that the model predicts the dynamics of movement neurons using parameters that were fit to behavior. This supports the identification of visual neurons with perceptual evidence and movement neurons with integration of evidence to threshold. This study is published in *The Journal of Neuroscience* (Purcell et al., 2012b).

Chapter IV further tests the link between model components and neuronal populations by analyzing the pattern of variability in FEF neurons during search. This study will show that the pattern of response variability in FEF movement neurons is consistent with the pattern of response variability predicted by accumulator models. In addition, this study evaluated how the variability of perceptual evidence may change under different conditions by analyzing the dynamics of visual neuron response variability. We found that the mean, but not the variability, of visual neuron firing rates is modulated by the strength of perceptual evidence. This indicates that evidence is encoded via signal enhancement rather than noise reduction. This study is published in *Journal of Neurophysiology* (Purcell et al., 2012c).

Chapter V tests the potential link between neuronal activity in posterior parietal cortex and FEF visual neurons through to represent perceptual evidence. To address this question, we recorded extracranial voltage potentials over posterior visual cortex simultaneously with intracranial neuronal activity from FEF. One advantage of this approach is that ERPs can amplify the representation of perceptual evidence in posterior visual cortex by integrating neuronal

activity across many centimeters of cortex. In addition, by using a noninvasive technique, we can attempt to identify a potential index of perceptual evidence that can be measured in healthy humans. This study finds that potentials recorded over posterior visual cortex modulate in much the same way as FEF neurons and local field potentials. The timing of these modulations suggests that FEF may be a source of input driving the generators of these potentials. This study is published in *Journal of Neurophysiology* (Purcell et al., 2013).

Chapter VI tests whether SEF visual neurons represent perceptual evidence. Although data exist to suggest that SEF may not be directly involved in the accumulation of evidence to initiate saccades (Stuphorn et al., 2010), less is known about the role that SEF may play in representing perceptual evidence for a particular response. We recorded single unit activity and LFP from the SEF of monkeys performing a visual search task. Surprisingly, we found that SEF neurons do not represent the salience (top-down or bottom-up) of stimuli in their receptive field and therefore cannot be identified with perceptual evidence for a response. Instead, SEF neurons signal search errors. This suggests that accumulator model processes do not map onto any SEF neurons. Instead, SEF may be involved in performance monitoring processes that are used to adjust performance on subsequent trials. This study is published in *The Journal of Neuroscience* (Purcell et al., 2012a)

Each study addresses the degree to which particular neurophysiological signals could correspond to accumulator model processes. In some cases, the studies support a close mapping between models and physiology. However, this work also highlights several limitations underlying the assumption that simple cognitive models will map cleanly onto discrete neural elements. In the final section (Chapter VII), I will discuss open questions that are raised by this work and address potential future approaches with which they could be answered.

CHAPTER II

MIMICRY IN MODEL DYNAMICS: RELATING STOCHASTIC ACCUMULATOR MODEL PARAMETERS TO NEURAL DYNAMICS

2.1 Abstract

Accumulator models explain perceptual decisions as the accumulation of evidence to a response threshold. The relationship between model parameters and predicted behavior is well known, but the relationship between model parameters and accumulator dynamics has received less attention because dynamics were assumed to be unobservable. The recent identification of neuronal activity with the accumulation process suggests that neural dynamics could be used as a tool for model selection. We characterized the expected patterns of neural dynamics using different accumulator model parameters to determine when different sources of behavioral variability can be distinguished via observed dynamics. Whereas the mapping between model parameters and dynamics is straightforward in the absence of noise, we found that noise complicates this relationship. When noise is moderate to large, changes in the model starting point and threshold could be easily identified through model dynamics, but changes in drift rate were nearly indistinguishable from changes in the start time of the accumulation (i.e., the encoding delay). We suggest an alternative method for distinguishing changes in drift rate and encoding delay based on the across-trial variability of model dynamics. These results inform the interpretation of neurophysiological signals identified with evidence accumulation and suggest that researchers should directly compare neural dynamics to model dynamics, and not model parameters.

2.2 Introduction

Cognitive models allow us to infer the basic processes underlying simple perceptual tasks (Townsend and Ashby, 1984; Busemeyer and Diederich, 2009). These models decompose

response time (RT) into distinct processes (Meyer et al., 1988; Sternberg, 2001). Accumulator models (also termed *sequential sampling models*) currently provide the most complete account of perceptual decision-making behavior (Ratcliff and Smith, 2004). These models assume that perceptual evidence for a particular response is integrated over time by one or more accumulators. A response is selected when evidence reaches a threshold or boundary. These models can explain RT distributions for both correct and error saccades for a range of perceptual tasks.

Several parameters determine accumulator model predictions. For example, a *drift rate* parameter defines the mean rate of accumulation, a *threshold* parameter defines the level of evidence that must be reached for a response to be initiated, and a *starting point* parameter determines the initiate state of accumulation. Often, parameter values are selected to maximize the match between observed and predicted behavior. The resulting values can then be used to infer the processes that generated behavior. However, model parameters also determine the dynamics of the accumulation process that unfolds over time. Less attention has been paid to the relation between model parameters and dynamics because these dynamics were assumed to be unobservable mental operations.

Recently, several groups have begun to investigate potential linking propositions between accumulator models and neurophysiological measures (Schall, 2004; Smith and Ratcliff, 2004; Gold and Shadlen, 2007). During decision-making tasks, the firing rates of neurons in frontal eye field (Hanes and Schall, 1996), superior colliculus (Ratcliff et al., 2003), lateral intraparietal area (Roitman and Shadlen, 2002), and premotor cortex (Cisek, 2006) have been identified with accumulation to a threshold. Other groups have identified event-related potentials (ERPs) that seem to reflect the evidence-integration process. During certain perceptual decisions, ERPs recorded over parietal cortex demonstrate dynamics consistent with evidence accumulation (O'Connell et al., 2012). In addition, the lateralized readiness potential (LRP), an ERP related to

motor preparation, has been identified with accumulation to a response boundary (Gratton et al., 1988; De Jong et al., 1990; Osman et al., 2000; Rinkenauer et al., 2004; Schurger et al., 2012).

If valid linking propositions can be identified, then accumulator dynamics could be directly observed. This means that accumulator model dynamics that are generated by parameter values fit to behavior could be interpreted as predictions for neural dynamics. If the mapping between model parameters and model dynamics is one-to-one, then predictions for changes in neural dynamics could be derived directly from changes in model parameters. For example, if the model requires a change in drift rate to predict behavior, then one might assume a change in growth rate of underlying spike trains must have occurred. Likewise, if appropriate neurophysiological data are collected, then one might be able to infer changes in parameters simply by analyzing the neural dynamics. For example, if the growth rate of spike trains changes across stimulus conditions, then one might assume that accumulator models will require changes in drift rate to explain behavior.

One potential problem with this approach is that the mapping between model parameters and model dynamics may not be one-to-one. This isn't a problem for deterministic models in which evidence accumulation is ballistic (Brown and Heathcote, 2005; Brown and Heathcote, 2008), but many accumulator models assume that evidence is noisy (e.g., Usher and McClelland, 2001; Ratcliff and McKoon, 2008; Smith and Ratcliff, 2009). Furthermore, noise is ubiquitous in neural activity (Faisal et al., 2008). Given sufficient levels of noise, it is possible that different model parameters could predict indistinguishable changes in model dynamics. In other words, the models may exhibit mimicry at the level of dynamics rather than behavior. However, the degree to which this is a problem for the noise levels typically assumed by accumulator models is an open question.

The goal of this study was to characterize the relationship between accumulator model parameters and dynamics. This is a crucial intermediate step towards understanding the relationship between model parameters and neural dynamics that has been unaddressed in

previous work. Previous studies have directly compared the model dynamics with neural dynamics (Mazurek et al., 2003; Ratcliff et al., 2003; Boucher et al., 2007; Ratcliff et al., 2007; Purcell et al., 2010; Purcell et al., 2012b), but the relation to model parameters was not always clear. For example, Purcell et al. (2010) showed that accumulator models predict the firing rates of certain frontal eye field neurons during perceptual decisions, but the effect of specific parameters on accumulator dynamics was unclear because the models assumed a complex, time-varying drift rate. Other studies have reported model dynamics for sets of parameters that were fit to behavioral data (e.g., Ratcliff et al., 2003; Ratcliff et al., 2007), but it is difficult to know which parameters contributed to which aspects of the dynamics without systematically manipulating the value of individual parameters.

In order to characterize the relationship between parameters and dynamics, we quantified four measures of model dynamics (onset, growth rate, baseline, and measured threshold) that would be expected to correspond to model parameters. These measures of model dynamics were based on established methods that have been applied to neurophysiological data in previous studies (Woodman et al., 2008; Purcell et al., 2010; Purcell et al., 2012b). If the mapping between parameters and dynamics is one-to-one, then variation in certain parameters should correspond to variation in specific measures of dynamics. This would mean that model parameters could be uniquely identified with specific neural dynamics. Alternatively, when noise is present, changes in one parameter may result in changes in one or more measures of dynamics. If so, then measures of neural dynamics cannot be uniquely identified with one parameter. This would mean that inferring changes in a specific model parameter based on changes in a specific measure of model dynamics may be invalid.

We find that when models include noise, the mapping between some model parameters and model dynamics is not one-to-one. In particular, noisy accumulator models will predict variability in the growth rate and onset of dynamics regardless of actual sources of across-trial variability. This can lead to changes in the measured onset across conditions even if the actual

encoding delay is unchanged. We suggest two alternative methods for identifying changes in the model encoding delay in the face of noise. In addition, we find that when models are noisy, parameters such as leakage, feed-forward inhibition, and lateral inhibition become very difficult to distinguish at the level of model dynamics. Altogether, these results suggest that, in general, model parameters should not be compared directly to neural dynamics.

2.3 Method

2.3.1 Overview of models

Different accumulator models make different assumptions about the nature of evidence accumulation. We first evaluated a general *independent race model* architecture in which one accumulator is assumed to accumulate evidence for a single response. If multiple responses are present, then multiple accumulators race to threshold to determine which response is executed and the time at which it is executed. This model is similar to several existing models that assume noisy independent accumulators for each response (Vickers, 1970; Smith and Van Zandt, 2000). If this model includes no intra-trial noise, then it is similar to the linear ballistic accumulator model (Brown and Heathcote, 2008; Palmer et al.) or LATER model (Reddi & Carpenter, 1995). We also evaluated a *bounded race model* that assumes a single accumulator with boundaries in both the positive and negative directions representing alternative responses. This model is similar to the well-known drift-diffusion model (Ratcliff, 1978; Ratcliff and Rouder, 1998). Results for the bounded model were highly similar to the independent race model, and therefore we summarize them in the Appendix (Figure A.1-A.3).

All accumulator models share several common assumptions. We use the term *primary parameter* to refer to parameters that determine basic properties of the accumulation process under a single experimental condition (Donkin et al., 2011). Accumulator models assume four primary parameters. First, the *drift* or *drift rate* (v) determines the mean rate of accumulation. This parameter is assumed to reflect the strength of sensory evidence for a particular response;

strong evidence results in a higher drift rate. Second, the *starting point* determines the level at which evidence accumulation begins. Adjustments in the relative values of the starting point across different accumulators can introduce response biases. Third, the *model threshold* (*a*) determines the level of evidence that must be accumulated before a response is initiated. Increasing or decreasing the threshold for all accumulators emphasizes accuracy or speed, respectively. Note we use the term *model threshold* rather than simply *threshold* to distinguish the model parameter from our measure of model dynamics described below. The fourth primary parameter of interest is the *encoding delay* (*D*) or the delay between the onset of a stimulus and the start of the accumulation process. This is assumed to be the time during which the properties of the stimulus are be encoded with respect to task demands. Typically, the encoding delay is combined with motor delay time that is assumed to follow the accumulation process into a single *non-decision time* parameter, but the two can be distinguished in neurophysiological signals. Here, we focus specifically on the encoding delay because the motor delay is known to be relatively short and invariant for many neurophysiological signals identified with evidence accumulation (e.g., Gratton et al., 1988; Scudder et al., 2002).

Different models make different assumptions about sources of behavioral variability. The first way in which models differ in their assumptions about variability is whether or not they assume intra-trial variability (i.e., *noise*) in accumulation. For example, the diffusion model (Ratcliff, 1978) assumes that the accumulation process is noisy (i.e., stochastic), whereas LBA (Brown and Heathcote, 2008) assumes that the accumulation is noiseless (i.e., deterministic). Noise is assumed to be sampled from a Gaussian distribution with mean 0 and standard deviation, *s*. A primary goal of this work was to understand the effect of noise on the relation between model parameters and model dynamics. We did this in two ways. First, we contrasted *noiseless models* ($s = 0$) to *noisy models* ($s = 0.1$). We choose $s = 0.1$ because *s* is commonly fixed to this value when fitting models to empirical data by convention (Ratcliff and Rouder, 1998; Ratcliff and Tuerlinckx, 2002; Ratcliff and Smith, 2004), although this may not be necessary for all

conditions (Donkin et al., 2009). Second, we report the changes in model dynamics while systematically varying the level of noise, drift rate, and model threshold. This allowed us to characterize how the effect of noise on model dynamics depends on the relative values of these parameters.

The second way in which models differ in their assumptions about variability is whether or not they assume across-trial variability in certain model processes. For each primary parameter, there is one additional *secondary parameter* that determines how that parameter varies across trials. The drift rate varies across trials according to a Gaussian distribution with standard deviation, η. The starting point varies according to a Uniform distribution with range, *sz*. The encoding delay varies according to a uniform distribution with range, *st*. The model threshold varies according to a Gaussian distribution with standard deviation, *sa*. Typically, different models assume different sources of across-trial variability. For example, LBA assumes across-trial variability in only the drift rate and the starting point. Our goal was to understand how well each of these secondary parameters could be identified through measures of model dynamics. Therefore, rather than focus on a single model architecture with specific assumptions about sources of variability, we independently assessed the effect of different sources of variability on model dynamics[2]. We evaluated different versions of each model that assumed a single source of variability by systematically varying one secondary parameter and setting all other secondary parameters to zero.

In addition to primary and secondary parameters, some accumulator models assume additional parameters that determine the degree to which integration is perfect or leaky, and whether or not there are competitive interactions among accumulators (e.g., Usher and

[2] Note that many accumulator models allow for multiple sources of across-trial variability, so these simulations represent an idealized situation. Even if we can show that a source of across-trial variability can be uniquely identified with one measure of model dynamics, we cannot be sure that this is true when interactions with other sources of variability are present. However, our simulations will demonstrate that even in this idealized situation, we still cannot identify certain sources of variability based on dynamics alone. This problem could only be exacerbated by additional sources of variability.

McClelland, 2001). Therefore, we also evaluated three additional model architectures to determine the degree to which leakage and competition can be identified in model dynamics. The *leaky race model* assumes that integration of evidence is not perfect, but decays with some time constant. This model is similar to the leaky competing accumulator model (Usher and McClelland, 2001) without competition and similar to an Ornstein-Uhlenbeck process in which the rate of accumulation decreases as the amount of accumulated evidence increases (e.g., Busemeyer and Townsend, 1993; Smith, 1995). The *competitive model* assumes that competing accumulators represent different responses. This model is also similar to the leaky competing accumulator model (LCA; Usher and McClelland, 2001) without leakage. Competition can be implemented as either feed-forward (Ditterich, 2006; Ratcliff et al., 2007) or lateral (Usher and McClelland, 2001) inhibition (see also Bogacz et al., 2006).

2.3.2 Measures of model dynamics

We investigated whether there was a one-to-one mapping between accumulator model parameters and four changes in model dynamics that could potentially explain changes in behavior. Measures of model dynamics were selected so that each measure should correspond to a specific model parameter if models were noiseless. First, we measured the *onset time* of accumulation relative to the appearance of the stimulus. This is the point when activity first increased from baseline towards the threshold. In the absence of noise, changes in the measured onset of accumulation should correspond to changes in the encoding delay parameters, D and st. Second, we measured the *growth rate* of accumulation to threshold. This is the average rate of change in activation from the time when activity first began increasing until the time when the threshold was reached. In the absence of noise, changes in the measured growth rate should correspond to changes in the drift rate parameters, v and η. Third, we measured the *baseline* of accumulation. This is the initial level of evidence prior to the start of the accumulation process. In the absence of noise, this should correspond to the starting point parameters, z and sz. Fourth,

we measured the *measured threshold* activation. This is the level of activation when the response was initiated. Here, we use the term *measured threshold* to distinguish the measure of dynamics from the model threshold parameter. In the absence of noise, this should correspond to the model threshold parameter, *a* and *sa*. The critical question was whether these relationships will hold when the accumulator is noisy ($s > 0.01$).

We used established methods for quantifying model and neurophysiological dynamics that have been used in previous studies (Woodman et al., 2008; Purcell et al., 2010; Pouget et al., 2011; Purcell et al., 2012b). To quantify the onset of activation, we used a sliding-window algorithm (+/- 50 ms) that moves backward in 1 ms increments beginning at the time when the threshold is reached. The onset of activation was determined as the time when the following criteria are met: (1) activity no longer increases according to a Spearman correlation (alpha = 0.05) within the window around the current time; (2) activity at that time was lower than activity during the 20 ms preceding saccade onset; and (3), as the window was moved backwards in time, the correlation remains nonsignificant for 90ms. We also tested whether the results are similar when the onset is computed using an alternative approach in which the onset is determined by the time at which activation first exceeds 10% of the distance from baseline to threshold (Schwarzenau et al., 1998). To quantify the growth rate, we divided the distance from starting point to threshold by the time from onset until RT. To quantify the baseline, I will compute the average activation in the initial 50ms of the simulation, which was always less than the minimum encoding delay. To quantify the measured threshold, I will compute the average model activation from 10 s before until 10 s after the threshold was reached.

For the most analyses, we report measures of model dynamics computed directly from the average accumulation process. This continuous signal may be most comparable to ERP components. However, accumulator models have also been mapped to the activity of individual neurons, which discharge action potentials (spikes) at discrete time points. The spiking statistics of cortical neurons have been modeled according to a Poisson process with a time-varying rate

parameter (e.g., Nawrot et al., 2008). Here, the accumulation process would be more akin to the rate parameter, and the Poisson spiking would introduce additional variability that could alter measured dynamics. Therefore, we also simulated a Poisson process using our model dynamics as the rate parameter. Model trajectories were rescaled by dividing by model threshold, a, and then multiplying by 50 to produce mean firing rates on the order of typical cortical neurons (e.g., Purcell et al., 2012b). As in neurophysiological studies, we converted simulated spike trains to a continuous function by convolving them with a kernel shaped like a post-synaptic potential (Thompson et al., 1996). The resulting activity can then be analyzed exactly as was done for the raw model dynamics.

2.3.3 Simulation methods

To understand the relationship between model parameters and dynamics, it was necessary to use numerical simulations in order to analyze the model trajectory associated with each response. Our motivation was to inform the comparison of accumulator models and neurophysiology, and therefore our simulation methods aimed to approximate the statistical power of neurophysiological recordings. For a given set of parameters, each model will first generate 200 simulated trials. We refer to this set of trials as a *simulated session* because it roughly corresponds to the number trials obtained from one condition of a single experimental session. For each simulated session, trials were grouped into RT deciles (bins of size 20) and the average model trajectory was computed for each decile. This process was repeated for 200 simulated sessions. This approach afforded some noise reduction via averaging, but avoids major distortions of model dynamics that can result from averaging trials that result in very different RTs. This approach also allowed us to ask how model dynamics change with RT when models assume different sources of across-trial variability. We found that our results are robust to large variations in the number of trials in a given simulated session (Figure A.4).

We report the results from two different approaches to measuring model dynamics. First, we could analyze individual simulated sessions and the pool across sessions. This approach approximates the statistical power expected in typical neurophysiological experiments in which measurements are made on individual neurons or subjects. Alternatively, model dynamics could be averaged across all simulated sessions to first eliminate noise, and then measurements could be computed based on this population *grand average.* This approach will test whether the noise reduction afforded by pooling across subjects or neurons can change our results.

2.4 Independent race model simulations

We first simulated an independent race model using a range of parameters in order to understand the relationship between model parameters and measured dynamics. Model activation, X, was set to an initial point, z for the duration of the stimulus encoding delay, D. Following the encoding delay, model dynamics are governed by the following stochastic differential equation:

$$\frac{\quad}{\quad} = \frac{\quad}{\quad} .$$

For each simulated trial, I is sampled from a Gaussian distribution with mean v and standard deviation η. is a Gaussian noise term with a mean of zero and standard deviation, s. RT is given as the time when activation, X, reaches a fixed threshold. Model threshold, a, varies according to a Gaussian distribution with standard deviation sa. Encoding delay, D, varies across trials according to a Uniform distribution with range st. Baseline, z, can vary across trials according to a Uniform distribution with standard deviation, sz. All model activation which drops below zero will be set to zero because spike rates cannot fall below zero. All simulations used an integration time step of dt = 1 ms.

2.4.1 Identifying sources of across-trial variability from model dynamics: noiseless independent race

We first evaluated whether distinct sources of across-trial variability (i.e., secondary parameters) could be identified based on patterns of model dynamics. To validate our measures of model dynamics, we first evaluated an independent race model with no noise. This model architecture is similar to LBA (Brown and Heathcote, 2008) or LATER (Reddi and Carpenter, 2000) models. Whereas LATER and LBA assume only across-trial variability in drift rate and starting point, we evaluated four versions of this model that each assumed a different source of across-trial variability. This was done by first setting default values of the primary model parameters (Tr = 0.2, v = 0.2, z = 0.018, a = 0.5) and initially setting noise to zero (s = 0). For each version of the model, one of the secondary parameters (i.e., st, η, sz, sa) was set to a positive value and all other secondary parameters were set to zero. Parameter values were selected to produce response times on the order of those typically observed in perceptual decision-making experiments. To introduce the problem, we first present results using default values of these parameters. Later, we present a more thorough exploration of parameter space to demonstrate the generality of these results.

The first version of the noiseless independent race model assumed that across-trial variability in the encoding delay was the only source of behavioral variability (st = 0.2, η = 0, sz = 0, sa = 0). Figure 2.1A plots the average trajectories for six representative RT groups. If encoding delay maps directly onto measured onset, then we would expect slower RTs to be associated with longer delays. Indeed, this is exactly what was observed (Figure 2.1A). Similarly, Figure 2.1B-D shows that each measure of model dynamics can be uniquely identified with a different source of across-trial variability. The second version of the model assumed that across-trial variability in drift rate is the only source of variability (st = 0, η = 0.1, sz = 0, sa = 0). For this version, longer RTs are associated with slower rates of accumulation (Figure 2.1B). The third version of the model assumed that across-trial variability in starting point was the only

source of variability (*st* = 0, η = 0, *sz* = .02, *sa* = 0). For this version, longer RTs are caused by trials in which the baseline level was lower (Figure 2.1C). Finally, when variability in threshold is the only source of behavioral variability (*st* = 0, η = 0, *sz* = 0, *sa* = 0.01), longer RTs are caused by greater levels at which the accumulation terminates (Figure 2.1D). These results are in line with general intuitions about how accumulator model dynamics behave in the absence of noise.

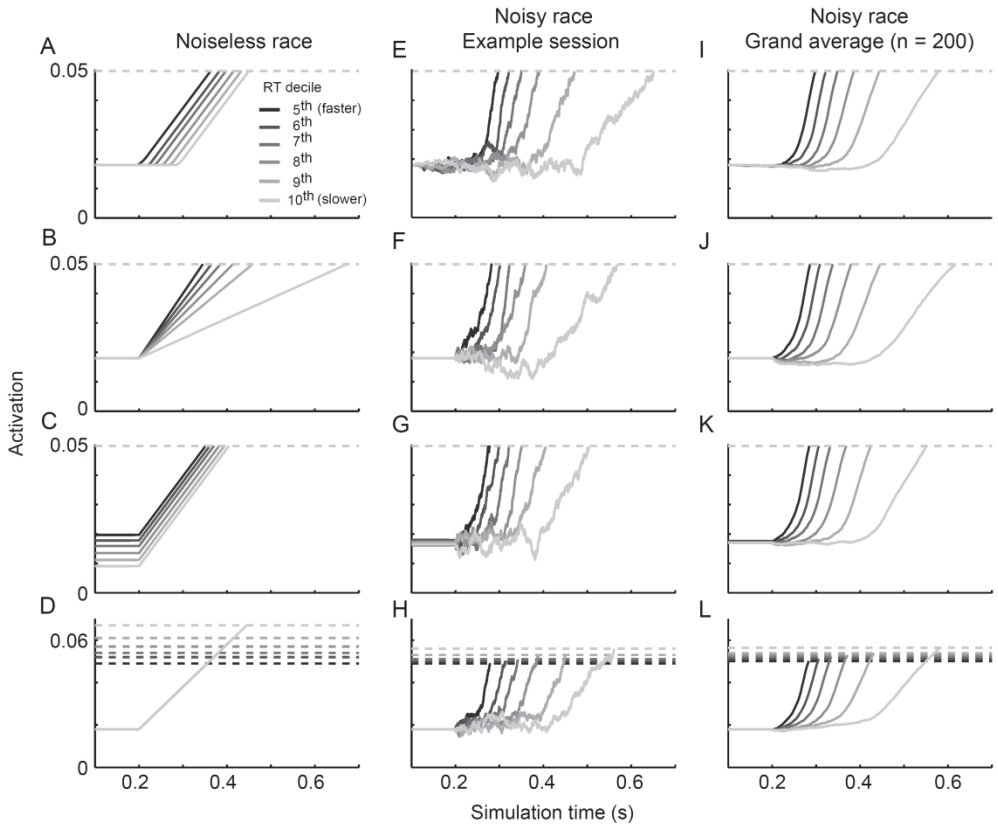

Figure 2.1 Independent race model dynamics. Plotted trajectories are averages from RT deciles. For clarity, only the 5th – 10th decile is plotted. Horizontal dashed lines indicate measured threshold. All simulations used the following primary parameters: *D* = 0.2, *v* = 0.2, *z* = 0.018, *a* = 0.05. **A-D**: Simulated trajectories from a single simulated session (200 trials) of a noiseless independent race model (*s* = 0). Rows differ according to the source of across trial variability (**A**: across-trial variability in encoding delay; *st* = 0.2, η = 0, *sz* = 0, *sa* = 0; **B**: across-trial variability in drift rate; *st* = 0, η = 0.1, *sz* = 0, *sa* = 0; **C**: across-trial variability in starting point; *st* = 0, η = 0, *sz* = 0.02, *sa* = 0; **D**: across-trial variability in threshold; *st* = 0, η = 0, *sz* = 0, *sa* = 0.01). **E-H**: Same as A-D, but with the addition of noise (*s* = 0.1). All other parameters are identical across rows. **I-L**: Grand average trajectories for 200 simulated sessions using the same parameters as in **E-H**.

We used these noiseless model trajectories to evaluate the validity of our quantitative measures of model dynamics. Figure 2.2 plots our measures of model dynamics as a function of

RT decile for the four versions of the model with different sources of across-trial variability. If the mapping between measures of model dynamics and secondary model parameters is one-to-one, then each model should produce significantly correlations between only one measure of model dynamics and RT. Indeed, there is a clear one-to-one mapping between each secondary parameter and each measure of model dynamics. The version of the model that assumed only across-trial variability in the encoding delay (column 1) predicts that the measured onset correlates perfectly with RT, and there is no significant correlation between RT and any other measures (all $p > 0.05$). Similarly, the version of the model that assumed only across-trial variability in drift rate (column 2) predicts that the measured growth rate is strongly inversely correlated with RT, and there is no significantly correlation between RT and any other measure (all $p > 0.05$). The correlation is not perfect due to the geometry of the accumulation process. The version of the model that assumed only across-trial variability in starting point (column 3) predicts that the measured baseline is perfectly inversely correlated with RT, and there is no significant correlation between RT and any other measure (all $p > 0.05$). Finally, the final version of the model that assumed only across-trial variability in model threshold (column 4) predicts that the measured threshold is perfectly correlated with RT, and there is no significant correlation between RT and any other measure (all $p > 0.050$. These results validate our measures of growth rate and onset and confirm our intuitions about noiseless accumulator dynamics.

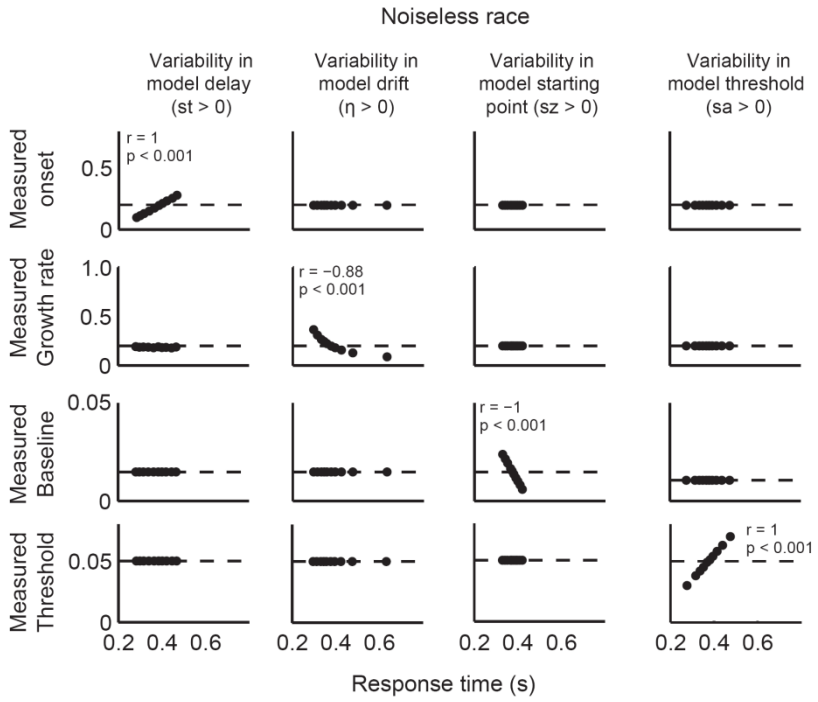

Figure 2.2 Measures of model dynamics for a noiseless independent race model ($s = 0$). Scatterplots show the measured onset (row 1), growth rate (row 2), baseline (row 3), and threshold (row 4) as a function of the mean RT for all ten RT deciles for four versions of the model in which all across-trial variability was due to variability in encoding delay (column 1; $st = 0.2$), drift (column 2; $\eta = 0.1$), starting point (column 3; $sz = 0.02$), or threshold (column 4; $sz = 0.01$). All other parameters governing across-trial variability were set to zero. The four columns correspond to the trajectories plotted in Figure 2.1A-D. Scatterplots that produced a significant correlation between mean RT and the measure of model dynamics are indicated with the Pearson correlation coefficient, r, and corresponding p-value. All other $p > 0.05$.

2.4.2 Identifying sources of across-trial variability from model dynamics: noisy independent race

The preceding section showed that each measure of model dynamics can be uniquely identified with a specific measure of model dynamics when the accumulation process is noiseless. However, many models assume that the accumulation process is noisy. Noise will contribute to predicted behavioral variability and will also affect model dynamics. Moreover, all neurophysiological signals are inherently noisy. Therefore, we must evaluate the degree to which alternative sources of variability can be uniquely identified with measures of model dynamics when models assume noise. To explore the effects of noise on model dynamics, we next simulated the independent race model using identical parameters as described above, but with the

addition of conventional levels of noise (s = 0.1). Later, we will report results from simulations in which the level of noise was varied.

To provide an intuition for how noise can affect model dynamics, we first consider a single representative simulated session (200 trials) from each version of the model that assumed a different source of across-trial variability (Figure 2.1E-H). Figure 2.1E shows example model trajectories for six RT deciles when variability in the encoding delay was the only additional source of across-trial variability (st > 0). The accumulation is noisier, but the onset of accumulation still appears to increase with RT as it did for the noiseless model (Figure 2.1A). Figure 2.1F shows example model trajectories from a simulated session in which variability in drift rate was the only source of across-trial variability in addition to noise ($\eta > 0$). In contrast to the noiseless model (Figure 2.1B), the onset of accumulation appears to increase with RT although the model assumed no variability in the encoding delay. Similarly Figures 2.1G,H show example model trajectories from a version of the model in which variability in starting point (sz > 0) and model threshold (sa > 0), respectively, were the only sources of across trial variability. These models also show an apparent increase in the onset of accumulation, despite assuming no across-trial variability in the encoding delay (st = 0). Qualitatively, it appears that the onset of model activation increases with RT for each version of the noise race model, irrespective of actual sources of across-trial variability.

The example sessions in Figure 2.1E-H suggests that the one-to-one mapping between model parameters and dynamics may break down with noise. To quantify this effect, we computed the measured onset, growth rate, baseline, and measured threshold for each RT decile of 200 simulated sessions. Figure 2.3 summarizes the results for each version of the model that assumed a different sources of across-trial variability (delay, drift, starting point, or model threshold). First, consider the relationship between measured onset and RT for each version (row 1). As in the example simulated session (Figure 2.1E-H), the measured onset correlates strongly and consistently with RT for all four versions of the model. Therefore, correlations between

onset and RT cannot be uniquely identified with a single source of across-trial variability for noisy accumulators. Second, consider the relationship between measured growth rate and RT for each version (row 2). All models predict that growth rate is inversely correlated with RT. The correlation is strongest and most consistent for model that included variability in drift, starting point, or model threshold and slightly weaker for the model that assumed variability in encoding delay. Therefore, correlations between growth rate and RT cannot be uniquely identified with a single source of across-trial variability for noisy accumulators. Third, consider the relationship between the measured baseline and RT for each version (row 3). Only the model that included variability in starting point predicted a correlation between measured baseline and RT. Therefore, correlations between baseline and RT can be uniquely identified with across-trial variability in starting point, but note that the effect is weaker in the upper tail as noise begins to explain larger proportions RT variability. Fourth, consider the relationship between the measured threshold and RT for each version of the model (row 4). All versions of the independent race model that did not include variability in model threshold show no correlation between measured threshold and RT. However, the model that included threshold variability showed a strong and consistent correlation. Therefore, correlations between threshold and RT can be uniquely identified with across-trial variability in model threshold.

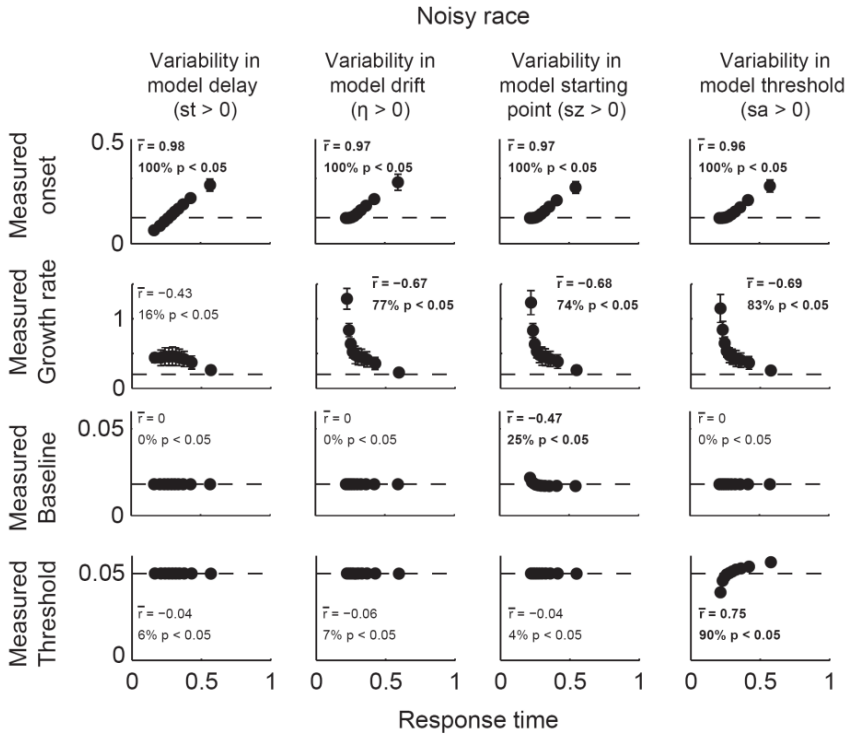

Figure 2.3 Measures of model dynamics for a noisy independent race model (s = 0.1). Conventions as in Figure 2.2 except that points now indicate the mean measures of model dynamics across 200 simulated sessions. Errorbars are ±SD. Each panel also shows the average Pearson correlation coefficient across all simulated sessions, , and the percentage of simulated sessions that produced a significant correlation ($p < 0.05$).

Across simulated sessions, correlations between RT and the growth rate or onset of accumulation were present regardless of actual sources of across-trial variability. One potential explanation is that a single simulated session with only 200 trials is still too noisy to reliably detect the actual end of the encoding delay (i.e., start of the accumulation). Signal averaging is the most common approach to noise reduction in neurophysiological analyses (e.g., Luck, 2005). Therefore, we tested whether we could more reliably detect variability in encoding delay (*st*) and drft rate (η) by averaging model trajectories for each RT decile across 200 simulated sessions (4000 total simulated trials) before computing our measures. Figure 2.1I-L shows the grand average model trajectories for six example RT bins across 200 simulated sessions. Qualitatively, the change in the onset and growth rate of the average trajectories appears remarkably similar regardless of the source of across-trial variability (contrast with Figure 2.1A-D). Figure 2.4

shows the relationship between RT and each measure of model dynamics computed from the grand average model trajectories. In general, the patterns are very similar to those based on individual simulated sessions. These results indicate that averaging cannot eliminate the observed correlations between RT and measured onset and growth rate and indicate that our results are unlikely to be due to a lack of power. In other words, if these were actual neurophysiological signals, then simply collecting more data cannot alleviate the problem.

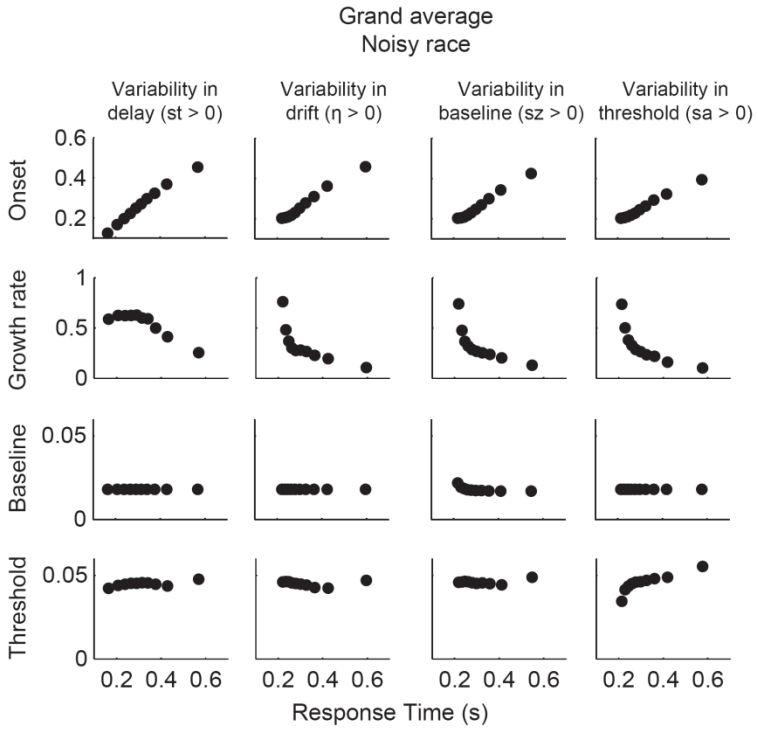

Figure 2.4 Measures of grand average model dynamics for a noisy independent race model. Conventions as in Figure 2.2 except that points now indicate measures of model dynamics computed directly from the grand average of 200 simulated sessions as plotted in Figure 2.1 (I-L).

2.4.3 Generalization across parameter space

Thus far we have reported results for only four sets of parameters with and without noise, but it is important to verify that these results generalize to broader regions of parameter space that are typically encountered when fitting accumulator models to empirical data. One concern is that we simply selected unrealistically small values of across-trial variability. To test whether this was the case, we evaluated a range of values for each secondary parameter. We selected ranges

of parameters based on the relative value of the corresponding primary parameter to encompass the ranges typically found for fits of LBA and diffusion models to empirical data (Matzke and Wagenmakers, 2009; Donkin et al., 2011). Figure 2.5 shows the average correlation (±SD) between RT and each measure of model dynamics from 200 simulated sessions as a function of each secondary parameter. There are several important observations. First, there is a strong positive correlation between measured onset and RT (row 1) and between measured growth rate and RT (row 2) regardless of the values of η ,*st*, *sz*, or *sa*. Thus, given conventional noise levels (s = 0.1), the measured onset and growth rate will correlate strongly with RT irrespective of actual sources of variability. Second, there is a monotonic relationship between *sz* and the strength of correlation between RT and baseline. Thus, this correlation serves as a good indicator for the magnitude of across-trial variability in starting point. Third, there is a monotonic relationship between *sa* and the strength of correlation between RT and measured threshold. Thus, this correlation serves as a good indicator of the magnitude of across-trial variability in threshold. Altogether, these results suggest that these effects are robust to variation across a range of values of parameters governing across-trial variability.

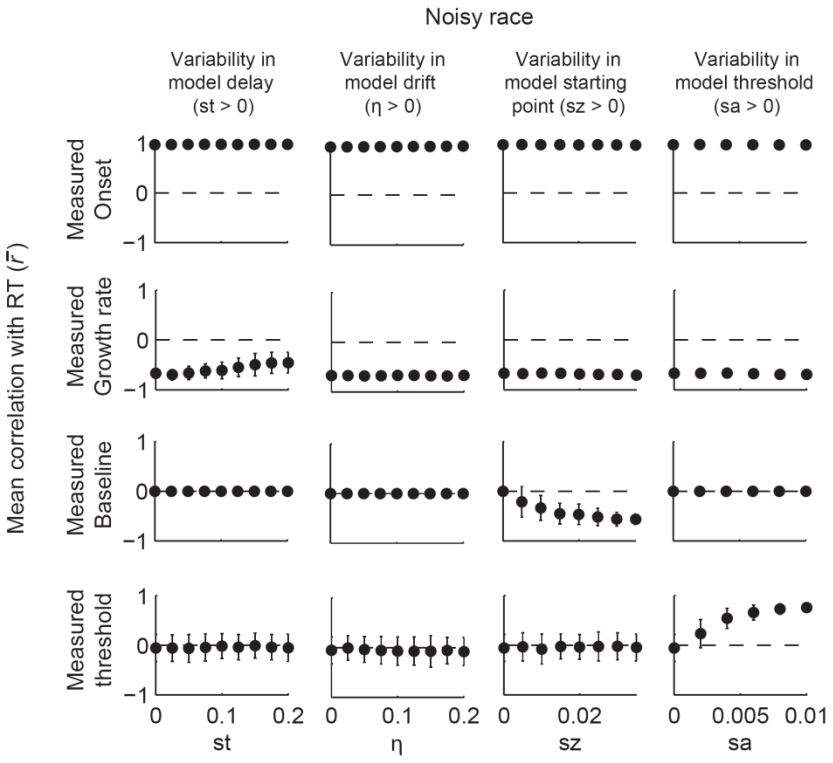

Figure 2.5 Correlations between measures of model dynamics and RT for a noisy independent race model (s = 0.1) with increasing levels across-trial variability. All simulations used the same primary parameters as preceding figures (D = 0.2, v = 0.2, z = 0.018, a = 0.5). For each column, one parameter determining across-trial variability was varied and all other parameters determining across-trial variability were set to zero. For versions of the model that included variability in delay (st) and drift (η), these parameter were varied from 0 to 100% of the value of the corresponding primary parameters (D and v), respectively. For versions of the model that included variability in starting point (sz) and model threshold (sa), these parameters were varied from zero until the maximum possible value constrained by the distance from starting point to threshold ($a - z$).

The preceding analyses indicate that the measured onset and growth rate will correlate with RT irrespective of additional sources of variability when conventional levels of noise are added. Moreover, these effects could not be eliminated with additional signal averaging. Why is this the case? To elucidate the effect of noise on accumulator dynamics, we simulated the noisy independent race model with no additional sources of across-trial variability (s = 0.1, η = 0, st = 0, sz = 0, sa = 0). Figure 2.6A-C shows examples of individual simulated trials and Figure 2.6D-F shows the probability of a particular activation level at each time point given that the process terminated in a fast, medium, or slow RT. The first feature to note is that relatively direct paths to the threshold are the only model trajectories that can have produced the fastest RTs

(Figure 2.6A,D). Hence, the fasted RTs occur when, by chance, noise is repeatedly sampled in the positive direction. This produces the elevated measured growth rate that was described above. The second feature to note is that many different paths can produce slower RTs (Figure 2.6B,C), but the paths must always have remained between the two boundaries (Figure 2.6E,F). The result is that, on average, the trajectories remain near baseline until shortly before the response is initiated. This pattern of dynamics has been noted before for versions of the drift diffusion model (Ratcliff, 1988; Ratcliff et al., 2003; Ratcliff et al., 2007), but the impact of noise on measures of neurophysiology dynamics has never been quantified and the effect has never been systematically explored.

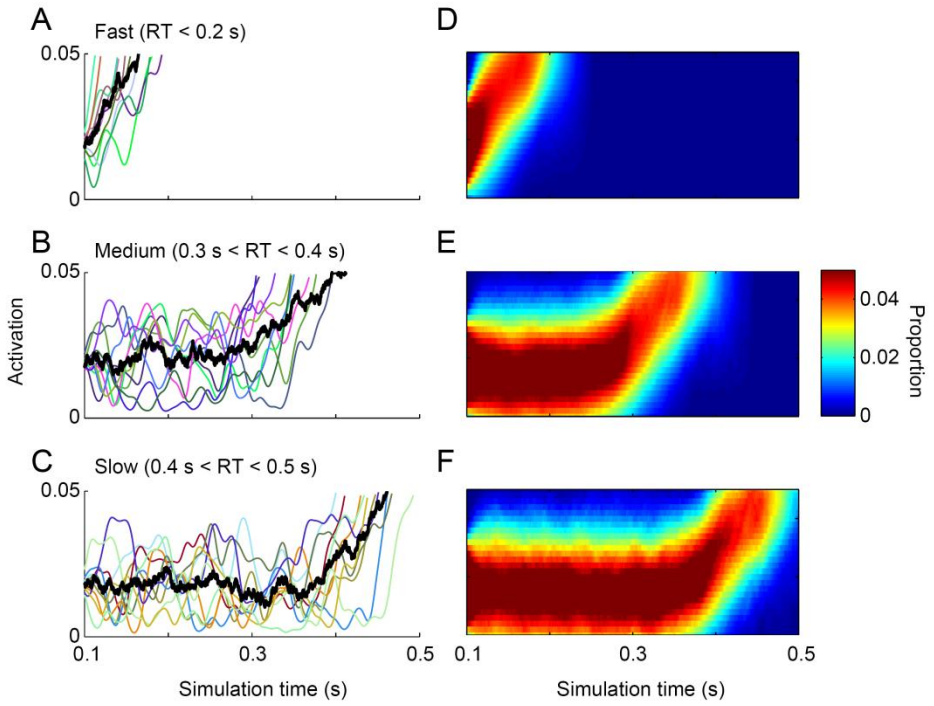

Figure 2.6 The impact of noise (s = 0.01) on independent race model dynamics for simulations resulting in fast (top; RT < 0.2 s), medium (middle; 0.3 s < RT < 0.4 s) and slow (bottom; 0.4 s < RT < 0.5 s) responses. All simulations used the same primary parameters as preceding figures (D = 0.2, v = 0.2, z = 0.018, a = 0.5), but with no sources of across-trial variability other than noise ($st = \eta = sz = sa = 0$). **A-C**: Simulated trajectories for 10 individual trials (colored lines) and their average (black). Here, individual trails have been low-pass filtered for illustrative purposes only. All other figures and analyses used unfiltered model trajectories. **D-F**: The conditional probability that the model trajectory was at an activation level at each time step given that the simulation produced a correct fast, medium, or slow RTs.

To what extent does this pattern generalize across values of primary parameters? To address this question, we again consider a model with no sources of across-trial variability ($\eta = st = sz = sa = 0$). The encoding delay parameter D simply shifts RTs and the start of the model dynamics by a constant amount, and can therefore be ignored for these analyses. Therefore, the predicted model dynamics will depend on the relative values of three parameters: v, a, and s. We computed the correlation between each measure of dynamics and RT while varying the coefficient of variation s/v (CV), v ($v = 0.1 – 0.3$) and a ($a = 0.04 – 1.6$). The ratio of z/a was fixed so that the position of the starting point relative to the bound was constant ($z/a = 0.36$, as above). Figure 2.7A shows the mean RT across 200 simulated sessions as a function of a, v, and CV. As expected, RTs increase with a, and decreases with v and CV. The important point is that our chosen parameter ranges span a broad range of mean RTs that are typically observed in perceptual decision-making tasks. Thus, we can at least be certain that our conclusions are valid for a large subset of plausible parameter values although an exhaustive exploration of parameter space is not possible. Figure 2.7B shows the mean correlation between each measure of model dynamics and RT across 200 simulated sessions. First, consider the effect of each parameter on the correlation between measured onset and RT (column 1). These panels show that even though the encoding delay is fixed ($st = 0$), the model predicts a strong correlation between measured onset and RT so long as CV is greater than ~0.3 regardless of the level of drift rate or threshold. This result is important because it means that so long as the CV of the model is high, one would expect to see an increase in measured onset with RT even when the encoding delay is constant. Second, consider the effect of each parameter on the correlation between measured growth rate and RT (column 2). Irrespective of other parameter values, even small amounts of noise will predict a negative correlation between growth rate and RT. This result is important because it means that decreases in the correlations between growth and RT do not imply across-trial variability in drift rate. Rather, this may simply be due to noisy accumulation. Finally, consider lack of an effect on each parameter on the measured baseline and measured threshold (columns 3

and 4). Regardless of the CV, *v*, or *a* these measures will not correlate with RT unless across-trial variability in these parameters (i.e., *sz* or *sa*) is explicitly built into the model. Altogether, these results help to shed light on the potential inferences about model parameters that can be made based on the pattern of observed neural dynamics.

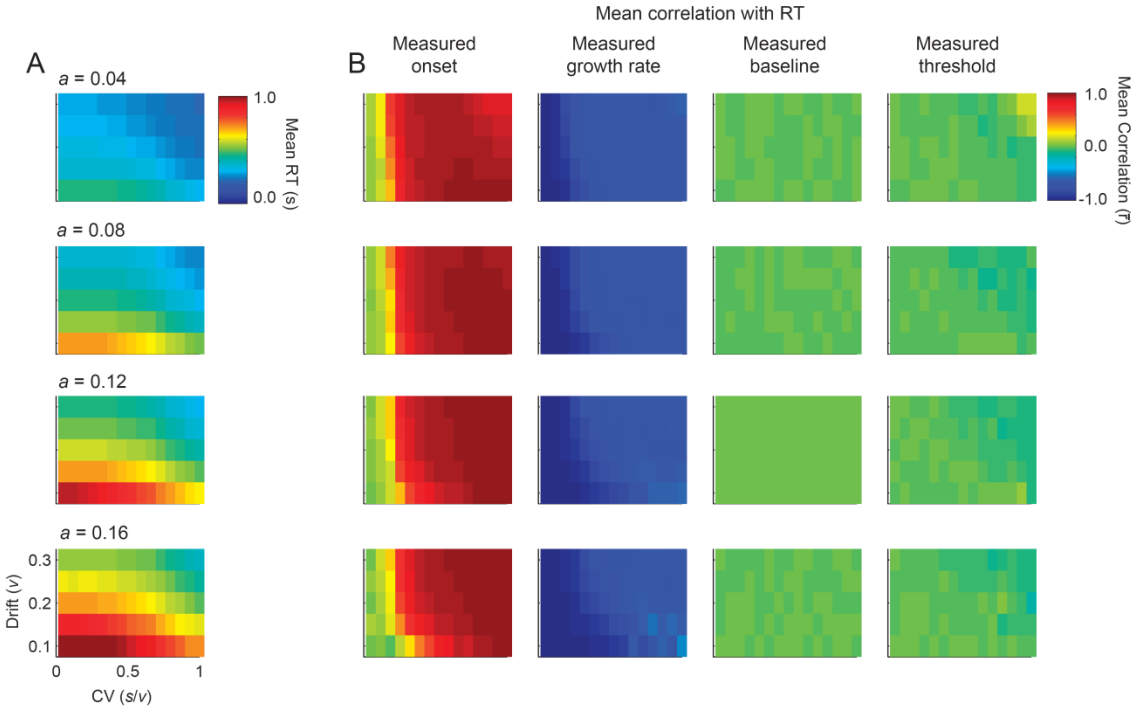

Figure 2.7 The effect of drift rate (*v*), threshold (*a*), and coefficient of variation (CV = *s*/*v*) on mean RT (**A**), and the mean predicted correlation between each measure of neural dynamics and RT (**B**). Values are the average across 200 simulated sessions. Encoding delay was fixed at $D = 0.2$ and starting point was fixed at $a/z = 0.36$. Noise was the only source of across trial variability ($st = \eta = sz = sa = 0$).

2.4.4 Accumulator noise, not Poisson spiking, distorts response dynamics

Thus far we have measured the onset, growth rate, threshold, and baseline directly from the continuous model dynamics, but accumulator models have been identified with single-unit spiking. Intrinsic spiking will increase the variability of the accumulation process, and could affect our measures of model dynamics. For example, perhaps the total synaptic input to a neuron is essentially captured by a noiseless accumulator model, but spiking is still variable due to biophysical properties of neurons (e.g., volume of neurotransmitter release, proportion of ion

channels open, etc). Would spiking variability also distort the relationship between model parameters and dynamics? To address this question we used our model dynamics as the rate parameter for Poisson process to simulate spike trains. Trajectories were rescaled to approximate the mean firing rates of cortical neurons identified with evidence accumulation (e.g., Purcell et al., 2012b), but the dynamics were unchanged. Following conventional neurophysiological methods, we converted those spike trains to a spike density function by convolving them with a kernel shaped like a post-synaptic potential (Thompson et al., 1996), and analyzed the resulting spike density function using the identical methods as were used above for the raw model dynamics.

We analyzed the dynamics of the independent race model using the same default parameters as in the preceding section (v = 0.2, z = 0.018, a = 0.5), but with the addition of Poisson spiking variability. We also increased D to 0.3 to avoid edge effects of the convolution used to generate the spike density function. We simulated the same four versions of a noiseless independent race model (s = 0) that assumed different sources of across-trial variability (Figure 2.8A-D). Even with the addition of Poisson spiking, the parameters of the noiseless independent race model could be uniquely identified through accumulator dynamics. This is because the spiking variability, unlike accumulator noise, is independent of RT. Although individual trial dynamics are noisier, the noise is independent across trials and averages out. We next simulated four versions of a noisy race model (s = 0.1) that assumed different sources of across-trial variability (Figure 2.8E-H). Similarly, we found that our conclusions are essentially unchanged when Poisson spiking is added to a noisy independent race model. Although the Poisson noise averages out across trials, the accumulator noise still distorts the relationship between model parameters and dynamics. Thus, as long as spiking is independent of RT, Poisson noise will average out and will not substantially distort observed model dynamics. In other words, if these were actual neurophysiological signals, simply collecting more data would be sufficient to eliminate variability due to Poisson spiking.

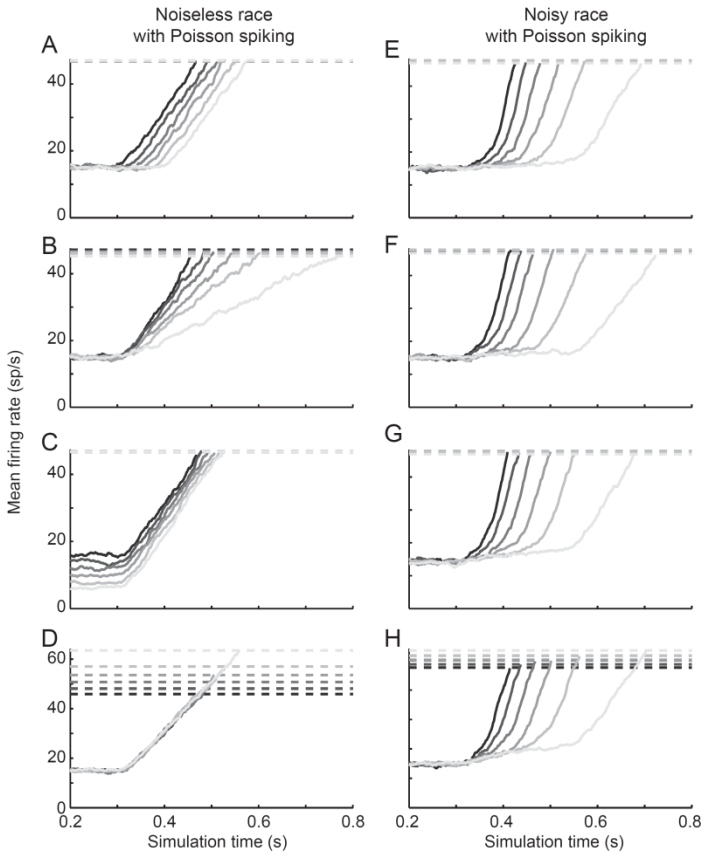

Figure 2.8 Independent race model dynamics with Poisson spiking. Plotted trajectories are averages from the 5^{th}-10^{th} RT decile. The model trajectory for each simulated trial was rescaled to have a measured threshold of 50 spikes/second (sp/s) and then used as the time-inhomogeneous mean rate to a Poisson process. **A-D**: Grand average spike density functions (n=200 simulated sessions) generated from the dynamics of a noiseless independent race model (s = 0). All parameters are identical to Figure 2.1A-D. **E-H**: Grand average spike density functions (n=200 simulated sessions) generated from the dynamics of a noisy independent race model (s = 0.1). All parameters are identical to Figure 2.1I-L.

2.4.5 Across-condition changes in model parmeters and dynamics

The preceding section demonstrated that distinct sources of across-trial variability may be nearly indistinguishable at the level of model dynamics. Often, however, researchers are primarily interested in parameter changes that are necessary to capture observed behavioral changes across experimental conditions. Therefore, we also tested whether potential sources of across-condition variability can be identified through measured dynamics.

To test whether parameter changes can be uniquely identified with changes in dynamics, we simulated the independent race model with no sources of across-trial variability ($st = \eta = sz = sa = 0$). We fixed other primary parameters at the same default values as before (v = 0.2, Tr =

0.2, z = 0.018, a = 0.05) and varied one parameter at a time. We first evaluated a model that included no noise (s = 0) for comparison with noisy models. The left column of panels in Figure 9A-D shows the simulated trajectories for four different versions of a noiseless independent race model with different sources of across-trial variability. As expected, changes in all primary parameters could be uniquely identified with changes in noiseless model dynamics.

We next evaluated a noisy accumulator model with conventional levels of noise (s = 0.1). For each simulated condition (i.e., parameter set), we independently analyzed each RT decile to avoid averaging across trials with very different durations. Figure 2.9 shows the grand average trajectories from 200 simulated sessions for the 1st, 5th, and 9th RT deciles. We quantified each measure of model dynamics independently for each RT decile and then averaged across deciles and sessions (Figure 2.11). First, consider the effect of changing the encoding delay on predicted model dynamics (row 1). The measured onset increases with the encoding delay for all RT deciles, although it is increasingly biased at slower RTs as described above. Second, consider the effect of changing the drift rate on model dynamics (row 2). When the model is noiseless, the change in drift rate is clearly identifiable through changes in the growth rate, but the model exhibits very different changes in dynamics when noise is included. For the fastest RTs (1st decile) , the predicted trajectories are indistinguishable regardless of drift rate changes. This is because the fastest RTs always occur when positive noise early in the trial causes a rapid rise to threshold. For slower RTs (9th decile), the onset of accumulation is later when the drift rate is lower, in addition to changes in the measured growth rate (Figure 2.11). In other words, noisy race models can predict that changes in the drift rate produce changes in both the onset of accumulation and growth rate if all RT deciles are used. Third, consider the effect of changing baseline on model dynamics (row 3). Changes in starting point cause changes in baseline regardless of RT, and so starting point can be uniquely identified with changes in baseline (Figure 2.11). Note, however, that accumulator dynamics become complex for slow RTs as the ratio z/a is altered. When z/a is high, the mean model trajectory dips away from threshold following the

encoding delay. This is because in order for trials to terminate with long RTs, negative noise must have moved the accumulation away from threshold early in the trial. When *z*/*a* is low, model trajectories are sigmoidal, and our standard measures of model dynamics no longer adequately characterize these trends. These dynamics pose a challenge when comparing fitted model parameters to neurophysiology, If the *z*/*a* ratio must be very large or small to explain behavior, then a neural signal must exhibit these dynamics with large RTs to be identified with evidence accumulation. Finally, consider the effect of changing the threshold on model dynamics. Regardless of RT, changes in the model threshold cause changes in the measured threshold (Figure 2.10). Thus, changes of model threshold across conditions can be uniquely identified with changes in measured threshold.

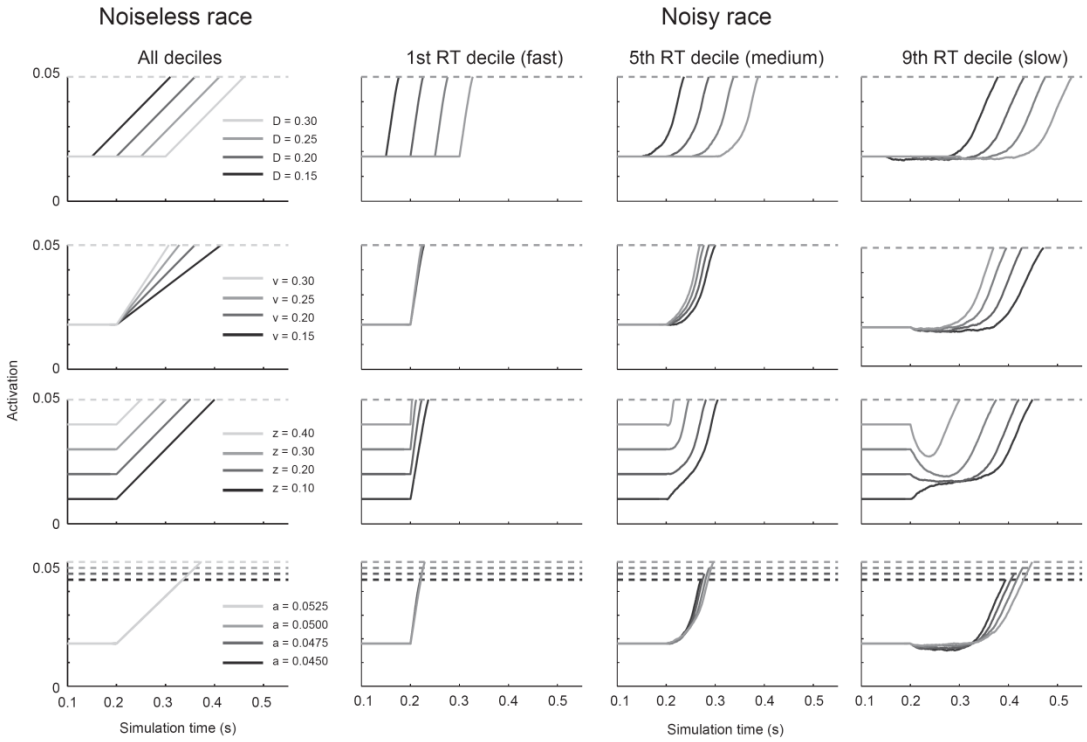

Figure 2.9 Across-condition changes in independent race model dynamics. The left panels show predicted model dynamics for a noiseless race model (left column; $s = 0$). All other panels show predicted model dynamics for a noisy race model at the 1st, 5th, or 9th RT decile, but with the addition of noise ($s = 0.1$). For each row, we selectively manipulated one parameter (delay, *D;* drift, *v;* starting point, *z;* **or** model threshold, *a)* and all other parameters were fixed at default values ($D = 0.2$, $v = 0.2$, $z = 0.018$, $a = 0.5$). All parameters determining across-trial variability were set to 0 ($st = \eta = sz = sa = 0$). Each plot shows the grand average trajectory across 200 simulated sessions for a single RT decile (9th decile).

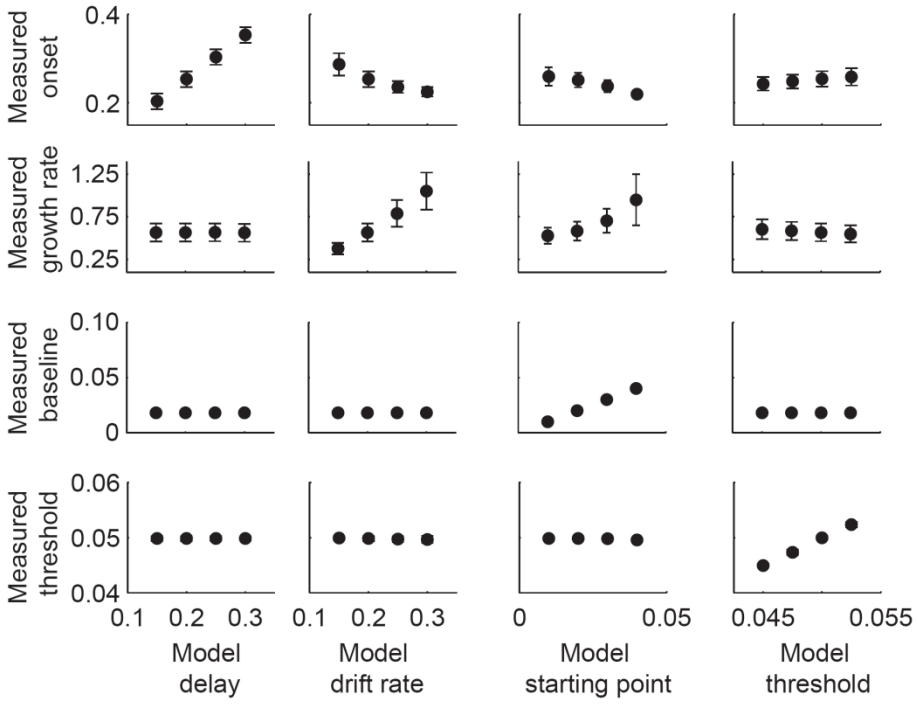

Figure 2.10 Across-condition changes in measures of model dynamics. Across-condition changes in measures of noisy independent race model dynamics. For each column of panels, we selectively manipulated one parameter (delay, drift, starting point, or model threshold) and all other parameters were fixed at default values (D = 0.2, v = 0.2, z = 0.018, a = 0.5). For each simulated session, each measure was computed for individual RT deciles and then averaged. Plots show the mean of each measure across 200 simulated sessions. Error bars are ±1SD.

To understand how changes in drift rate can produce changes in the measured onset of accumulation, we computed the measured onset, averaged across RT deciles, as a function of CV (s/v) for different levels of drift rate (Figure 2.11A). At low levels of noise (CV < 0.2), the measured onset closely matches the model encoding delay (D = 0.2) for any drift rate. As noise increases (0.2 < CV < 0.4), the measured onset is biased later than the actual delay, which was illustrated above (Figure 2.6). However, at higher levels of noise (CV > 0.4), the mean onset peaks and declines, but the peak varies inversely with the drift rate. This is because RTs become shorter and less variable as drift rate and noise increase, and the onset bias is only possible for long RTs (Figure 2.10; Figure 2.6). Hence, slower drift rates produce a larger bias for a fixed CV. Note that this problem would be exacerbated if we fixed s across conditions rather than fixing CV, as is typically done when fitting behavioral data. Similarly, when the model is noisy,

it is possible for changes in threshold to produce changes in the measured onset (Figure 2.11B). For comparison, Figure 2.11C shows changes in measured onset as a function of different levels of model encoding delay and CV. The measured onset is biased when noise increases, but the magnitude of the bias is not affected by the encoding delay. Altogether, these simulations demonstrate that changes in the measured onset could be explained by changes in drift rate, threshold, or encoding delay if the accumulation is sufficiently noisy.

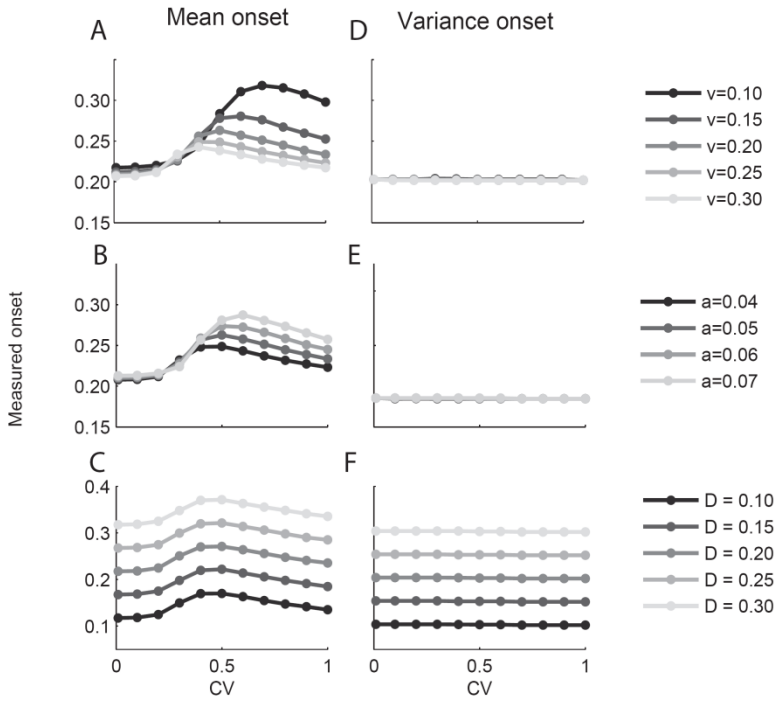

Figure 2.11 Encoding delay (i.e., the beginning of the accumulation process) can be more reliably measured using the variance onset. Other model parameters were fixed at their default values as above with no across-trial variability. Measured mean onset (left) and variance onset (right) are plotted as a function of CV (*s*/*v*) for five values of encoding delay (**A, D**), threshold (**B, E**), and drift rate (**C,F**). Measured onset was computed individually for each decile and averaged across deciles.

The observation that changes in drift rate can cause changes in the measured onset has important implications for the interpretation of neurophysiological signals. For example, if the measured onset of neuronal spiking increases with the difficulty of a perceptual discrimination, it would not be possible to determine whether this was due to an increase in the time necessary to compute the representation of perceptual evidence (i.e., encoding delay), or a decrease in the

quality of the evidence itself (i.e., drift rate). Therefore, we evaluated two alternative methods to more reliably identify the start of the accumulation. The first method is to compute the onset using only the fastest RT decile. The preceding sections showed that the measured onset is primarily biased by trials resulting in longer RTs (Figure 2.6; Figure 2.10). Thus, this method provides a more reliable measure of accumulator onset because only trajectories that abruptly rise to threshold will produce the fastest RTs. However, one limitation of this approach is that it requires a large sample of trials so that the lower tail of the distribution is sufficiently sampled.

A second alternative method is to measure the onset of across-trial variability rather than the mean; that is, the time when across-trial variability first increases from baseline. This method provides a more reliable measure of accumulator onset because individual trials begin to fluctuate around the mean as soon as the accumulation begins even if the mean trajectory remains near the starting point (Figure 2.6). To illustrate this approach, Figure 2.12 shows the population activation mean and simulated activation variance for a noisy race model using the same default primary parameters as above (s = 0.1, D = 0.2, v = 0.2, z = 0.18, a = 0.05) and all secondary parameters fixed at zero. The measured mean onset increases substantially with RT (Figure 2.12A), but the variance onset is fixed as a function of RT (Figure 2.12B). Later in the trial, variance dynamics change with RT deciles because accumulator models predict skewed RT distributions (i.e., greater variability in the upper tail), but the variance onset is constant. The utility of this approach is further illustrated by Figure 2.11. The variance onset is constant for all values of noise, drift rate, and threshold when the encoding delay is fixed (Figure 2.11D,E), but closely tracks the model encoding delay as it is varied (Figure 2.11F). Thus, measuring the onset of neural variance could be used to disambiguate the cause for observed changes in the measured onset.

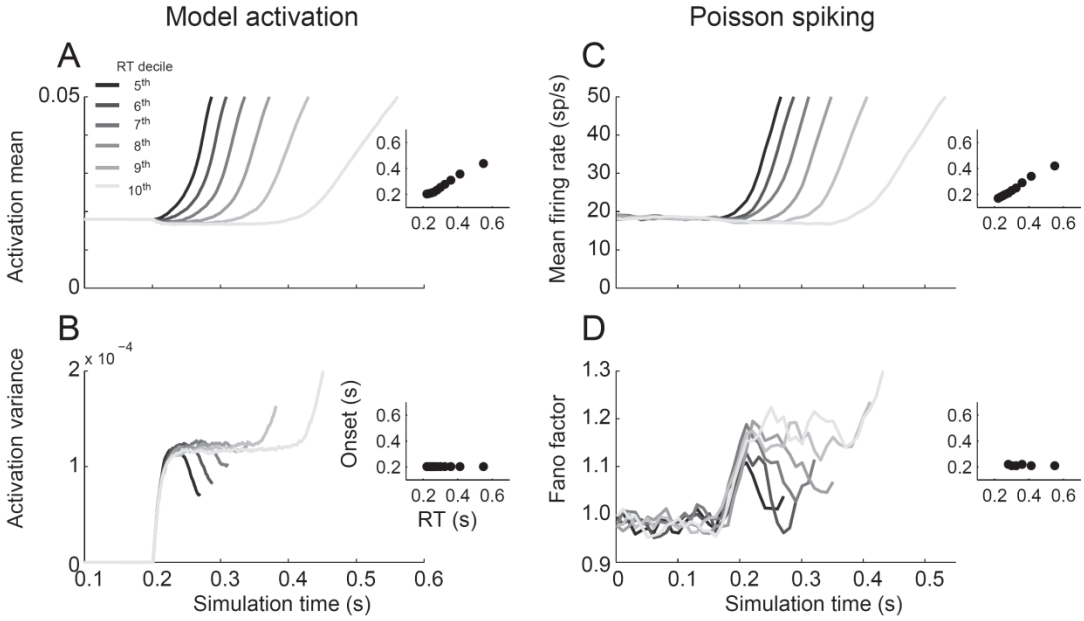

Figure 2.12 Independent race model mean and variance dynamics. Changes in model activation mean (**A**) and variance (**B**) over time. Only the 5th-10th RT deciles are plotted for clarity. Simulations used the following parameters: $s = 0.1$, $D = 0.2$, $v = 0.2$, $z = 0.18$, $a = 0.05$. Changes in mean firing rate (**C**) and Fano factor (**D**) compute using spike times simulated from predicted model trajectories (see text for details). Same parameters as in **A**-**B**. Insets show measured onset as a function of RT.

One potential concern with identify changes in the start of the accumulation based on changes in variance is that our simulations assumed a baseline variance of zero, which is not physiologically plausible. To mitigate this concern, we also evaluated changes in variance for a model in which model trajectories were used to generate Poisson spikes. We computed the ratio of the spike count variance to the spike count mean (i.e., the *Fano factor*) in a 50ms running window. We then computed the variance onset based on the resulting Fano factor as described above, but with a slightly more conservative threshold (15%) to exclude baseline noise. We also computed the onset of the mean firing rate for comparison. Even with the addition of Poisson spiking noise, the onset of variance was still a more reliable indicator of the accumulation start than the onset of the mean spike count (Figure 2.12C,D).

2.4.6 Noise obscures leakage dynamics

The time constant of integration for individual neurons must be finite due to their known biophysical properties (Amit and Tsodyks, 1991). This neurally-motivated property has been incorporated into leaky accumulator models (e.g., Usher and McClelland, 2001). However, neural integration is thought to be implemented at the network level (e.g., Wang, 2002), which could result in near-perfect integration. Moreover, leakage is often not necessary to explain behavior (Ratcliff and Smith, 2004). If we can identify a signature of leakage in model dynamics, then we could use it to assess whether leakage is present in a neurophysiological signal.

We simulated a leaky race model to determine whether changes in leakage can be identified with specific changes in accumulator dynamics. Like the race model, activation, X, is set to an initial point, z for the duration of the encoding delay, D. Following encoding time, the dynamics of the leaky race model are governed by the following:

[illegible] .

All simulations were run using the same general method as the independent race model, but with the addition of a k parameter that determined the strength of leakage.

We asked whether we could find evidence for leaky integration based on predicted patterns of model dynamics. A characteristic property of leaky integrates is that the rate of accumulation decreases as the accumulation increases. This will result in a decelerating function over time given a constant input (i.e., drift). Therefore, we asked whether the rate of deceleration could serve as a signature of leakage in model dynamics. To identify whether our model trajectories were decelerating, we fit model activation, X, as a function of the time, t, from the measured onset with a simple power function, [illegible]. The p parameter determines the acceleration of the function. Values of $p > 1$ indicate acceleration, values of $p < 1$ indicate deceleration, and $p = 1$ indicates a linear rise to threshold. Thus, we would expect a model with

no leakage to predict dynamics that are best described by a linear function ($p = 1$) and a model with leakage to be best described by a power function with $p < 1$.

To evaluate the validity of this approach, we first tested a noiseless leaky race model with the following parameters: ($v = 1$, $Tr = 0.2$, $a = 0.05$, $z = 0.018$), in addition to varying levels leakage ($k = 0$ to ~0.002). The model included no additional sources of across trial variability ($\eta = st = sz = sa = 0$). Figure 2.11A (left) shows examples of predicted model trajectories as k was increased. It is clear that the rate of deceleration is greater as k increases. Figure 2.11A (right) shows that this deceleration was adequately captured by the exponent p in our power function. As k increases, the best fitting p parameter decreases from one towards zero indicating that the function becomes less linear and more concave. This result confirms what we know about the effect of leakage on model dynamics and shows that fitting power functions to model dynamics can adequately track changes in leakage for noiseless race models.

The key question is whether this approach is still adequate when noise is present. To test how noise affects the measured deceleration of model activation, we simulated a leaky race model parameterized exactly as described above, but with increasing levels of noise ($s = 0.1 – 0.3$). Figure 2.11B shows examples of predicted model trajectories as k was increased and $s = 0.1$. In contrast to the noiseless leaky race model, the model trajectories become increasingly sigmoidal as k increases. As a result, the p exponent of the power function no longer tracks increases in k because a power function no longer adequately describes the model dynamics. When $s > 0.2$, the model trajectories are accelerating regardless of the level of k; that is, the function is almost entirely convex. This results in values of p that are consistently higher than one regardless of the level of leakage. This means that any accumulator model with sufficient noise will predict an accelerating function regardless of the level of leak. Thus, deceleration is not longer a defining characteristic of leaky integrators when noise is present.

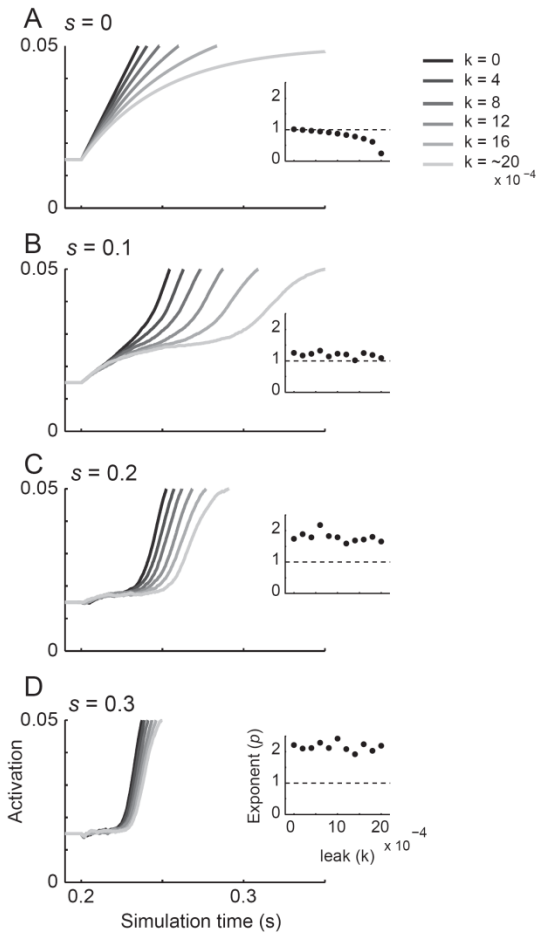

Figure 2.13 Leaky race model dynamics. Predicted model trajectories and best fitting power function exponent, *p*, (insets) for a leaky race model with varying levels of leak (*k*) and noise (*s*). Only the trajectory of the 9th RT decile is shown for clarity. The insets shows *p* computed independently for each RT decile and averaged. Noise was varied across panels (**A**: *s* = 0; **B**: *s* 0.1; **C**: *s* = 0.2; **D**: *s* = 0.3). The leakage constant was varied from 0 to slightly less than 0.002 (the maximum value of leakage that will not cause activation to reach asymptote before the threshold is crossed). Primary model parameters were set to $D = 0.2$, $v = 1$, $z/a = 0.36$ and there were no sources of across-trial variability other than noise ($st = \eta = sz = sa = 0$).

2.4.7 Noise obscures feed-forward and lateral inhibition

Neurophysiological studies suggest that competition may be a fundamental component of neural circuits (e.g., Cohen et al., 2010). Different models have incorporated different forms of competitive interactions, but the precise form of competition has been difficult to identify via behavior alone. Some models propose that competition takes place at the level of model inputs (i.e., feed-forward competition Mazurek et al., 2003; Ditterich, 2006; Ratcliff et al., 2007). Bounded accumulator models with alternative responses represented in opposite directions {} can

be interpreted as a form of feed-forward competition (Bogacz et al., 2006). Other models assume direct competition between accumulators (Usher and McClelland, 2001). These two forms of competition can be very difficult to distinguish behaviorally (Ratcliff and Smith, 2004). More recent studies have suggested that analyzing the form of model dynamics can provide a way to resolve this behavioral mimicry (Ditterich, 2010), but these methods have not been evaluated under varying levels of noise.

We simulated a competitive model to test whether feed-forward and lateral competition can be discriminated based on the pattern of predicted model dynamics with varying levels of noise. The model is comprised of two accumulators representing different potential responses. Like the independent and leaky race model, activation for accumulator *i*, X_i, is set to an initial point, *z* for the duration of the encoding delay, *D*. Following encoding time, the full competitive model is described by the following system of stochastic differential equations:

$$\frac{dX_1}{dt} = \quad \quad .$$

$$\frac{dX_2}{dt} = \quad \quad .$$

All simulations followed the same general approach as the independent race and leaky race model, but extended to multiple accumulators. For each simulated trial, I_1 and I_2 are sampled from independent Gaussian distributions with mean v_1 and $v_2 = 1\text{-}v_1$, respectively. $_{1 \text{ and } 2}$ are independent Gaussian noises terms with a mean of zero and standard deviation, *s*. RT is given as the time of the first activation, X_i, to reach a fixed threshold, *a*. We did not explore versions of this model with across-trial variability in primary parameters. All model activation which drops below zero was reset to zero. All simulations used an integration time step of $dt = 1$ ms. The model also includes two parameters that govern the nature of competitive interactions. A β parameter determines the strength of lateral inhibition. A *u* parameter determines the strength of feed-forward inhibition. I will manipulate each of these parameters independently to assess their

effects on model dynamics. That is, the *feed-forward competitive* model will assume $u > 0$ and $\beta = 0$, and the *lateral competitive* model will assume $u = 0$ and $\beta > 0$.

Unlike the independent race and leaky models, identifying potential signatures of competition must take into account the dynamics of both accumulators. The key difference that distinguishes the two forms of competition is that feed-forward inhibition assumes that the strength of inhibition depends on the strength of model inputs (I), whereas lateral competition assumes that the strength of inhibition depends on the current level of the competing accumulator (X). Because most models assume a constant drift throughout the trial, this means that feed-forward inhibition will be constant over time whereas the strength of inhibition for the competitive model will be time-inhomogeneous. Specifically, lateral inhibition is initially equal for both accumulators, but over time the inhibition applied to the winning accumulator will decrease (as the losing accumulator declines to zero) and the inhibition applied to the losing accumulator will increases (as the winning accumulator rises to threshold). Based on these observations, we reasoned that the two forms of accumulation could be discriminated based on the temporal evolution of the difference between the winning and losing accumulator. Because feed-forward inhibition is constant, the evolution of this difference should increase at a fixed rate. In contrast, because lateral inhibition increases over time, the separation between accumulators should increase as the losing accumulator is suppressed toward zero. In other words, the feed-forward model predicts that the difference between the winning and losing accumulator should grow linearly, whereas the lateral inhibition model predicts an accelerating difference.

Based on these properties of the model, we reasoned that these two forms of inhibition could be distinguished by measuring the degree to which the difference between the winning and losing accumulators was linear versus accelerating over time. We quantified this by fitting a power function to the difference in model activation of the winning (X_1) and losing (X_2) accumulators ($X_D = X_1 - X_2$). We limited our analysis to only simulated correct trials in which X_1 was defined as the correct response (i.e., $v_1 > v_2$). We fit X_D as a function of the time, t, from

the measured with a power function, . Thus, we would expect a model with feed-forward inhibition to be best explained by a function with $p = 1$, and we would expect a model with lateral inhibition to be best explained by a function with $p > 1$.

To test whether this was a valid method to distinguish alternative forms of competition, we first evaluated a competitive model with feed-forward inhibition. We used the following primary model parameters: $v_1 = 0.55$, $Tr = 0.2$, $a = 0.1$, $z = 0.036$), but we added varying levels of feed-forward competition ($u = 0$ to ~0.002) and no lateral competition ($\beta = 0$). The model included no across trial variability ($\eta = st = sz = sa = 0$). Figure 2.12A-C shows examples of predicted model trajectories for the winning target (X_1), the losing target (X_2), and the difference between the two (X_D) as u increased. As u increases, X_D increases at a faster rate, but remained linear. This was indicated by the exponent of the best fitting power function (p) that remained near one regardless of the strength of feed-forward inhibition (u). Note that a noiseless model without feed-forward inhibition would also predict a linear rise in X_D, and therefore this method is not adequate to distinguish feed-forward models from models with no feed-forward inhibition. Figure 2.12D-F plots the same trajectories for a model that included the same parameters as above, but with varying levels of lateral competition ($\beta = 0$ to 12) and no feed-forward competition ($u = 0$). In contrast to the competitive model with feed-forward inhibition, X_D accelerates at a faster rate as β increases. This was indicated by an increase in p as β increased. Thus, if accumulators are noiseless, then an acceleration of the difference of alternative response accumulators can provide a signature of lateral inhibition.

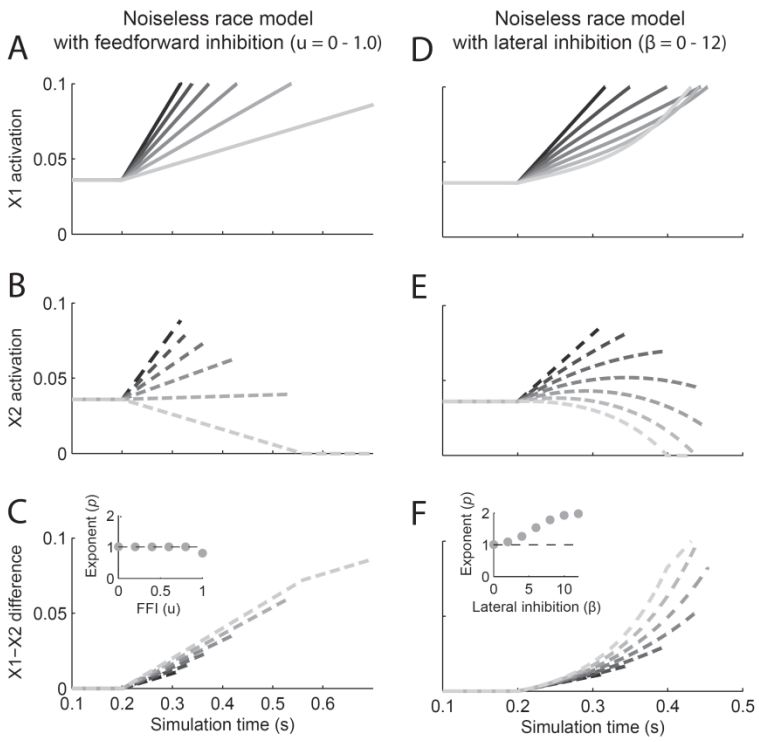

Figure 2.14 Noiseless race model dynamics with feed-forward (**A-C**) and lateral (**D-F**) inhibition. Primary model parameters were set to $D = 0.2$, $v = 0.55$, $z/a = 0.36$, $a = 0.1$ and there were no sources of across-trial variability other than noise ($st = \eta = sz = sa = 0$). The first row plots the simulated dynamics of the winning accumulator (X_1) under increasing values of feed-forward (**A**) or lateral (**B**) competition. The second row plots the simulated dynamics of the losing accumulator (X_2) under increasing values of feed-forward (**B**) and lateral (**E**) competition. The final row plots the difference between the winning and losing accumulators ($X_D = X_1 - X_2$) with increasing values of feed-forward (**C**) and lateral (**F**) inhibition. The insets show the exponent p of the best fitting power function to the difference in activation as a function of increasing feed-forward (**C**) and lateral (**F**) inhibition.

Finally, we tested whether these different forms of competition can be distinguished when noise is present. To test how noise affects our ability to discriminate feed-forward and lateral competition, we simulated the same models described above with the addition of a small amount of noise ($s = 0.011$). Figure 2.13 shows examples of predicted model trajectories for competitive race models with feedforward (Figure 2.13A-C) and lateral (Figure 2.13D-F) competition. In contrast to the noiseless models, both forms of competition predict that X_D should follow an accelerating function. As a result, p remains consistently above 1 regardless of the strength of feed-forward and lateral inhibition. This result places limitations on the use of neural signals to discriminate forms of competition.

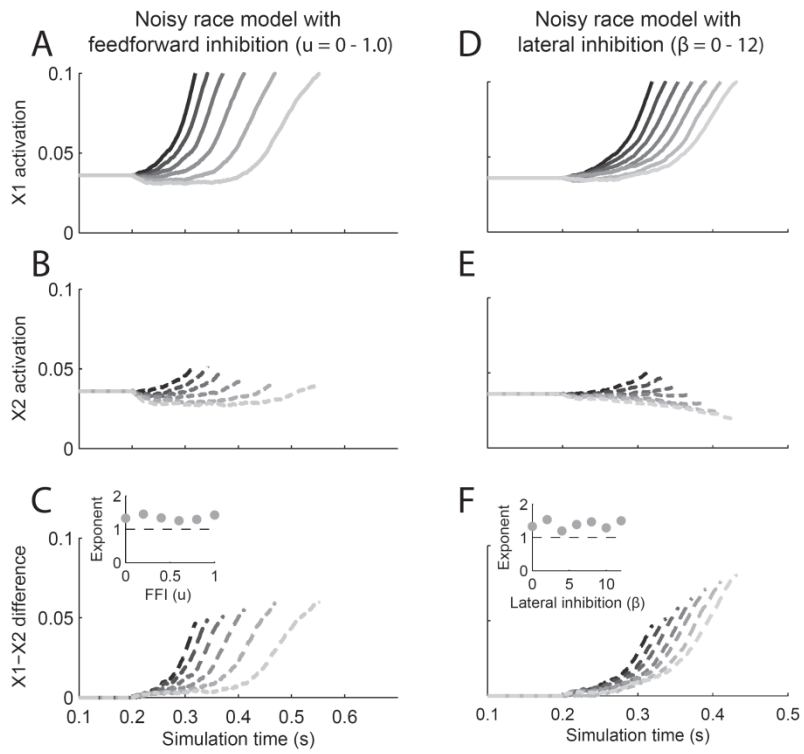

Figure 2.15 Noisy race model dynamics with feed-forward (**A-C**) and lateral (**D-F**) inhibition. Conventions as in Figure 2.14, but with the addition of noise (*s* = 0.11).

2.5 Discussion

Until recently, cognitive psychologists have largely ignored the dynamics of stochastic accumulator models. The possibility that evidence accumulation may be directly observable through neurophysiological measurements means that we could potentially discriminate competing models based on their predicted dynamics (Ditterich, 2010; Purcell et al., 2010; Forstmann et al., 2011). The utility of this approach depends on the degree to which alternative models predict dynamics that can be distinguished in neurophysiological signals. When models are noiseless, we confirmed that distinguishing models with different sources of variability is trivial. However, many models assume some noise, and all neurophysiological signals are noisy.

We found that not only do conventional levels of noise obscure the relation between model parameters and dynamics, but it does so in ways that can be potentially misleading if not taken into account. In the next several sections we discuss the implications of these results for the identification and interpretation of neurophysiological signals implementing evidence accumulation, and the use of these signals to test competing models.

2.5.1 On the identification of neurophysiological signals identified with evidence accumulation

One goal of this work was to clarify predictions for how a neurophysiological signal should modulate during decision-making if it implements evidence accumulation. Based on intuitions about the dynamics of noiseless accumulators, it has commonly been assumed that the critical hallmark of evidence accumulation is a variation of growth rate with changes in RT (Hanes and Schall, 1996; Roitman and Shadlen, 2002). Our simulations demonstrate that variation in the measured onset with RT should also be considered a signature of noisy evidence accumulation. Previous studies have described this property of accumulator models (Ratcliff, 1988; Ratcliff et al., 2003; Ratcliff et al., 2007), but those models also included encoding delay variability, and so the actual cause of changes in onset was not clear. In addition, no previous study has quantified this effect and systematically explored the range of parameters under which it is observed. We found that correlations between onset and RT are observed under a broad range of parameterizations that predict response times on the order of those observed empirically.

Overall, our results inform the methods that researchers should choose to compare model processes with neurophysiological activity. For evaluating neurophysiological processes that are directly identified with evidence accumulation, our recommendation is straightforward: Model dynamics should be directly compared to neural dynamics rather than assuming patterns of model dynamics based on parameter values (e.g. Mazurek et al., 2003; Ratcliff et al., 2007; Purcell et al., 2010; Purcell et al., 2012b). This approach is ideal for electrophysiological measurements with high temporal resolution such as single-unit recordings, intracranial local field potentials, and

extracranial EEG. However, putative correlates of evidence accumulation in BOLD responses (i.e., Heekeren et al., 2004) will lack the temporal resolution to distinguish onset changes from drift rate changes. A different approach to using cognitive models to understand the brain is to correlate model parameters with the magnitude of BOLD responses throughout the brain (Forstmann et al., 2008; van Maanen et al., 2011; Wenzlaff et al., 2011; Mulder et al., 2012). In these studies, the goal is not necessarily to identify the actual implementation of evidence accumulation, but instead to identify where the cognitive process indexed by a parameter might cause elevated neuronal activity (Reilly and Mars, 2011). For this purpose, correlations between model parameters and the BOLD response should be sufficient, although these correlations cannot be interpreted in terms actual biological mechanisms.

2.5.2 On the interpretation of neurophysiological signals identified with evidence accumulation

Based on the properties of noiseless accumulators, it has seemed reasonable to identify the onset of neural dynamics with the start of the decision process (i.e., the end of the encoding delay). However, we found that noisy accumulator models predict changes in the onset of accumulation with RT even when the encoding delay remains fixed. This suggests that correlations between the onset of activation and RT may simply indicate a noisy accumulation process and not changes the duration of stimulus encoding.

This finding has important implications for the nature of information flow across stages that comprise RT. Many behavioral observations can be explained equally well models that assume either continuous or discrete flow of information across stages (e.g., Meyer et al., 1988; Ratcliff, 1988). According to the stochastic accumulator model framework, the start of the accumulation process marks a transition from a discrete stimulus encoding stage to the start of continuous evidence accumulation. If the onset of neurophysiological signals indicate this transition, then it could be used to infer the degree to which processing is discrete or continuous for a given task. For example, motor related ERP components have been identified with

stochastic accumulation to threshold (Gratton et al., 1988; Schurger et al., 2012). Some studies have reported within-condition correlations between the onset of the LRP and RT (Miller, 1998). Other studies have reported changes in the LRP onset across different levels of speed and accuracy emphasis (Osman et al., 2000; Rinkenauer et al., 2004), congruent or incongruent distractor stimuli (Gratton et al., 1988), and target discriminability (Smulders et al., 1995). If the onset of the LRP was identified as the start of a new stage of evidence accumulation or response preparation, then these data would be incorrectly interpreted as evidence that these manipulations extend the duration of a discrete stimulus encoding stage. Our simulations suggest that these changes in onset could also be due to changes in the strength of evidence (i.e., drift rate) across conditions or simply noisy accumulation

In addition, several studies have reported correlations between the firing rate onset and RT in neurons thought to implement evidence accumulation. For example, during a motion detection task, the onset time when neurons in parietal cortex begin increasing their firing rate correlates strongly with RT (Cook and Maunsell, 2002). In addition, the onset time of FEF neurons correlates strongly with RT during visual search (Woodman et al., 2008), motion discrimination tasks (Ding and Gold, 2012), and when animals slow following errors (Pouget et al., 2011). Similar increases in onset have also been observed in superior colliculus neurons during perceptual decision tasks (Ratcliff et al., 2003; Ratcliff et al., 2007). As with the ERP data, it is tempting to conclude that the changes in onset found in these studies indicate the extension of a distinct perceptual process stage, but we cannot rule out changes in the strength of perceptual evidence or simply noise.

In addition to changes in the onset of accumulation with RT, we found that correlations between growth rate and RT are expected even if the drift rate is fixed across conditions so long as any amount of accumulator noise is present. Growth rate is faster when, by chance, noise is more often sampled above the mean and slower when noise is more often sampled below the mean. This observation has important implications for identifying sources of across-trial

variability. Many models predict that across-trial variability in drift rate, instead of or in addition to noise, is a key source of behavioral variability (Ratcliff and Rouder, 1998; Reddi and Carpenter, 2000; Brown and Heathcote, 2005; Brown and Heathcote, 2008). Across-trial variability in drift rate provides a potential mechanism to explain the observation that many subjects produce error response times that are slower than correct response times (Ratcliff and Rouder, 1998; Ratcliff et al., 1999). The observation that the measured growth rate of FEF (Hanes and Schall, 1996), LIP (Roitman and Shadlen, 2002; Maimon and Assad, 2006), and SC (Ratcliff et al., 2003) neurons varies with RT seems to support this modeling assumption. However, our results suggest that these dynamics may simply reflect noisy accumulation of fixed mean rate. Moreover, several groups have shown that slow errors relative to correct RTs can be explained by an urgency gain that increases throughout the duration of the trial (Ditterich, 2006; Churchland et al., 2008; Cisek et al., 2009). In addition, an analysis of across-trial variability in LIP neurons during a motion discrimination task shows that variability increases approximately linearly, which is inconsistent with models that assume across-trial drift is a major source of variability (Churchland et al., 2011). It remains to be seen whether this same pattern of variability dynamics is consistently observed across other areas and tasks.

In contrast to changes in the measured onset and growth rate, we found that variability in the measured threshold was only observed when that variability was explicitly built into the model. This finding validates the fixed activity threshold as a key signature of evidence accumulation. The observation that the firing rates of FEF (Hanes and Schall, 1996), LIP (Roitman and Shadlen, 2002), and SC (Dorris et al., 1997) neurons reach a fixed firing rate threshold immediately prior to saccades was the original basis for the hypothesis that these models implement a form of evidence accumulation. Likewise, the observation that the LRP reaches a fixed voltage at the start of electromyographic activity supports the identification of that component with accumulation to a response threshold (Gratton et al., 1988). In particular, our results reinforce the conclusion that variability in RT is not explained by variability in a response

threshold as proposed by some decision-making models (Grice, 1968). More recently, it has been demonstrated that the measured threshold of FEF neurons during adjustments of speed and accuracy does not conform to changes of threshold predicted by LBA (Heitz and Schall, 2012). Our results suggest that this is not an averaging artifact or consequence of noise; rather, the neurophysiological data are inconsistent with hypothesis that FEF neurons implement the evidence accumulation process predicted by LBA.

We found that changes in the measured baseline could be uniquely identified with changes in the model starting point. Several studies have reported changes in baseline activity during perceptual decision tasks that affect the baseline firing rates of sensorimotor neurons involved in evidence accumulation. For example, when the number of potential responses is known in advance, the baseline firing rates of LIP (Churchland et al., 2008) and SC (Basso and Wurtz, 1998) neurons decrease with added response alternatives. More recently, FEF neurons have been shown to increase their baseline firing rate with speed stress (Heitz and Schall, 2012). Our simulations indicate that these modulations of baseline firing rate are not due to noise. In addition, our simulations show that correlations between baseline and RT will be substantially weaker at longer RTs relative to shorter RTs when the accumulation process is noisy. This is because additional noise accumulates as the trial progresses, and thus the early offset in starting point has relatively less of an effect on the overall RT. Notably, a similar effect has been reported in LIP neurons during a motion discrimination task in which manipulations of the prior probability of a particular motion direction induced response biases in monkeys (Rao et al., 2012). LIP neurons showed clear shifts in baseline activity for the biased response, but those biases faded as the trial progressed, which was consistent with predicted accumulator model dynamics.

One caveat to our finding that shifts in baseline with RT reflect explicit variability in starting point is that our simulations assumed a discrete perceptual processing stage in which no accumulation took place, followed by a decision stage in which evidence began to accumulate.

We have previously shown how these discrete stages of processing can be implemented neurophysiologically if model inputs are gated (inhibited) prior to the trial (Purcell et al., 2010; Purcell et al., 2012b). However, Purcell et al. (2010; 2012) also found that leaky integrators without gating will predict a strongly correlation between baseline and RT even without assuming any changes in the starting point offset. Since many neurophysiological signals do not exhibit correlations between baseline and RT, we concluded that some type of gating inhibition must be operating.

2.5.3 On the use of neurophysiological signals to discriminate alternative models

We found that the actual start of the accumulation was not reliably indicated by the mean onset of accumulation and we suggested two alternative approaches with which it could be more reliably identified. First, we found that the measured mean onset of the fastest response times more accurately reflect the start of the accumulation process. This is because the fastest RTs can only occur when evidence accumulation takes a relatively direct path to threshold. This approach may be suitable when large quantities of data are available, but this method assumes that the lower tail of the RT distribution is sufficiently sampled. As a second alternative, we found that measuring the time when across-trial variability first increased above baseline was a reliable indicator of the start time of accumulation. This is because although the mean activity level tends to remain near the starting point, individual trails tend to vary considerably above and below the mean. Studies that have measured the dynamics of response variability in LIP (Churchland et al., 2011) and FEF (Purcell et al., 2012c) neurons during perceptual decision-making tasks have reported no changes in the time when variability first diverges from baseline when the difficulty of the perceptual decision is manipulated. This suggests that the encoding delay is relatively constant during these tasks. One difference between the neurophysiology and our simulations is that both studies report brief dips in variability prior to increasing, which is commonly observed across cortical areas (Churchland et al., 2010). However, Purcell et al. (2012) showed that leaky

accumulator models that assume some variability in baseline firing rate can predict this brief decline.

We evaluated whether leaky evidence accumulation can be distinguished from perfect evidence accumulation by fitting mean accumulator trajectories with a power function. When models were noiseless, we found that leakage could be clearly identified with decelerating functions. However, when models included noise, the mean rate of accumulation appears to accelerate over time regardless of whether leakage is present or absent. This means that observing a linear or accelerating rise to threshold is not sufficient to rule out leaky accumulation. Note that this apparent acceleration is due to averaging across trials with slightly different model trajectories, although the drift rate is constant throughout the trail (Schurger et al., 2012). Depending on the nature of the task, neurons identified with evidence accumulation typically exhibit approximately linear (Hanes and Schall, 1996; Hanes et al., 1998; Brown et al., 2008) or accelerating (Hanks et al., 2011; Schall et al., 2011; Ding and Gold, 2012) rates of rise to threshold. Linear or accelerating dynamics are also observed in motor-related ERP components (e.g. Gratton et al., 1988; O'Connell et al., 2012). We have shown that these dynamics could be produced by either leaky or perfect integrators with noisy accumulation.

Given that the mean accumulator trajectory may be uninformative about whether or not an accumulator is leaky, can we identify alternative methods by which leakage could be identified? One approach is to consider activity prior to the onset of the stimulus. We have found that even gated accumulator models require a small amount of leakage to prevent the early accumulation of evidence that exceeds the level of the gate (Purcell et al., 2012b). This is not surprising because the time constant of integration for any individual neuron is necessarily limited by the biophysical properties of the cell (Amit and Tsodyks, 1991); that is, all neurons are inherently leaky. An alternative approach is to evaluate the functional relevance of leakage by using time-varying stimuli to identify the temporal window during which stimulus fluctuations most strongly affected perceptual decisions. Behavioral studies that have used this approach

consistently find that subjects are more strongly influenced by early rather than later evidence, which is inconsistent with leaky integration (Ludwig et al., 2005; Kiani et al., 2008; Nienborg and Cumming, 2009). In addition, Huk & Shadlen (2005) found that the effects of brief pulses of motion on LIP neurons during a motion discrimination task affected the firing rate of LIP neurons in a manner roughly consistent with perfect, but not leaky, integration of motion evidence. Finally, leakage is often unimportant to predict decision-making behavior (Ratcliff and Smith, 2004). One possible way to reconcile these findings is to appreciate that long time-scale integration that is necessary for decision-making is thought to be a property of networks endowed with strong recurrent excitation (Wang, 2002). It may be the case that leakage is important to maintaining stable baseline firing rates in the inter-trial intervals, but functionally negated during evidence accumulation due to strong recurrent excitation.

We evaluated whether feed-forward and lateral competition could be discriminated in model trajectories by fitting a power function to the mean difference of two competing accumulators. When the competing accumulators were noiseless, we found that lateral competition could be distinguished from feed-forward competition because it predicted that the difference between accumulators should increase over time. However, when the models included noise, the difference was accelerating regardless of the form of competition. We have previously shown that these two forms of competition may be indistinguishable at the level of neural dynamics when models were driven by a time-varying input function derived from observed neurophysiology (Purcell et al., 2010; Purcell et al., 2012b). Other studies have suggested that there may be subtle differences in the form of accumulation depending on the precise form of competition (Ditterich, 2010), but those differences may be undetectable with higher levels of noise expected in neurophysiological signals. Our results here suggest that even when model inputs are fixed, it may be very difficult to distinguish feed-forward and lateral competition based solely on patterns of mean firing rate dynamics.

A more fruitful approach to identifying differences in feed-forward versus lateral inhibition may be to analyze the precise spike time correlations across neurons representing alternative responses. Feed-forward inhibition predicts a dip in the cross-correlogram around 0 ms, whereas lateral inhibition would predict a dip following some time lag. Using this approach, Ratcliff et al., (2011) observed no appreciable dip in spike time coincidences for pairs of neurons recorded in opposite colliculi during a perceptual decision task. In contrast, Cohen et al. (2010) observed reduced spike time coincidences when the target of visual search was inside the RF of on neuron, but outside the RF of the second neuron. This could reflect across area differences in the form of inhibition; however, the sample size for both studies was relatively low, and therefore more data are needed before strong conclusions can be drawn. Bollimunta & Ditterich (2012) used a different approach to distinguish lateral from feed-forward inhibition by recording from LIP neurons while monkeys performed a three-alternative motion discrimination task in which support for the target (strongest motion direction) could be manipulated independently of support for distractors (weaker motion direction). They found that modulations of the strength of evidence against the target were present in LIP neurons ~80ms before modulations of evidence supporting the target, which seems inconsistent with a lateral inhibition mechanism. However, it is also unclear why a feed-forward model would predict such a large delay between the arrival inhibition and excitation. Simultaneous recordings of much larger populations of neurons could help to resolve this issue.

2.5.4 Conclusions

We characterized the relationship between model parameters and model dynamics as an intermediate step for comparisons of model parameters to neuronal populations thought to implement the accumulator process proposed by the model. We found that the mapping between model parameters and model dynamics is more complex when the accumulation process is noisy. We conclude that the most valid method of comparison models to data may be to directly

compare simulated model trajectories to observed neural dynamics. Additional data will be necessary to determine if firing rates can be best described by lateral or feed-forward inhibition.

CHAPTER III

FROM SALIENCE TO SACCADES: MULTIPLE-ALTERNATIVE GATED STOCHASTIC ACCUMULATOR MODEL OF VISUAL SEARCH

3.1 Abstract

We describe a stochastic accumulator model demonstrating that visual search performance can be understood as a gated feed-forward cascade from a salience map to multiple competing accumulators. The model quantitatively accounts for behavior and predicts neural dynamics of macaque monkeys performing visual search for a target stimulus among different numbers of distractors. The salience accumulated in the model is equated with the spike trains recorded from visually-responsive neurons in the frontal eye field. Accumulated variability in the firing rates of these neurons explains choice probabilities and the distributions of correct and error response times with search arrays of different set sizes if the accumulators are mutually inhibitory. The dynamics of the stochastic accumulators quantitatively predict the activity of presaccadic movement neurons that initiate eye movements if gating inhibition prevents accumulation before the representation of stimulus salience emerges. Adjustments in the level of gating inhibition can control tradeoffs in speed and accuracy that optimize visual search performance.

3.2 Introduction

Many models of visual search and attention assume a map that combines bottom-up and top-down *salience* (also referred to as *priority*) to guide shifts of attention and eye movements (Treisman and Gormican, 1988; Duncan and Humphreys, 1989; Bundesen et al., 2005; Navalpakkam and Itti, 2007; Wolfe, 2007). *Visually-responsive neurons* in frontal eye field (FEF), superior colliculus (SC) and posterior parietal cortex modulate their firing rate according to both physical conspicuity (bottom-up salience) and behavioral relevance (top-down salience; Schall and Hanes, 1993; Gottlieb et al., 1998; Bichot and Schall, 1999a; Findlay and Walker,

1999; Constantinidis and Steinmetz, 2005; Ipata et al., 2006; Thomas and Pare, 2007; Balan et al., 2008; Cohen et al., 2009a; White and Munoz, 2011). However, it is poorly understood how neurons that encode salience are read out to guide saccades. Furthermore, no current model of visual search accounts for full response time (RT) distributions of error and correct responses (Wolfe et al., 2010; Palmer et al., 2011). Alternative models that make very different predictions about underlying mechanisms can often explain mean correct RTs equally well, but predicting errors and full RT distributions imposes more stringent constraints that can often distinguish alternative models (Ratcliff and Smith, 2004).

Stochastic accumulator models of perceptual decision making explain how a single stimulus guides selection of one response among alternative responses (Usher and McClelland, 2001; McMillen and Holmes, 2006; Beck et al., 2008; Churchland et al., 2008; Furman and Wang, 2008; Ditterich, 2010; Leite and Ratcliff, 2010), but the natural world consists of many stimuli. FEF and SC *movement neurons* project to oculomotor brainstem nuclei and initiate a saccade when a fixed firing threshold is reached (Hanes and Schall, 1996; Hanes et al., 1998; Pare and Hanes, 2003). The firing rate dynamics of movement neurons are well explained by stochastic accumulator models (Boucher et al., 2007; Ratcliff et al., 2007), but the source of inputs driving movement neurons to threshold is not known. Furthermore, neurally-plausible implementations of these models have never been generalized to decisions among multiple stimuli, as in visual search.

We present the first neural model of visual search formulated as a multiple-accumulator decision process. We significantly extend a novel modeling technique that defines the source of inputs driving accumulators with the observed discharge rates from FEF visually-responsive neurons (Purcell et al., 2010). Our new work assumes that this dynamically-modulated representation of stimulus salience drives a network of multiple competing accumulators associated with alternative stimuli in a visual search display. The transformation from salience to saccades is controlled by a tonic gating inhibition. Unlike our earlier work developing and

validating this modeling technique, our new model incorporates multiple accumulators and explains choice probabilities and full correct and error response time distributions as a function of set size during visual search. We identify the accumulators with FEF movement neurons that select and initiate saccades when threshold is reached. Accumulator dynamics correspond quantitatively to movement neuron dynamics. We show that gating and lateral inhibition are necessary by ruling out alternative models which do not include these mechanisms. We also show how the gating inhibition provides a novel mechanism to control tradeoffs in speed and accuracy.

3.3 Materials and methods

3.3.1 Behavior and physiology

Behavioral and neurophysiological data were collected from two adult male macaques (*Macaca radiata)* trained to perform a visual search task in which the number of items in the display (set size) varied randomly across trials (Figure 3.1A, inset). Basic behavioral and physiological analyses of these data have been published previously (Woodman et al., 2008; Cohen et al., 2009b; Heitz et al., 2010). Briefly, after fixating a central stimulus for ~600 ms, a stimulus array appeared containing a target (**T** or **L**) among one, three, or seven distractors (random 90^{o} orientations of the other letter). The eccentricity of the array was always 10^{o}. When the array contained two objects, they were always presented at opposite locations and when the array contained four items they were always separated by an unfilled location. Thus, stimuli were spaced ~7.7^{o}, 14^{o}, 19^{o} or 20^{o} apart in the visual field. Target identity was varied across sessions. Monkeys were rewarded for making a single saccade to the location of the target within 2000ms and fixating it for 1000 ms. Search performance was qualitative similar across monkeys, therefore we data pooled across monkeys in addition to fitting to individual monkey data.

Neurons were classified using a memory-guided saccade task. A single target (filled gray disk) was presented in isolation for 100 ms. Monkeys were trained to maintain fixation for 400-

800 ms after target onset. When the fixation spot disappeared, the monkey was rewarded for making a saccade to the remembered location of the target. Neurons with a consistent visual response <100 ms following target onset and persistent firing during the delay period were classified as *visually-responsive neurons* (59 neurons; monkey Q, 40 neurons; monkey S, 19 neurons) and were used to derive input to the stochastic accumulators in the model. This included both visual neurons with no presaccadic discharge and visuomovement neurons with both visual and presaccadic discharge. We included both pure visual and visuomovement neurons as input to the model because previous work has shown that visuomovement neurons, like pure visual neurons, represent the salience of objects in their receptive field (Thompson et al., 1996; Cohen et al., 2009b), but do not have activity sufficient to directly control saccade initiation (Ray et al., 2009). Neurons with a brisk pre-saccadic discharge, but little or no visual response, were classified as *movement neurons* (22 neurons; monkey Q, 15 neurons; monkey S, 7 neurons) and were compared qualitatively and quantitatively to model accumulator dynamics.

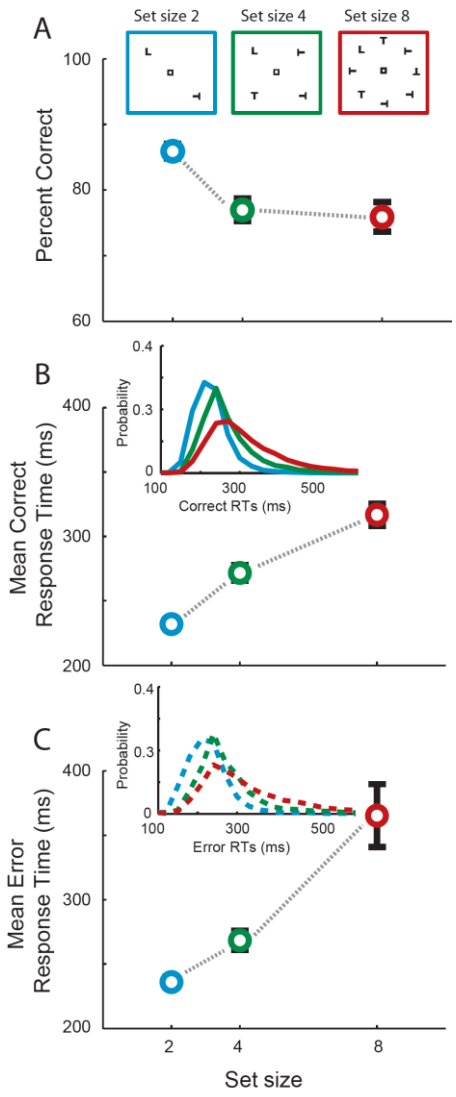

Figure 3.1: Visual search task and behavior. After fixating for a variable delay, an array of stimuli was presented, one of which was the target (e.g., L) and the rest were distractors of random 90^{o} orientations (e.g., T). Monkeys were required to make a single saccade to the target for reward. When the array contained two objects, they were always presented at opposite locations and when the array contained four items, each was separated by an unfilled location. All stimuli were presented at 10^{o} eccentricity. Target identity varied across sessions. Set size varied randomly across trials. **A-C**, Mean ± SEM percent correct (**A**), correct (**B**) and error (**C**) response times for set size 2 (blue), 4 (green), and 8 (red). Insets show search array illustration (**A**), correct (**B**), and error (**C**) response time distributions. Data are pooled across subjects. See Figure 3.5 for individual subject data.

3.3.2 Simulation methology

Neurophysiologically-derived representation of visual salience. Our model assumes that output from pools of visually-responsive neurons encoding stimulus salience converge on movement neurons that initiate saccades. Observed spike trains of visually-responsive neurons define the model input to stochastic accumulators that are identified with movement neurons. Here we describe how those observed spike trains are converted into model input on each simulated trial. In the next section we describe the architecture of the network of accumulators that integrate that model input over time to generate a saccade to a particular stimulus in the visual search array at a particular time. Predicted proportions of error and correct responses and their associated response time distributions are generated by simulating thousands of trials.

Model input was derived directly from the spike trains recorded from visually-responsive neurons following previously described methods (Figure 3.2; Purcell et al., 2010). For each simulated trial, we randomly sampled, with replacement, *N* spike trains from individual trials and generated a spike density function for each trial by convolving the spike trains with a function of the form , which mimics the post synaptic influence of each spike (Thompson et al., 1996); the growth constant, τ_g, is 1 ms, and the decay constant, τ_d, is 20 ms. The pool size, *N*, was varied to identify the value which optimally predicted behavior (Table 3.1). Each spike density function was normalized to the maximum firing rate of the neuron, and all spike density functions in the sample were summed. The resulting spike density function is mathematically similar to a Poisson shot noise process (Smith, 2010).

Spike trains from all neurons were sorted according to the set size (2, 4, or 8) presented and response (correct or error) made when they were recorded. Trials in which the animal prematurely broke fixation were excluded (<1%). Spike trains recorded from a particular set size condition were used to generate behavioral and neural predictions for that set size. The observed choice probabilities for the set size being simulated determined the proportion of simulations that used spike trains sampled from correct or error trials. Thus, the spike trains that drive the model

represent the responses of visually-responsive neurons recorded under the exact conditions being simulated. Simulations that used input from trials in which the animal erroneously looked to a distractor most often predicted erroneous responses due to the form of sampled input (Heitz et al., 2010), but we did not force this to be the case. Indeed, we present examples of models that fail to adequately predict error probabilities.

Post-saccadic spikes cannot contribute to the saccade choice and must be excluded. However, simply eliminating those spikes would artificially increase noise as the simulation progressed because different trials terminate with different RTs. Instead, we extended each trial with firing rates generated according to a Poisson process with a mean rate determined by the spike rate 20 to 10 ms prior to the saccade. Practically, this prevented the parameter optimization routine from failing when certain parameter values could not produce any RT or choice. Ultimately, these extrapolated spikes contribute very little to simulations of well-fitting models because simulated trials ended within the observed RT range.

The use of trial-by-trial spike trains recorded while animals performed the visual search task distinguishes our modeling approach from other stochastic accumulator models in several important ways: First, simulations began well before the presentation of the stimulus array and proceeded until the response was initiated (Figure 3.2B). Afferent delays were determined by visually-responsive neuron physiology and efferent delays were short and well-established quantities (Scudder et al., 2002), so no "non-decision time" parameter is necessary. Second, this approach takes into account the heterogeneous nature of neuronal response properties. Whereas many models assume highly simplified, prototypical, or idealized neural response function, our model is subject to the heterogeneity inherent in neuronal populations. Third, most models make specific assumptions about the mathematical form of the input to stochastic accumulators (e.g., Churchland et al., 2008; Furman and Wang, 2008; Smith and Ratcliff, 2009). Here, we make no a priori assumptions about the form, timing, and variability of inputs within and across trials and conditions; instead, the form, timing, and variability are given by the pattern of activity of

visually-responsive neurons representing visual salience. Although this approach does not speak to the mechanisms that generate salience (e.g., Tsotsos et al., 1995; Itti and Koch, 2001), it provides strong constraints on the mechanism by which salience is used to generate a saccade. We see this as a crucial first step to constrain new models that explain how the neural representation of salience is generated.

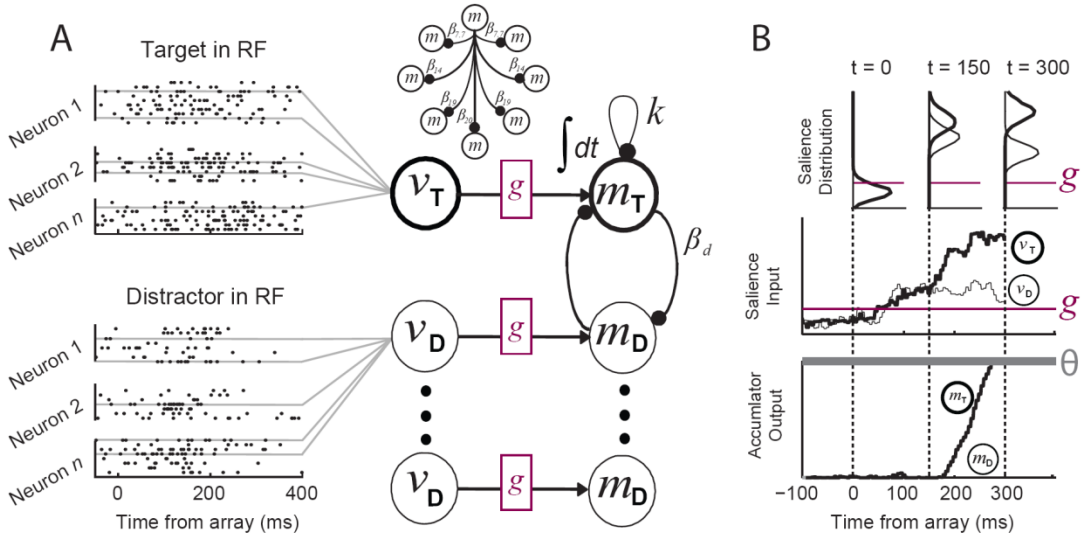

Figure 3.2: A, Gated competitive accumulator model architecture. Spike trains generated by visually-responsive neurons during visual search (left) were pooled to generate a dynamic input function to each accumulator unit (v_i). Input from visually-responsive neurons is integrated by eight accumulator units (m_i) to a fixed threshold. Parameters that determine threshold (θ), leakage (k), gating inhibition (g), and lateral inhibitory connections (β_d) were optimized to fit performance. Only 2 of 7 distractor units are illustrated. Leakage is illustrated for only the target unit, but was of equal value for all units. Lateral inhibition varied by distance, *d*, where *d* denotes the approximate degrees of visual angle between two stimuli (top), but was symmetrical between all units. **B**, Example simulated trial. The distribution of visual inputs when the target (thick, v_T) or a distractor (thin, v_D) were in the receptive field of the neuron varies dynamically over time as determined by visually-response neuron physiology (top). Sampled visual inputs (middle) drive accumulator units (bottom) that initiate saccades to the location of the target (thick, m_T) or a distractor (thin, m_D). Inputs for this example were generated from spike trains recorded during set size 8. Only one of seven distractor units is shown. Predicted RT is the time when the threshold, θ (gray), is reached plus 15ms for the eyes to move. The level of gating inhibition, *g* (magenta), was fit to performance. Accumulation begins only after the gate is exceeded and the salience of the target salience of the distractors unit due to lateral inhibition (i.e., *target selection time*).

Stochastic accumulation of visual salience. The physiologically-defined inputs are pooled and integrated by a network of leaky, competing accumulators (Figure 3.2A). Trials in which a

target was in the RF of a visually-responsive neuron were used as input to the accumulator unit encoding the location of the target. Trials in which distractors were in the RF of a visually-responsive neuron were used as input to units encoding the locations of distractors. Trials when the target was near the RF edge were excluded.

The network always consisted of eight accumulator units regardless of the set size being simulated. For set sizes 2 and 4, input to an accumulator representing a location without a stimulus was defined by visually-responsive neuron firing rates on trials in which no stimulus appeared in the cell's RF. Thus, the model requires no reconfiguration across set size conditions and can generalize naturally to situations with more than eight stimuli. We simulated neural activity from 300 ms before stimulus presentation until the initiation of the saccade. A simulated choice was made to the location represented by the first accumulator unit to reach a constant threshold (Figure 3.2B, bottom). Simulated saccade RT was defined as the time when the threshold was crossed plus a fixed ballistic time of 15 ms that accounts for the time necessary for brainstem processes that shift gaze (Scudder et al., 2002).

Model parameters define for all accumulators the threshold (θ), leakage (k), gating inhibition (g), and lateral inhibition (β_d). Lateral inhibition varied as a function of distance between locations, but was symmetrical between any two locations. Critically, no parameters varied across set size or with the choice of saccade target or distractor. Therefore, variability in search performance was directly determined by variability in the visually-responsive neuron representation of salience and how that representation impacts the dynamics of the stochastic accumulator network. Thus, the model assumes that set size effects can be understood as a consequence of changes in the salience representation that is integrated by stochastic accumulators. It is possible that models assuming architectural or parametric differences across set size could also predict the observed behavior, but this would be a far less parsimonious account.

Each accumulator was governed by the following stochastic differential equation:

— —
— , (1)

where m_i is the mean activity of the accumulator unit representing location i and v_i is the input from visually-responsive neurons representing the same location. As with other neural stochastic accumulator models (e.g., Usher and McClelland, 2001), we rectified m_i to be greater than zero because firing rates cannot be negative. Interactions between units were determined by symmetrical feed-forward, u_d, and lateral, β_d, inhibition weights (e.g., Usher and McClelland, 2001), where d indexes the distance between two stimuli in the array (Figure 3.2A, inset; 4 total values corresponding to approximately d = 7.7, 14, 19, and 20 degrees of visual angle separating the two stimuli). k is the leakage constant, g is the gating constant, and $^+$ denotes rectification above zero. The time constant was set to τ = 1 ms and the time-steps were set to dt = 5 ms for all simulations. All models included a modest amount of Gaussian noise intrinsic to the accumulator, ξ, with mean, $\mu = 0$, and standard deviation, $\sigma = 0.05$; this variability is quite small relative to variability in the visual inputs. Initial model exploration showed that models explain search performance with $\sigma = 0$, but we include some intrinsic variability to allow for tonic neuronal drive when salience input falls below the level of the gate. We also found that models that assume tonic excitation ($\mu > 0$) in addition to salience inputs can predict elevated baseline firing rates as observed in our movement neuron sample, but note that movement neurons with little or no tonic firing rate are commonly observed (e.g., Pare and Hanes, 2003).

Gating inhibition. Effective visual search performance requires that saccades are withheld until visually-responsive neurons have processed stimulus salience. The model solves this problem with a combination of gating and lateral inhibition. Computationally, g is a tonic inhibition applied to the salience input, which is rectified to be greater than zero after the inhibition is applied (Equation 1). Functionally, gating imposes a firing rate that must be

exceeded before the inputs from visually-responsive neurons begin to influence the accumulators. All models assumed that gating is independent of set size and stimulus strength. We assumed a tonic inhibition for computational simplicity and because it could be easily implemented by neurons (see *Neurophysiological Implementation* in Discussion). The precise form of nonlinearity mediating the transformation from visually-responsive neurons to accumulator units is probably not critical, so long as accumulator units have little or no response until the inputs exceed some critical level. Alternative nonlinearities such as sigmoid or power functions may also work if the slope or acceleration is sufficiently steep (e.g., Simen et al., 2006; Simen and Cohen, 2009).

Figure 3.2B illustrates how gating inhibition and lateral inhibition mediate the transformation of salience into response accumulator dynamics. Drive from visually-responsive neurons exists even before the search array appears, but no accumulation takes place because baseline input firing rates are below the gate. By 100 ms after array presentation, visually-responsive neuron firing rates exceed the gate, but top-down salience has not yet emerged. Salience for targets and distractors is equal and balanced; lateral competition holds the system at a temporary equilibrium. After 150 ms, salience for the target exceeds salience for distractors, which triggers a rise in the accumulator unit encoding the target location. Thus, gating and lateral inhibition explain how the selection of salient saccade targets by visually-responsive neurons is transformed into a competition for saccade execution in movement neurons.

Alternative model architectures. We evaluated several different model architectures by fixing various subsets of the parameters in Equation 1 to zero and varying others to fit search performance. Different model architectures instantiate competing hypotheses about the processes that lead to the observed response. We compared models on their quality of fit to search performance (see Fits to visual search performance) and their ability to predict the time course of movement neuron activity (see Measures of movement neuron and accumulator dynamics). Models that failed to fit the observed pattern of behavior, that fit significantly worse than alternative model architectures, or that failed to predict movement neuron dynamics were

rejected. This application of strong inference (Platt, 1964) allowed us systematically to eliminate several plausible neural architectures for using salience to make saccades.

The best performing model architecture across all of our criteria was the gated competitive model (Figures 3.4-3.7; Figure 3.12). This model was defined by setting ud = 0 (no feed-forward inhibition) and included gating inhibition (g), leakage (k), and lateral inhibitory connections (βd) between units (8 free parameters). The term gated accumulator model refers to this particular architecture unless otherwise specified.

We evaluated two alternative model architectures that did not assume competitive interactions. The gated race model (Figure 3.9A) was defined by setting ud = 0 and βd = 0; this model included gating inhibition and leakage, but no competition (4 total free parameters). The gated diffusion-like model (Figure 3.9B) was defined by setting βd = 0; this model included gating inhibition, leakage, and feed-forward, but not lateral, inhibitory connections (8 total free parameters). We also evaluated a model with both diffusion-like and competitive interactions (12 total free parameters), but the fit was not significantly improved relative to the gated competitive model.

We evaluated two other model architectures without gating inhibition. The non-gated, non-leaky model (Figure 3.9C) was defined by setting ud = 0, k = 0, and g = 0; this model included lateral inhibition, but integration of the salience occurred without loss (6 total free parameters). The non-gated, leaky model (Figure 3.9D; Figure 3.10) was defined by setting ud = 0 and g = 0, and included leaky integration and lateral inhibition, but no gating inhibition (7 total free parameters).

Fits to visual search performance. We identified parameters values that best fit search performance. We simulated 5000 trials to generate RT distributions and response probabilities for each set size. All models were fit to behavioral data using a custom combination of a hybrid genetic algorithm (Goldberg, 1989) with a Simplex routine (Nelder and Mead, 1965) implemented in MATLAB (The MathWorks). Parameters were optimized to fit both pooled and

individual monkey performance (Table 3.1). We used a Pearson χ^2 statistic to quantify the discrepancies between the frequency of observed and predicted RTs falling within time bins defined by the 10^{th}, 30^{th},50^{th}, 70^{th} and 90^{th} percentiles (Van Zandt, 2000; Ratcliff and Tuerlinckx, 2002). The χ^2 statistic was summed across each set size condition and choice as follows:

———. (2)

The summation over *i* indexes response time bins defined by the quantiles of the observed response time distribution corresponding to the cumulative probabilities of 0.1, 0.3, 0.5, 0.7, and 0.9. O_i are the observed proportion of response times and P_i are the predicted proportion of response times within the bins. With these quantiles, the six O_i are 0.1, 0.2, 0.2, 0.2, 0.2, and 0.1, respectively. P_i are the predicted proportion of response times falling within each bin. The probabilities are converted to frequencies by multiplying by the observed number of data points, *n*. The summation over *r* indexes responses (correct, error) and the summation over *s* indexes set size (2, 4, 8). We count the number of predicted responses falling within each response time distribution; therefore, minimizing this statistic simultaneously fits both the observed response probabilities and the response time distribution (Van Zandt, 2000).

We used a second statistic, the Akaike information criterion (AIC), a penalized maximum likelihood statistic, to test whether improvements in fit can be explained by increases in the number of free parameters (Bozdogan, 2000):

(3)

where O_i and P_i are the same as described above. M is the number of free parameters in the model.

We used nonparametric bootstrapping to compare goodness of fit and gauge the reliability with which optimally-fitting parameters could be estimated (Efron and Tibshirani, 1993; Wichmann and Hill, 2001). We randomly sampled, with replacement, sets of responses (correct or error) and response times equivalent to the average number of trials in a session (2137 trials).

We fit each model to sampled data 5000 times using different initial states and pseudo-random number generator seeds to account for noise in the fit statistic and parameter estimates. Standard error and confidence intervals were determined directly from the resulting distributions of fit statistics and estimated parameters. Simulations were run in parallel on a high-performance computing cluster supported by the Vanderbilt Advanced Center for Computing for Research and Education (ACCRE).

Measures of movement neuron and accumulator dynamics. Following Woodman et al. (2008), we analyzed four changes in movement neuron dynamics related to changes in RT across and within set size: *baseline* firing rate before search array presentation, *onset* of presaccadic firing rate increase, *growth rate* of this increase to threshold, and the presaccadic firing rate *threshold* immediately prior to a saccade. Trials in which a saccade was made to the neuron's movement field were sorted by RT and binned into groups of ten to analyze the relationship of movement neuron dynamics to RT. A bin size of ten was selected because averaging eliminates some noise, but RT variability within a bin is small enough to avoid distortions due to averaging across trials with very different RTs. Only neurons that were recorded for at least 30 trials (3 bins) were included for a particular set size, which precluded an analysis of error trials.

To calculate the onset of activation, we used a sliding-window algorithm (+/- 20 ms) that moved backward in 1-ms increments beginning 15 ms before the mean time of saccade initiation for the bin being analyzed. The onset of activation was determined to be the time when the following three criteria were met: (a) Activity no longer increased according to a Spearman correlation ($\alpha = 0.05$) within the window around the current time, (b) activity at that time was lower than activity during the 20 ms preceding saccade onset, and (c) as the window was moved backward in time, the correlation remained nonsignificant for 20 ms. Results were qualitatively similar when the onset was computed as the time point when activity first exceeded two standard deviations above baseline. The growth rate was the slope coefficient of a least squares regression line fit to the activity from 100 ms to 15 ms presaccade. Baseline was computed as the average

firing rate in the 200 ms prior to the appearance of the search array. Threshold was computed as the average activity level of a neuron in the interval 20 to 10 ms relative to saccade (Hanes and Schall, 1996).

To allow commensurate statistical comparisons of models and neurophysiology, model dynamics were analyzed in the following way: (a) We simulated gated accumulator model trajectories using the best fitting parameters to search performance from the pooled data set, (b) we normalized and rescaled the model trajectories by the threshold firing rate observed in recorded movement neurons, (c) we generated one spike train for each trial according to a time inhomogeneous Poisson process with the rate given by the model activation trajectory for that trial, (d) we binned the simulated spike trains into groups of 10 trials according to the predicted RT and generated a spike density function from the predicted spikes exactly as was done for the actual spikes. This transformed a model prediction in terms of spikes per second into a single predicted spike train. These steps were repeated 500 times using numbers of simulated trials matched to actual numbers of trials recorded from individual movement neurons.

We analyzed how each measurement accounted for variation in RT across and within set size. To determine how changes in each measure accounted for variation in RT across set size, we averaged each measure across bins and computed the slope of the average measure as a function of set size. To determine how changes in each measure accounted for variation in RT within each set size, we computed the correlation coefficient between each measurement and the mean RT for all bins of trials. We report median measures of neural dynamics ± standard error of the median, which was obtained using a statistical bootstrap approach (1000 samples).

It is critical to emphasize that all predicted accumulator dynamics were generated using parameters that were first optimized to fit search performance. No parameters were hand-tuned to match neural dynamics. Thus, the simulated model dynamics are true predictions and not optimized fits to physiology. As predictions, we focus on the general changes in response

dynamics across and within conditions, as opposed to specific details that are likely to be idiosyncratic to particular neurons.

ROC analysis. We assessed how reliably FEF neurons signaled the target location by computing the area under the receiver operating characteristic (ROC) curve from the distribution of trials in which the target appeared inside the receptive field of the neuron and trials in which the target appeared outside the receptive field (see Thompson et al., 1996). The ROC was computed by incrementing a criterion from 0 spikes/s to the maximum firing rate observed across all trials in steps of 1 spike/s. For this analysis we measured the average area under the ROC curve from 100 to 200 ms after array presentation.

Speed-accuracy tradeoff simulations. We explored how the gated competitive accumulator model could accomplish speed-accuracy tradeoffs by systematically varying two key parameters of the model. We computed the mean RT, percent correct, and expected reward rate while varying the gate or threshold parameters and fixing all other parameters at the values fitted to pooled performance data. Each simulation consisted of 700 trials of each set size corresponding approximately to the average number of trials in an actual recording session. Reward rate is defined by $R = P/T$, where P is the average proportion of correct choices across all set size conditions and T is the average trial duration (Gold and Shadlen, 2002; Lo and Wang, 2006). T was defined by T = where p is the response proportion and RT is the average RT for each set size, s (2, 4, or 8), and response, r (correct or error). The intertrial interval, ITI, was 1 s as in the experiment protocol. Confidence intervals were computed from the distribution of reward rates obtained by simulating expected reward rate 1000 times for each set of parameters with randomly sampled inputs.

3.4 Results

3.4.1 Visual search behavior and neurophysiology

We modeled behavior and neurophysiology observed from macaque monkeys trained to perform an attentionally-demanding visual search task (Figure 3.1A), details of which have been previously published (Cohen et al., 2009a; Heitz et al., 2010). Monkey behavior exhibited hallmarks of inefficient search as observed in humans. Percent correct declined (Figure 3.1A) and mean RTs increased (Figure 3.1B; Figure 3.1C) with increasing set size (Cohen et al., 2009b). Monkeys also exhibited substantial variability in RTs within each set size (Figure 3.1B and Figure 3.1C, insets). The variance of the distribution increases with set size and there is a systematic lengthening of the upper tail of the distribution, which is also observed in human search performance (Ward and McClelland, 1989; Palmer et al., 2011). No current model of search explains full response time distributions (Wolfe et al., 2010) or the neural source of this variability. Our new model explains both the systematic and random variability in RT driven by single-unit physiology recorded during visual search.

The first observation guiding our modeling is that visually-responsive neurons in FEF, SC, and lateral intraparietal area (LIP) appear to encode salience of potential saccade targets. All single-unit data in the present report were collected in FEF, but note that neurons with very similar response properties are observed in other oculomotor areas. Thus, although we used the discharge rate of visually-responsive FEF neurons as model input, we believe that similar results would be observed using discharge rates from visually-responsive SC or LIP neurons. During the visual search task, the firing rates of visually-responsive neurons increase following the onset of the search array and are maintained at a higher level if the target is within the cell's RF (Figure 3.3A). The average time of target selection increases with set size and the average firing rate decreases with set size (Cohen et al., 2009b). Decreases in the average firing rate with set size have also been reported in LIP (Balan et al., 2008). In addition, we found that visually-responsive neurons signaled the location of the target less reliably as set size increased, as indicated by a

decline in the average (±SE) area under the ROC curve (set size 2: 0.63 ± 0.05; set size 4: 0.55 ± 0.03; set size 8: 0.54 ± 0.03). All differences were significant (paired t-test, all $p < 0.05$). These changes may reflect the limited capacity of the visual system to simultaneously analyze all stimuli in the visual field, although we cannot make strong claims about the specific mechanisms responsible for this limitation. Importantly, the decrease in firing rate with set size is consistent with the identification of these neurons as encoding visual salience. A model that explains how salience is translated into a saccade command must explain how these firing rate dynamics are read out to initiate a saccade.

The second observation guiding our modeling is that movement neurons in FEF and SC initiate saccades at a fixed firing rate threshold. Note that LIP has very few movement neurons without visual responses (e.g., Gottlieb and Goldberg, 1999) and LIP neurons do not project directly to oculomotor brainstem nuclei, therefore we do not identify our model accumulator with LIP neurons. Figure 3.3B illustrates the population response of FEF movement neurons during the T/L search task. In contrast to the visual neuron population, the firing rates of these neurons converge at a fixed firing rate threshold immediately prior to the saccade regardless of the set size and RT. This adds to converging evidence that presaccadic movement neurons initiate a saccade when a fixed firing rate threshold is reached (Hanes and Schall, 1996; Hanes et al., 1998; Pare and Hanes, 2003). A model that explains how stimulus salience is translated into a saccade command must explain how presaccadic movement neurons are driven to threshold.

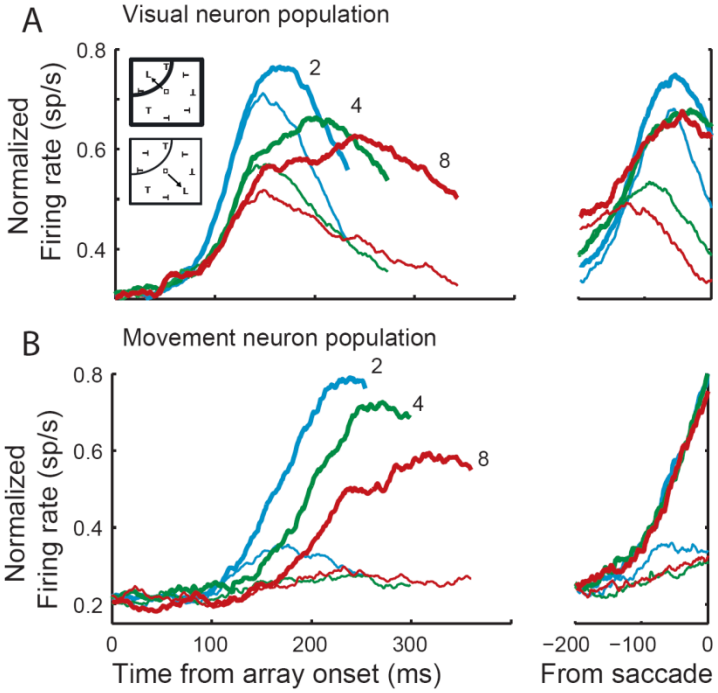

Figure 3.3: Frontal eye field physiology during visual search**. A**,**B**, Normalized population firing rates for FEF visual (**A**) and movement (**B**) neurons during visual search with set size 2 (blue), 4 (green), and 8 (red). Spike density functions were generated from trials in which the target (thick) or a distractor (thin) was inside the RF of the neuron. Spike density functions are aligned on the stimulus array presentation (left) and saccade (right). Stimulus-aligned spike density functions end at the median RT.

3.4.2 Gated competitive accumulation explains search performance

The gated accumulator model quantitatively accounts for all aspects of visual search performance. We optimized parameters to simultaneously fit the observed choice probabilities and RT distributions for both correct saccades to the target and error saccades to distractors (Table 3.1). Figure 3.4 compares observed search performance with simulated performance of the network. The model accounts for the increase in mean RT with set size (Figure 3.4A) because the average firing rate of visually-responsive neurons declines with set size (Figure 3.3A) and because neurons encoding competing locations are increasingly active due to the presence of distractors in their RF. In other words, as set size increases, more locations become activated on the salience map. The model accounts for the decrease in percent correct with set size because

increased activation at competing locations decreases the reliability with which the target can be discriminated and because visually-responsive neurons select distractors when the monkey makes an error (Thompson et al., 2005b; Heitz et al., 2010). Predicted errors are slow relative to correct responses because firing rates are lower, on average, on error trials. Thus, the properties of visually-responsive neurons coupled to a network of stochastic accumulators have exactly the properties necessary to explain the basic properties of search performance. Although we only manipulated set size here, we note past results showing that visually-responsive neuron firing rates decrease with target-distractor similarity as expected of a salience representation (Bichot and Schall, 1999a; Ipata et al., 2006; White and Munoz, 2011). This is exactly the pattern of modulation that would be required for our model to predict the observed decreases in performance with increased target-distractor similarity, as we have demonstrated previously (Purcell et al., 2010).

The model explains the basic changes in mean RT and accuracy during inefficient visual search, which must be true for any viable model of search, but a more rigorous evaluation of model performance is whether the model can predict full RT distributions. Figure 3.4 plots the observed and predicted RT distributions for correct (Figure 3.4C) and error (Figure 3.4D) trials for each set size condition. The model captures the increasing spread and the systematic lengthening of the upper tail of the distribution, which is characteristic of inefficient visual search in humans and our monkeys (Wolfe et al., 2010; Palmer et al., 2011). We verified that this was also true for individual monkeys (Figure 3.5). These results demonstrate that nearly all of the variability in search performance can be explained by a gated accumulation of the neural representation of stimulus salience.

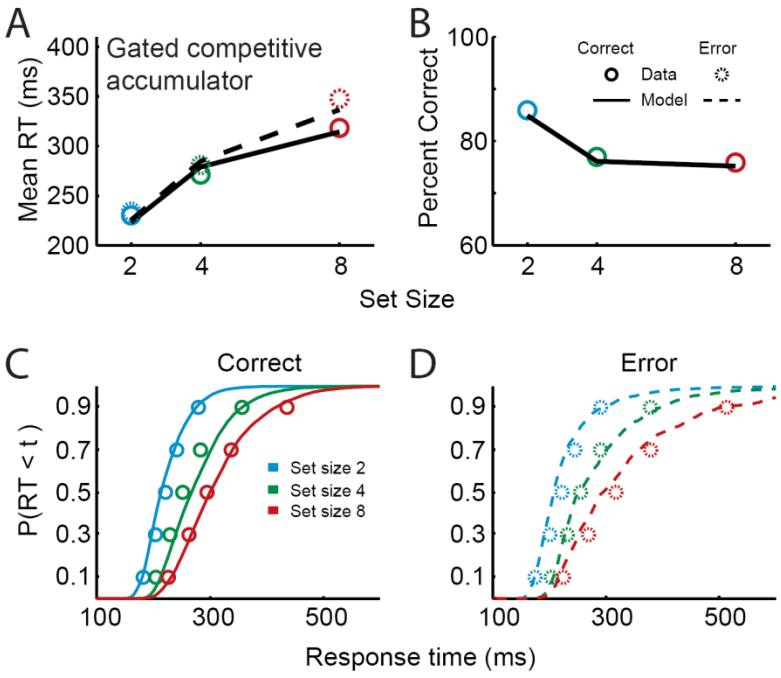

Figure 3.4: Gated competitive accumulator model fits to pooled search performance**. A**, Mean observed (circles) and predicted (lines) correct (solid) and error (dashed) response times for set size 2 (blue), 4 (green), and 8 (red). **B**, Mean observed and predicted percent correct. **C**,**D**, Observed cumulative response time distribution quantiles (circles) and predicted response time distributions (lines) for correct (**C**) and error (**D**) responses.

Table 3.1: Best fitting parameter values and fit statistics (χ^2 and *AIC*) for all model architectures and data sets. *N*: number of spike trains sampled from visually-responsive neurons to generate salience input for all conditions. θ: threshold. *k*: leakage constant. *g*: gate constant. β_d : lateral inhibition weights between two units spaced *i* degrees of visual angle apart. u_d : feed-forward inhibition weights between two units spaced *i* degrees of visual angle apart. Bold values indicate the best fitting model (minimum χ^2). Dashes indicate that parameters were fixed to zero for a given architecture.

Data set/Architecture	χ^2	*AIC*	*N*	θ	k	g	$\beta_{7.7}$	β_{14}	β_{19}	β_{20}	$u_{7.7}$	u_{14}	u_{19}	u_{20}
Pooled														
Gated race	623	6583	130	1.337	0.430	0.427	-	-	-	-	-	-	-	-
Gated diffusion-like	265	6398	40	2.658	0.001	0.511	-	-	-	-	0.039	0.050	0.041	0.050
Gated competitive	**123**	**6199**	108	11.605	0.017	0.330	0.048	0.038	0.024	0.024	-	-	-	-
Non-gated, non-leaky	234	6583	550	60.302	-	-	0.003	0.004	0.003	0.002	-	-	-	-
Non-gated, leaky	165	6237	80	17.707	0.022	-	0.004	0.022	0.006	0.013	-	-	-	-
Monkey Q														
Gated race	403	6543	66	3.373	0.018	0.599	-	-	-	-	-	-	-	-
Gated diffusion-like	244	6624	66	3.298	0.001	0.520	-	-	-	-	0.048	0.028	0.041	0.047
Gated competitive	**106**	6497	134	13.607	0.014	0.330	0.050	0.034	0.018	0.021	-	-	-	-
Non-gated, non-leaky	331	6917	450	60.238	-	-	0.004	0.004	0.004	0.004	-	-	-	-
Non-gated, leaky	159	**6434**	100	17.573	0.027	-	0.031	0.027	0.014	0.012	-	-	-	-
Monkey S														
Gated race	631	6193	50	1.095	0.519	0.500	-	-	-	-	-	-	-	-
Gated diffusion-like	351	6120	45	1.001	0.424	0.377	-	-	-	-	0.040	0.050	0.007	0.050
Gated competitive	**157**	**6006**	70	9.816	0.028	0.269	0.004	0.047	0.000	0.025	-	-	-	-
Non-gated, non-leaky	324	6411	500	55.363	-	-	0.003	0.005	0.003	0.004	-	-	-	-
Non-gated, leaky	181	6021	70	14.018	0.027	-	0.008	0.030	0.008	0.020	-	-	-	-

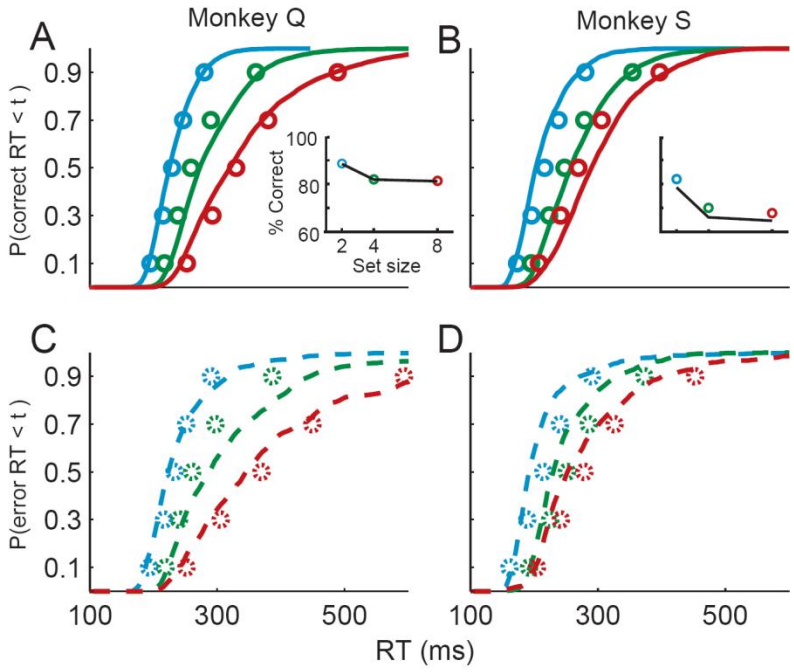

Figure 3.5: Gated competitive accumulator model fits to individual monkey search performance. **A**,**B**, Observed correct response time quantiles and predicted response time distributions for monkey Q (**A**) and monkey S (**B**). Insets show observed and predicted percent correct. **C**,**D**, Observed error response time quantiles and predicted response time distributions for monkey Q (**C**) and monkey S (**D**). Conventions as in Figure 3.4.

3.4.3 Gated competitive accumulation predicts dynamics of presaccadic movement activity

We identify model accumulator units with movement neurons in FEF and SC. If this mapping is correct, then accumulator dynamics should correspond to movement neuron dynamics observed during visual search. Figure 3.6 (A-C) plots observed movement neuron spiking dynamics for slow, intermediate, and fast responses within each set size condition. The onset of neuronal modulations is later, on average, when the monkey responds slower whether within or across set size conditions (Woodman et al., 2008), but there is little change in the rate of growth across set size when aligned on saccade initiation; the apparent differences in rate of growth when aligned on array onset are merely a consequence of averaging across trials with different RTs. Consistent with a fixed response threshold, the presaccadic firing rate remains constant regardless of task difficulty or response speed. The onset of activation also increases within each set size condition and there is a slight decline in the rate of growth to threshold.

Figure 3.6 (D-F) plots the average simulated trajectories sorted according to the same procedure as the movement neuron data. We simulated each set size condition 5000 times and generated spikes trains according to a Poisson process with a non-homogenous rate given by the simulated model trajectories (see Materials and Methods). The model qualitatively captures key physiological observations in the movement neurons. The time when the accumulated activation first modulates above baseline increases across and within set size. When aligned on saccade initiation, there is little or no change in the rate of growth across set size and only marginal change in the rate of growth within set size. Finally, the model reaches a fixed threshold prior to the response by design.

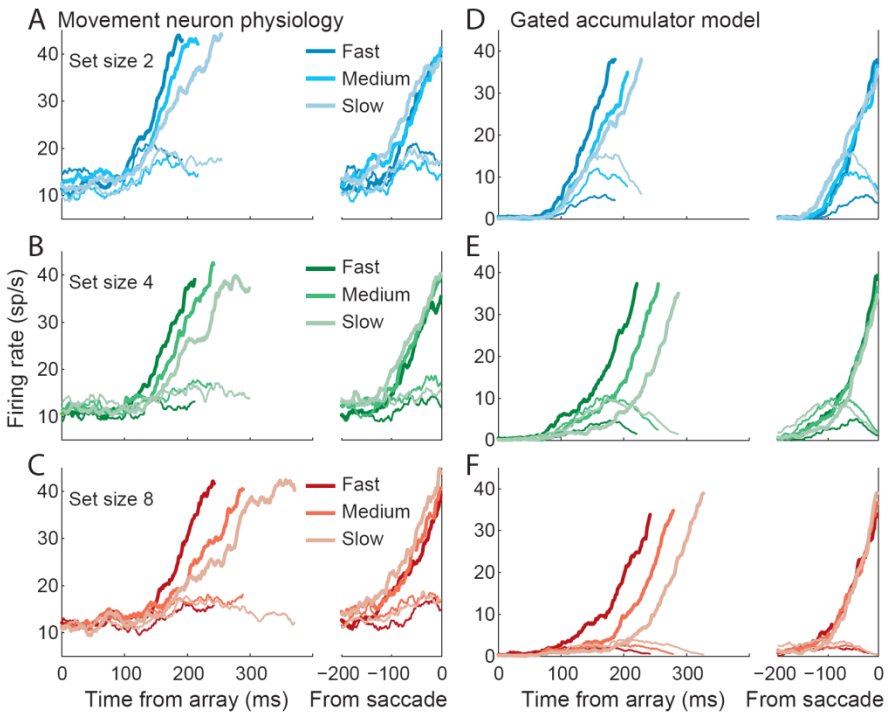

Figure 3.6: Movement neuron and gated accumulator dynamics. **A-C**, Spike density functions for FEF movement neurons conditionalized on set size (A – 2, B – 4, C – 8) and response time (dark – fast, intermediate – medium, light – slow). Fast, medium, and slow SDFs were generated from ten trials sampled at the 20th, 40th, and 80th RT percentile, respectively, to avoid averaging distortions. **D-F**, Simulated neural dynamics from the best fitting parameters of the gated accumulator model to the pooled data set (Table 3.1).

Following Woodman et al. (2008), we quantified four measures of neural dynamics to verify the correspondence between accumulators and movement neurons: delays in the onset of the presaccadic rise (onset), the average rate of rise (growth rate), the starting point (baseline), and the firing level at the time of saccade (threshold; see Materials and Methods). All simulations used parameters fitted to search performance (Table 3.1). Critically, no parameters were adjusted to generate predicted model dynamics.

First, for the across set size assessment, we computed the average of each measure across RT groups and computed the least squares regression slope of that measure as a function of set size. Figure 3.7A-D shows the resulting slopes for a representative movement neuron. Only the onset of accumulation increases significantly with set size. Figure 3.7E-H shows the resulting slopes for the population of all movement neurons (bar histogram) and simulations of the gated competitive

accumulator model (line histogram). Across the movement neuron population, the median slope of onset as a function of set size is significantly greater than zero (14.4 ± 2.5 ms/item, Wilcoxon rank sum test, $p < 0.001$), but does not differ significantly from the median slope of model predictions (14.9 ms/item, $p = 0.47$). No other slope distribution was statistically different from zero or from model predictions (all $p \geq 0.05$). Thus, the model predicts changes in neural dynamics with changes in set size that are comparable to observed movement neuron dynamics.

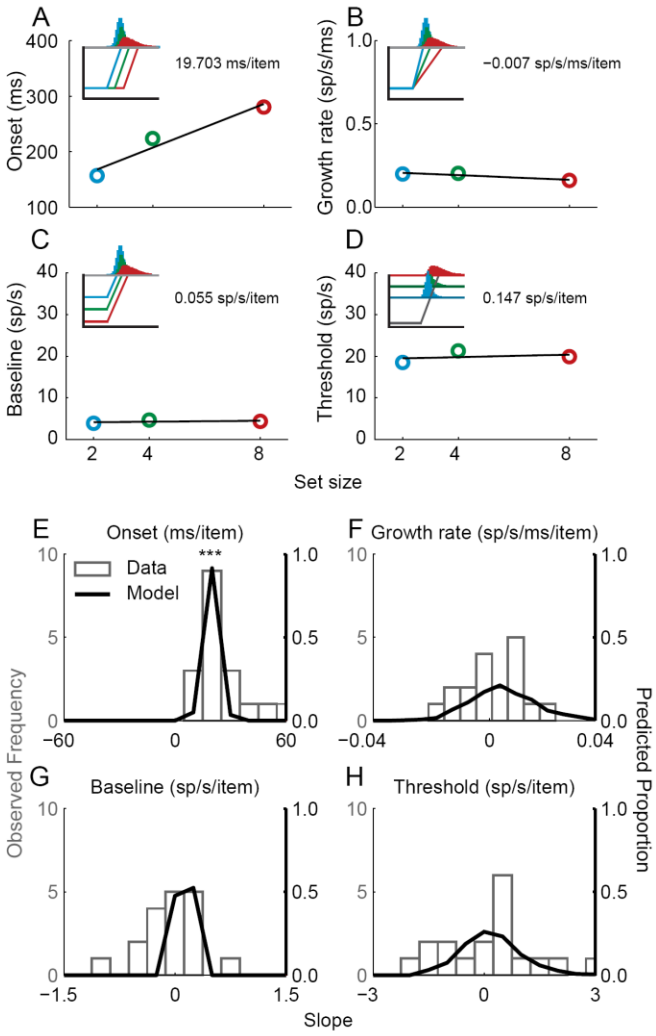

Figure 3.7: Quantification of movement neuron and gated competitive accumulator model dynamics across set size. **A-D**, onset of the presaccadic burst (**A**), growth rate of firing rate rise to threshold (**B**), baseline firing rate (**C**), and presaccadic firing rate threshold (**D**) as a function of set size for a representative neuron (see Materials and Methods for details). Black line illustrates the slope of each measure of neural dynamics as a function of set. The insets illustrate the idealized expected dynamics if a given measure accounts for variability in set size. **E-H**, Population of slopes of each measure of neural dynamics as a function of set size for FEF movement neurons (open gray bars; 22 neurons) and simulated model dynamics (black lines; 500 simulations). Asterisks denote significant that the distribution of movement neuron slopes is significantly different from zero (Wilcoxon rank-sum test; *** for $p < 0.001$).

Next, for the within set size assessment, we computed the correlation between each measure of neural dynamics and RT within each set size independently. Figure 3.8A-D illustrates the correlation between each measure of neural dynamics and RT bins from a representative neuron recorded during set size 4 trials. Only the onset of the presaccadic burst correlates significantly

with response time (Figure 3.8A), although there is a small, but nonsignificant, decrease in the rate of growth (Figure 3.8B). Figure 3.8E-H plots the median observed correlation between each measure of neural dynamics and RT across the population of movement neurons for all set sizes. The median correlation is significantly greater than zero for the onset of the presaccadic burst (Figure 3.8E; Wilcoxon rank-sum test, set size 2: 0.67 ± 0.12; set size 4: 0.81 ± 0.05; set size 8: 0.93 ± 0.02; all $p < 0.01$). We also observed a weak correlation between baseline and RT in set size two that was marginally significant (Figure 3.8G; set size 2: -0.24 ± 0.07, $p = 0.04$), but no other measures of neural dynamics correlated significantly with RT (all $p > 0.05$). Importantly, the strength of correlation with RT was statistically indistinguishable between movement neurons and model predictions for most measures of neural dynamics (all $p > 0.05$). The only exceptions were the median correlation between baseline and RT for set size 4 (data: 0.03; model: -0.29; $p = 0.02$) and between threshold and RT for set size 4 (data: 0.12; model: -0.17; $p = 0.03$) which differed slightly, but significantly from the data. However, the lack of a systematic relationship with set size suggests that this deviation can be attributed to noise. Thus, the model predicts the essential quantities seen in the neural dynamics using the same parameters that were optimized to fit search performance.

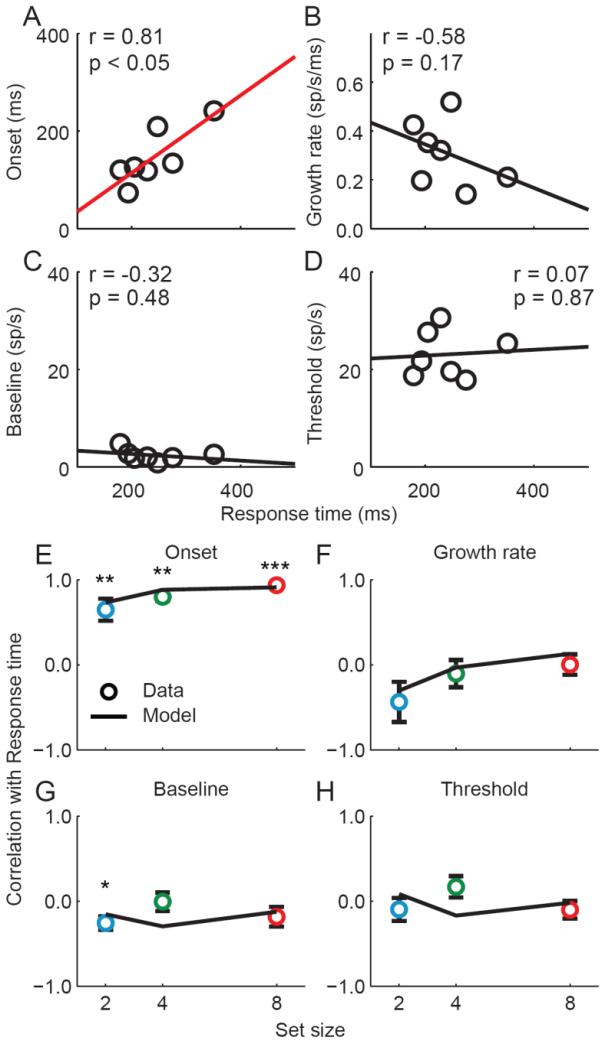

Figure 3.8: Quantification of movement neuron and gated competitive accumulator model dynamics across response time bins within each set size. **A-D**, onset of the presaccadic burst (**A**), growth rate of firing rate rise to threshold (**B**), baseline firing rate (**C**), and presaccadic firing rate threshold (**D**) as a function of RT bins for a representative neuron (see Materials and Methods for details). Only set size 4 is shown for simplicity. Lines illustrate the least squares regression line fit to the data. Red lines indicate significant Pearson correlation coefficients ($p < 0.05$). **E-H**, median correlation between each measure of neural dynamics and response time for observed movement neurons (circles) and simulated model dynamics (lines). Error bars indicate standard error of the median for observed data (bootstrap, 1000 samples). Asterisks indicate median correlations that significantly differed from zero (Wilcoxon rank-sum test; * for $p < 0.05$; ** for $p < 0.01$; *** for $p < 0.001$).

3.4.4 Gating inhibition and lateral competition are necessary

Using the logic of nested model testing, we determined which model elements are necessary to account for visual search performance and replicate movement neuron physiology. First, we explored a gated race model architecture without competitive interactions (all $\beta_d = 0$). This architecture qualitatively failed to predict the ordering of mean error RTs (Figure 3.9A). This

architecture failed because it has no mechanism to suppress the initial visual responses that drive saccades to distractors. Quantitatively, this produced significantly elevated χ^2 relative to the gated competitive model for both individual and pooled monkey data ($p < 0.05$, non-parametric bootstrap, 5000 simulations; Figure 3.10). The difference was not statistically significant using AIC (all $p > 0.05$), but there are several reasons to believe that this additional complexity is warranted. First, the gated race model cannot predict the correct ordering of error RTs and therefore qualitatively fails to predict a key component of visual search performance. Second, the need for competition is supported by studies demonstrating that microstimulation of FEF can suppress firing rates in the opposite hemifield (Schlag et al., 1998) and the presentation of a visual distractor in the ipsilateral visual field reduces the firing rate of SC movement neurons (Dorris et al., 2007). Lastly, existing theoretical work has demonstrated some form of competitive interaction is necessary to optimize the rate of reward for a set amount of sensory evidence (Bogacz et al., 2006). Thus, some form of competitive interaction appears to be necessary.

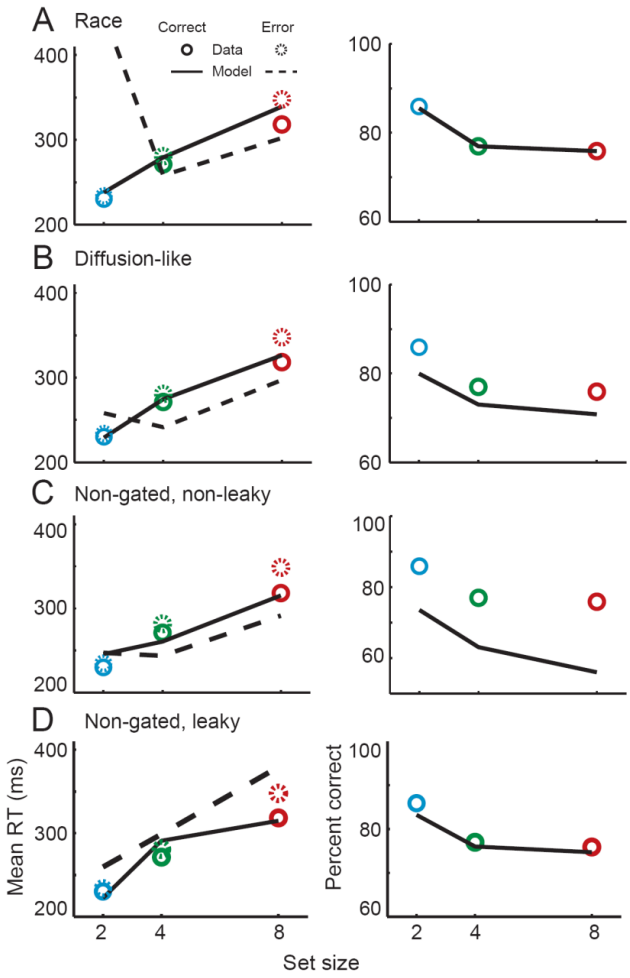

Figure 3.9: Rejection of alternatives to gated competitive accumulation. **A-D**, mean correct and error response times (left) and percent correct (right) for observed data and model predictions from alternative architectures. Poor performance of a gated independent race architecture (**A**, $\beta_d = 0$, $u_d = 0$), gated diffusion-like architecture (**B**, $\beta_d = 0$, u_d is fit), non-gated, non-leaky architecture (**C**, $k = 0$, $g = 0$) and non-gated, leaky architecture (**D**, $g = 0$). Conventions as in Figure 3.4.

We next explored a diffusion-like gated accumulator model with feed-forward inhibition between model inputs but no competition between model units (all u_d were allowed to vary, but all $\beta_d = 0$). This architecture failed to predict both the ordering of error RTs and the observed percentages of correct responses (Figure 3.9B). We observed a significantly worse fit for this model than the gated competitive model for all data sets whether or not model complexity is taken into account (all $P < 0.05$; Figure 3.10). This model fails because some mechanism must

suppress the initial visual responses to distractor locations, but feed-forward inhibition must necessarily be weak when the number of interacting accumulators is >2. If feed-forward inhibition is strong, then the inhibition from distractors will overwhelm excitation to the target location resulting in excessively long RTs (Usher and McClelland, 2001). These results appear to challenge the generality of a large class of drift diffusion models that require feed-forward inhibition for their neurophysiological implementation (Gold and Shadlen, 2001; Bogacz et al., 2006; Ratcliff et al., 2007; Churchland et al., 2008; Ditterich, 2010; Purcell et al., 2010).

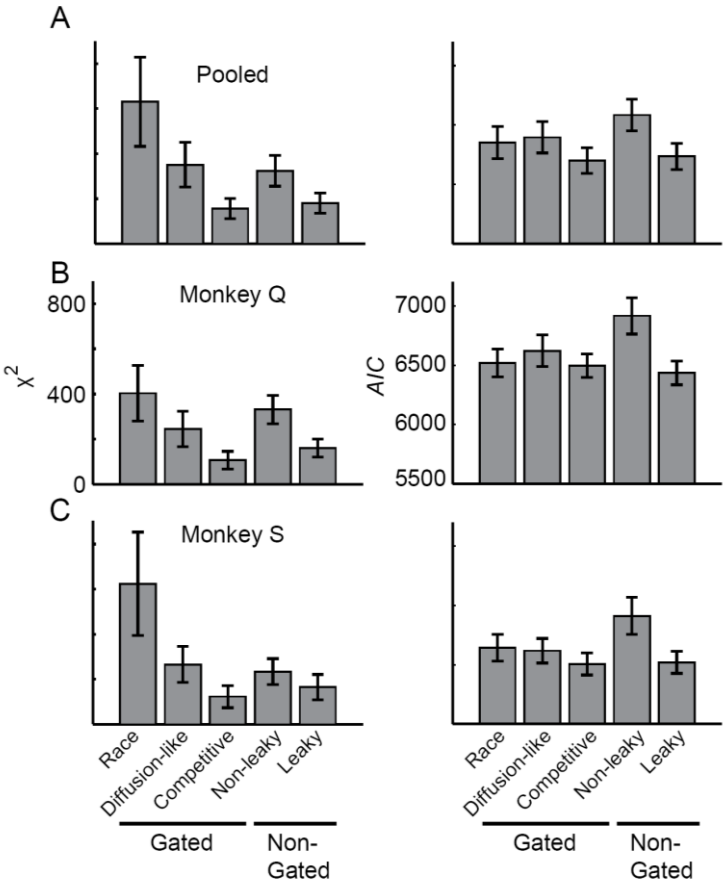

Figure 3.10: Fit summary for alternative model architectures fit to pooled (**A**), monkey Q (**B**), and monkey S (**C**) search performance data. Values are median χ^2 (left) or *AIC* (right) ± 95% confidence interval (Non-parametric bootstrap; 5000 simulations).

To investigate the necessity of gating inhibition and leakage, we explored a non-gated, non-leaky model architecture with lateral inhibition but no gate or leak. This architecture failed to quantitatively predict both correct and error RTs as well as the percentage of correct responses (Figure 3.9C). The fit was significantly worse than the gated competitive model even when taking into account differences in model complexity (Figure 3.10). It fails because tonic activity of visually-responsive neurons propagates directly to accumulators that initiate saccades before salience can be computed. Thus, some mechanism is needed to limit the rate of integration until an informative salience signal can be generated, and leakage or gating or both are viable mechanisms.

To investigate the necessity of gating inhibition, we explored a non-gated, leaky architecture with lateral inhibition and leakage, but no gating inhibition. This architecture accounted qualitatively for the basic pattern of search performance (Figure 3.9D). Although the fit appears qualititatively worse than the gated competitive model architecture, this difference was not statistically significant for both fit statistics and all data sets (Figure 3.10). We previously found the same result using a simplified two-accumulator model framework (Purcell et al., 2010). Thus, leaky and gated models cannot be discriminated by behavioral data alone even in this more complex network that explains richer behavioral data. However, gated accumulation is necessary to for the accumulators to replicate movement neuron dynamics. Models that do not include gating predict a strong negative correlation between the baseline and RT that is not observed in the data. Figure 3.11 shows that this result replicates in a multiple-accumulator framework. Thus, gating inhibition is necessary to explain movement neuron physiology during visual search.

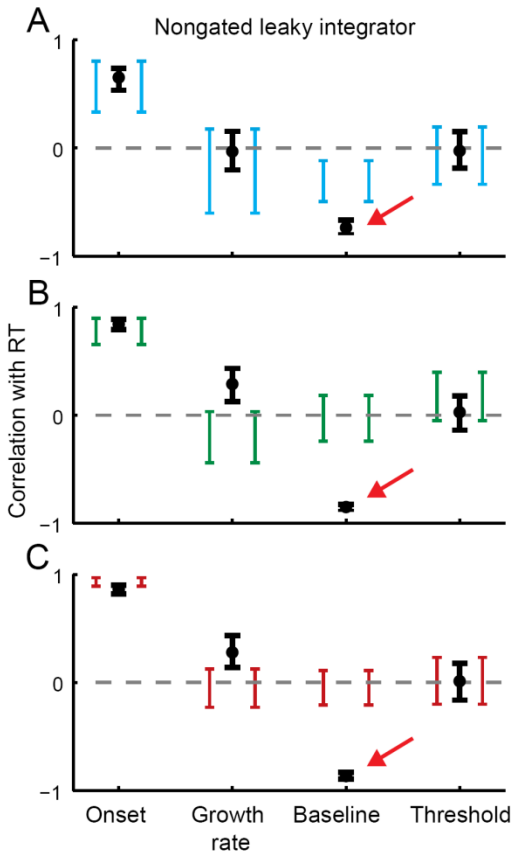

Figure 3.11: Models with no gate fail to predict observed movement neuron dynamics. Observed (brackets) and predicted (points) median correlation between response time and four measures of neural dynamics for set size 2 (**A**), 4 (**B**), and 8 (**C**). Brackets and error bars are 95% confidence intervals around the observed and predicted median correlation, respectively (bootstrap, 1000 simulations). Red arrows highlight the key difference between the predicted and observed baseline correlation with RT (see also Purcell et al., 2010).

3.4.5 Control of speed-accuracy tradeoff

Most stochastic accumulator models assume that adjustments in speed and accuracy are controlled via adjustments in the height of the response threshold (Gold and Shadlen, 2002; Bogacz et al., 2006; Lo and Wang, 2006; Nakahara et al., 2006; Simen et al., 2006; Ratcliff and McKoon, 2008). However, no current study has reported changes in threshold firing rate at the level of individual neurons, and in fact, recent neurophysiological evidence indicates that systematic adjustments of RT are accomplished through changes in the onset of accumulation (Pouget et al., 2011). We found that the gated accumulator model produces a speed and accuracy

tradeoff when either threshold or gating inhibition is varied. Rather than fit parameters to data as in the preceding section, we manipulated the level of the threshold or the gate while fixing all other parameters at values fitted to pooled search performance. When the threshold increases, the system is more likely to correctly locate and respond to the target, but requires more time to accumulate additional salience (Figure 3.12A, inset). When the gate increases, visual salience is processed to a higher resolution before it begins to drive saccade initiation (Figure 3.12B, inset; see Figure 3.2B). Thus, gating inhibition provides an alternative account for trade-offs between speed and accuracy during visual search.

Mechanisms that trade speed for accuracy should optimize behavior. As one measure of optimization, we computed the expected reward rate as a function of threshold and gate. Consistent with previous studies, we found that varying threshold produced a non-monotonic change in the expected reward rate such that a range of threshold values maximized reward (Figure 3.12A). However, we also found that systematically varying the level of the gate produced a non-monotonic change in reward rate (Figure 3.12B). Furthermore, the value of threshold and gate that best fit the monkey's performance fell within the range of parameter values that maximized reward rate. This suggests that after extensive practice, the circuitry of the network responsible for visual search performance adapted precisely to optimize performance.

Monkeys could strategically adjust their performance via adjustments in threshold or gating, but the alternative mechanisms are indistinguishable in terms of both maximal reward rate and robustness to parameter variation. However, the alternative mechanisms make clearly distinguishable predictions about how movement neuron dynamics should change when monkeys emphasize speed or accuracy. Increases in threshold will obviously increase the presaccadic firing rate of neurons (Figure 3.12C), whereas increases in gating will decrease the baseline and delay the beginning of accumulation of activity leading to the saccade (Figure 3.12D). New data from tasks in which animals are explicitly cued to trade speed and accuracy can be incorporated into our modeling framework to discriminate these alternative mechanisms.

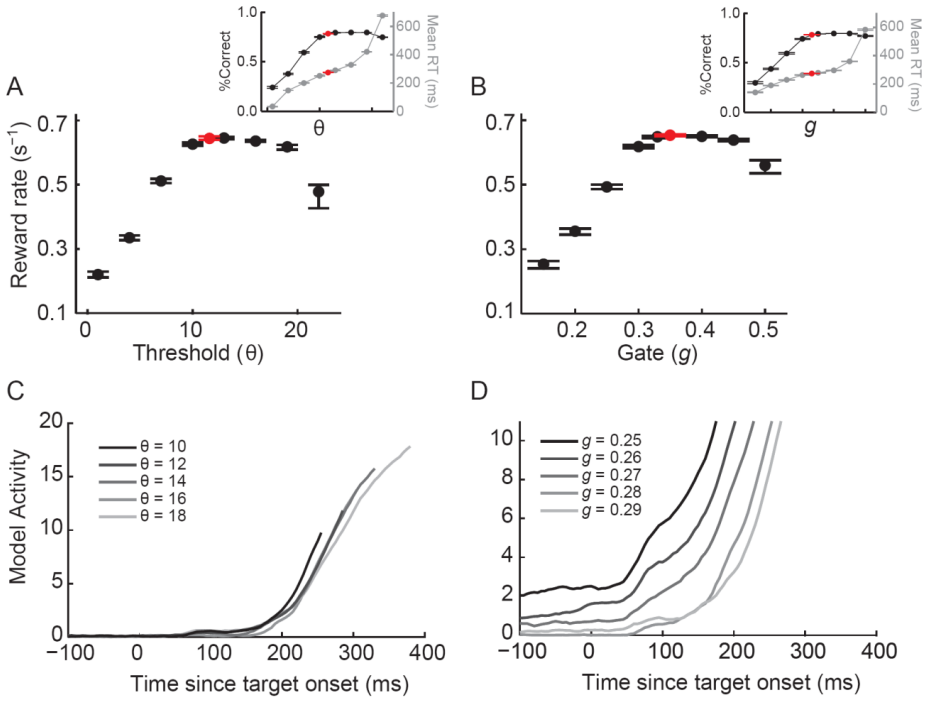

Figure 3.12: Threshold and gating inhibition can explain speed-accuracy tradeoffs. **A**,**B**, Mean expected reward rate as a function of the threshold (**A**) and gate (**B**) values when other parameters are fixed at the values which best fit the pooled search performance. Insets show simulated mean percent correct (black) and RT (gray) corresponding to the parameter values used to simulated the reward rates in A and B. Each point is calculated by a simulated session with 700 trials per set size, which approximates the average number of trials recorded per session. Error bars are 95% confidence intervals around the mean which may be asymmetric due to skewed distributions (bootstrap, 1000 simulations). The red points show expected reward rate using parameters which best fit the animal's performance. **C**,**D**, Gated accumulator dynamics for threshold (**C**) and gate (**D**) spanning a range of reward rates. Each trajectory reflects the average of 1000 simulated trajectories for a given set of parameters. As threshold increases, the accumulation begins at the same time, but reaches progressively higher levels. As gate increases, baseline activity decreases and accumulation begins rising later.

3.5 Discussion

We formalized and tested a model of visual search comprised of a network of gated, competing units that accumulate a dynamic salience representation. The model accounts for the probabilities and RTs of correct and error saccades and also replicates the dynamics of presaccadic movement neurons by identifying them with the process of accumulating salience. The model also provides a new perspective on the mechanism for speed-accuracy adjustments.

3.5.1 A neurophysiologically-constrained account of visual search

Visually responsive neurons in FEF, LIP, and SC have been identified as a neurophysiological salience map (Findlay and Walker, 1999; Thompson and Bichot, 2005; Fecteau and Munoz, 2006; Gottlieb, 2007; Bisley and Goldberg, 2010) because these neurons modulate their firing rate according to both physical properties of the stimuli in the display (Bichot and Schall, 1999b; Ipata et al., 2006; White and Munoz, 2011), reflecting bottom-up salience, as well as variables which determine the significance of a stimulus such as its expected reward (Ding and Hikosaka, 2006) or stimulus history (Bichot et al., 1996; Bichot and Schall, 1999a, 2002; Sato et al., 2003), reflecting top-down salience. This salience representation does not depend on response or effector (Thompson et al., 1997; Bisley and Goldberg, 2003; Sato and Schall, 2003; Gottlieb et al., 2005; Thompson and Bichot, 2005; Murthy et al., 2009; White and Munoz, 2011).

Rather than assuming some model of the salience map endowed with properties that might predict search performance, we used the salience representation provided by visually-responsive neurons in FEF to investigate the mechanisms sufficient to translate the salience map into a saccade. We found that gated integration with lateral inhibition is sufficient. This is the first model to explicitly link the neural representation of salience to a multiple-alternative stochastic accumulator network. Some previous search models include stochastic accumulation, but these have only been formulated conceptually (Wolfe, 2007) or are not grounded in physiology (Ward and McClelland, 1989; Thornton and Gilden, 2007). We previously modeled correct search RTs using a simple two-unit accumulator network (Purcell et al., 2010). This preliminary model accounted for systematic variation of RT with search efficiency, but the data set was insufficient to investigate error rates or set size effects; therefore, it was not a viable model of visual search. The substantial behavioral and neurophysiological data afforded by the data set modeled here impose substantially greater model constraint.

We found that gating inhibition is necessary to limit the accumulator input until explicit visual salience is present. Many models assume a static salience representation (Palmer et al., 2000; Navalpakkam and Itti, 2007), but the neural representation of salience evolves dynamically over time (Figure 3.3A). In our model, saccade preparation cannot begin until the visual response exceeds the gate and an informative salience signal evolves (Figure 3.2B). This mechanism contrasts with all previous stochastic accumulator models that require the *ad hoc* assumption that accumulation is simply delayed by an arbitrary non-decision time parameter (Lo and Wang, 2006; Ratcliff et al., 2007; Churchland et al., 2008; Stanford et al., 2010). Other work has demonstrated that balanced excitation and inhibition can delay the onset of accumulation (e.g., Furman and Wang, 2008), but such a system can be susceptible to perturbations that can disrupt stability leading to premature threshold crossings.

3.5.2 Extending perceptual decision tasks to multiple stimuli

Several frameworks have been proposed to explain perceptual decisions about individual stimuli and many include discrete or continuous networks of accumulators (Usher et al., 2002; Beck et al., 2008; Churchland et al., 2008; Furman and Wang, 2008; Ditterich, 2010; Leite and Ratcliff, 2010). Some of these models refer to how visually-responsive LIP and FEF neurons integrate the firing rates of neurons encoding visual features to categorize information from a single foveal stimulus (Roitman and Shadlen, 2002; Ding and Gold, 2011). However, a general theory of perceptual decision making must explain more complex conditions involving multiple stimuli; not just multiple responses. These models identify the same visually-responsive neurons that encode salience with accumulators that signal the end of stimulus categorization when discharge rates reach a fixed threshold. However, the dynamics of these neurons are markedly different during search tasks where one or more stimuli appear abruptly in the RF of the neuron and must be categorized and selected to guide response selection. The initial visual response often exceeds the presaccadic firing rate and these neurons do not reach a fixed threshold prior to

saccade initiation (Figure 3.3A; Hanes et al., 1998; Brown et al., 2008). Therefore, we propose a new framework to account for neural dynamics and search performance.

According to this framework, visual neurons in FEF, SC, and LIP have already integrated and reweighted sensory inputs according to task demands before being input to the accumulator network. This interpretation is consistent with cognitive models of perceptual decision making in which perceptual processing precedes the start of the accumulation process to determine the degree of support for a particular response (Nosofsky and Palmeri, 1997; Logan, 2002). This interpretation also highlights the distinct role of different populations of neurons in decision making. While the decision that a stimulus belongs to a particular category could be identified with selection of the target location by visually-responsive neurons in FEF, SC, and LIP, the decision to act requires additional processing by movement-related neurons (Schall, 2001). Our model formalizes this distinction.

3.5.3 Strategic adjustments in speed and accuracy

Threshold adjustments seem to provide a simple and intuitive account of speed-accuracy tradeoffs. However, we found that variation of gating inhibition can produce equivalent speed-accuracy tradeoffs by either promoting or delaying the accumulation of salience as has been observed in another study (Pouget et al., 2011). This model predicts that changes in gating inhibition will produce a qualitatively different pattern of movement neuron dynamics than changes in threshold when tested during speed-accuracy tradeoffs. This also suggests that a neuron which implements the gating inhibition will modulate its firing rate inversely with speed-stress.

Other recent models have indicated that speed-accuracy tradeoffs can be implemented by a time-varying multiplicative gain or “urgency” signal applied to the inputs to stochastic accumulators (Churchland et al., 2008; Cisek et al., 2009). Increasing noise and variance are intrinsic properties of our neurophysiologically-derived model input (Figure 3.2B). Our model

predicts that this could take place via changes in the firing rates of visually-responsive neurons without assuming an explicit multiplicative gain parameter. Altogether, our model makes clear predictions to discriminate alternative accounts of the neural basis of speed-accuracy tradeoffs.

3.5.4 Neurophysiological implications

FEF, SC, and LIP neurons have anatomical connectivity to perform the functions proposed by our model. These areas receive inputs from diverse regions of extrastriate visual cortex and prefrontal areas to compute stimulus salience (e.g., Blatt et al., 1990; Lui et al., 1995; Schall et al., 1995a). Neurons representing visual salience reside in both supragranular and infragranular layers of FEF (Thompson et al., 1996) and intermediate layers of SC (White and Munoz, 2011). Movement neurons reside in layer 5 of FEF and the intermediate layers of SC and project to oculomotor brainstem nuclei that control saccade initiation (Moschovakis et al., 1988; Segraves, 1992). Visually-responsive LIP neurons could drive SC and FEF movement neurons to threshold via known projections (Blatt et al., 1990; Pare and Wurtz, 2001). The constant presaccadic firing rate observed in FEF and SC movement neurons may correspond to the fixed degree of excitation necessary to tip the balance from gaze-holding to gaze-shifting via excitation of long-lead burst neurons and inhibition of omnipause neurons (Munoz et al., 2000; Scudder et al., 2002).

Our model assumes that a gating mechanism intervenes between visually-responsive and movement neurons. Gating inhibition is a simple operation that can be realized through several different neural mechanisms. First, gating could be implemented by inhibitory interneurons within FEF and SC that can adjust the level of excitation necessary to initiate spiking in individual neurons (Somogyi, 1977; Markram et al., 2004). Simple neural networks that balance interneuron inhibition with self-excitation exhibit bistable dynamics that limit integration until inputs exceed a critical level (e.g., Simen and Cohen, 2009). Second, gating could be mediated by FEF and SC fixation neurons, which fire tonically during fixation but cease firing prior to a saccade at a time coinciding with the onset of movement neuron firing across conditions (Munoz

and Wurtz, 1993; Everling et al., 1998; Hanes et al., 1998). Finally, gating inhibition could also be implemented via basal ganglia circuitry as posited by other models (Brown et al., 2004; Frank, 2006). FEF neurons project to the caudate nucleus which sends inhibitory projections to the substantia nigra pars reticulate (SNpr; Hikosaka et al., 2000). SNpr neurons cease firing around the time of target selection during search (Basso and Wurtz, 2002). SNpr sends direct projections to SC and also to the mediodorsal (MD) and ventroanterio (VA) nuclei (Parent and Hazrati, 1995); thalamic nuclei with saccade-related responses (Tanaka, 2007) and reciprocal connections with FEF (Huerta et al., 1987).

3.5.5 Conclusions

We showed that a feed-forward cascade of salience into a network of multiple competing stochastic accumulators can account for visual search performance and replicate the dynamics of presaccadic movement neurons activity. By forgoing the details of spike generation in exchange for the ability to relate specific network mechanisms to comprehensive behavioral data, this approach allowed us to reject plausible model architectures and identify key mechanisms necessary and sufficient to explain how the brain decides among multiple stimuli. We can further test our model's premise of a feed-forward visual-to-motor cascade by using visually-responsive neuron physiology recorded in the context of additional tasks as model input to our framework. Factorial manipulations of search efficiency and set size, variations in stimulus-response mapping, and tasks in which animals are cued to trade speed for accuracy will provide critical tests of the basic model assumptions.

CHAPTER IV

RESPONSE VARIABILITY OF FRONTAL EYE FIELD NEURONS MODULATES WITH SENSORY INPUT AND SACCADE PREPARATION BUT NOT VISUAL SEARCH SALIENCE

4.1 Abstract

Discharge rate modulation of frontal eye field (FEF) neurons has been identified with a representation of visual search salience (physical conspicuity and behavioral relevance) and saccade preparation. We tested whether salience or saccade preparation are evident in the trial-to-trial variability of discharge rate. We quantified response variability via the Fano factor in FEF neurons recorded in monkeys performing efficient and inefficient visual search tasks. Response variability declined following stimulus presentation in most neurons, but despite clear discharge rate modulation, variability did not change with target salience. Instead, we found that response variability was modulated by stimulus luminance and the number of items in the visual field independent of attentional demands. Response variability declined to a minimum before saccade initiation and pre-saccadic response variability was directionally tuned. In addition, response variability was correlated with the response time of memory-guided saccades. These results indicate that the trial-by-trial response variability of FEF neurons reflects saccade preparation and the strength of sensory input, but not visual search salience or attentional allocation.

4.2 Introduction

Visually-responsive neurons in the frontal eye field (FEF) have been identified with a map of visual *salience* (Thompson and Bichot, 2005). By salience we refer to the representation guiding the allocation of attention and gaze; some use the term *priority* (Bisley and Goldberg, 2010). The mean discharge rate of these neurons varies with the physical-conspicuity (bottom-up

salience; Bichot and Schall, 1999a; Sato et al., 2001; Cohen et al., 2009b) and behavioral relevance (top-down salience; Thompson et al., 1996; Bichot and Schall, 2002) of items in their response field (RF), regardless of whether a saccade is executed to the RF (Thompson et al., 1997; Thompson et al., 2005a; Murthy et al., 2009). In addition, saccade-related neurons in FEF have been identified with saccade preparation (Bruce and Goldberg, 1985; Hanes and Schall, 1996; Boucher et al., 2007; Murthy et al., 2009; Purcell et al., 2010; Purcell et al., 2012b). The mean discharge rate of these neurons increases to a fixed threshold immediately prior to saccades (Hanes and Schall, 1996; Hanes et al., 1998). Thus far, the identification of FEF neurons with visual salience and saccade preparation is based entirely on changes in mean discharge rate.

Recent studies have demonstrated that the trial-by-trial variability of cortical neurons may be modulated by the behavioral relevance of objects in their RF. Response variability of V4 neurons declines with attention to an RF stimulus (Mitchell et al., 2007; Cohen and Maunsell, 2009). Reduced firing variability of neurons representing behaviorally relevant stimuli could improve the reliability with which a search target is discriminated and thereby improve search performance (Palmer et al., 2000). In FEF, neuronal response variability declines following stimulus onset, but is not maintained in the absence of sensory input and the magnitude of the visually-evoked decline does not depend on whether or not the animal was cued to attend to the RF stimulus (Chang et al., 2012). A previous study from this laboratory reported that response variability of FEF neurons did not distinguish targets from distractors in distinct time intervals (Bichot et al., 2001b), but the time course of response variability during visual search has never been systematically examined under differing attentional demands.

Other investigators have suggested that trial-by-trial variability can be a signature of motor preparation. Response variability in pre-motor cortex declines following presentation of a reach target and reaches a minimum immediately prior to arm movements (Churchland et al., 2006). Similar declines in variability prior to saccades have been reported in V4 (Steinmetz and Moore, 2010) and LIP (Churchland et al., 2011). If FEF neurons initiate saccades at a response

threshold, as suggested by discharge rate modulation, then variability should be minimal at saccade initiation. It is not known whether the response variability of FEF neurons declines in a manner consistent with this model.

We computed the time-varying Fano factor as an index of response variability in FEF neurons recorded from monkeys performing a visual search task. If the response variability of FEF neurons depends on visual salience, then Fano factor should be modulated by the behavioral relevance and physical conspicuity of an RF stimulus. If response variability of FEF neurons depends on motor preparation, then Fano factor should decline to a minimum prior to saccade initiation. In addition, we would expect Fano factor to vary according to saccade direction and correlate with response time (RT).

4.3 Materials and Methods

4.3.1 Behavioral tasks and recordings

We recorded single-unit spiking from the FEF of three macaques (*Macaca mulatta*). Monkeys were surgically implanted with a head post, a subconjunctive eye coil, and recording chambers during aseptic surgery under isoflurane anesthesia. Antibiotics and analgesics were administered postoperatively. All surgical and experimental procedures were in accordance with the National Institute of Health *Guide for the Care and Use of Laboratory Animals* and approved by the Vanderbilt Institutional Animal Care and Use Committee.

Neurons were recorded from both hemispheres of all monkeys using tungsten microelectrodes (2-4 MΩ, FHC) and were referenced to a guide tube in contact with the dura. All FEF recordings were acquired from the rostral bank of the arcuate sulcus at sites where saccades were evoked with low-intensity electrical microstimulation (<50 μA; Bruce and Goldberg, 1985). Spikes were sampled at 40 kHz. Waveforms were sorted online using a time-amplitude window discriminator and offline using principal component analysis and template matching (Plexon). Eye position was recorded at a sampling rate of 1kHz.

The monkeys performed visual search tasks of varying difficulty. Each monkey performed a subset of three variants of a search task in which either set size or target-distractor similarity was manipulated. Basic analyses of these data have been published previously (Sato et al., 2001; Cohen et al., 2009b; Purcell et al., 2010; Purcell et al., 2013).

In the first search task (Figure 4.1A), monkey F searched for a target (green or red disk) among seven distractors. Each trial began with the monkey fixating a central spot for ~600ms. A target was then presented at one of eight isoeccentric locations equally spaced around the fixation spot (8-10^{o} eccentricity). The other seven locations contained distractor stimuli. Search efficiency was varied randomly across trials by manipulating target-distractor similarity. For efficient search, distractors were red or green disks for green or red targets, respectively. For inefficient search, distractors were yellow-green disks for green targets. The monkey was rewarded for making a single saccade to the target and fixating it for ~400ms.

In the second search task (Figure 4.1B), monkeys Q and S searched for a target (T or L rotated 0^{o}, 90^{o}, 180^{o}, or 270^{o}) among distractors (rotated L or T). Each trial began with the monkey fixating a central spot for ~600ms. A target was then presented at one of eight isoeccentric locations equally spaced around the fixation spot (8-10^{o} eccentricity). The number of distractors varied randomly across trials (set size 2, 4, or 8). Stimuli were always arranged in diametrically opposite locations. The target and distractor identities remained constant throughout a session and target identity was varied across sessions. The monkey was rewarded for making a single saccade to the location of the target within 2000 ms of array onset and fixating the target for 500 ms.

In the third search task (Figure 4.1C), monkeys Q and S searched for a color target (green or red disks) among one, three, or seven distractors of the other color. The experimental protocol was otherwise identical to the form search. The form search task was considered inefficient search and the color pop-out search task was considered efficient search based on behavioral patterns (see Results).

All monkeys performed a memory-guided saccade task to distinguish visual- from saccade-related activity (Hikosaka and Wurtz, 1983; Bruce and Goldberg, 1985). The target (filled gray circle) was presented without distractors for 80-150 ms. Monkeys were required to maintain fixation for 500-1000 ms after target onset. After the fixation point changed from filled to open, the monkeys were rewarded for making a saccade to the remembered location of the target and maintaining fixation for ~500ms. For monkeys Q and S, the target luminance was varied randomly across trials (0.01 to 8.05 cd/m^2). Unless otherwise stated, we used only trials in which target luminance was ≥0.99 cd/m^2 for basic analyses of this task because discharge rate and Fano factor varied little above this range.

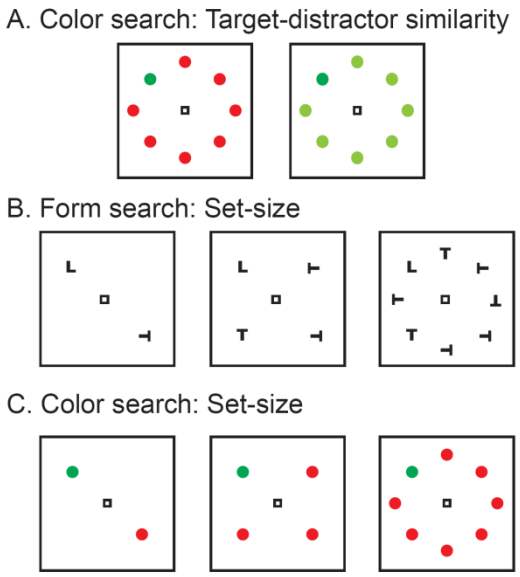

Figure 4.1 Color and form visual search tasks. After fixating for a variable delay, a search array appeared consisting of a target and distractors. Monkeys were trained to make a single saccade to the location of the target for reward. **A**, Color search task with target-distractor similarity manipulation. Monkey F searched for a green or red target. Target-distractor similarity varied across trials. Target color varied across sessions. **B**, Form search task with set size manipulation. Monkeys Q and S searched for a rotated L among Ts or T among Ls. Set size varied across trials (2, 4, and 8 stimulus). Target identity was consistent within a session. Stimuli were arranged such that one distractor was always diametrically opposite the target location. **C**, Color search task with set size manipulation. Monkeys Q and S searched for a green or red target among red or green distractors, respectively. The task was otherwise identical to the form search task.

4.3.2 Data analysis

For the search task, discharge rate and Fano factor were analyzed by sliding a 50 ms window in 10 ms steps across the spike train data. We verified that all visual search results were statistically identical using window sizes ranging from 10 to 150 ms. We used a larger window of 150 ms for the memory-guided saccade task because the average number of trials per condition (34 trials) was substantially less than search (110 trials). This provided additional smoothing at the expense of temporal smearing.

The discharge rate was calculated as the spike count in each time bin divided by the length of the window. The Fano factor was calculated as the ratio of the variance to the mean of spike counts across trials within each time bin. Discharge rate and Fano factor were computed separately for each individual neuron, search condition, and stimulus in RF and then averaged across neurons. Trials with incorrect responses were excluded from neural analyses. Time bins in which the mean discharge rate was 0 were excluded from the average. Only well-isolated neurons in which the waveform and average discharge rates were stable across the recording session were included. Unless otherwise noted, all units were included for analysis regardless of whether task-related modulations were observed. Results were identical whether or not nonmodulated neurons were included.

The center of the RF was determined by vector summation of the normalized response to each target location during the memory-guided saccade task. The angle of the resultant vector gave the preferred response location. To be conservative, we considered locations within 45^{o} of the preferred angle to be inside the RF, which is slightly smaller than the average RF width at 10^{o} eccentricity (~51^{o})(Purcell et al., 2012a). We verified that our results do not depend greatly on the exact size of the RF. Trials were sorted according to whether the target appeared inside the RF or diametrically opposite to the RF center. This ensured that at least one stimulus was present in the RF on every analyzed trial even when set size was <8.

Discharge rate and Fano factor modulations were assessed using identical statistical methods. To assess significant deviations from baseline, we compared discharge rate and Fano factor at each time bin to the average activity -100 to 0 ms relative to array onset (Wilcoxon rank-sum test, $p < 0.01$). The *visual latency* was defined as the time bin when activity first diverged from baseline and remained significantly different for 5 consecutive time bins. Discharge rate and Fano factor in each bin were computed from spike counts in a window as described above. To assess target and saccade-direction selectivity, we compared the discharge rate and Fano factor when the target or distractors were inside the neurons' RFs (Wilcoxon rank-sum test, $p < 0.01$). The *selection time* was defined as the time bin when activity first significantly diverged and remained significantly different for 5 consecutive bins. We used a bootstrapping procedure to compute standard error and confidence intervals. We randomly sampled, with replacement, 1000 times from our population of neurons, computed the visual latency and selection time for each sample, and estimated the standard error and confidence intervals directly from the resulting distribution.

In addition to bin-by-bin statistical comparisons, we also analyzed discharge rate and Fano factor in three key epochs. For spike times relative to stimulus presentation, we defined the *post-stimulus* period as the time interval from 100 ms after array onset until 100 ms before mean saccade response time for each neuron. This epoch was computed separately for each neuron, but fixed across trials. We used this epoch to analyze the earliest period of visual selection that followed the initial non-selective visual response, but preceded saccade initiation. This epoch corresponds approximately to the earliest times at which the target location can first be discriminated in individual FEF neurons (e.g., Thompson et al., 1996; Cohen et al., 2009b). Results were statistically identical using a more conservative window 100 to 150 ms relative to array onset for all neurons, which excluded saccades from all but ~1% of trials. For spike times relative to saccade, we defined the *pre-saccade* period as the time interval from 50 to 0 ms before saccade initiation. We used this epoch to analyze the state of motor preparation immediately

prior to saccade. This epoch allowed us to evaluate models of saccade preparation that predict reductions in variability before saccades of a particular direction (e.g., stochastic accumulator models). Results were statistically identical using a larger window of 100 to 0 ms before saccade initiation. During the memory-guided saccade task, we also analyzed the *pre-cue* interval -200 to 0 ms before cue (fixation point offset). We used this epoch to analyze spatial maintenance and motor preparation during the memory delay. Note that our selection of time epochs is not intended to imply serial processing of covert attention and saccade processing; rather, the two processes probably overlap temporally (Purcell et al., 2010; Purcell et al., 2012b).

To assess the effect of luminance on discharge rate and Fano factor, we divided responses according to target location and luminance for neurons recorded during the memory-guided saccade task. We grouped trials into three groups according to luminance (Low: 0.01 to 0.6 cd/m^2; Medium: 0.20 to 1.00 cd/m^2; High: 1.70 to 5.00 cd/m^2). These groupings were chosen such that the average number of trials per condition was sufficiently large and approximately equal across groups (~25 trials). We computed the slope of the least squares regression line for discharge rate and Fano factor in the post-target interval as a function of median luminance value for each group. It is likely that more complex nonlinear functions better explain the relationship between luminance and discharge rate or Fano factor (Albrecht and Hamilton, 1982), but we did not have sufficient data to more precisely quantify the relationship. Hence, our goal is only to show that discharge rate and Fano factor in FEF are monotonically modulated by stimulus luminance across the range of tested values. We used a 50 ms window when computing the visual latency of mean discharge rates for improved temporal resolution.

To assess the effect of set size on discharge rate and Fano factor, we divided responses according to search condition and stimulus in receptive field. We averaged discharge rate and Fano factor across time bins for each set size in a running window (±20 ms, four time bins) incremented in time steps of 10ms. The window moved from array onset until 50 ms before mean saccade response time for set size 2 to avoid comparisons across set sizes before and after

saccades had been initiated. At each time step, we computed the slope of the least squares regression line for discharge rate and Fano factor as a function of set size and assessed the statistical significance ($p < 0.01$). We also report the mean discharge rate and Fano factor in the window 50 to 125 ms following target onset because the strongest changes in response variability were observed in this early visual epoch.

We classified FEF neurons as visually-responsive or saccade-related based on responses during the memory-guided saccade task. We computed a visuomovement index (VMI) for each neuron as follows:

$$\frac{\quad}{\quad},$$

where V is the average discharge rate 50 to 200 ms following target onset and M is the average discharge rate 50 to 0 ms prior to saccade. The VMI is 1 for neurons with only visual responses and -1 for neurons with only saccade-related responses. To be classified as visually-responsive, the VMI must be greater than 0 and the discharge rate of a neuron must be significantly greater than baseline (-100 to 0 ms) following target onset (50 to 200 ms; Wilcoxon rank-sum test, $p < 0.01$). To be classified as saccade-related, the VMI must be less than 0 and the discharge rate must be significantly greater than baseline immediately prior to saccade (-50 to 0 ms). We also analyzed the subset of pure visual neuron with significant modulation in the post-stimulus epoch, but no significant modulation in the pre-saccadic epoch. Neurons without significant modulation in either epoch were considered nonmodulated.

We quantified spatial tuning by dividing discharge rate and Fano factor by distance from RF center (in polar angle) and averaging across neurons and search conditions. RF center was defined as the stimulus location closest to the neuron's preferred response location. We fit the average discharge rate or Fano factor as a function of target location with a Gaussian function of the form:

$$\frac{\quad}{\quad},$$

where activation (A) as a function of polar angle ( ) depends on the baseline (B), maximum/minimum response (R), optimum direction ( ), and directional tuning ( ) (Bruce and Goldberg, 1985; Schall et al., 1995b). Tuning width was estimated by the standard deviation ( ) of the best fitting Gaussian curve. Previous reports have demonstrated that some neurons exhibit flanking suppression (Schall et al., 1995b; Schall et al., 2004), which is best explained by a Difference-of-Gaussian function, but we found that the simpler Gaussian function accounted for most of the variance in the epoch of interest (all $R^2 > 0.95$). The data were fitted with a Simplex routine (Nelder and Mead, 1965) implemented in MATLAB (fminsearch.m) to minimize the sum of squared deviations between observed and predicted values. Fitting was repeated 20-30 times with different initial points to prevent settling in local minima. We used nonparametric bootstrapping to compare estimated tuning width for discharge rates and Fano factor (Efron and Tibshirani, 1993; Wichmann and Hill, 2001). We randomly sampled, with replacement, from the set of neurons and fit the Gaussian function to the data 500 times. Standard error and confidence intervals were determined from the resulting tuning width distribution.

We used a mean-matching procedure to control for a possible effect of discharge rate on Fano factor. This procedure has been described in detail elsewhere (Churchland et al., 2010). Briefly, the mean spike count was determined for each time bin, search condition, and stimulus in RF. The algorithm determined a common distribution of mean spike counts (but not variances) that can be found at all time points and for each stimulus-in-RF condition. We randomly eliminated mean counts from a given neuron and condition until a common distribution was achieved at each time point for both RF stimuli. The Fano factor was then computed at each time point using only the data points remaining in this common distribution. The process was repeated 10 times and averaged to control for variation due to random sampling. We independently mean-matched data aligned on target onset and saccade. We performed this analysis using the Variance

Toolbox for MATLAB (Churchland et al., 2010 http://www.stanford.edu/~shenoy/GroupCodePacks.htm).

To assess the relationship between Fano factor and RT, we divided trials into short RT and long RT according to whether they were faster or slower than the median RT, respectively. This analysis was only performed on neurons recorded during the memory-guided saccade task because short RTs during visual search made it impossible to distinguish whether variation in Fano factor preceded the earliest eye movements. Trials were divided into RT groups individually for each neuron and target location so these factors were not confounded across groups. We excluded the lower 10^{th} and upper 90^{th} percentiles to exclude unusually short and long RTs. RTs <100 ms were considered anticipatory and excluded from analysis.

4.3.3 Accumulator model simulations.

We implemented a simple accumulator model to compare with observed neurophysiology. The model was governed by the following differential equation:

– .

The model input, *I*, was set to baseline, *z*, until array onset plus some afferent delay, T_r, at which point it increased by an amount sampled from a Gaussian distribution with mean, *v*, and standard deviation η. RT was given as the time when activation, *X*, reached a fixed threshold, *a*, at which point *I* was reduced to baseline. The parameters, *z*, *v*, η, and *a*, were set to 0.2, 1.7, 0.1, and 155, respectively, to predict a distribution of RTs similar to that observed during our visual search tasks. All simulations began 500 ms prior to array onset to establish a stable baseline. We fixed T_r to 50 ms to account for afferent delays (Schmolesky et al., 1998; Pouget et al., 2005). The time constant, , was fixed at 100 ms. All simulations used an integration time step of dt = 1 ms.

We simulated 110 trials for 304 simulated neurons to match the statistical power of the experimental data. For each simulated neuron, we rescaled the parameters z, v, η, and a by a value sampled from a uniform distribution ranging from 0.8 to 1.2 to account for variability in average discharge rate across the population. For each simulated trial, we generated spike times according to a time-inhomogeneous Poisson process with mean rate given by the model dynamics for that simulation. Spike counts were binned across time, and mean discharge rate and Fano factor were computed exactly as described above for experimental data.

4.4 Results

Three monkeys performed variants of a visual search task requiring a single saccade to a target among distractors. Basic behavioral data have been described previously (Sato et al., 2001; Cohen et al., 2009b; Purcell et al., 2013). Monkey F performed a color search task in which search efficiency was varied randomly across trials by manipulating target-distractor similarity (Figure 4.1A). Mean RTs (±SE) were faster during efficient search (208 ± 16.8 ms) relative to inefficient search (251 ± 16.3 ms; $p < 0.001$; Wilcoxon signed-rank test). Percent correct was also higher during efficient (94 ± 1.2) relative to inefficient search (71 ± 1.2). Monkeys Q and S performed an inefficient form search task in which set size was varied across trials (Figure 4.1B). The search slope (RT by set size) was steep for both monkey Q (23 ± 1.6; $p < 0.001$; linear regression slope coefficient) and monkey S (11 ± 1.4; $p < 0.001$), confirming that the form search task is attentionally demanding. Monkeys Q and S also performed an efficient pop-out color search task in which set size was varied randomly across trials (Figure 4.1C). The search slope was shallow for both monkey Q (2 ± 0.8; $p < 0.01$) and monkey S (1 ± 1.0; $p = 0.51$), and significantly lower than form search for both monkeys (both $p < 0.001$; linear regression; set size and task interaction coefficient), confirming that attentional demands for the pop-out color search task are minimal. These behavioral patterns are consistent with well-established patterns of

efficient and inefficient search in humans (Duncan and Humphreys, 1989; Wolfe, 1998) and monkeys (Bichot and Schall, 1999b).

4.4.1 FEF response variability does not reflect behavioral relevance or physical conspicuity

We recorded activity from 304 FEF neurons while monkeys performed the visual search tasks. Of those, 133 neurons were recorded during singleton color search in which search efficiency varied randomly across trials (Monkey F; Figure 4.1A). Ninety-three neurons were recorded during an attentionally-demanding inefficient form search (59 from monkey Q, and 34 from monkey S; Figure 4.1B). Seventy-eight neurons were recorded during a pop-out color search (44 neurons from monkey Q, and 34 neurons from monkey S; Figure 4.1C). Our initial analyses use the full population of 304 neurons.

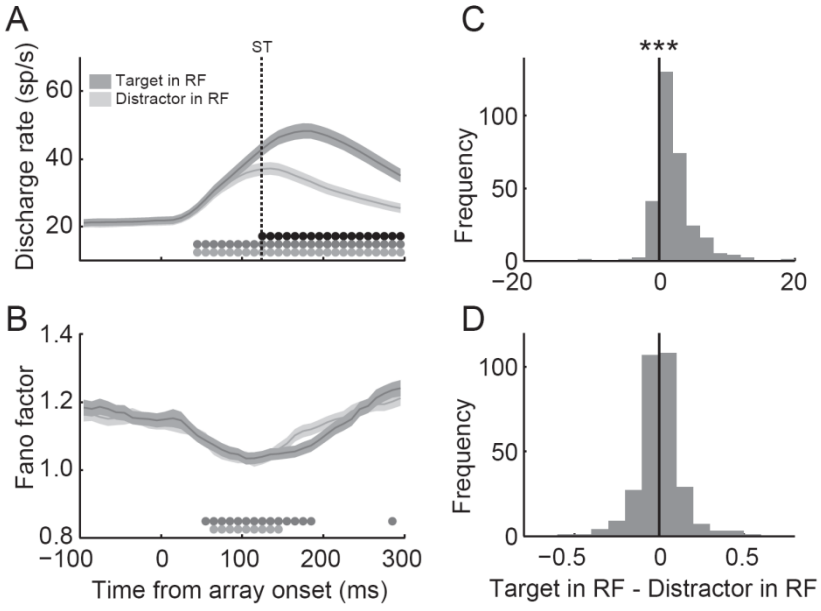

Figure 4.2 Temporal dynamics of discharge rate and Fano factor aligned on array onset for the full population of 304 neurons during all visual search tasks. **A**, Mean discharge rate (lines) and ±SE (shading) was computed in a 50 ms sliding window separately for trials in which the target or a distractor was in the RF. Gray dots indicate significance from baseline (100 ms before array onset) in steps of 10 ms when the target (dark gray) or distractors (light gray) were in the RF (Wilcoxon ranked-sum test, $p < 0.01$). Black dots indicate significant differences between discharge rates when the target or distractor were in the RF. The dotted vertical line indicates the selection time (ST), which is the time when the distribution of discharge rates for trials in which the target versus distractor were in the RF first diverged significantly for 5 consecutive time bins. **B**, Mean Fano factor computed in same analysis windows as described above. There is no ST labeled because the distribution of Fano factors for trials in which the target versus distractor were in the RF never significantly diverged. The brief, but non-significant separation around ~190ms can be attributed to saccade initiation. **C**, Distribution of differences in discharge rate when the target or a distractor was in the neurons' RFs computed in the post-stimulus epoch 100 ms after array presentation until 100 ms before mean saccade response

time. Asterisks denote significant difference of mean value from 0 (Wilcoxon signed-rank test, *** denotes $p < 0.001$). **D**, Distribution of differences for Fano factor.

Figure 4.2 shows the average population discharge rate and Fano factor for trials in which a target or a distractor appeared in the RF of the neuron. The population discharge rate increases significantly above baseline following the onset of the array regardless of the behavioral relevance of the RF stimulus (Figure 4.2A). The latency of the response (±SE) was similar when a target (46 ± 7.7 ms) or distractor (47 ± 8.3 ms) was in the RF ($p > 0.05$, bootstrap, 1000 samples). Discharge rates are initially equivalent regardless of the stimulus in RF, but diverge over time to significantly discriminate the target location 127 ± 4.0 ms following array onset. This timing is consistent with estimates of selection time from individual neurons (Cohen et al., 2009b). We quantified the magnitude of selectivity across the population by computing the difference in discharge rate when the target or distractors were in a neuron's RF during the post-stimulus epoch 100 to 150 ms (Figure 4.2C). The population fired significantly greater on average when the target was in their receptive field (7 ± 0.6 sp/s; $p < 0.001$, Wilcoxon signed-rank test). This observation was consistent across search tasks and monkeys (Table 4.1). These results demonstrate the classic observation that the discharge rates of FEF neurons select the location of behaviorally relevant objects irrespective of stimulus features (see Schall and Thompson, 1999 for review).

Table 4.1. Difference in mean discharge rate (DR) and Fano factor (FF) (±SE) for trials in which the target or distractors were in the RF.

	Post-array (100 to 150 ms)				Pre-saccade (-50 to 0 ms)			
Color search								
	Monkey F				Monkey F			
Efficient								
DR	11.30 ± 2.82	***			20.20 ± 4.48	***		
FF	0.01 ± 0.03				-0.06 ± 0.04			
Inefficient								
DR	3.40 ± 1.05	***			19.04 ± 3.93	***		
FF	0.05 ± 0.03	*			-0.08 ± 0.04	*		
Inefficient form search								
	Monkey Q		Monkey S		Monkey Q		Monkey S	
Set size 2								
DR	6.29 ± 0.98	***	12.65 ± 2.97	***	13.38 ± 2.00	***	26.20 ± 4.46	***
FF	-0.01 ± 0.04		-0.01 ± 0.04		-0.07 ± 0.04	*	-0.11 ± 0.05	**
Set size 4								
DR	4.57 ± 0.89	***	6.97 ± 2.02	***	17.77 ± 2.56	***	25.87 ± 4.11	***
FF	-0.05 ± 0.03		0.07 ± 0.10		-0.17 ± 0.04	***	-0.05 ± 0.07	*
Set size 8								
DR	3.56 ± 0.65	***	6.59 ± 2.29	**	19.13 ± 2.83	***	27.02 ± 4.33	***
FF	0.01 ± 0.04		0.04 ± 0.05		-0.09 ± 0.04	**	-0.15 ± 0.04	**
Efficient color search								
Set size 2								
DR	4.22 ± 0.89	***	4.41 ± 1.04	***	7.73 ± 1.25	***	11.82 ± 2.53	***
FF	-0.02 ± 0.03		0.02 ± 0.02		-0.04 ± 0.02	*	-0.07 ± 0.04	
Set size 4								
DR	3.81 ± 0.63	***	5.21 ± 0.82	***	7.29 ± 1.28	***	11.48 ± 2.42	***
FF	0.00 ± 0.02		-0.01 ± 0.03		-0.03 ± 0.02		-0.06 ± 0.03	*
Set size 8								
DR	4.34 ± 0.94	***	3.93 ± 0.98	***	8.92 ± 1.55	***	12.04 ± 2.53	***
FF	-0.02 ± 0.02		0.04 ± 0.03		-0.02 ± 0.03		-0.03 ± 0.03	

Figure 4.2B shows the average Fano factor computed using the same neurons, conditions, and time bins. The average baseline Fano factor for the population of neurons is 1.2 ± 0.03, which indicates slightly less regular spiking than a Poisson model (Fano factor = 1.0), and is similar to values observed in visual cortex (Dean, 1981; Tolhurst et al., 1983; Softky and Koch, 1993). The population Fano factor declines following the onset of the array regardless of RF stimulus. The latency of the decline was similar for targets (56 ± 11.9 ms) and distractors (62 ± 9.5 ms; $p > 0.05$; bootstrap, 1000 samples), and was not significantly different from the visual latency of mean discharge rate (both $p > 0.05$). This is consistent with previously reported declines in the Fano factor of FEF neurons following stimulus onset (Chang et al., 2012), which is commonly found in cortical neurons (Churchland et al., 2010). In contrast to the modulations in mean discharge rate, the magnitude of the post-array decline in Fano factor was equivalent for targets and distractors. There is a weak and fleeting divergence around 180 ms that never attains statistical significance and can be attributed to variability in the timing of saccades. The average post-stimulus difference in Fano factor when the target or distractors were in the neuron's receptive field was not significantly different from 0 (Figure 4.2D; $p = 0.74$). This observation was consistent across nearly every individual data set (Table 4.1). Only the Fano factor of neurons recorded from monkey F during inefficient search reached marginal significance, but the effect was opposite the expected direction (i.e., distractors were more reliably encoded than targets). Thus, response variability in FEF neurons declines following array onset, but does not distinguish behaviorally relevant targets from irrelevant distractors despite robust discharge rate modulation.

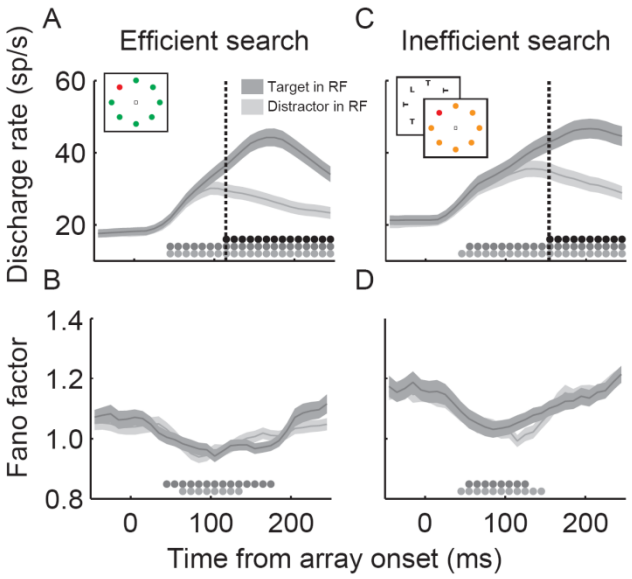

Figure 4.3 Temporal dynamics of discharge rate (top) and Fano factor (bottom) for efficient (left) and inefficient (right) search. Conventions as in Figure 4.2.

In addition to behavioral relevance, the discharge rate of FEF neurons varies with the physical conspicuity of objects in their receptive field (bottom-up salience; Bichot and Schall, 1999a). To test for an effect of physical conspicuity, we computed discharge rate and Fano factor separately for efficient and inefficient search. Only set size 8 trials were included to eliminate variability due to stimulus number. Figure 4.3 shows the discharge rate and Fano factor computed from efficient and inefficient search trials. As in previous reports, FEF discharge rates discriminate the location of the target significantly earlier during efficient search (112 ± 4.8 ms; Figure 4.3A) than inefficient search (150 ± 6.1 ms; $p < 0.01$; bootstrap, 1000 samples; Figure 4.3C)(Sato et al., 2001). In addition, the magnitude of discrimination was greater during inefficient search (10 ± 0.1 sp/s; $p < 0.001$; Wilcoxon rank-sum test).

Fano factor declined following array onset regardless of search efficiency, but it did not distinguish whether the target or a distractor was in the RF in either efficient or inefficient search (Figure 4.3B,D; Table 4.1). The average post-stimulus percent decline in Fano factor during efficient (-5.7 ± 1.69) and inefficient search (-8.1 ± 1.76) was statistically indistinguishable (p =

0.20). Although Figure 4.3 appears to suggest a variation in baseline variability across tasks, this difference is driven primarily by across-neuron differences in Fano factor for the two data sets. For neurons that were recorded during both efficient and inefficient search, we verified that no within-neuron baseline difference in search efficiency was observed in discharge rate ($p = 0.36$; Wilcoxon signed-rank) or Fano factor ($p = 0.20$). Thus, we see no evidence of changes in response variability with search efficiency, despite clear changes in mean discharge rate.

4.4.2 FEF response variability reflects the strength of sensory input.

The post-stimulus decline in Fano factor irrespective of behavioral relevance or physical conspicuity suggests that response variability is sensitive to sensory input independent of attentional allocation. To test this hypothesis, we measured Fano factor while varying the strength of sensory input using two manipulations. First, we systematically varied stimulus luminance during the memory-guided saccade task. The mean post-stimulus discharge rate increased with luminance (Figure 4.4A,C; 1.6 ± 0.13 sp/s/cd/m^2; $p < 0.001$; Wilcoxon signed-rank test). This effect was partially driven by a decrease in visual latency at high luminance levels (Low: 79 ± 7.3 ms; Medium: 74 ± 6.4 ms; High: 53 ± 5.1 ms), which is observed throughout the visual system including lateral geniculate nucleus (Maunsell et al., 1999), striate (Gawne et al., 1996) and extrastriate areas (Oram et al., 2002), and superior colliculus (White and Munoz, 2011). In addition, the magnitude of the post-stimulus Fano factor decline increased with luminance (Figure 4.4B,D; -0.1 ± 0.01 Fano factor/cd/m^2; $p < 0.001$). This effect was still apparent in the mean-matched Fano factor (Figure 4.4C, inset), indicating that the reduction cannot be solely attributed to increases in mean discharge rate. Neither discharge rate nor Fano factor showed significant modulation with luminance when the target appeared outside the neuron's RF (both $p > 0.05$). Thus, increased sensory input decreases trial-by-trial response variability in FEF neurons.

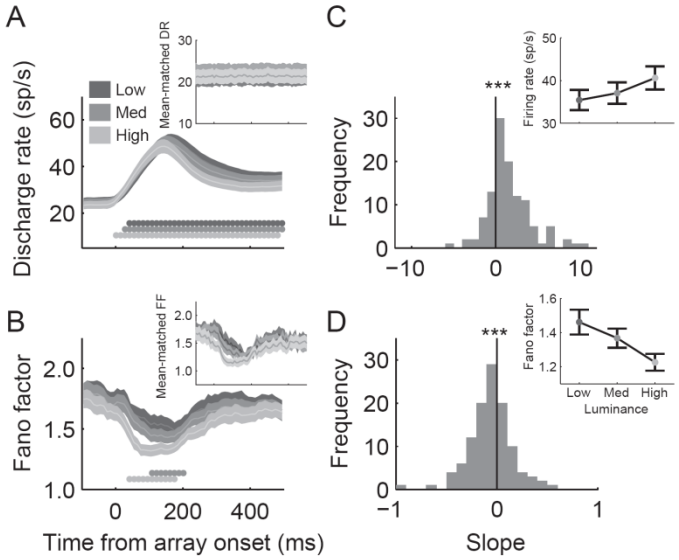

Figure 4.4. Effect of luminance on discharge rate (DR) and Fano factor (FF). **A**, Mean discharge rate (±SE) divided by target luminance (Low: 0.01 to 0.6 cd/m^2; Medium: 0.20 to 1.00 cd/m^2; High: 1.70 to 5.00 cd/m^2). Gray dots indicate significant differences from baseline (Wilcoxon rank-sum test, $p < 0.01$). Inset shows mean-matched discharge rate for each luminance group (see Materials and Methods; Churchland et al., 2010). The mean-matched discharge rate is invariant across time and luminance. **B**, Variations in Fano factor with luminance. Conventions as in panel A. Fano factor decreases significantly with luminance even when controlling for changes in mean discharge rate. **C**, Distribution of slopes of mean discharge rate as a function of luminance group in the post-stimulus epoch (sp/s/cd/m^2). Inset shows mean discharge rate (±SE) by luminance group. Asterisks denote significant difference of mean value from 0 (Wilcoxon signed-rank test, *** denotes $p < 0.001$). **D**, Same as panel C for Fano factor (Fano factor/cd/m^2). Note that discharge rate and Fano factor were computed using 150 ms time bins, therefore the visual latency may appear earlier due to temporal smearing. All latency estimates reported in the text used smaller 50 ms time bins.

Second, we manipulated the strength of sensory input by systematically varying the number of objects in the visual field. In the post-stimulus epoch, mean discharge rate significantly decreased as additional items appeared in the visual field (-0.914 ± 0.141 sp/s/item; $p < 0.001$; Cohen et al., 2009). In addition, Fano factor significantly decreased with additional items (-0.006 ± 0.003 per item; $p < 0.05$).

Interestingly, Fano factor modulation by set size was strongest shortly after stimulus onset, before an effect of set size on discharge rate was evident (Figure 4.5). Therefore, we also compared the effect of set size on discharge rate and Fano factor in this early visual epoch (50-125 ms). During the initial visual response, discharge rate did not vary with set size regardless of whether a target or distractor was in the neuron's RF (Figure 4.5A,B insets; both $p > 0.05$;

Wilcoxon signed-rank test). Although the mean discharge rate was invariant across set size at this time, Fano factor still significantly declined with set size when both the target (-0.009 ± 0.0037 per item; $p < 0.05$) or distractors (-0.011 ± 0.0033 per item; $p < 0.001$) were inside the neuron's RF (Figure 4.5C,D insets). Thus, in search, more objects in the visual field leads to an early reduction of neuronal variability independent of later changes in discharge rate.

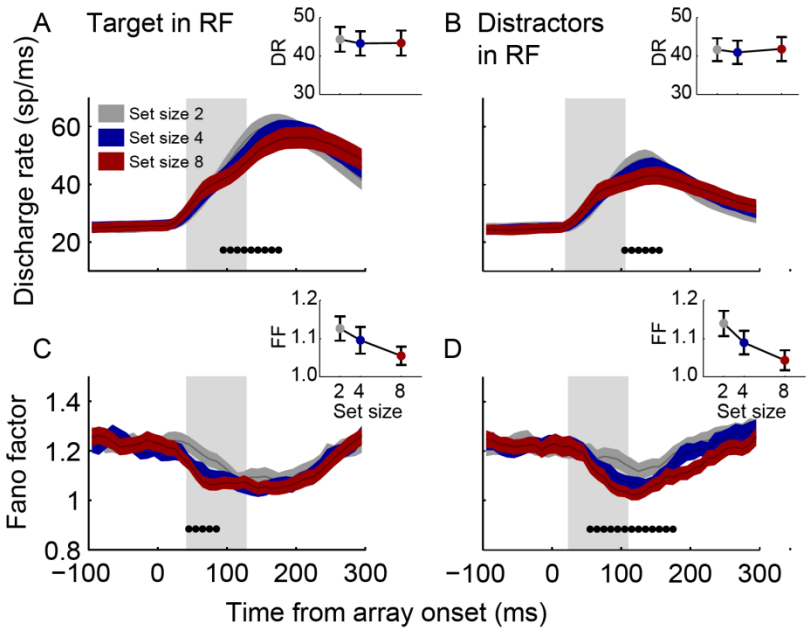

Figure 4.5. Effect of set size on discharge rate (DR) and Fano factor (FF) for trials in which the target (left) or distractors (right) were in the neurons' RFs. Mean discharge rate (top, **A,B**) and Fano factor (bottom, **C,D**) aligned on array onset for set size 2 (gray), 4 (blue), and 8 (red). Insets show mean discharge rate or Fano factor (±SE) for each set size in the time interval 50-125 ms after array onset (shaded region). Black dots indicate times in which slope of the least squares regression line for discharge rate and Fano factor as a function of set size decreased significantly ($p < 0.01$). The regression line was computed by averaging discharge rate and Fano factor across time bins for each set size in a running window (±20 ms) incremented in time steps of 10ms.

We next divided trials by search efficiency and combined across RF stimuli (Figure 4.6). If the decline in Fano factor with set size is due to increasing attentional demands, then it should be absent during efficient search. However, we found that Fano factor in the early visual epoch declined with set size for both inefficient (-0.012 ± 0.0050 per item; $p < 0.001$) and efficient (-

0.007 ± 0.0021 per item; $p < 0.01$) search (Figure 4.6B,D). There was no effect of set size on discharge rate at this time for either search task (Figure 4.6A,B; both $p > 0.05$; Wilcoxon signed-rank test). The decline in Fano factor with set size was slightly, but not significantly weaker during efficient search relative to inefficient search ($p = 0.19$). There are several reasons to believe that this is due to lower stimulus luminance and not decreased attentional demands. First, the variation of Fano factor with set size is present regardless of RF stimulus (Figure 4.5), and therefore lacks spatial specificity or sensitivity to object relevance. Second, the variation of Fano factor with set size appears ~50 ms after array onset, which corresponds to afferent delays in FEF (Schmolesky et al., 1998; Pouget et al., 2005), but is before attention-related signals are observed in discharge rate. Lastly, theories of visual attention predict that increased reliability should produce improved performance (Palmer et al., 2000), but FEF neurons fired more reliably as performance declined during inefficient search. Altogether, these results suggest that Fano factor in FEF is modulated by the strength of sensory input but not attentional demands.

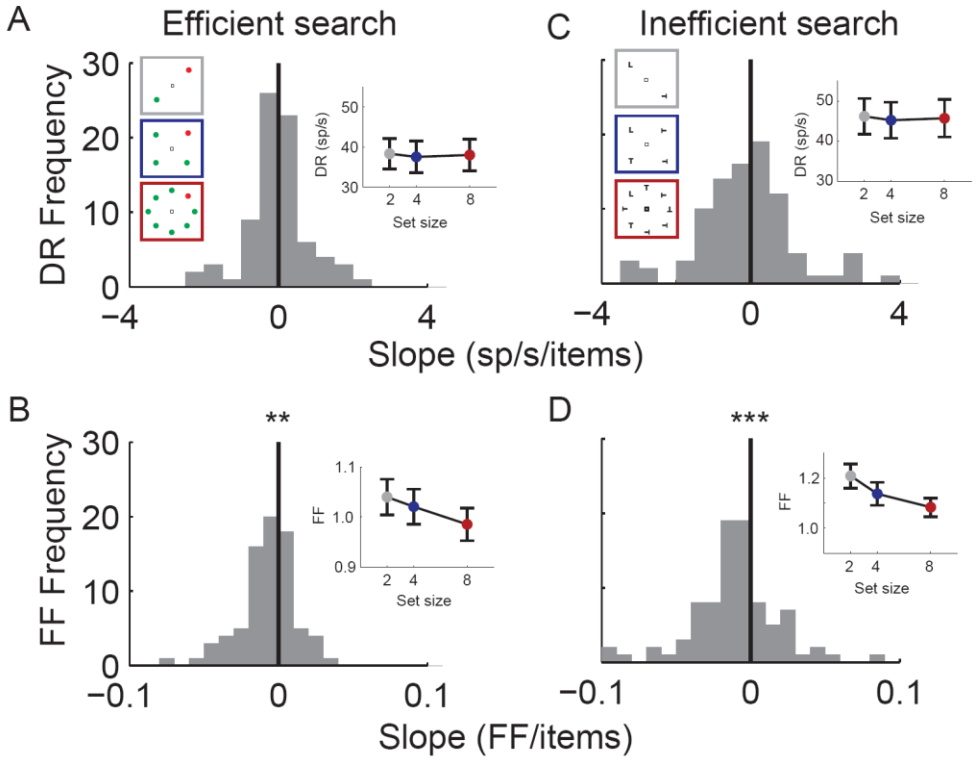

Figure 4.6. Effect of set size on discharge rate (DR) and Fano factor (FF) during efficient (left) and inefficient (right) visual search. Population histogram for slope coefficient of least squares regression line fit to mean discharge rate (**A,C**, top) and Fano factor (**B,D**, bottom) in the early visual epoch 50-125 ms after array onset as a function of set size during efficient (left) and inefficient (right) search. Inset shows population mean (±SE) discharge rate (DR) or Fano factor (FF) for each set size. Asterisks indicate that the population of slopes was significantly shifted from 0 (Wilcoxon signed-rank test, ** $p < 0.01$; *** $p < 0.001$).

4.4.3 FEF response variability reflects saccade preparation

In the preceding sections, we analyzed Fano factor in early time intervals aligned on stimulus presentation to determine how behavioral relevance, physical conspicuity, and the strength of sensory input influence response variability in FEF neurons. In addition to encoding visual salience, the discharge rates of FEF neurons have also been identified with saccade preparation (Hanes and Schall, 1996; Hanes et al., 1998; Murthy et al., 2009; Gregoriou et al., 2012). Specifically, the mean discharge rates of saccade-related FEF neurons have been identified with accumulator models of saccade preparation that predict saccades are initiated when discharge rates reach a fixed threshold (Ratcliff et al., 2003; Boucher et al., 2007; Purcell et al., 2010; Purcell et al., 2012b). This implies that response variability should reach a minimum

prior to saccades of a particular direction. We analyzed the Fano factor of FEF neurons relative to saccade initiation to determine whether changes in response variability were consistent with accumulator models of saccade preparation.

Figure 4.7 shows the population discharge rate and Fano factor aligned to the onset of saccades directed towards or away from the neuron's RF. The population discharge rate predicted the saccade direction 92 ± 5.2 ms before gaze shifted (Figure 4.7A). On average (±SE), neurons fired 21 ± 1.4 sp/s more when the saccade was directed towards versus away from the RF (Figure 4.7C; $p < 0.001$, Wilcoxon signed-rank test). The population Fano factor initially declined regardless of saccade direction, but evolved to predict saccade direction 58 ± 9.9 ms before the eyes moved (Figure 4.7B). Across the population, Fano factor was significantly lower when a saccade was made towards a neuron's RF (Figure 4.7D; -0.10 ± 0.01, $p > 0.05$). Importantly, the pre-saccadic magnitude of discrimination ($p = 0.95$) and percent Fano factor decline ($p = 0.53$) were statistically indistinguishable between efficient and inefficient search, which indicates that this pre-saccadic selectivity cannot be identified with visual salience. Although some individual data sets fail to reach statistical significance, this trend is consistent across all tasks and monkeys (Table 4.1). Thus, although FEF response variability was not affected by stimulus relevance, it robustly predicted the direction of an upcoming saccade.

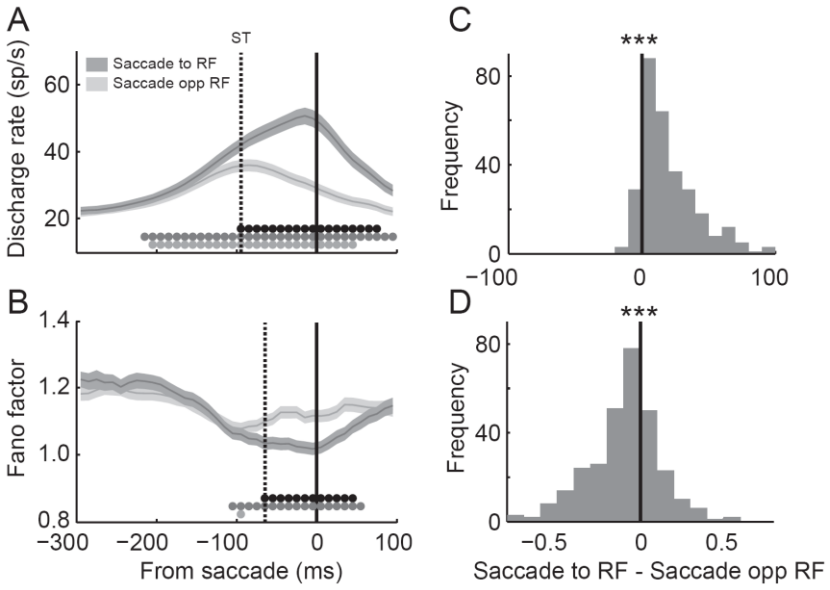

Figure 4.7 Temporal dynamics of discharge rate (**A**) and Fano factor (**B**) aligned on saccade initiation during visual search for the full population of 304 neurons. Conventions as in Figure 4.2. **C**, Distribution of difference in discharge rate when the saccade was directed towards or away from the neuron's RF in the pre-saccade epoch (50-0 ms before saccade). Asterisks denote significance from 0 (Wilcoxon signed-rank test, *** denotes $p < 0.001$). **D**, Same as panel C, but for Fano factor.

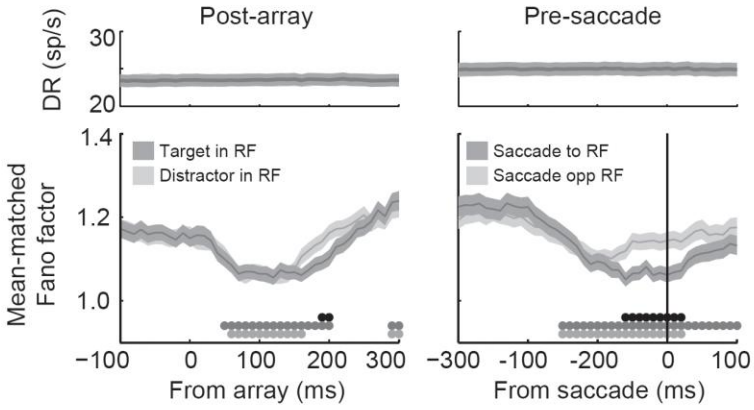

Figure 4.8 Mean-matched discharge rate (DR) (top) and Fano factor (bottom) as a function of time relative to array presentation (left) and saccade initiation (right). Solid vertical line indicates time of saccade. Mean-matching was performed across target locations and saccade directions, but independently for array-aligned and saccade-aligned data. Conventions as in Figure 4.2.

A potential concern is that the pre-saccadic Fano factor selectivity could be confounded by the differences in mean discharge rate. Higher discharge rates could impose more regular

spiking due to the spike refractory period (Kara et al., 2000; Mitchell et al., 2007). To control for this possibility, we recomputed Fano factor using a mean-matching procedure which subsamples neurons and conditions at each time point such that mean discharge rate remains constant across time and conditions (Churchland et al., 2010). In the post-stimulus epoch, the mean discharge rate is constant across time and regardless of the stimulus in the receptive field, but there is still a significant decline in the Fano factor regardless of stimulus identity (Figure 4.8). There is a brief, late difference in Fano factor around 190 ms that can be attributed to saccade initiation. Most importantly, the pre-saccadic Fano factor is still significantly lower when saccades were made to the RF despite identical discharge rates. Thus, changes in pre-saccadic Fano factor cannot be explained by changes in mean discharge rate.

We quantified the resolution of pre-saccadic spatial tuning during visual search by fitting a Gaussian curve to the mean discharge rate and Fano factor as a function of distance from the RF center. Consistent with previous results, the mean discharge rates in the post-stimulus interval were well explained by a Gaussian function (R^2 = 0.99; Figure 4.9A; but see Schall et al., 1995a; Schall et al., 2004), but the Fano factor was constant across target locations (Figure 4.9B). In contrast, pre-saccadic mean discharge rates (Figure 4.9C; R^2 > 0.99) and Fano factor (Figure 4.9D; R^2 = 0.96) were both well explained by a Gaussian function. We used the standard deviation of the best fitting Gaussian curve as an index of tuning width. The pre-saccadic Fano factor tuning width ($65^o \pm 8.6^o$) was slightly, but significantly more broadly tuned than the mean discharge rate ($51^o \pm 2.4^o$; $p < 0.05$, nonparametric bootstrap, 500 samples). Thus, response variability in FEF neurons reaches a minimum only prior to saccades of a particular direction. This is inconsistent with models of motor preparation that predict all neurons in a population reach a variability minimum irrespective of the movement (e.g., Churchland et al., 2006; Afshar et al., 2011).

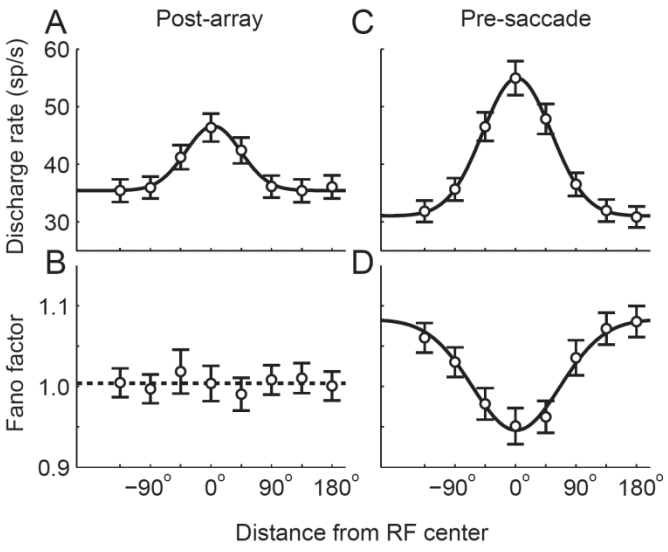

Figure 4.9. Spatial tuning of mean discharge rate (**A,C**) and Fano factor (**B,D**) as a function of distance from RF center (in degrees polar angle) during the post-array (left) and pre-saccadic (right) epochs. Solid lines are best fitting Gaussian curves. Dashed line is the mean across locations for data that did not exhibit significant selectivity in the interval of interest. Error bars are SE.

4.4.4 Visually-responsive and saccade-related subpopulations

Previous studies have proposed that salience and saccade preparation are encoded by functionally distinct subpopulations of FEF neurons. Specifically, visually-responsive neurons are proposed to represent salience, whereas saccade-related neurons are thought to integrate salience to a response threshold (Purcell et al., 2010; Purcell et al., 2012b). We classified neurons as visually-responsive and saccade-related based on their responses during a memory-guided saccade task to test whether they showed distinct patterns of response variability during search. We classified 108 neurons as visually-responsive and 124 neurons as saccade-related. These analyses excluded 28 neurons that were nonmodulated and neurons that were not recorded during the memory-guided saccade task.

We first asked whether a representation of stimulus relevance is selectively present in visually-responsive neurons. Figure 4.10 shows the mean discharge rate and Fano factor as a function of time since the array onset. Discharge rates of both visually-responsive and saccade-

related neurons evolve to select the target location at 154 ± 9.3 ms (Figure 4.10A, left) and 139 ± 5.5 ms (Figure 4.10C, left), respectively. The Fano factor significantly declined following array onset for both visually-responsive (Figure 4.10B, left) and saccade-related (Figure 4.10D, left) neurons, but Fano factor never significantly distinguished the RF stimulus in either population (both $p > 0.05$). This indicates that response variability does not change with stimulus relevance in both subpopulations.

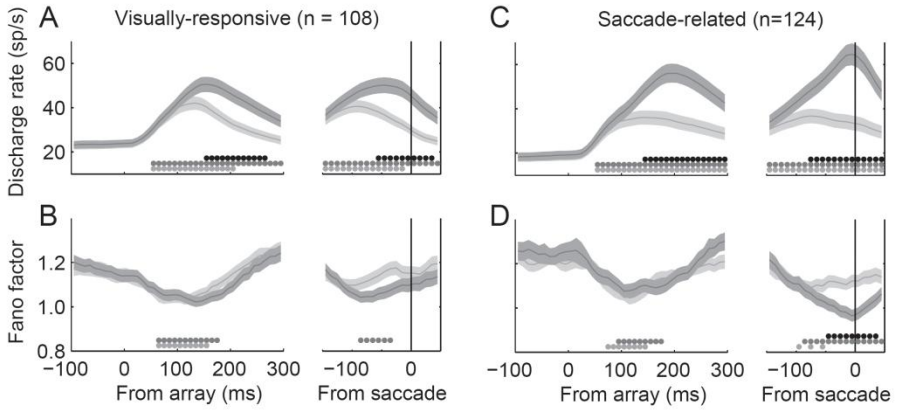

Figure 4.10. Visually-responsive and saccade-related subpopulations. Mean discharge rate (**A,C**) and Fano factor (**C,D**) for visually-responsive (left) and saccade-related (right) neurons during visual search. Conventions as in Figure 4.2.

We next asked whether a representation of saccade preparation is selectively present in saccade-related neurons. Discharge rates of both visually-responsive and saccade-related neurons evolved to predict the saccade direction 58 ± 7.6 ms and 80 ± 9.1 ms before the eyes moved, respectively (Figure 4.10A, 4.10C, right). However, the temporal dynamics of Fano factor were distinctly different for the two populations. Visually-responsive neurons never significantly distinguished the saccade direction on a bin-by-bin basis (Figure 4.10B), whereas saccade-related neurons predicted the saccade direction 51.6 ± 11.6 ms before the eyes moved (Figure 4.10D; $p < 0.01$). Likewise, the subset of 43 pure visual neurons which showed significant post-stimulus modulation, but no significant pre-saccadic modulation also exhibited saccade-direction

dependent modulation of discharge rate ($p < 0.001$), but not Fano factor ($p = 0.07$). The pre-saccadic Fano factor of visually-responsive neurons reached a minimum 75 ± 13.8 ms before saccade and increased before the eyes moved. Neurons in brainstem nuclei that control saccades become active ~15 ms prior to eye movements (Scudder et al., 2002), which means that variability has increased from the minimum when the saccade is triggered. In contrast, saccade-related neurons declined to a minimum immediately prior to saccades (3 ± 7.8 ms), which means that variability was nearing minimum when the saccade was triggered. There was also a significant positive correlation between VMI and pre-saccadic Fano factor ($r = 0.13$; $p < 0.05$), indicating that neurons with stronger saccade-related responses tended to have lower response variability prior to saccades. Altogether, the differences in pre-saccadic Fano factor suggest that saccade preparation can be identified with saccade-related, but not visually-responsive neurons (see also Hanes et al., 1998; Brown et al., 2008).

4.4.5 Stochastic accumulator simulations

Saccade-related neurons have been identified with stochastic accumulators that initiate a saccade when discharge rates reach a fixed threshold (Ratcliff et al., 2003; Boucher et al., 2007; Purcell et al., 2010; Purcell et al., 2012b). However, many accumulator models predict that variability increases over time (Ratcliff, 1978; Churchland et al., 2011), which appears to be inconsistent with the post-stimulus decline in Fano factor (Figure 4.10D). We evaluated a simple stochastic accumulator model to test whether the basic predictions of this framework are consistent with the observed changes in response variability of FEF neurons. As expected, the model predicts a decline in Fano factor before saccade initiation because responses are initiated at a fixed discharge rate threshold (Figure 4.11, bottom right). Surprisingly, the model also predicts the decline in Fano factor following stimulus presentation (Figure 4.11, bottom left). Variability declines observed because the average increase in mean input following array onset (v-z) is greater than the increase in variability (η) that gives the model its variable rate of rise. As long as

the ratio, $(v\text{-}z)/\eta$, is sufficiently high, the model will predict a post-stimulus decline in Fano factor. Critically, using the same parameterization, the model can predict an RT distribution comparable to the range observed during visual search tasks (Figure 4.11, top). We present this simple model as a proof of concept that the basic predictions of the accumulator model framework are consistent with response-variability dynamics observed in FEF. Systematic evaluation of alternative network architectures will be necessary to fully explore potential mechanisms underlying saccade generation and their contribution to response variability.

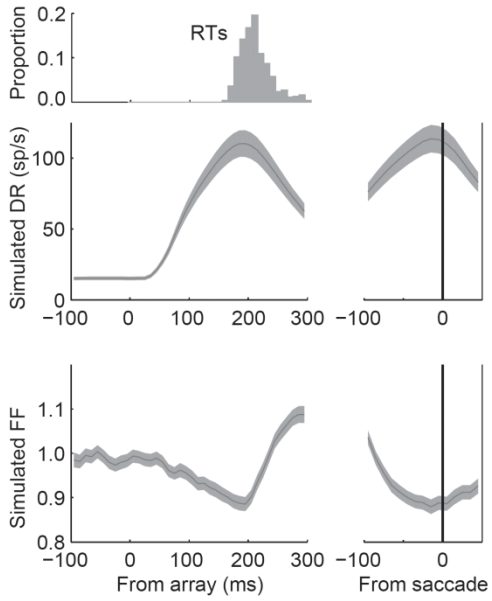

Figure 4.11. Accumulator model simulations. Simulated model discharge rates (DR) (top) and Fano factor (FF) (bottom) relative to array onset (left) and saccade (right). Lines are the averages (±SE) across 304 simulated neurons with 110 simulated trials to match the statistical power of the observed data. Gray histogram (top) is the quantile averaged response time (RT) probability distribution across all simulations. Only one accumulator representing a saccade to the neurons' response field was simulated. Note that Fano factor begins declining ~50 ms after target onset and reaches a minimum at the time of saccade initiation as observed in FEF neurons (see Figure 4.10C,D).

4.4.6 Response variability during memory-guided saccades

It is possible that response variability does not change with visual search salience because response variability lacks spatial tuning. We analyzed response variability following the onset of a single target during the memory-guided saccade task to evaluate this possibility. Discharge

rates increased when the target appeared inside the RF, but were unchanged when the target was outside the RF (Figure 4.12A). This produced significant selectivity following target onset (Figure 4.12C; 16 ± 1.2 sp/s; $p < 0.001$; Wilcoxon signed-rank test) that was maintained throughout the delay interval prior to the cue (9.8 ± 1.0 sp/s; $p < 0.001$) and the pre-saccadic epoch (14.9 ± 1.7 sp/s; $p < 0.001$). Thus, modulations in discharge rate were present throughout all critical task epochs.

In contrast, Fano factor declined when the target appeared inside or opposite the RF (Figure 4.12B). Importantly, the decline was greater when the target was inside the RF. This resulted in significant selectivity following target onset (-0.12 ± 0.04; $p < 0.001$; Wilcoxon signed-rank test), but Fano factor returned to baseline shortly after the target disappeared and selectivity was absent in the delay interval ($p > 0.05$). We verified that this effect was still present in the mean-matched Fano factor (Figure 4.12), and therefore cannot be solely due to differences in mean discharge rate. This is consistent with a recent study showing that the post-stimulus response variability of FEF neurons is broadly tuned, but is not maintained in the absence of the stimulus even when the location must later be used to guide saccades (Chang et al., 2012). In addition, we found that Fano factor declined prior to saccade initiation regardless of saccade direction. There was a tendency for variability to be lowest for saccades to the neuron's RF (Figure 4.12D), but this difference was not significant. This is probably due to increased end-point scatter in the absence of a visual target and a reduction in statistical power relative to the visual search data due to fewer recorded trials per neuron. Altogether, the pattern of Fano factor modulation during memory-guided saccades indicates that the absence of any influence of salience on response variability during search is not due to an absence of spatial selectivity in Fano factor and supports the hypothesis that strong modulation of Fano factor is more closely associated with sensory input and motor preparation.

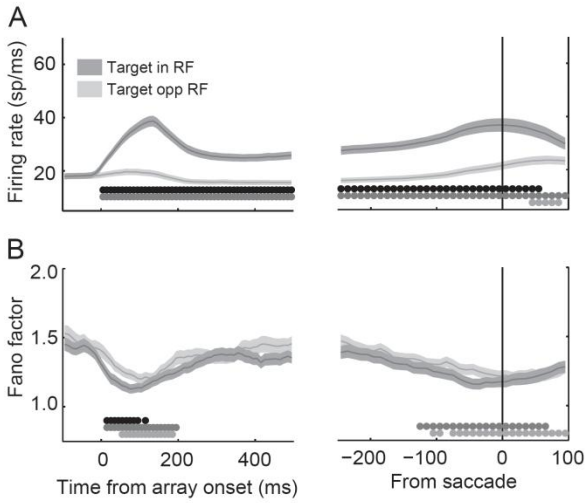

Figure 4.12. Memory-guided saccades. Mean discharge rate (**A**) and Fano factor (**B**) during memory-guided saccades aligned to target onset (left) or saccade (right) in which the target appeared inside (dark gray, Target in RF) or diametrically opposite (light gray, Target opp RF) the neurons' RFs. Stimulus duration was 80-150 ms and delay intervals ranged from 500-1000 ms. Insets show mean-matched discharge rate and Fano factor. Conventions as in Figure 4.2.

4.4.7 Response variability and RT

Previous studies have found that response variability in extrastriate and premotor cortex correlate with RT (Churchland et al., 2006; Steinmetz and Moore, 2010). We analyzed Fano factor conditionalized on RT during memory-guided saccades in the epoch prior to the cue. Figure 4.13A shows the mean discharge rates aligned on cue. Prior to the cue, there was no significant difference in mean discharge rate across RT groups regardless of whether the saccade was made towards ($p = 0.25$; Wilcoxon signed-rank test) or away from the RF ($p = 0.72$). In contrast, Fano factor was lower in the pre-cue epoch when RT was faster regardless of whether the saccade was made towards (-0.05 ± 0.019; $p < 0.05$; Wilcoxon signed-rank) or away (-0.11 ± 0.072; $p < 0.05$) from the RF. When combining across saccade directions, this difference remained significant for the subpopulation of saccade-related neurons (-0.05 ± 0.026; $p < 0.05$), but not visually-responsive neurons (-0.03 ± 0.033; $p = 0.47$), although a similar trend was evident. Pre-saccadic discharge rate and Fano factor did not depend on the speed of the response (Figure 4.13C-D; both $p > 0.05$), which is consistent with accumulator model predictions. These

results support our conclusion that Fano factor reflects motor preparation in FEF and introduces new constraints on models of saccade generation.

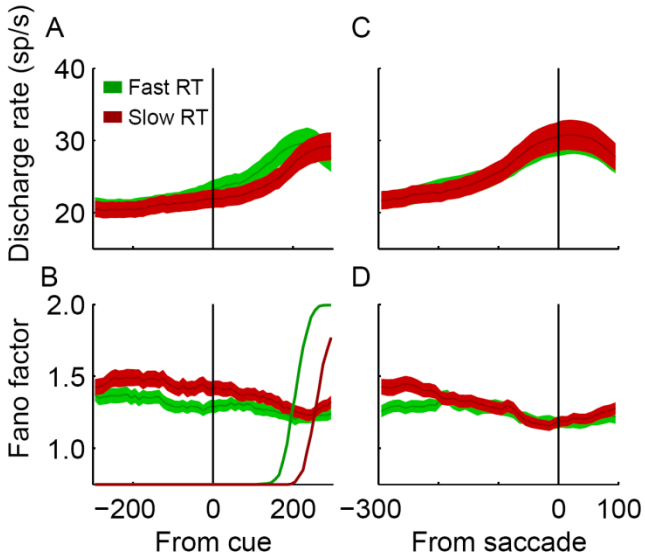

Figure 4.13. Mean discharge rate (**A,C**) and Fano factor (**B,D**) aligned on the cue (left) and saccade (right) for memory-guided saccade trials with RT earlier (green) and later (red) than median RT. The thin colors lines in panel (**A,C**) indicate cumulative distributions of fast (green) and slow (red) RTs. This analysis includes all neurons recorded during the memory-guided saccade task and all trials regardless of whether the target was inside or opposite the neurons' RFs. Whereas discharge rate varied with RT mainly after the response cue, Fano factor varied with RT mainly before the response cue. Discharge rate and Fano factor were indistinguishable across RT samples at the time of saccade initiation.

4.5 Discussion

We found that response variability of FEF neurons declines following stimulus presentation, but the magnitude of decline is equal for search targets and distractors. Response variability did not change with search efficiency, despite clear modulation of mean discharge rate. Instead, we found that response variability was modulated by the strength of sensory input and declined to minimum before saccades to a neuron's RF. These results inform models of visual search and saccade generation.

4.5.1 Relation to theories of visual search and attention

Theories of visual search propose that a salience map guides attention and eye movements to locations of maximal activation (Itti and Koch, 2001; Bundesen et al., 2005; Wolfe, 2007). FEF is part of a network of oculomotor areas including superior colliculus and lateral intraparietal area, but not supplementary eye field (Purcell et al., 2012a), that have been identified with the salience map (Findlay and Walker, 1999; Thompson and Bichot, 2005; Gottlieb, 2007; Bisley and Goldberg, 2010). According to this framework, the decline in response variability that we observed following stimulus presentation could improve the reliability with which the location of maximal activation can be distinguished. Importantly, declines in variability at all locations on the map will actually increase the signal-to-noise ratio. In other words, considered in a signal detection theory framework (Palmer et al., 2000), target discriminability is increased by a reduction in variability for both the noise (distractor) and noise + signal (target) distribution. Thus, our observation that variability declines equally irrespective of object relevance could produce greater target discriminability of the point of maximal activation. These results are consistent with a previous study that failed to find target-distractor differences in FEF variability during search (Bichot et al., 2001b), but this study only analyzed stimulus-aligned responses during the initial nonselective visual response (0 to 50 ms). Here, we show that response variability in FEF is not modulated by stimulus salience (relevance or conspicuity) during visual search despite large changes in mean discharge rate. This observation is also consistent with a previous study which found that the mean discharge rate, but not response variability, of FEF neurons was modulated when animals were cued to attend to the neuron's RF (Chang et al., 2012). Our results extend this observation to visual search tasks in which the target must be discriminated from among distractors to appropriately allocate attention (i.e., exogenous attention).

Considered in a signal detection theory framework (Palmer et al., 2000), changes in behavioral performance with search efficiency could potentially be explained by increases in

response magnitude (target enhancement) or decreases in response variability (noise reduction). We found that the discharge rates, but not response variability, of FEF neurons was modulated by search efficiency. This is consistent with the hypothesis that attention does not affect FEF response variability (Chang et al., 2012). This contrasts with observations in V4, in which spatial attention reduces response variability (Mitchell et al., 2007; Cohen and Maunsell, 2009). Similarly, although attention has been found to reduce trial-by-trial discharge rate correlations in V4 (Cohen and Maunsell, 2009; Mitchell et al., 2009) and MT (Cohen and Newsome, 2008), FEF neurons show increased correlations when search targets fall within the overlapping RFs of two neurons (Cohen et al., 2010). Thus, although both V4 and FEF neurons show elevated discharge rates when representing the location of behaviorally relevant objects (Zhou and Desimone, 2010) and FEF is proposed to be a source of attentional modulations in V4 (Moore and Armstrong, 2003; Gregoriou et al., 2012), measures of response variability and correlated rate variations suggest very different mechanisms of selection are operating in frontal and posterior visual areas.

This result also challenges models of attention which propose a serial scan of locations on the salience map (e.g., Treisman and Gelade, 1980; Buschman and Miller, 2009). Serial search, which entails greater variability in the time when attention is focused on an object, should produce greater variability in discharge rate during inefficient search. Our observation that Fano factor declines equivalently for efficient and inefficient search is inconsistent with this implication.

4.5.2 Stronger sensory input decreases response variability

Discharge rate increases with luminance-contrast throughout the visual system (Dean, 1981; Albrecht and Hamilton, 1982; Schiller and Colby, 1983; Tolhurst et al., 1983). This includes neurons in extrastriate areas V4 and superior temporal sulcus (Reynolds et al., 2000; Oram et al., 2002) that project topographically to FEF (Huerta et al., 1987; Stanton et al., 1988; Schall et al., 1995a). Thus, increasing luminance can be identified with increasing the strength of

sensory input to FEF. We found that FEF neurons fired more consistently following the onset of higher luminance stimuli. Similar declines in variability are observed in LGN neurons with increased retinal stimulation and microstimulation of afferent sources (Hartveit and Heggelund, 1994). Moreover, the effect was preserved after mean-matching, which indicates that the improvement must be due to decreases in noise above and beyond increases in mean discharge rates. This indicates an improved signal-to-noise ratio for higher luminance stimuli that could be partially responsible for variations in performance during saccade detection tasks (Carpenter, 2004).

During memory-guided saccades, response variability declined following presentation of a single target anywhere in the visual field, but the decline was greatest in the neuron's RF. This is consistent with a recent study, which found broad tuning of response variability in FEF in response to single targets (Chang et al., 2012). The monkeys in the Chang et al. (2012) study were trained to remember the target location in order to perform a subsequent change detection task. Unlike that study, our monkeys were trained to make an oculomotor response to the location of the remember target, and therefore could begin preparing a saccade to the remembered location during the delay interval. We observed an additional decline in Fano factor as the time of saccade approaches that was similar to the decline observed in neurons recorded from the dorsolateral pre-frontal cortex of macaques performing a visual discrimination task (Hussar and Pasternak, 2010). Like Chang et al. (2012), we found that selectivity vanishes shortly after the stimulus is removed despite sustained discharge rates during the memory delay. This provides converging evidence that maintenance of spatial information in the absence of sensory input does not alter response variability. Unlike sensory input which is necessarily feed-forward, maintenance of spatial information is thought to be implemented through local recurrent excitation (Wang, 1999; Compte et al., 2000). Therefore, our results are consistent with the hypothesis that feed-forward, but not recurrent, excitation causes a decline in response variability. This hypothesis is also supported by the observation that inactivation of primary visual cortex via

electrical stimulation does not alter variability in membrane potential and that changes in variability with contrast can be entirely accounted for by changes in variability in feedforward inputs form the lateral geniculate nucleus (Sadagopan and Ferster, 2012).

4.5.3 Response variability as a signature of saccade preparation

During the visual search task, response variability declined to a minimum before saccades. This result was unexpected because a previous study failed to find differences in pre-saccadic response variability (Bichot et al., 2001b). This is probably because Bichot et al. (2001) included mostly visually-responsive neurons, which were found to show little to no pre-saccadic Fano factor selectivity. Importantly, we found that variability was minimal only for saccades directed to the neuron's RF. The population Fano factor was spatially tuned only slightly more broadly than discharge rates prior to saccade initiation, which is consistent with observations that pre-saccadic response variability reaches a minimum before saccades to the RF in LIP (Churchland et al., 2011). In contrast, response variability in pre-motor cortex was found to be invariant across arm reaches in different directions (Churchland et al., 2006) and the influence of saccade direction on Fano factor variability in V4 is weak (Steinmetz and Moore, 2010). Weak spatial tuning of response variability has been interpreted in support of an 'optimal subspace hypothesis' in which all neurons in a cortical area initiate a movement when discharge rates converge to a specific value (Afshar et al., 2011). The observation that pre-saccadic Fano factor is sharply tuned in FEF neurons means that only neurons that encode the end-point of the upcoming saccade are reaching a minimum variance. Moreover, we showed that only saccade-related, but not visually-responsive, neurons reach a minimum variance before saccades. Altogether, these results suggest that the optimal subspace hypothesis does not generalize to the oculomotor system.

Saccade-related FEF and SC neurons have been identified with stochastic accumulators to a response threshold that is invariant with RT within a condition (Ratcliff et al., 2003; Boucher

et al., 2007; Purcell et al., 2010; Purcell et al., 2012b). The most basic prediction of this framework is that variability should decline to a minimum at the time of the response. We showed that saccade-related neurons conform to this prediction. Many forms of stochastic accumulator models also predict an increase in variability as a function of time (Ratcliff, 1978; Carpenter and Williams, 1995; Brown and Heathcote, 2005), which is inconsistent with the post-stimulus decline in response variability that we observed. However, we demonstrated that a simple accumulator model can predict both the decline in response variability and RT distributions corresponding to those observed during visual search. The model demonstrates that Fano factor will decline so long as the increase in mean input following array onset is sufficiently larger than the increase in variability that produces varying rates of rise. This result provides additional constraint on computational models of saccade choice and decision-making. Future modeling work will be necessary to rule out network architectures that fail to predict this decline in variability.

During memory-guided saccades, RTs were fastest when variability was lower prior to the imperative stimulus. This is consistent with our conclusion that response variability in FEF reflects saccade preparation. Similar correlations between response variability and RT have been observed in premotor cortex (Churchland et al., 2006) and V4 (Steinmetz and Moore, 2010). In premotor cortex, this observation has been interpreted as evidence that pools of neurons are approaching an optimal discharge rate (Churchland et al., 2006; Afshar et al., 2011), but our results indicate that, at least for the oculomotor system, accumulator models provide a complete account of saccade preparation and initiation. Why then does variability decline before fast saccades? Several potential mechanisms can cause reduce variability without influencing discharge rates, for example increases in balanced excitation and inhibition or self-inhibition. Thus, this observation provides additional constraints on future models of saccade generation.

CHAPTER V

ON THE ORIGIN OF EVENT-RELATED POTENTIALS INDEXING COVERT ATTENTIONAL SELECTION DURING VISUAL SEARCH: TIMING OF SELECTION BY MACAQUE FRONTAL EYE FIELD AND EVENT-RELATED POTENTIALS DURING POP-OUT SEARCH

5.1 Abstract

Event-related potentials (ERP) have provided crucial data concerning the time course of psychological processes, but the neural mechanisms producing ERP components remain poorly understood. This study continues a program of research investigating the neural basis of human ERP components by simultaneously recording intracranially and extracranially from macaque monkeys. Here, we compare the timing of attentional selection by the macaque homologue of the human N2pc component (m-N2pc) with the timing of selection in the frontal eye field (FEF), an attentional-control structure believed to influence posterior visual areas thought to generate the N2pc. We recorded FEF single-unit spiking and local field potentials (LFP) simultaneously with the m-N2pc in monkeys performing an efficient pop-out search task. We assessed how the timing of attentional selection depends on task demands by direct comparison to a previous study of inefficient search in the same monkeys (i.e., finding a T among Ls). Target selection by FEF spikes, LFPs and the m-N2pc was earlier during efficient, pop-out search than during inefficient search. The timing and magnitude of selection in all three signals varied with set size during inefficient, but not efficient search. During pop-out search, attentional selection was evident in FEF spiking and LFP before the m-N2pc, following the same sequence observed during inefficient search. These observations are consistent with the hypothesis that feedback from FEF modulates neural activity in posterior regions that appear to generate the m-N2pc even when competition for attention among items in a visual scene is minimal.

5.2 Introduction

Event-related potentials (ERPs) provide crucial information on the timing of specific cognitive operations (Luck, 2005). Attention-related ERPs can track shifts in attentional allocation in humans processing complex scenes (Woodman and Luck, 1999, 2003). Specifically, the N2pc component provides an index of attentional allocation across the visual field (Luck and Hillyard, 1994b, a), but a thorough investigation into the neural mechanisms that generate the N2pc is precluded by the difficulty in obtaining intracranial recordings from human subjects. Current source density and source estimation procedures suggest that the N2pc is generated by attentional modulations in posterior visual regions (Luck and Hillyard, 1994b; Hopf et al., 2000; Hopf et al., 2004; Boehler et al., 2011), but these methods are under-constrained without intracranial data (Helmholtz, 1853; Luck, 2005; Nunez and Srinivasan, 2006) and cannot resolve hypotheses concerning the influence of more distal regions that drive the underlying neural generator.

We have addressed this methodological shortcoming by simultaneously recording ERPs with intracranial signals in non-human primates (Woodman, 2011). We recently identified a macaque homologue of the N2pc component, termed the m-N2pc, which is a relative positivity contralateral to an attended item (Woodman et al., 2007; Cohen et al., 2009a; Heitz et al., 2010). The human N2pc was originally hypothesized to be due to feedback from attentional-control structures because of its relatively long latency and sensitivity to task-demands (Luck and Hillyard, 1994b), but until recently it has been impossible to test this hypothesis directly. ERPs lack the spatial resolution to distinguish the attention-related modulations in visual cortex from control structures in frontal cortex thought to drive those modulations. This has lead to controversy about the degree to which the N2pc reflects bottom-up versus top-down attentional signals (Eimer and Kiss, 2010; Theeuwes, 2010). Having established a homologous component in monkeys, we can test this hypothesis using targeted, invasive procedures that are impossible in healthy humans.

The frontal eye field (FEF) is a region of prefrontal cortex thought to be involved in attentional control. FEF single-unit spiking and local field potentials (LFP) evolve to identify the location of behaviorally-relevant search targets (Bichot and Schall, 1999a; Sato et al., 2001; Thompson and Bichot, 2005; Monosov et al., 2008; Cohen et al., 2009a; Cohen et al., 2009b), whether or not a saccade is generated (Thompson et al., 1997; Thompson et al., 2005a). For this reason, FEF has been identified with a salience map that guides attentional deployment (Thompson and Bichot, 2005), possibly via projections to extrastriate visual cortex (Pouget et al., 2009; Anderson et al., 2011; Ninomiya et al., 2012). The role of FEF in top-down attentional control is further supported by the effects of FEF microstimulation on activity in extrastriate visual cortex (Moore and Armstrong, 2003; Ekstrom et al., 2008). Thus, FEF is a prime candidate for an attentional-control structure that could drive the neural generator of the N2pc.

We recently found that FEF neurons and LFPs select the location of search targets before the m-N2pc during an inefficient visual search task (Cohen et al., 2009a). This result is consistent with the hypothesis that feedback from FEF participates in driving the putative posterior generator of the m-N2pc. This hypothesis is also supported by intracranial recordings demonstrating that attentional selection occurs in prefrontal cortex before LIP (Buschman and Miller, 2007), V4 (Zhou and Desimone, 2010) and IT (Monosov et al., 2010) during attentionally-demanding tasks. However, it is not clear how this timing depends on task demands. For example, one study has found that the ordering of selection across cortex depends on search difficulty (Buschman and Miller, 2007), which could influence the timing of the N2pc relative to FEF. In addition, a recent study reported an N2pc in response to a task-irrelevant singleton (Hickey et al., 2006), suggesting that this component may not depend on top-down influences. Moreover, some theories of visual attention propose that efficient search for a target defined by a single feature can be performed pre-attentively (Treisman and Gelade, 1980). Thus, it could be the case that the onset of the N2pc followed attentional selection in FEF because the task required explicit top-down control, but the same may not hold true during efficient search tasks.

To determine the degree to which the timing of selection in FEF and the m-N2pc depends on attentional demands, we recorded ERPs from monkeys performing an efficient pop-out visual search task simultaneously with FEF single-unit activity and LFPs. The experimental protocol, analytical and statistical methods, and monkeys were the same as those used in a previous report on attentional selection during inefficient T versus L search to allow for direct comparison across studies (Cohen et al., 2009a). If these three signals reflect the timing of attentional allocation, then the timing of selection should modulate with set size when search is inefficient, but not when search is efficient. In addition, if efficient search requires feedback from the saliency map of FEF to the neural generator of the m-N2pc, then we would expect selection in FEF to precede or coincide with the m-N2pc as was observed during inefficient search. We would also expect to see trial-by-trial correlations between FEF activity and the m-N2pc.

5.3 Materials and method

5.3.1 Behavioral tasks and recordings

Recording procedure. We simultaneously recorded neuronal spikes, LFPs, and the extracranial electroencephalogram (EEG) from two male macaques (*Macaca radiata*, identified as Q and S). Monkeys were surgically implanted with a head post, a subconjunctive eye coil, and recording chambers during aseptic surgery under isoflurane anesthesia. Antibiotics and analgesics were administered postoperative. All surgical and experimental procedures were in accordance with the National Institute of Health Guide for the Care and Use of Laboratory Animals and approved by the Vanderbilt Institutional Animal Care and Use Committee.

Neurons and LFPs were recorded from the right and left FEF of both monkeys using tungsten microelectrodes (2-4 MΩ, FHC) and were referenced to a guide tube in contact with the dura. All FEF recordings were acquired from the rostral bank of the arcuate sulcus at sites where saccades were evoked with low-intensity electrical microstimulation (<50 μA; Bruce et al., 1985). Spikes

were sampled at 40 kHz and LFPs were sampled at 1 kHz. LFPs were band-pass filtered between 0.2 and 300 Hz and amplified using a Plexon HST/8o50-G1 head-stage. LFPs were baseline corrected using the average voltage during the window from 100 to 0 ms before array presentation. Spikes were sorted online using a time-amplitude window discriminator and offline using principal component analysis and template matching (Plexon Inc.). We generated spike density functions by convolving each spike train with a kernel resembling a postsynaptic potential (Thompson et al., 1996).

Following the method of Woodman et al. (2007), we recorded ERPs from gold skull electrodes implanted 1 mm into the skull. Electrodes were located at approximately T5/T6 in the human 10-20 system scaled to the macaque skull. EEG signals were sampled at 1 kHz and filtered between 0.7 and 170 Hz. A frontal EEG electrode (approximating human Fz) was used as the reference for the lateral, posterior EEG signals.

Behavioral tasks. The monkeys performed a pop-out visual search task and a memory-guided saccade task, the latter allowed for the classification of different cell types. All tasks began with the monkey fixating a central white spot for ~500ms. In the pop-out visual search task (see Figure 5.1A), the fixation point changed from a filled to an unfilled white square (10.3 cd/m^2) simultaneously with the presentation of a colored target and one, three, or seven distractors of the opposite color. The number of distractors varied randomly across trials. Targets and distractors were either red (CIE chromaticity coordinates x = 0.620, y = 0.337) or green (CIE x = 0.289, y = 0.605). The target and distractor color remained constant throughout the session and target color was varied across sessions. The monkey was rewarded for making a single saccade to the location of the target within 2000 ms of array presentation and fixating that target for 500 ms.

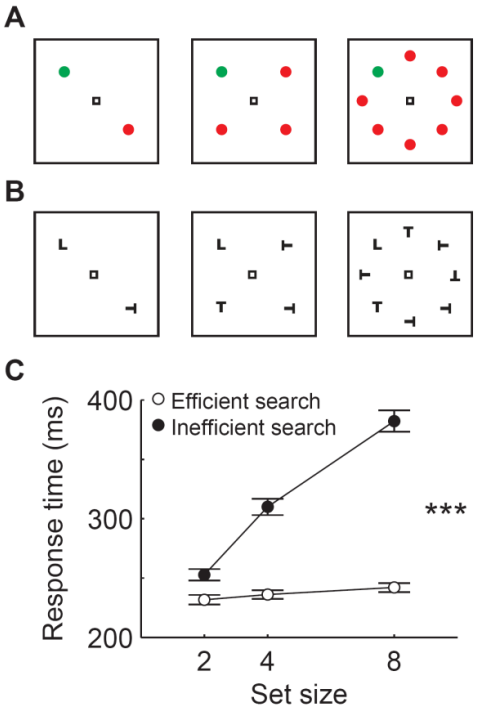

Figure 5.1 Visual search task and behavior. **A**, After fixating for a variable delay, a search array appeared consisting of one target (e.g., green disk) and 1, 3, or 7 distractors (e.g., red disks). Monkeys were required to make a single saccade to the target for reward. Target identity varied across sessions. **B**, We directly compared our new results from efficient pop-out search with previously published data collected from the same monkeys performing an inefficient visual search task (Cohen et al., 2009a). All procedures were identical to efficient search except that the monkeys searched for a T versus L (or vice versa). **C**, mean response time (RT) to the target as a function of set size for both search tasks. Error bars represent SE around the mean of the session means. Asterisks indicate significant differences in slope across tasks (*** for $p < 0.001$).

Each neuron was also recorded during a memory-guided saccade task to distinguish visual- from movement-related activity (Hikosaka and Wurtz, 1983; Bruce and Goldberg, 1985). In this task, a target (filled gray disk) was presented for 100 ms at one of eight isoeccentric locations equally spaced around the fixation spot at 10° eccentricity. The animal was required to maintain fixation for 400-800 ms (uniform distribution) after the target presentation. After the fixation point changed from a filled square to an unfilled square, the monkeys were rewarded for making a saccade to the remembered location of the target and maintaining fixation at that remembered location for 500 ms.

We also analyzed previously published FEF neurons, FEF LFPs, and the m-N2pc recorded from the same monkeys during an inefficient visual search (Figure 5.1B; Woodman et al., 2008;

Cohen et al., 2009a; Cohen et al., 2009b). The task was identical to the pop-out search task described above except that monkeys searched for a target defined by form (T or L in one of four orientations) among distractors (Ls or Ts, respectively). Target identity varied across sessions. Analytical and procedural methods were identical for data collected during both tasks. This allowed us to perform statistical comparisons between our new data collected during pop-out search and previously published data collected during inefficient search.

5.3.2 Data analysis

Neuron classification. We identified task-related neurons and LFPs by comparing activity to the baseline period 50 ms before presentation of the array. A neuron or LFP signal was classified as *visually responsive* if activity (discharge rate or voltage) was significantly different from baseline in the interval 50-200 ms following stimulus presentation during the memory-guided saccade task and in the interval 50-150 ms during search (Wilcoxon rank-sum test, $P < 0.05$). A neuron or LFP was classified as *saccade-related* if activity was significantly different from baseline in the interval -100 to 100 ms relative to saccade initiation for all tasks. Unless otherwise noted, our analyses focused on visually-responsive units with or without saccade-related modulation because these are the neurons known to represent visual salience (Bichot and Schall, 1999a; Sato et al., 2001; Thompson and Bichot, 2005) and likely to project to posterior visual areas thought to generate the N2pc (Thompson et al., 1996; Pouget et al., 2009; Gregoriou et al., 2012). Of the 102 total neurons we recorded, 84 neurons (82%) exhibited significant visual responses. Of the 141 total LFP sites we recorded, 133 LFPs (94%) exhibited significant visual responses. Of the 84 sites in which visually responsive neurons were recorded, 81 (96%) also exhibited visually-responsive LFPs. Thus, the sample size was 81 for the paired comparisons of simultaneously recorded neurons, LFPs, and ERPs. Of the 99 visually-responsive LFP sites in which neurons were concurrently recorded, 18 neurons (18%) did not exhibit visual responses.

Selection time. We used a "neuron-antineuron" approach to determine the selection time when the target location could be reliably discriminated in single-unit spiking, LFPs, and ERPs (Britten et al., 1992; Thompson et al., 1996). The selection time is defined as the time at which the distribution of activity when the search target is inside a receptive field is significantly greater than the distribution of activity when the target is opposite the receptive field for 10 consecutive milliseconds with a conservative α value of 0.01 (Wilcoxon rank-sum test). These criteria are identical to a previous report (Cohen et al., 2009a). For all signals, we defined the receptive field (or preferred location) as the three adjacent target locations in which the firing rate or voltage modulation maximally deviated from baseline. To ensure that our results were not the artifact of the orientation of the corneoretinal potential that changed during the saccade (Godlove et al., 2011a), we also computed selection time with signals aligned on saccade initiation. Only signals which selected the target >20ms before saccade initiation were included in this analysis.

For direct comparison with a previous study, we also estimated selection time by a running an ANOVA at each millisecond following target presentation (Monosov et al., 2008). The resulting p-value gave the probability that the activity did not vary across target locations. The selection time was the first millisecond that the p-value dropped below 0.05 before continuing past 0.001 and remaining below 0.05 for 20 out of 25 subsequent milliseconds. This ensured that differences across studies cannot be explained by differences in analytical methods. This method also ensures that our results are not due to our definition of receptive fields.

We also computed population selection times based on all 102 FEF single-units, 141 LFPs, and the m-N2pc conditionalized on whether the target was contralateral or ipsilateral to the hemisphere in which the signal was recorded. This is the approach more commonly used to study the human N2pc. This included neurons and LFP with and without significant visual responses and with both contralateral and ipsilateral preferred locations. Since the average firing rates of cortical neurons vary markedly, we normalized responses between 0 and 1 by subtracting the minimum response and dividing by the range so that variability across recording sites didn't

inflate selection times. The population selection time is defined as the time when the distributions of activity when the target is contralateral and ipsilateral significantly diverge for 10 consecutive milliseconds with $\alpha = 0.01$ (Wilcoxon rank-sum test). Here, the distribution is across neurons and recording sites, whereas individual selection times were based on the distribution across trials. All signals were truncated at saccade.

Magnitude of selection. We quantified the magnitude of selection as the difference in response magnitude when the target or a distractor was in the receptive field (preferred location) for each signal. For spiking activity, the magnitude of selection was computed as the difference in average normalized firing rate from 125 to 200 ms after the array presentation. For LFPs and the m-N2pc, the magnitude of selection was computed as the integral of the voltage in the same time window divided by the length of the window (Cohen et al., 2009a). All signals were truncated at saccade.

Set size effects. To assess how RT, selection time, and magnitude of selection depended on set size and search efficiency, we fit a multiple linear regression model of the form,

,

where the independent variable, *y*, is the mean RT for each session, or the selection time and magnitude of selection for each single-unit, LFP, or ERP. The predictor *s* is the set size (in items) and the predictor *e* is a dummy variable representing search efficiency (0 = efficient, 1 = inefficient). We assessed whether the coefficient β_1 was significantly different from zero to test for significant set size effects. We assessed whether the coefficient, β_2, was significantly different from zero to test for a significant effect of search efficiency.

Visual response latency. The latency of the visual response was determined by comparing baseline activity to activity during a ms-by-ms sliding window starting at array presentation. For FEF spiking activity and LFPs, the visual onset was the time when activity first became significantly different from baseline and remained significant for 10 consecutive ms (Wilcoxon

rank-sum test, $p < 0.01$). For ERPs, we required significance to be maintained for 30 consecutive ms to eliminate false alarms indicated by bimodality in the distribution and visual inspection.

Trial-by-trial correlations of spike rate, LFP, and ERP amplitude. We computed the Pearson correlation coefficient between the trial-by-trial amplitude modulation of simultaneously recorded neurons, LFPs, and ERPs. We used only signals that selected the target in these analyses. For spiking activity, amplitude was computed as the average firing rate in the window from 150 ms after the array presentation until saccadic response to exclude the nonselective initial visual response. For LFPs, amplitude was computed as the integral of the voltage in the same time window divided by the length of the window. We compared simultaneously recorded neurons and LFPs that were recorded from the same electrode or spaced ~1 mm apart. For comparison with a previous study (Cohen et al., 2009a), the ERP amplitude was first computed as the integral of the voltage in the same time window divided by the length of the time window. However, it is possible for this method to yield spurious correlations due to common noise picked up at the frontal reference. As a control, we also computed the ERP amplitude as the integral of the voltage difference between the two posterior electrodes divided by the length of the time window. We computed the correlation using trials in which the target appeared inside the receptive field of the neuron and LFP. As an additional control, we also computed the correlation during the baseline period 100 ms before array presentation. This allowed us to determine the inherent correlations between these signals independent of those elicited by the analysis of the elements in the search arrays. For this analysis, we baseline corrected 250-150 ms before the time window (i.e., 350-250 ms before array presentation).

Control for differences in signal-to-noise ratio. We measured the change in selection time with the number of trials to test whether differences in the signal and noise characteristics of the neural measures could explain observed differences in selection time. Following the methodology of Cohen et al. (2009a), we characterized the change in selection time as a function of trial number (randomly sampled, with replacement) using an exponential function of the form,

—

,

where *ST* is selection time; *n* is the number of trials; is the decay (in units of trials); $ST_{max+min}$ is the baseline (ms); and ST_{min} (ms) is the asymptote. We optimized parameters to fit ST as a function of the number of trials individually for each neuron, LFP site, and ERP. If the signal-to-noise ratio is comparable across signals, then the rate of decay, , should not vary across signals. If the timing of selection varies across signals, then the asymptote, ST_{min}, should vary across signals despite similar rates of decay.

5.4 Results

5.4. 1 Behavior

Two monkeys searched for a red or green target stimulus among one, three, or seven distractors of the opposite color (Figure 5.1A). Both monkeys exhibited behavioral hallmarks of efficient, pop-out visual search. The slopes of RT by set size (i.e., search slopes) were shallow for both monkeys (Figure 5.1C and Table 5.1). These search slopes are characteristic of pop-out search in humans (Wolfe, 1998) and monkeys (Bichot and Schall, 1999a). We compared our new effect search data to previous published data from the same monkeys performing an inefficient search task for a T among L's, and vice versa (Figure 5.1B; Cohen et al., 2009b). Both monkey's search slopes were significantly shallower during efficient search (Figure 5.1C; Table 5.1). During efficient search, the slope of percent correct by set size was not significant for monkey Q (0.001 ± 0.002; $p = 0.43$; Wilcoxon rank-sum test) and monkey S (-0.004 ± 0.005; $p = 0.72$). These results clearly indicate more efficient processing during pop-out search and demonstrate the low attentional demands of the task. It is the neural basis of this difference in processing efficiency which we turn to next.

Table 5.1. Response time and selection time search slopes, in ms/items, for each neural signal during efficient (pop-out) and inefficient visual search. Values are slope of linear regression ±SE. Asterisks indicate significant slope coefficient for set size: $p < 0.05$; $^{**}p < 0.01$; $^{***}p < 0.001$. Pairwise comparisons indicate significant interaction term for set size and task. Inefficient search data have been previously described (Cohen et al., 2009a).

	Monkey Q		Monkey S	
Response time				
Inefficient	22.6 ± 1.6 ***	***	10.5 ± 1.4 ***	***
Efficient	2.3 ± 0.8 *		0.7 ± 1.0	
FEF single-units				
Inefficient	4.6 ± 1.5 ***	***	5.3 ± 1.7 ***	
Efficient	1.2 ± 1.1		2.3 ± 1.1	
FEF LFP				
Inefficient	8.2 ± 1.4 ***	***	6.3 ± 1.3 ***	***
Efficient	1.1 ± 1.0		0.4 ± 1.5	
m-N2pc				
Inefficient	9.7 ± 0.5 ***	***	6.2 ± 0.9 ***	
Efficient	0.9 ± 1.0		1.0 ± 0.9	

5.4.2 Selection time

We recorded 102 FEF neurons (48 from monkey S and 54 from monkey Q) that exhibited discharge rate modulations following stimulus presentation or around the time of saccade initiation. This report focuses on the subset of 65/102 neurons (64%) that exhibited spatially tuned visual responses. We also recorded LFP from 141 sites (60 in monkey S and 81 in monkey Q). Of these, 109/141 (77%) exhibited spatially tuned visual responses. The neurons and LFP sites were verified to be in FEF based on low threshold microstimulation (Bruce et al., 1985). During all of these recordings we simultaneously recorded the m-N2pc from EEG electrodes over posterior lateral cortex (Figure 5.2).

We compared the *selection time,* the time when each signal first reliably signaled the target location, in FEF single-units, FEF LFPs, and the m-N2pc. Figure 5.2 shows a representative session of simultaneously recorded FEF single-unit spikes, FEF LFPs, and the m-N2pc. All three signals show an initial visual response regardless of the target's location in the visual field. However, each signal evolves over time to discriminate the location of the target stimulus before the saccade is executed. In our example session, the neuron signaled the target location with an

elevated firing rate when the target is inside the RF relative to when it is outside the RF (165 ms after the presentation of the search array; Figure 5.2A). The LFP recorded from the same electrode, signaled the target location with a greater negativity for the target relative to distractors at approximately the same time (161 ms; Figure 5.2B). The m-N2pc signaled the target location with a greater positivity contralateral to the target, but this selection did not occur until well after selection by both FEF spikes and LFP (179 ms; Figure 5.2C).

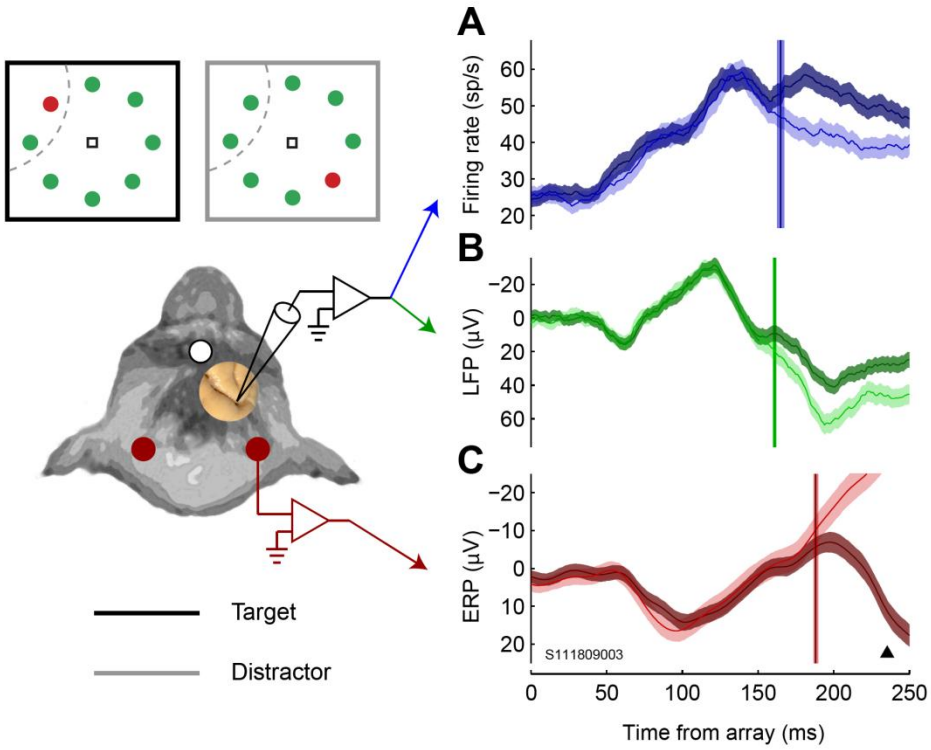

Figure 5.2 Target selection during a representative session. Average activity of one neuron (**A**), LFP site (**B**), and ERP over visual cortex (**C**) when the search target was inside (dark) and opposite (light) the receptive field (or preferred location) of the signal. Bands around average activity indicate 95% confidence intervals. Vertical lines indicate selection time when the two curves became significantly different. Bands around selection time indicate SE estimated using a bootstrap procedure (100 samples). Solid triangle indicates mean response time for this session.

Figure 5.3 shows the distribution of selection times for all three signals across our sample of all FEF neurons, FEF LFPs, and concurrently recorded m-N2pc. Overall, the m-N2pc selected

the target later (mean ± SE, 192 ± 3.9 ms) than FEF single-unit spikes (160 ± 4.1 ms; $p < 0.001$; Wilcoxon rank-sum test) and FEF LFPs (171 ± 3.9 ms; $p < 0.001$; Table 5.2). This chronology was also observed when these monkeys performed an inefficient T versus L search task (Cohen et al., 2009a), but average selection time was later in all three signals (single-units: 167 ± 3.6 ms, $p = 0.05$; LFP: 194 ± 3.2, $p < 0.001$; m-N2pc: 202 ± 1.9 ms, $p < 0.001$). In general, the selection time difference between FEF and the m-N2pc was smaller in monkey Q than monkey S (Table 5.2). One possible explanation is that FEF feedback was integrated and processed more efficiently in the visual cortex of monkey Q, which could explain his superior behavioral performance (mean RT: 223 ± 3.0 ms; percent correct: 97 ± 0.7%) relative to monkey S (mean RT: 254 ± 4.2 ms; percent correct: 83 ± 0.1%), and larger amplitude m-N2pc (4.0 ± 0.47 μV) relative to monkey S (1.9 ± 0.65 μV). Regardless, it is clear that the m-N2pc never preceded selection in FEF for both monkeys, which is inconsistent with a feed-forward hypothesis. Importantly, selection took place well before mean saccadic response time, indicating that all signals selected the target sufficiently early to have played a role in the covert attention processes that precedes saccade execution. Accordingly, the same pattern of results were observed when we computed selection time with all signals aligned on the time of saccade initiation; the m-N2pc selected the target significantly later (-71 ± 8.7 ms relative to saccade) than both FEF single-units (-113 ± 7.9 ms; $p < 0.01$) and LFP (-105 ± 6.0 ms; $p < 0.01$).

Table 5.2 Comparisons of target selection time and latency of visual onset across signals during efficient (pop-out) search. Values are means ± SE. Brackets with asterisks indicate significant differences between signals (Wilcoxon rank-sum test). Asterisks alone indicate significant difference from zero (Wilcoxon signed-rank test). * for P < 0.05; ** for P < 0.001

	Monkey Q		Monkey S	
Visual onset time, ms				
Single-units	71 ± 3.8	**	66 ± 2.6	*
LFP	52 ± 1.9	**	61 ± 2.6	*
ERP	67 ± 3.1		68 ± 4.6	
Selection time, ms				
Single-units	155 ± 4.2	*	160 ± 5.6	**
LFP	160 ± 3.7		167 ± 6.1	**
ERP	168 ± 4.1		203 ± 4.2	
Selection time difference				
ERP - Single-units	9 ± 4.3		39 ± 4.6	**
ERP - LFP	6 ± 2.6	*	31 ± 4.7	**
LFP - Single-units	3 ± 3.2		8 ± 4.6	

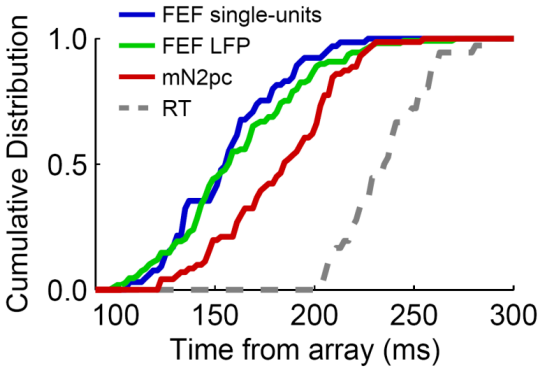

Figure 5.3 Population selection times for each type of signal. Cumulative distributions of selection times measured from intracranial FEF single-unit spiking (blue), FEF LFPs (green), and the posterior m-N2pc (red) during pop-out search. Selection precedes saccadic response time (RT, dashed grey line).

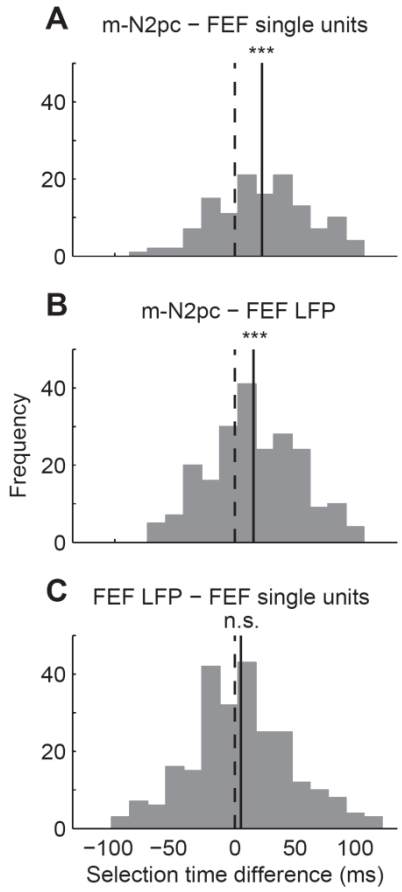

Figure 5.4 Within-session selection time differences across signals. Differences between selection time measured from simultaneously recorded m-N2pc and FEF single-unit spikes (**A**), mN2pc and FEF LFPs (**B**), and FEF LFPs and single-unit spikes (**C**). The solid vertical line indicates the mean of the distribution. The dashed vertical line indicates zero. Asterisks indicate significant differences from zero (Wilcoxon rank-sum test, *** for $p < 0.001$; n.s. for nonsignificant).

Figure 5.4A,B shows that the simultaneously recorded FEF single-units and LFPs typically selected the target before the m-N2pc (Table 5.2). The average difference between the FEF single-unit selection time and m-N2pc selection time was 23 ± 3.4 ms ($p < 0.001$; Wilcoxon signed-rank test). The average difference between FEF LFP and m-N2pc selection time was 16 ± 2.5 ms ($p < 0.001$). When we recomputed selection time using a running ms-by-ms ANOVA (Monosov et al., 2008), the selection time difference between the m-N2pc and FEF single-units and LFPs remained positive and significant ($p < 0.001$), indicating that this result cannot be due to our selection of preferred locations for each signal. This sequence of selection supports the

hypothesis that feedback from FEF contributes to the generation of the m-N2pc even during pop-out search.

One potential explanation is that the m-N2pc is delayed relative to FEF because ERPs are summing across neurons with different RFs. To test for this possibility we also computed population selection times based on all FEF single-units, LFPs, and the m-N2pc conditionalized on whether the target was in the contralateral or ipsilateral hemifield. Analyzed in this way, all three population signals reflect summation across individual signals with different RFs within a hemisphere. Population selection times (±SE, bootstrap, 500 samples) for both FEF single-units (145 ± 18) and LFPs (133 ± 15.8) were still earlier than the m-N2pc (176 ± 27). The population selection time for FEF LFP is earlier than the FEF single-unit selection time because LFP in FEF are more strongly contralaterally biased than single-units (Purcell et al., in press). It is likely that the contribution of LFPs and single-units to surface ERPs is more complex than simple summation across signals, but this result gives us a degree of confidence that the summation of scattered RFs alone cannot explain our results.

We also compared the relative timing of FEF single-units and LFPs to assess mechanisms of efficient target selection within FEF. During inefficient search tasks, FEF single-units select the target before FEF LFPs (Monosov et al., 2008; Cohen et al., 2009a). However, across the population of signals, the selection time for FEF single-units and LFPs was not significantly different during efficient search (Figure 5.3; Table 5.2; $p = 0.40$; Wilcoxon rank-sum test). Likewise, during efficient search, there was no systematic selection time difference between FEF single-units and LFPs recorded simultaneously on the same electrode (Figure 5.4C; 0.3 ± 5.1 ms; $p = 0.5$; Wilcoxon signed-rank test). We verified that the selection time difference between FEF single-units and LFP was significantly smaller during efficient search relative to inefficient search task (22 ± 3.0 ms; $p < 0.001$). This across-task difference was also evident when selection time was computed using a running ANOVA method ($p < 0.001$; Monosov et al., 2008). These results

show that when search is efficient, the FEF population activity indexed by the LFPs can discriminate the target location as rapidly as individual single-units in the population.

We measured the latency of the initial visual response in each signal to ensure that the differences in selection time were not a consequence of our recording procedures. For example, maybe all electrophysiological activity is earlier when measuring high-frequency spikes or lower frequency LFPs on the microelectrodes relative to the surface ERPs. However, this was not the case. Across monkeys, the mean latency (± SE) of the earliest visual response in each neural signal was 68 ± 2.4 ms for FEF neurons, 56 ± 1.6 ms for FEF LFPs, and 68 ± 2.7 ms for the initial visual ERP component (Table 5.2). These values are consistent with recent reports (Pouget et al., 2005; Monosov et al., 2008; Cohen et al., 2009a). The visual latency of the FEF LFPs was significantly earlier than both FEF neurons and the posterior ERPs ($p < 0.001$, Wilcoxon rank-sum test), but the mean latency of FEF neurons and posterior ERPs were statistically indistinguishable.

5.4.3 Timing and magnitude of selection during efficient and inefficient search

Previous studies have shown that discrimination of a target from distractors by visually responsive FEF neurons marks the outcome of visual processing for attentional selection (e.g., Thompson et al. 1996, 1997; Sato & Schall 2003). During inefficient search, selection time increases with set size in FEF neurons, LFPs, and the m-N2pc (Bichot et al., 2001b; Sato et al., 2001; Cohen et al., 2009a; Cohen et al., 2009b), which is consistent with delays in the time required to reliably focus attention on the target. Essentially all models of visual attention propose that distractors do not effectively compete for selection during pop-out search (e.g., Duncan and Humphreys, 1989; Treisman and Sato, 1990; Wolfe, 2007). Therefore, if selection time represents an index of attentional allocation, then we would expect it to remain invariant over set size when search is efficient and the target pops out. Indeed, we found that the mean (±SE) slope of selection time by set size during efficient search was not significant for FEF

neurons (1.7 ± 1.02 ms/item; $p = 0.09$), FEF LFP (0.6 ± 0.87 μV/item; $p = 0.48$), and the m-N2pc (0.9 ± 0.9 μV/item; p = 0.32; linear regression; Figure 5.5; Table 5.1). This contrasts sharply with the significant increases in selection time observed during inefficient search for all three signals (FEF single-units: 4.9 ± 1.14 ms/item; $p < 0.001$, FEF LFP: 7.3 ± 0.96 μV/item; $p < 0.001$, m-N2pc: 3.3 ± 0.49 μV/item; $p < 0.001$; Cohen et al., 2009a). The difference in slope of selection time by set size for inefficient search relative to efficient search was significant for all three signals (all $p < 0.001$). This result indicates that selection time increases with the attentional demands of the search task and not simply the number of objects in the visual field.

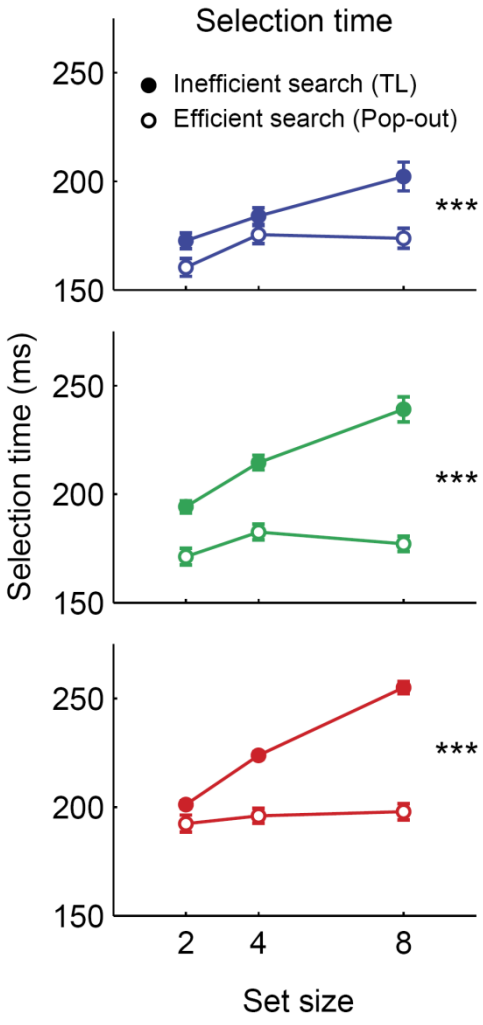

Figure 5.5 Average selection time for FEF single-unit spikes (top), FEF LFPs (middle), and m-N2pc (bottom) at each set size. Asterisks indicate significant difference in slope across efficient (pop-out) and inefficient (T versus L) search (multiple linear regression; * for p < 0.05; ** for p < 0.01; *** for p < 0.001). Error bars indicate SE.

Previous studies have also found that the amplitude of the N2pc (Luck and Hillyard, 1990, 1994b; Luck et al., 1997a) and FEF neurons (Bichot and Schall, 1999a; Cohen et al., 2009b) depends on attentional demands. During inefficient search, the amplitude of the m-N2pc (Woodman et al., 2007) and FEF neurons (Cohen et al., 2009b) declines with set size. The amplitude of ERP components is related to the variability in the latency (Luck, 2005); greater amplitude is expected with lower latency variability and lower amplitude is expected with greater latency variability. Thus, if the latency of the N2pc truly reflects an index of attentional allocation, amplitude should decline with set size during inefficient search when selection time variability increases, but should remain constant with set size during pop-out when selection time variability is constant. Indeed, we found that the slope of amplitude by set size during efficient search was not significantly different from 0 for FEF single-units (0.01 ± 0.27 sp/s/item), FEF LFP (-0.01 ± 0.16 μV/item), and m-N2pc (0.04 ± 0.13 μV/item; all $p > 0.05$; Figure 5.6). In contrast, the average slope of amplitude by set size during inefficient search significantly declined for FEF single-units (-0.59 ± 0.30 sp/s/item; $p < 0.05$), FEF LFP (-0.35 ± 0.13; $p < 0.001$), and the m-N2pc (-0.19 ± 0.04; $p < 0.001$). This resulted in a significantly smaller magnitude of selection for FEF LFPs and the m-N2pc during inefficient search (LFPs: 3.0 ± 0.56 μV; m-N2pc: 2.2 ± 0.15 μV) relative to efficient search (LFPs: 5.1 ± 0.65 μV, $p < 0.01$; m-N2pc: 3.4 ± 0.47 μV, $p < 0.01$; Wilcoxon rank-sum test). This pattern of modulation is very similar to effects seen in the human N2pc (Luck and Hillyard, 1990; Eimer, 1996). Altogether, these results indicate that selection time and amplitude in FEF neurons are sensitive to attentional demands and extends these observations to LFPs and the m-N2pc.

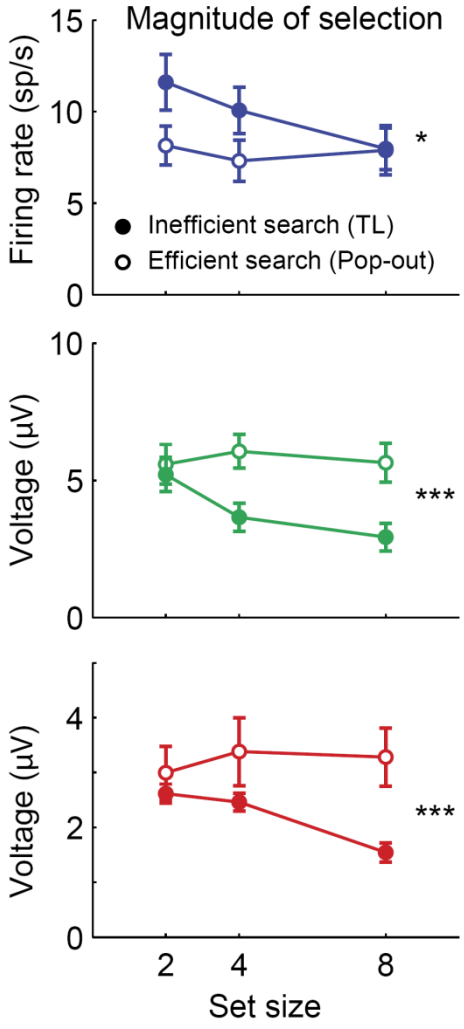

Figure 5.6 Average magnitude of selection (response amplitude when the target was in the preferred location of the signal minus the response amplitude when a distractr was in the preferred location) for FEF single-unit spikes, FEF LFPs, and the m-N2pc at each set size. Conventions as in Figure 5.5.

5.4.4 Trial-by-trial correlation of spike rate, LFP, and ERP amplitude

The similar pattern of modulation in all three signals suggests that FEF may be one source of modulations in posterior visual areas that generate the N2pc. If feedback from FEF is present during pop-out search and influences the neural mechanisms that generate the m-N2pc, then the trial-by-trial amplitude of FEF LFPs should covary with posterior ERP amplitude. The mean correlation between FEF LFP and the m-N2pc was significantly greater than zero (0.53 ± 0.02; $p < 0.001$; Wilcoxon signed-rank test) and comparable to values observed during inefficient search

(Cohen et al., 2009a). We verified that the correlation remained significant when performed on the difference in amplitude between posterior surface electrodes (Figure 5.6A; r = 0.03 ± 0.009; $p < 0.01$), which rules out the possibility that it is simply due to shared noise at the reference. Moreover, this correlation was absent during the baseline period before array presentation ($p = 0.46$) and when only distractors were in the receptive field of the LFP ($p = 0.20$), illustrating both spatial and temporal specificity. It is known that only the superficial layers of FEF feed back to visual cortex (Pouget et al., 2009), which is a likely reason why some LFP sites show negligible correlations with the m-N2pc (Figure 5.6A).

The spike rates of FEF single-units were significantly correlated with LFPs recorded from the same electrode (Figure 5.6B; r = -0.09 ± 0.008; $P < 0.001$), which is consistent with the hypothesis that LFPs reflect postsynaptic activity of neurons surrounding the electrode tip. This correlation dropped, but remained significant, when it was performed across electrodes spaced ~1mm apart (r = -0.02 ± 0.008; $p < 0.001$), suggesting that these units were nearing the edge of the area over which the LFP integrated (Katzner et al., 2009). In contrast, the mean correlation between FEF spiking and the m-N2pc measured at posterior ERP electrodes was not significantly different from zero (Figure 5.6C; r = 0.004, $p = 0.61$), which is consistent with studies showing a negligible relationship between these electrophysiological signals (Cohen et al., 2009a).

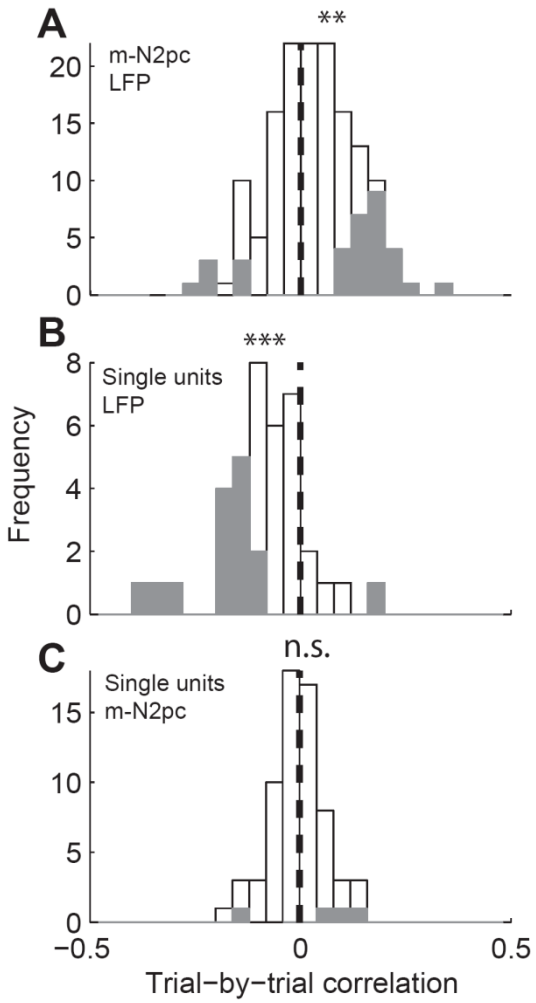

Figure 5.7 Trial-by-trial correlations between FEF LFP amplitude and the amplitude difference between posterior EEG electrodes (**A**), between FEF LFP amplitude and FEF single-unit firing rate recorded on the same electrode (**B**), and between FEF single-unit firing rate and the amplitude difference between posterior EEG electrodes (**C**). Asterisks indicate significance from zero, indicated by the vertical dashed line (Wilcoxon rank-sum; n.s. for nonsignificance; ** for $p < 0.01$; *** for $p < 0.001$).

5.4.5 Control for differences in signal-to-noise ratio across measures of neural activity

A potential concern is that the observed differences in selection time across the electrophysiological signals are due to differences in the signal-to-noise properties of each signal. The pattern of target selection times could just be a difference inherent in the neural measures at different spatial scales. In particular, the signal-to-noise characteristics of the spike times of single neurons may be different from the signal-to-noise characteristics of an LFP derived from a

weighted average of ~10^5 neurons within ~1 mm^2 of the electrode tip (Katzner et al., 2009) and from the signal-to-noise characteristics of an ERP component derived from a weighted average of many cm of cortex (Nunez and Srinivasan, 2006) It may be that through summation, the LFPs and ERPs become more reliable measures, or the summation may introduce more noise into the LFP and ERP. Following Cohen et al. (2009a), we reasoned that the signal-to-noise characteristics of each neural signal will determine how increasing trial numbers affects the reliability with which the target can be discriminated (see also Bichot et al., 2001b). We fit an exponential curve to selection times as a function of trial number measured from FEF neurons, LFP, and the m-N2pc. The average number of trials per session was greater than the number of trials necessary for all signals to reach asymptote (Figure 5.7A, black point). The rate of decay, τ, was statistically indistinguishable for neurons (101 ± 26.4; median ± SE), LFP (139 ± 33.0), and the m-N2pc (129 ± 24.9; Figure 5.7B; all $p > 0.09$; Wilcoxon rank-sum test). In a previous study of inefficient search (Cohen et al., 2009a), the corresponding values were 94 ± 14.2, 144 ± 21.7, and 97 ± 17.5 for neurons, LFP, and the m-N2pc, respectively (all $p > 0.14$). This result is consistent with the comparable confidence intervals that are apparent in Figure 5.2. However, the level at which selection time reached asymptote was lowest for neurons (138 ± 4.3), followed by LFP (150 ± 4.2), and latest by the m-N2pc (180 ± 4.0; Figure 5.7C; all $p < 0.05$, Wilcoxon rank-sum test). This result is consistent with the ordering of selection times reported above (Figure 5.3). In a previous study of inefficient search (Cohen et al., 2009a), the corresponding values were 151 ± 3.2, 172 ± 5.2, and 188 ± 2.7 for neurons, LFP, and the m-N2pc, respectively (all $p < 0.01$). Thus, we can conclude that the timing differences across the signals are not due to different signal-to-noise characteristics of the neural measures.

5.5 Discussion

To understand the neural mechanisms that generate attention-related ERPs in humans, we recorded the macaque homologue of the N2pc component simultaneously with single-unit spiking

and LFPs in FEF. We asked how the timing of selection in all three signals depends on the attentional demands of the task by directly comparing the timing of selection during an efficient pop-out search task with an inefficient form search task (Cohen et al., 2009a). We showed that both the timing and magnitude of selection in all three signals depends on the attentional demands of the task. However, selection was evident in FEF before the m-N2pc regardless of search efficiency. These results are consistent with the hypothesis that the primate N2pc is due to feedback from higher cortical areas, even when bottom-up salience is sufficient for task performance. These results also inform us about the neural mechanisms that generate the N2pc and constrain theories of visual attention.

5.5.1 Comparison of human and macaque N2pc

Before we consider the relevance of our findings to the study of human ERPs, we must first ask whether the macaque m-N2pc indexes the same cognitive operations as the human N2pc. The m-N2pc satisfies several established criteria for across-species homology (Woodman, 2011). Previous studies have shown that the spatial distribution of the N2pc is maximal over posterior electrodes in both humans (Luck and Hillyard, 1994b) and monkeys (Woodman et al., 2007; Cohen et al., 2009a). In addition, previous studies have found that the latency of the N2pc increases with set size in both humans (Luck and Hillyard, 1990) and monkeys (Woodman et al., 2007) when search is inefficient. We found that the latency and amplitude of the macaque N2pc (m-N2pc) are insensitive to changes in set size during efficient pop-out search, which is consistent with an index of attentional demands and not simply the number of objects on the screen. We also found that the amplitude of the m-N2pc is greatest during efficient search, which is observed with the human N2pc (Eimer, 1996). Thus, the m-N2pc satisfies multiple criteria for homology including a similar spatial distribution, task dependence, and timing. Our findings provide new support for this across-species homology.

One notable across-species difference is that the polarity of the N2pc is reversed. Humans show a contralateral negativity and monkeys show a contralateral positivity. This is likely due to differences in cortical folding in posterior visual areas across the species. For example, macaque V4 is located on the surface of the prelunate gyrus (Zeki, 1971), but the human homologue spans several sulci (Orban et al., 2004). Another potential across-species difference is that several studies of the human N2pc have reported increases in amplitude with attentional demands (Luck et al., 1997a; Hopf et al., 2002), whereas we observed declines in the m-N2pc. This is likely due to differences in task design rather than species. In humans, this effect is observed when targets and distractors are tightly grouped in a limited portion of the visual field. In contrast, when stimuli are well spaced across hemifields as in our monkey studies, amplitude decreases with additional stimuli (Eimer, 1996). Future experiments that directly compare the N2pc observed in humans and monkeys under identical experimental design (e.g., Godlove et al., 2011b; Reinhart et al., 2012a; Reinhart et al., 2012b) can further establish the homology across species.

5.5.2 The origin and interpretation of the N2pc

We found that the pattern of modulation in FEF LFP and the N2pc were similar during inefficient and efficient visual search and the signals were correlated on a trial-by-trial basis. This suggests that FEF is influencing the generation of the N2pc, but it seems unlikely that the contribution is direct. First, voltage distributions, current source density topography, and dipole source modeling suggests that the dipole seen as the N2pc on the scalp originates in posterior visual cortex in humans (Luck et al., 1997b; Hopf et al., 2000; Hopf et al., 2004) and monkeys (Woodman et al., 2007; Cohen et al., 2009a; Young et al., 2011). Second, the timing differences that we observed seem inconsistent with identification of FEF as the direct neural generator because extracranial EEG is not delayed relative to intracranial synaptic activity (Nunez and Srinivasan, 2006). The electrical fields generated in FEF are probably actively canceled or the dipole is oriented such that it does not produce an observable extracranial signal.

Instead, these observations are consistent with the hypothesis that FEF is part of a frontal-parietal network involved in driving attentional shifts in posterior visual areas thought to generate the m-N2pc (Corbetta, 1998). FEF is part of a distributed network of structures shown to encode a representation of visual salience for guiding attentional deployments (Thompson and Bichot, 2005). Our observation that activity in FEF modulates concurrently with the m-N2pc during both efficient and inefficient search suggests that this network is engaged regardless of search efficiency. Some studies have questioned the need for an influence of frontal structures during efficient search tasks based on BOLD responses (Leonards et al., 2000) and effects of transcranial magnetic stimulation (Muggleton et al., 2003) in prefrontal areas during inefficient, but not efficient search. However, these results are inconsistent with findings from monkey studies showing that reversible inactivation of FEF with the GABA agonist muscimol impairs performance on pop-out search tasks (Wardak et al., 2006; Monosov and Thompson, 2009). In addition, other studies report comparable BOLD activation in human (Anderson et al., 2007) and monkey (Wardak et al., 2010) FEF irrespective of search efficiency. Thus, our results add to converging evidence suggesting that FEF plays an important role in processing visual targets even during efficient search tasks.

Our results also inform the interpretation of the cognitive processes indexed by the primate N2pc. The degree to which the human N2pc reflects the initial spatial selection of a target or post-selection processing has been unclear (Eimer and Kiss, 2010; Theeuwes, 2010). Our data place clear limits on the degree to which the latency of the N2pc can be interpreted as the time of initial spatial selection because the N2pc followed selection in prefrontal cortex even during an efficient search task that required minimal feature analysis. One limitation of the current task design is that the singleton was always task relevant, and therefore we cannot make strong claims about the relative timing of selectivity based on pure bottom-up physical salience. However, our results are consistent with a growing body of work demonstrating the sensitivity of the N2pc to top-down factors and extend that work by suggesting that FEF is a likely source of this top-down

modulation. When a color singleton is not task relevant, the N2pc is small or absent (Luck and Hillyard, 1994b; Eimer et al., 2009) and selectivity in FEF is minimal (Bichot et al., 2001a). The N2pc is also sensitive to rewards associated with target localization and identification (Kiss et al., 2009), as are FEF neurons (Ding and Hikosaka, 2006). Lastly, trial history and experience influence both the N2pc (Eimer et al., 2010; An et al., 2012) and FEF neurons (Bichot et al., 1996; Bichot and Schall, 1999a, 2002). The same FEF neurons that are modulated by these top-down factors project to earlier visual areas thought to generate the N2pc (Pouget et al., 2009), which is consistent with the hypothesis that FEF is the source of these modulations.

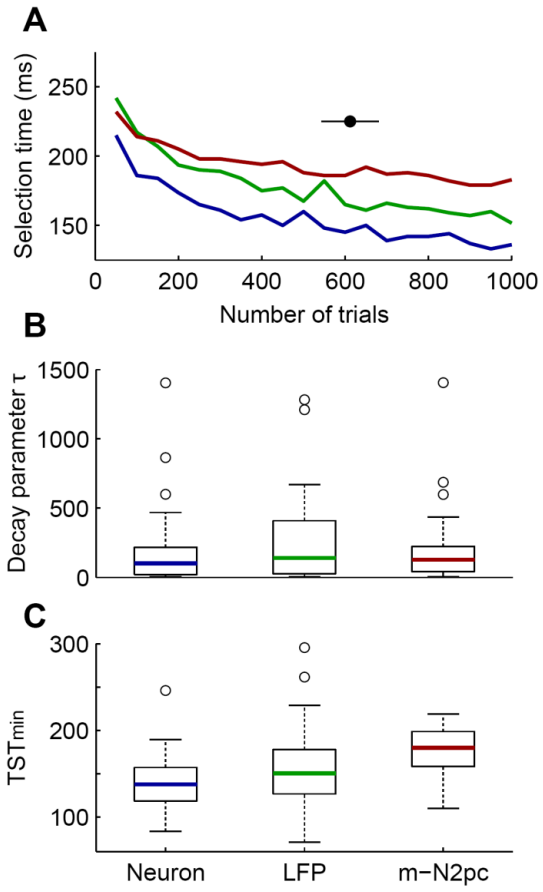

Figure 5.8 Selection time by number of trials. A: average selection time as a function of number of trials (randomly sampled, with replacement) across recordings of FEF single-units (blue), LFP (green), and m-N2pc (red). The black point (with SE line) indicates the average number of trials in our data set. B: decay parameter (τ) estimates from exponential fits to the selection time by number of trials. C: asymptote parameter (TST_{min}) estimates from the exponential fits plotted in B.

5.5.3 Relation to previous studies of attentional selection across cortex

Several recent studies have investigated the timing of attentional selection across cortex using paired intracranial recordings. Zhou and Desimone (2011) observed earlier selection in FEF neurons relative to V4 neurons during an inefficient conjunction search tasks. Similarly, during inefficient conjunction search, Buschman & Miller (2007) observed earlier selection in FEF and dorsolateral prefrontal neurons. In addition, Monosov et al., (2010) found that FEF neurons exhibited significant spatial selectivity before IT neurons exhibited significant object selectivity during a difficult search and identification task. Thus, converging evidence supports the hypothesis that attentional selection in FEF neurons precedes attentional selection in several earlier visual areas when tasks are attentionally demanding (see also Cohen et al., 2009a), but findings during efficient pop-out search are less consistent. One study found that selectivity in lateral intraparietal area precedes selectivity in FEF and dorsolateral prefrontal cortex during pop-out search (Buschman and Miller, 2007), but preliminary evidence from another study found the opposite; frontal areas selected before parietal areas during pop-out (Katsuki and Constantinidis, 2011). In addition, studies using nearly identical task designs and analytical methods found that both FEF and LIP select the location of a color singleton at approximately the same time (Thompson et al., 1996; Thomas and Pare, 2007). Our observation that the m-N2pc selects the target location later than FEF is consistent with studies suggesting that FEF selectivity precedes selectivity in early visual areas, but it is important to note that ERPs cannot be regarded as a direct proxy for underlying neural activity. ERPs are thought to reflect the summation of synchronous activity across many centimeters of cortex (Nunez and Srinivasan, 2006), and the N2pc likely reflects attentional selection across multiple visual areas. Thus, additional simultaneous recordings in frontal and parietal areas will be necessary to conclusively determine the degree to which the timing of selection across neurons in different cortical areas depends on task demands.

In addition to our observations regarding the timing relationship between FEF and the m-N2pc, we also observed differences in the relative timing of selection in FEF single-units and LFP depending on the attentional demands of the task. Previous studies have found that FEF LFPs select the target later than FEF single-units (Monosov et al., 2008; Cohen et al., 2009a). We found that the delay in selection time between FEF single-units and LFPs was absent during pop-out. LFPs reflect the synaptic activity of thousands of neurons surrounding the electrode tip (Mitzdorf, 1985; Katzner et al., 2009), whereas spiking activity reflects only a single neuron. Therefore, one interpretation of this result is that the population of FEF neurons contributing to the LFP reached a consensus about target identity more efficiently during pop out. The absence of a delay between selection in FEF single-units and LFP was unexpected given a previous report showing a significant delay between the two signals in one monkey performing a covert pop-out search task in which target location was reported via lever turn (Monosov et al., 2008). Covert visual search requires active suppression of saccade generating neurons in FEF (Thompson et al., 2005a), which could have postponed LFP selectivity. In line with the present findings, another interpretation is that the delayed LFP selection time relative to single-units during covert search reflects the increased attentional demands required to map target location to the lever turn.

5.5.4 Relation to theories of visual search and attention

Early models of visual attention proposed that targets that could be distinguished by a single feature could be localized "pre-attentively" solely through bottom-up selection of local feature differences (Treisman and Gelade, 1980; Itti and Koch, 2001). Other studies have shown that prior knowledge and expectation have a strong influence on pop-out performance (Treisman and Gormican, 1988; Maljkovic and Nakayama, 1994; Joseph et al., 1997). Our finding that an attentional control area, FEF, contributes to the generation of the N2pc during efficient search is consistent with theories of visual attention that propose no strong dichotomy between efficient and inefficient search (Treisman and Sato, 1990; Desimone and Duncan, 1995; Bundesen et al.,

2005; Wolfe, 2007). This result is consistent with a recent study which found that the enhanced response of V4 neurons to a pop-out stimulus is eliminated when attention is directed elsewhere in the visual field (Burrows and Moore, 2009). Thus, our findings add to behavioral and neurophysiological evidence that top-down input from frontal cortex may guide attentional selection even during pop-out search.

CHAPTER VI

SUPPLEMENTARY EYE FIELD DURING VISUAL SEARCH: SALIENCE, COGNITIVE CONTROL, AND PERFORMANCE MONITORING

6.1 Abstract

How supplementary eye field (SEF) contributes to visual search is unknown. Inputs from cortical and subcortical structures known to represent visual salience suggest that SEF may serve as an additional node in this network. This hypothesis was tested by recording action potentials and local field potentials (LFP) in two monkeys performing an efficient pop-out visual search task. Target selection modulation, tuning width, and response magnitude of spikes and LFP in SEF were compared with those in frontal eye field. Surprisingly, only ~2% of SEF neurons and ~8% of SEF LFP sites selected the location of the search target. The absence of salience in SEF may be due to an absence of appropriate visual afferents, which suggests that these inputs are a necessary anatomical feature of areas representing salience. We also tested whether SEF contributes to overcoming the automatic tendency to respond to a primed color when the target identity switches during priming of pop-out. Very few SEF neurons or LFP sites modulated in association with performance deficits following target switches. However, a subset of SEF neurons and LFP exhibited strong modulation following erroneous saccades to a distractor. Altogether, these results suggest that SEF plays a limited role in controlling ongoing visual search behavior, but may play a larger role in monitoring search performance.

6.2 Introduction

Natural vision requires an organism to select important objects from irrelevant objects to guide responses. Models of visual search propose that a *salience* map (also termed *priority*) combines bottom-up physical conspicuousness with top-down knowledge of target features to guide attention and eye movements (Tsotsos et al., 1995; Itti and Koch, 2001; Bundesen et al.,

2005; Wolfe, 2007). A distributed network of visuomotor areas encodes a representation of salience (Findlay and Walker, 1999; Thompson and Bichot, 2005; Gottlieb, 2007; Bisley and Goldberg, 2010). This includes the frontal eye field (FEF; Thompson et al., 1996; Bichot and Schall, 1999a; Purcell et al., 2012b), superior colliculus (SC; McPeek and Keller, 2002; Shen and Paré, 2007), substantia nigra pars reticulata (SNpr; Basso and Wurtz, 2002), lateral intraparietal area (LIP; Ipata et al., 2006; Thomas and Pare, 2007; Balan et al., 2008; Arcizet et al., 2011) and parietal area 7A (Constantinidis and Steinmetz, 2001). Supplementary eye field (SEF) receives cortical afferents from FEF, LIP, and 7A (Andersen et al., 1990; Huerta and Kaas, 1990; Schall and Hanes, 1993) as well as from the superior temporal polysensory area and nuclei in the central thalamus that are innervated by SC and SNpr (Lynch et al., 1994; Parent and Hazrati, 1995) and contribute to saccade target selection (Schall and Thompson, 1994; Wyder et al., 2004) (Figure 6.1).

Connectivity with these visuomotor areas suggests that SEF may represent just one more node in the cortical network representing salience. Furthermore, SEF neurons exhibit clear visual responsiveness (Schlag and Schlag-Rey, 1987; Schall, 1991a, b; Russo and Bruce, 2000; Pouget et al., 2005). SEF neurons respond selectively to a number of stimulus categories including the type of information they provide (Campos et al., 2009), arbitrary stimulus response associations (Chen and Wise, 1995a, b, 1996; Olson and Tremblay, 2000), expected reward (Seo and Lee, 2009; So and Stuphorn, 2010), and their rank order in a sequence (Lu et al., 2002; Berdyyeva and Olson, 2009). However, similarity of elementary physiological properties may belie important functional differences in more complex contexts; for example, although many neurons in FEF, SC, and SEF discharge before saccades, saccade-initiation is directly controlled by FEF (Hanes et al., 1998) and SC (Pare and Hanes, 2003), but not SEF (Schiller et al., 1979; Schiller and Chou, 1998; Stuphorn et al., 2010).

Other research suggests that medial frontal areas, including SEF, are involved in the monitoring and control processes recruited when errors are made and habitual actions must be

overcome (Schlag-Rey et al., 1997; Stuphorn et al., 2000; Stuphorn and Schall, 2006; Isoda and Hikosaka, 2007; Emeric et al., 2010; Isoda and Hikosaka, 2011). Priming of pop-out tasks in which the target and distractor features switch randomly every few trials requires overcoming the primed tendency to respond to a distractor following switches (Maljkovic and Nakayama, 1994). FEF neurons that encode salience modulate in parallel with changes of performance during priming (Bichot and Schall, 2002), but it is not known whether medial frontal cortex is involved in suppressing the primed tendency to respond to a distractor or facilitating the controlled response to the new target.

We tested the hypothesis that SEF encodes visual salience to select saccade targets by recording spiking activity and local field potentials (LFP) in the SEF of two monkeys trained to perform a visual search task. We also asked whether SEF controls or monitors changes in performance during priming of pop-out. The data also provide new quantitative comparisons between SEF and FEF.

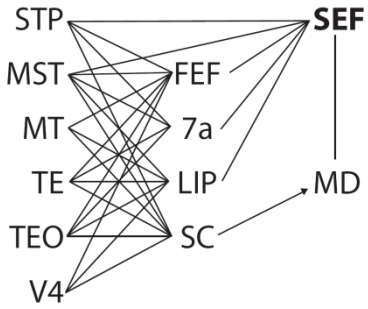

Figure 6.1 Distribution of visual afferents to supplementary eye field (SEF). Lines indicate reciprocal connections. Arrow indicates one way projection. SEF is densely connected with visuomotor areas that are known to represent visual salience (bold) including frontal eye field (FEF) and lateral intraparietal area (LIP), area 7a, as well as from superior colliculus (SC) via the medial dorsal nucleus of the thalamus (MD). These areas receive afferents from diverse areas in visual cortex that encode various target features (italicized). In contrast, SEF does not receive direct input from areas representing stimulus features from which a salience map is computed. Not pictured are efferent connections to SC and reciprocal connections with the ventral anterior and ventrolateral nuclei of the thalamus which are innervated by substantia nigra pars reticulata.

6.3 Materials and methods

6.3.1 Behavioral tasks and recordings

Recording procedure. We recorded neuronal spikes and simultaneous LFP from the SEF of one male bonnet macaque monkey (*Macaca radiata* ~8.5 kg, monkey F) and one male rhesus macaque monkey (*Macaca mulatta* ~12.5 kg, monkey Z). Monkeys were surgically implanted with a head post and recording chambers during aseptic surgery with animals under isoflurane anesthesia. Antibiotics and analgesics were administered post-operatively. All surgical and experimental procedures were in accordance with the National Institute of Health *Guide for the Care and Use of Laboratory Animals* and approved by the Vanderbilt Institutional Animal Care and Use Committee.

Neurons and LFP were recorded simultaneously from the right hemisphere of both monkeys using tungsten microelectrodes (2-4 MΩ, FHC) and were referenced to a guide tube in contact with the dura. Spikes were sampled at 40 kHz and LFP were sampled at 1kHz. LFP were band-pass filtered between 0.2 and 300 Hz and amplified using a Plexon HST/8o50-G1 head-stage. A 60 Hz second-order IIR notch filter was applied offline to reduce electrical noise. LFP were baseline corrected using the average voltage 50ms until the array onset. Spikes were sorted online using a time-amplitude window discriminator and offline using principal component analysis and template matching (Plexon). We generated spike density functions by convolving each spike train with a kernel resembling a postsynaptic potential (Thompson et al., 1996). Eye movements were monitored with an infrared corneal reflection system (SR Research) at a sampling rate of 1 kHz.

Behavioral tasks. Monkeys were trained to perform three tasks: a visual search task, a detection task, and a memory-guided saccade task (Figure 6.2). Tasks were run in blocks and task order was counterbalanced across recording sessions. All tasks began with the monkey fixating a central white spot for ~500ms. In the color visual search task, the fixation point

changed from filled to open simultaneously with the onset of a colored target and seven isoluminant distractors (2.8 cd/m^2) of the opposite color. Targets and distractors were either red (CIE chromaticity coordinates x = 0.648, y = 0.331) or green (CIE x = 0.321, y = 0.598). The monkey was rewarded for making a single saccade to the location of the target within 2000 ms and fixating for 500 ms. For some experimental sessions target and distractor color remained constant throughout the session and target color was varied across sessions. For other sessions target and distractor color were swapped in successive blocks of trials to investigate priming of pop-out. Block duration was sampled from a uniform distribution ranging over 8-16 trials. This task required animals to discriminate the singleton target from distractors and then shift gaze to that location as quickly as possible while maintaining reasonable accuracy.

In the detection task, the target (red or green disk) was presented at one of the same eight locations and remained on the screen. Simultaneous with the onset of the target, the fixation point changed from filled to open, instructing the animal to make a saccade to the target location within 2000 ms and maintain fixation for 500 ms for reward. This task was identical to the visual search task, but included no distractor stimuli.

In the memory-guided saccade task, a target (filled gray disk) was presented for 100 ms at one of eight isoeccentric locations equally spaced around the fixation spot at 10^o eccentricity. The animal was required to maintain fixation for 400-800 ms (uniform distribution) after the target onset. After the fixation point changed from filled to open, the monkeys were rewarded for making a saccade to the remembered location of the target and maintaining fixation for 500 ms. For monkey Z, this task also included a small fraction (~15%) of "NoGo trials" in which a change in fixation point color cued the monkey to maintain fixation for reward. The memory-guided saccade task was used to temporally dissociate sensory and motor-related responses for neuron and LFP classification (Bruce and Goldberg, 1985).

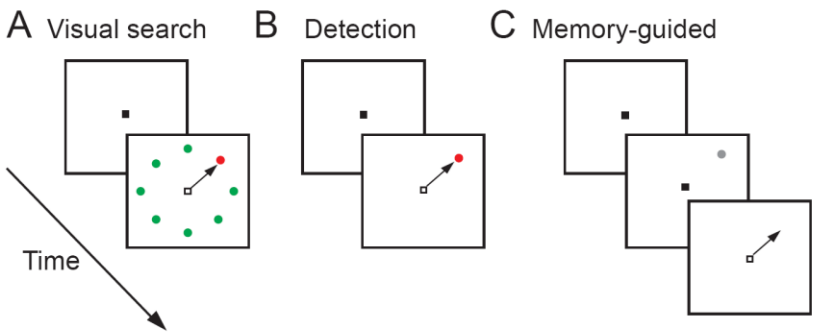

Figure 6.2 A, Visual search task. After fixating a central point for a variable delay (top frame), an array of stimuli was presented (bottom frame), one of which was the target (e.g., red disk) and the rest were distractors (e.g., green disks). Monkeys were required to make a single saccade (indicated by the arrow) to the target for reward. **B**, Detection task. This task is identical to the visual search task except the target appeared alone without distractors. **C**. Memory-guided saccade task. After fixating for a variable delay (top frame), the target was flashed for 100 ms at one of eight locations (middle frame). The animal was required to maintain fixation for a variable delay until the fixation point changed from filled to open (bottom frame), which signaled the animal to make a single saccade to the remembered target location for reward.

Localization of SEF. In both monkeys, we determined the location of SEF by the effects of intracortical microstimulation and histology (Figure 6.3). Microstimulation parameters were conventional (100ms trains of 333 Hz biphasic pulses of 0.2 ms pulse duration). After the experiment, monkey F was deeply anesthetized with pentobarbital and perfused with 0.1 M phosphate buffered saline (PBS), followed by 4% paraformaldehyde (PFA) in PBS followed by buffered sucrose solution (10% surcrose, 4% PFA in PBS). Monkey Z could not be perfused, so the brain was post-fixed in 4% PFA for 10 days. Both brains were photographed in situ. Fiduciary guide pins in the recording chamber were located relative to the hemisphere midline and arcuate and principal sulci. The sites of neurons and LFP with task-related responses and sites from which saccades could be elicited with low threshold ($\leq$50 μA) microstimulation were located in Nissl-stained sections relative to previously described cytoarchitectural landmarks (Mitz and Wise, 1987; Luppino et al., 1991; Matelli et al., 1991; Schall, 1991a).

Frontal eye field data. We analyzed FEF neurons and LFP recorded during the same visual search task to compare directly with SEF. We analyzed single-unit activity and LFP recorded in the FEF of two additional monkeys (monkey Q, *Macaca radiata* ~7.5 kg; monkey S, *Macaca*

radiata ~8.5 kg) during a color visual search task. This task included a set size manipulation in which the number of distractors (1, 3, or 7) varied randomly across trials, but was otherwise identical to the visual search task described above. We also analyzed previously published single-unit activity recorded from the FEF of monkey F while he performed the identical color search task (Sato et al., 2001). All FEF recordings were acquired from the rostral bank of the arcuate sulcus at sites where saccades were evoked with low-intensity electrical microstimulation (<50 μA; Bruce and Goldberg, 1985). Analytical methods were identical for SEF and FEF data.

Behavioral performance was consistent across species. There was no systematic difference in percent correct (87% for monkey F: 85% for monkey Z; 96% for monkey Q; 86% for monkey S) or mean RT (210 ms for monkey F; 216 ms for monkey Z; 222 ms for monkey Q; 254 ms for monkey S).

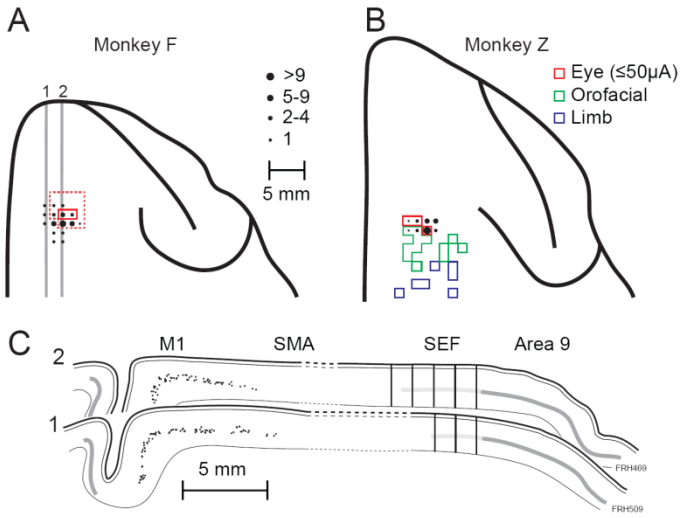

Figure 6.3 Localization of SEF. **A,B.** Dorsal view of recording sites in monkey F (**A**) and monkey Z (**B**). Circle size indicates the number of neurons with task-related responses. Xs indicate sites that were sampled, but no task-related neuron was found. Solid colored lines indicate areas in which limb, orofacial, and saccadic eye movements were elicited by electrical microstimulation. Red dashed lines indicate areas in which low threshold saccades were elicited at the symmetric position in the opposite hemisphere. **C.** Sagittal sections from monkey F at levels indicated in panel **A** (gray lines 1 and 2) illustrate location of penetrations relative to cytoarchitectural landmarks. Black vertical lines indicate reconstructed penetration locations. The caudal penetration (**C2**, left) is 27 mm anterior to the interaural line. **C1** and **C2** are ~4.7 mm and ~6.7 mm lateral of midline, respectively. Dots mark locations of Betz cells in primary motor cortex (M1) and supplementary motor area (SMA). Dark shading indicates granular layer in prefrontal cortex (area 9) and light shading indicates the incipient granular layer that is characteristic of SEF. Dashed lines indicate a damaged region. **D.** Sagittal sections from monkey Z at levels indicated in panel **B** (gray lines 3 and 4). **C3** and **C4** are ~6.0 mm and ~8.0 mm lateral of midline, respectively. Conventions as in panel C.

6.3.2 Data analysis

Neuron and LFP classification. We identified task-related neurons and LFP by comparing discharge rates or voltage to the baseline period 50 ms before presentation of the array. A neuron or LFP site was classified as *visually responsive* if discharge rate or polarization remained significantly different from baseline for five consecutive 10 ms time bins in the interval 50 to 200 ms following stimulus presentation for the memory-guided saccade task and in the interval 50 to 150 ms for the detection or search tasks (Wilcoxon rank-sum test, $P < 0.05$). A neuron or LFP site was classified as *saccade-related* if discharge rate or polarization remained significantly different from baseline for five consecutive 10 ms time bins in the interval -100 to 100 ms relative to saccade initiation for all tasks. Only visually-responsive neurons are included in our analyses of visual salience; although, we verified that results were identical for neurons with saccade-related discharge modulation. As in previous reports, many saccade-related neurons did exhibit direction selectivity, but it emerged too late to represent a covert salience representation that guided saccade target selection (<20 ms before saccade onset; Scudder et al., 2002 see also Stuphorn et al., 2010). All neurons were included in our priming analyses regardless of when task-related modulations were observed.

Spatial selectivity. The selectivity of spikes and LFP to target location was quantified by vector summation of the normalized response to each target (Batschelet, 1981; Schall, 1991a). The angle of the resultant vector gave the preferred response location of the neuron or LFP site (0^o – ipsilateral; 180^o – contralateral). The length of the resultant vector was defined as the direction bias. Direction bias ranged from 0 (equal responses for all locations) to 1 (maximal response to a single location). When measured during the detection task with a single stimulus, this quantified the location and tuning width of the receptive field (RF) for a given eccentricity. When measured during the visual search task, this quantified the extent to which the target was localized. For visual search and detection, we used the average voltage or discharge rate from 50

ms after stimulus presentation until 50 ms before mean saccade initiation time to exclude saccade-related responses. For the memory-guided saccade task, we used the average voltage or discharge rate in the time interval from 50 to 200 ms after stimulus onset. We assessed the significance of spatial selectivity using a permutation test which determined the probability of obtaining the preferred location by chance alone (Georgopoulos et al., 1988 ; 1000 simulations, $P < 0.01$).

We also quantified the selectivity of SEF and FEF neurons and LFP to the target versus distractors using a "neuron-antineuron" analysis (Thompson et al., 1996). We computed the area under the receiver operating characteristic (ROC) curve from the distribution of discharge rate or polarization in trials in which the target appeared inside the RF and trials in which only distractors appeared inside the RF. The area under the curve reflects the probability that an ideal observed could correctly specify whether the target was in the neuron's RF. For this analysis the RF was conservatively defined as the stimulus locations within 45^{o} of the preferred angle, although tuning width was also measured more rigorously (see *Receptive field width*). For neurons, the ROC was computed by incrementing a criterion from 0 spikes/s to the maximum discharge rate observed across all trials in steps of 1 spike/s. For LFP, the criterion was incremented from the minimum voltage observed to the maximum voltage observed in steps of 10 μV. The distribution of discharge rates and voltages was obtained for 5-ms intervals averaged from 5 ms before to 5 ms after each time point to smooth the data. The average area under the ROC curve from 50 ms after array onset to 50 ms before mean RT determined the magnitude of target selectivity for each neuron and LFP site.

Visual response latency. The latency of the visual response was determined by comparing baseline activity 10 ms before array onset to a ms-by-ms sliding window starting at array onset. The visual onset was the time when activity first became significantly different from baseline and remained significant for 10 consecutive ms (Wilcoxon rank-sum test, $P < 0.01$).

Spatial tuning width. We quantified the spatial tuning width by fitting the variation in discharge rate or voltage as a function of target location with a Gaussian function of the form:

_____

where activation (*A*) as a function of meridional direction ( ) depends on the baseline discharge rate (*B*), maximum discharge rate (*R*), optimum direction ( ), and directional tuning ( ) (Bruce and Goldberg, 1985; Schall et al., 1995b; Russo and Bruce, 2000; Schall et al., 2004; Monosov et al., 2008). Tuning width was estimated by the standard deviation ( ) of the best fitting Gaussian curve. The data were fitted with a Simplex routine implemented in MATLAB (The MathWorks) to minimize the sum of squared deviations between observed and predicted values. We excluded neurons and LFP sites for which the Gaussian curve accounted for <50% of the variance in the data indicating very poor fit (8 neurons; 26 LFP). The eccentricity was matched for SEF and FEF recordings, which allows for direct comparison across areas and signals, but note that the tuning width of SEF and FEF neurons will vary with eccentricity (Bruce and Goldberg, 1985; Russo and Bruce, 2000).

Visual response magnitude. The magnitude of the initial visual response in SEF neurons and LFP was computed as the mean discharge rate or voltage in the interval 50 ms to 150 ms minus the baseline in the interval - 50 ms to 0 ms relative to stimulus onset.

Error signal analysis. We identified error-related neurons and LFP by comparing firing rates and voltage on trials in which the animal made a correct saccade to the target with trials in which the animal made an incorrect saccade to a distractor. Errors in which the monkey prematurely broke fixation, failed to maintain fixation on the target, or initiated a saccade to an empty location were rare and are not considered further. LFP were baseline corrected -50 to 0 ms relative to saccade onset to eliminate differences in pre-saccadic modulation. A neuron or LFP was classified as *error-related* if modulation was significantly greater when the monkey made an erroneous saccade to a distractor as when the monkey made a correct saccade to the target in the

interval 100 to 300 ms after the saccade (t-test, $p < 0.05$). The number of trials in which erroneous saccades were made to each location was matched across locations by excluding random trials. The number of trials in which correct saccades were made to each location was matched to the trial counts for error saccades by excluding random trials. Thus, the distributions of saccade directions was identical when comparing correct and error trials. Trials in which the animal failed to maintain fixation for 400 ms were excluded to eliminate the influence of non-task-related eye movements (e.g., unrewarded corrective saccades to the target). This analysis used only neurons and LFP recorded during sessions in which the target was varied across blocks because monkeys made few errors when the target remained constant (~93% correct). Most errors occurred on trials following changes in target identity, but we found no difference in post-saccadic activity on switch and non-switch trials, therefore we combined across all error trials regardless of the number of trials since the switch.

6.4 Results

6.4.1 Absence of salience in SEF spiking activity during visual search

We recorded 135 SEF neurons (92 from monkey F; 43 from monkey Z) that exhibited discharge rate modulation following stimulus presentation or around the time of saccade initiation. The neurons were verified to be in SEF based on histology and relation to microstimulation landmarks (Figure 6.3). Our analysis of visual salience focuses on the subset of 95 visually-responsive neurons that exhibited discharge rate modulation following stimulus presentation. This included neurons recorded during sessions in which the target was constant and sessions in which the target changed in blocks. Of these neurons, 36 (38%) were classified as pure *visual neurons* which responded only following the stimulus onset and 59 (62%) were classified as *visuomovement* neurons which responded both following stimulus onset and around

the time of saccade. The mean SEF neuron visual latency (±SE) was 71 ± 2.4 ms, which approximately corresponds to previous reports (Pouget et al., 2005).

Table 6.1 Numbers (percentages) of visually-responsive neurons and LFP that selected targets.

	Neurons			LFP		
Monkey	Total	Select single target	search target	Total	Select single target	Select search target
F	69	44 (63.8%)	1 (1.4%)	145	51 (35.2%)	13 (9.0%)
Z	26	14 (53.8%)	1 (3.8%)	40	11 (27.5%)	2 (5.0%)
Total	95	58 (61.1%)	2 (2.1%)	185	62 (33.5%)	15 (8.1%)

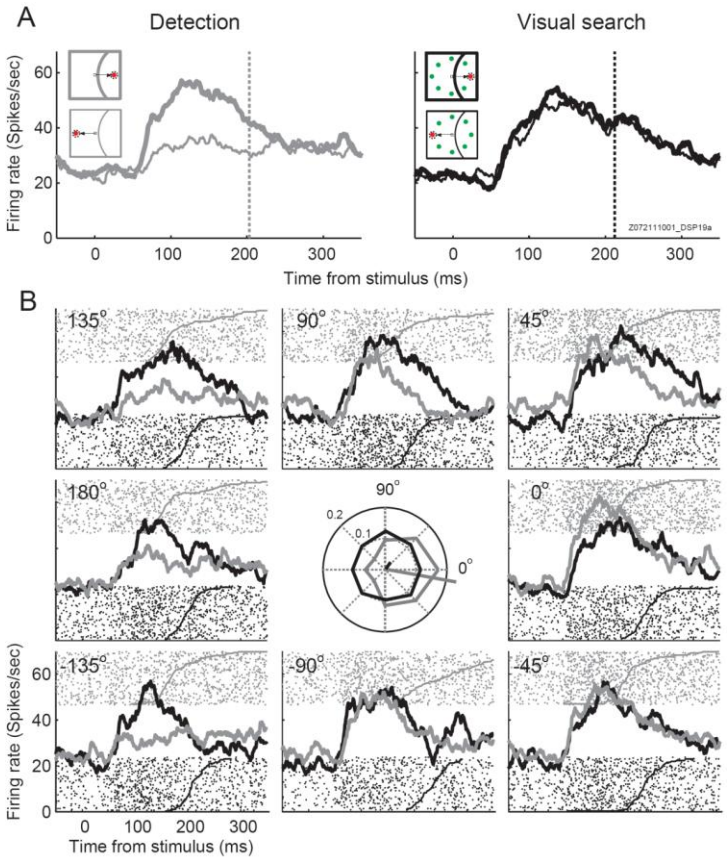

Figure 6.4 Representative visually-responsive neuron during detection and search. **A.** Average spike density functions on trials when the target was inside (thick) or opposite (thin) the receptive field (RF) of the neuron during the detection (left) and visual search (right) tasks. Vertical dotted line indicates mean saccade response time. **B.** Rasters and average spike density functions of the representative neuron when the target was located at each of eight isoeccentric location during the detection (gray) and search (black) tasks. Lines indicate response time distributions. The central polar plot indicates the normalized response of the neuron to each target location during both tasks. The vector sum of the response to the target at each location is indicated by the radial line, the length of which indicates the directional bias, or strength of spatial tuning.

Figure 6.4 shows the discharge rate of a representative visually-responsive neuron during the detection and visual search tasks. We quantified the spatial selectivity of the neuron by computing a normalized vector sum of the neuron's response to the target at each polar angle. The angle of the resultant vector quantifies the direction of the center of a neuron's RF in polar angle and the length quantifies the degree of selectivity. A neuron with a response field restricted to one target location would give a vector length of 1, and a neuron with no response field and equal responsiveness to stimuli in all directions would give a vector length near 0. During detection, the visual response of the neuron was significantly spatially selective with the RF center at -4.6^{o} (bootstrap, 1000 samples, $P < 0.001$). During visual search, however, this neuron exhibited no spatially selectivity in the RT interval ($P = 0.31$). In other words, this neuron has a clear RF, but does not discriminate whether it contained a salient singleton or a distractor.

Across the population of visually-responsive neurons, we identified many neurons with spatially localized RFs as evidenced by significant spatial selectivity during the single-target tasks (Table 6.1; Figure 6.5A). The RF centers tended to be located in the contralateral hemifield during both the detection (circular mean angle = -160^{o}; V-test, $u = 4.89$, $P < 0.001$) and memory-guided saccade task (circular mean angle = -162^{o}; $u = 4.66$, $P < 0.001$). These observations are consistent with previous reports (Schlag and Schlag-Rey, 1987; Schall, 1991a; Russo and Bruce, 2000).

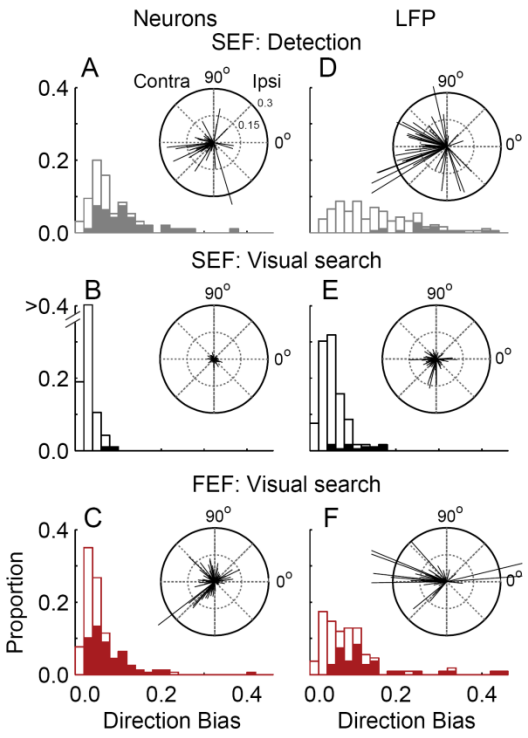

Figure 6.5 A-F, Distribution of directional biases for visually-responsive SEF and FEF neurons and LFP. Filled histograms indicate neurons and LFP sites that were individually significant ($P < 0.01$). Insets illustrate the distribution of preferred locations (vector angle) and directional bias (vector length) for the population of neurons and LFP (180^o – contralateral; 0^o – ipsilateral).

Although we observed many SEF neurons with well localized RFs, we found that vanishingly few exhibited significant target selectivity during visual search (Table 6.1). Figure 6.5B summarizes the measure of vector tuning during search and detection. The mean directional bias during visual search (0.02 ± 0.002) was significantly lower than that measured during both detection (0.11 ± 0.01; Wilcoxon rank sum test, $P < 0.001$) and memory-guided saccade tasks (0.10 ± 0.01; $P < 0.001$), indicating that no spatial selectivity could be identified during search. No contralateral bias was present during search ($u = 0.77$, $P = 0.22$). Thus, SEF neurons with clear RFs during single-target tasks failed to discriminate the target during visual search.

It is unclear from the preceding analysis whether the reduced selectivity reflects a true absence of salience or whether the reduced directional bias merely reflects reduced salience when additional stimuli are in the visual field. Therefore, we also analyzed single-unit activity recorded

from FEF, an area known to encode salience (Thompson and Bichot, 2005). The FEF data were recorded from monkey F and two additional monkeys to compare directly the spatial selectivity during visual search across areas. The data from monkey F were previously published (Sato et al., 2001). The FEF dataset was comprised of 157 neurons (101 from monkey F; 32 from monkey Q; 24 from monkey S) with significant visual responses. The mean visual latency of the FEF neurons was 68 ± 1.4 ms, which is consistent with previous reports (Thompson et al., 1996; Schmolesky et al., 1998). Results were qualitatively similar across monkeys, so we combined data to increase statistical power.

In contrast to SEF, many FEF neurons (77/157, 49%) exhibited significant target selectivity during search when measured in the same way (Figure 6.5C). Spatial selectivity in FEF was significantly biased to the contralateral hemifield during search (circular mean angle = 157^{o}; V-test, $u = 3.95$, $P < 0.001$) consistent with previous studies (Schall et al., 1995b). The mean strength of directional bias in FEF (0.04 ± 0.007) was significantly greater than SEF neurons recorded during visual search (Wilcoxon rank-sum test, $P < 0.001$). This value is lower than previously reported values using single target tasks (e.g., Schall, 1991a) because the visual response to distractors decreases the length of the vector sum. Thus, our results reflect genuine differences in the role of these areas in representing visual salience.

To facilitate comparisons across areas and studies, we also quantified the magnitude of selectivity using a "neuron-antineuron" approach (Figure 6.6). The magnitude of selectivity was determined as the area under the ROC curve when the target or distractors were inside a neuron's RF. During visual search, the neuron's discharge rate was approximately equal regardless of whether the target was inside or opposite the neuron's RF resulting in ROC values near 0.5 throughout the trial (Figure 6.6A). Figure 6.6B compares the mean magnitude of selectivity for SEF and FEF neurons that exhibited spatial selectivity when the target was presented alone during detection or memory-guided saccades. The mean magnitude of selectivity (± SE) for SEF neurons is only slightly, but significantly, greater than 0.5 (0.51 ± 0.003; $P < 0.01$). Thus,

visually responsive SEF neurons are highly unreliable predictors of target location. In contrast, the mean magnitude of selectivity of FEF neurons is markedly and significantly greater than 0.5 (0.58 ± 0.003; $P < 0.001$; Wilcoxon sign-rank test) and also significantly greater than the SEF neuron population ($P < 0.001$, Wilcoxon rank-sum). Thus, neurons in SEF, unlike FEF, SC, LIP, and 7a, do not reliably discriminate the target from distractors.

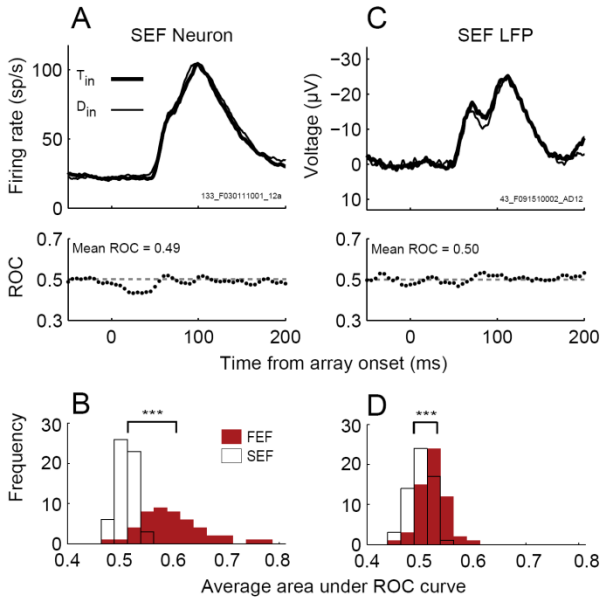

Figure 6.6 Neuron-antineuron test for target selectivity. Top, Response of a representative neuron (**A**) and LFP site (**C**) during the visual search task in which a target (thick line) or distractor (thin line) appeared in the preferred location. Middle, The mean area under the receive operating characteristic (ROC) curve in a running 10 ms window. Bottom, Distribution of average area under the ROC curve in the window 50 ms after array onset until 50 ms before mean saccade response time for SEF and FEF neurons (**B**) and LFP (**D**). Asterisks indicate significant difference between areas (Wilcoxon rank-sum test; *** for $P < 0.001$).

6.4.2 Absence of salience in SEF LFP during visual search

LFP recorded in FEF exhibit differential polarization that discriminates the location of salient targets (Monosov et al., 2008; Cohen et al., 2009a), but little is known about the spatial tuning or stimulus selectivity of SEF LFP (but see Emeric et al., 2010). We have demonstrated that the spiking activity of SEF neurons does not encode a representation of visual search salience, but all single-unit recording studies are based on a limited sample of individual neurons within a given region of cortex. Therefore, it is possible that we did not encounter neurons in SEF that do represent search salience. To mitigate this concern, we also analyzed LFP because they reflect

the summed synaptic activity of thousands of neurons in the region of cortex surrounding the electrode tip (Mitzdorf, 1985; Katzner et al., 2009) and thus provide a more complete sampling of a region. In addition, LFP reflect subthreshold fluctuations in membrane potential that may not have produced a spike (e.g., Poulet and Petersen, 2008; Okun et al., 2010) and may reflect both intrinsic processing and inputs from distant cortical areas (Logothetis and Wandell, 2004). Therefore, the LFP in SEF may select the target despite an absence of spiking selectivity.

We recorded LFP from 216 sites in SEF that exhibited task-related polarization (161 from monkey F; 55 from monkey Z), of which185 sites exhibited significantly visually-evoked polarization (Table 6.1). Of the 185 visually-responsive LFP sites that formed the data set for our analyses, 23 (11%) were classified as pure *visual* LFP that showed significant modulation following only the stimulus onset and 162 (75%) were classified as *visuomovement* LFP, which showed significant modulation following both stimulus onset and around the time of saccade initiation. The greater percentage of visuomovement LFP relative to neurons likely reflects summed activity across both visual and saccade-related neurons, which is consistent with the lack of evidence for modular or laminar differences in SEF neuron types. The visual latency of the SEF LFP was 54 ± 0.7 ms, which is significantly earlier than the latency of SEF neuron spike rate modulation ($P < 0.001$, Wilcoxon rank-sum test). This value is earlier than previous reports (Emeric et al., 2010), which were based on limited numbers of trials. All of our sessions included >1000 trials; therefore, we believe our latency estimate is more accurate.

Figure 6.7 shows the average response of a representative LFP site recorded during the detection and visual search tasks. During detection, the visually elicited polarization of the LFP varies significantly with target location with an RF center at -142^{o} (bootstrap, 1000 samples, $P < 0.001$). During visual search, however, the LFP recorded at the same site did not distinguish the target from distractors ($P = 0.08$).

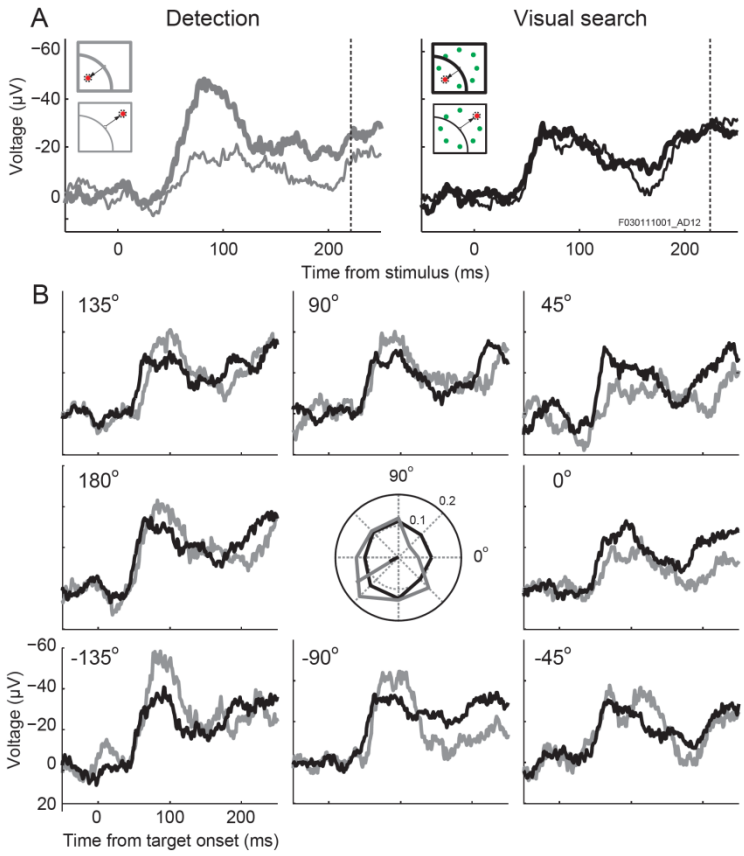

Figure 6.7 Representative visually-responsive LFP site during detection and search. Conventions as in Figure 6.4.

We quantified the RF location and spatial selectivity of each LFP site using vector summation of the modulation at each target location as described above. Figure 6.5D illustrates the preferred locations and directional bias for the 185 visually-responsive LFP sites. Across the population of visually-responsive LFP sites, many exhibited significant spatial selectivity when a single saccade target was presented (Table 6.1). The reduced percentage of visually-responsive LFP relative to neurons likely reflects summed activity across neurons with different preferred locations. There is a clear bias to the contralatereal hemifield during detection (circular mean angle = -167^{o}; V test, u = 5.2, P < 0.001) and memory-guided saccades (circular mean angle = -176^{o}; u = 6.8, P < 0.001), which has been previously reported using only two targets on the horizontal meridian (Emeric et al., 2010).

Although many LFP sites had spatially selective modulation, very few LFP sites exhibited significant target selectivity during visual search (Table 6.1). Figure 6.5D-E summarizes the strength of directional bias during search and detection. The mean strength of directional bias during search (0.05 ± 0.005) was significantly reduced relative to both detection (0.21 ± 0.02) and memory-guided saccade (0.22 ± 0.01) tasks (Wilcoxon rank-sum test, $P < 0.001$). There was no significant difference in the strength of spatial selectivity between detection and memory-guided saccade tasks ($P = 0.48$). Thus, many LFP sites with spatially selective modulation during single target tasks fail to select the target during search.

We compared the strength of target selection in SEF LFP to LFP recorded from the FEF of two additional monkeys that performed the color visual search task. The dataset was comprised of 109 LFP with significant visual modulation following stimulus onset (73 from Monkey Q: 36 from Monkey S). Of these, 42/109 (38%) exhibited significant target selectivity during search. The mean visual latency of the FEF LFP was 53.0 ± 2.0 ms, which is consistent with previous reports (Monosov et al., 2008; Cohen et al., 2009a). Figure 6.5F illustrates the distribution of FEF LFP preferred directions and directional biases. Directional selectivity was significantly biased to the contralateral hemified during search (circular mean angle = 174^{o}; V-test, $u = 6.03$, $P < 0.001$), consistent with previous reports (Monosov et al., 2008). During search, the strength of directional bias in FEF (0.35 ± 0.21) was significantly greater than the directional bias in SEF (Wilcoxon rank-sum test, $P < 0.001$). Thus, target selectivity is evident in FEF, but not SEF, LFP.

We confirmed the absence of selectivity in SEF LFP by computing the area under the ROC curve over the course of the trial (Figure 6.6C-D). The mean magnitude of selectivity for SEF LFP was not significantly different than 0.5 (0.48 ± 0.014; $P = 0.85$). In contrast, the mean magnitude of selectivity for FEF neurons was significantly greater than 0.5 (0.53 ± 0.004; $P = 0.85$) and also significantly greater than the SEF LFP population ($P < 0.001$). Thus, we found no

evidence that SEF represents salience during search even when taking into account population level signals that include subthreshold synaptic activity.

6.4.3 Comparison of visual responses in SEF and FEF

We characterized two properties of SEF neurons and LFP to determine whether they distinguish SEF from other visuomotor areas that encode salience. First, we compared the tuning width of neurons and LFP. Following Bruce & Goldberg (1985), we used the standard deviation of a Gaussian function fitted to the mean discharge rate/voltage of each neuron/LFP as a function of target position during the memory-guided saccade task as an indicator of tuning width. The mean tuning width for SEF neurons ($56^o \pm 4.0^o$, degrees of polar angle) was significantly narrower than the mean tuning width for SEF LFP ($82^o \pm 3.8^o$; Wicoxon rank-sum test; $P < 0.001$) (Figure 6.8). Similarly, the mean tuning width of FEF neurons ($51^o \pm 3.1^o$) was significantly narrower than the mean tuning width for FEF LFP ($65^o \pm 3.3^o$). This is consistent with the hypothesis that LFP in both areas are integrating across neurons with scattered RFs (Monosov et al., 2008). The slight increase in mean tuning width in SEF relative to FEF was significant for LFP ($P < 0.01$), but not neurons ($P = 0.38$). When converted to visual field angles using the law of cosines, the estimated RF width at 10^o eccentricity was $9^o \pm 0.6^o$ for SEF neurons and $13^o \pm 0.5^o$ for SEF LFP. The estimated RF width of FEF neurons was $8^o \pm 0.4^o$ and FEF LFP was $11^o \pm 0.5^o$. Note that these estimates are based on only a single eccentricity (10^o visual angle) and RF width is known to vary with eccentricity in both FEF and SEF (Bruce and Goldberg, 1985; Russo and Bruce, 2000). However, at the eccentricity tested, the tuning width of SEF neurons and LFP are roughly comparable to those observed in FEF (Schall, 1991b; Russo and Bruce, 2000).

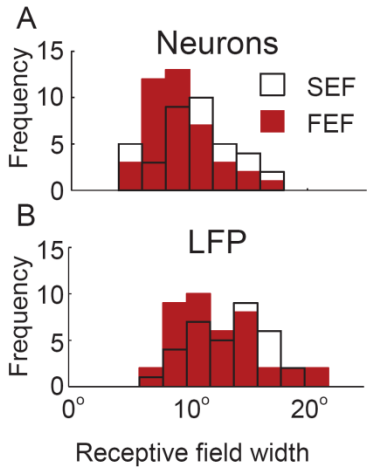

Figure 6.8 The distribution of receptive field widths for SEF (open histogram) and FEF (solid red histogram) across the population of neurons across the population of neurons (top) and LFP (bottom) during the memory-guided saccade task.

Second, we determined whether adding distractor stimuli to the visual field inhibited SEF visual responses. FEF, LIP, and SC neurons are suppressed by the addition of stimuli outside their RF (Schall et al., 1995b; Basso and Wurtz, 1998; McPeek and Keller, 2002; Falkner et al., 2010), which suggests some form of lateral inhibition that is thought to be critical for generating a salience representation (e.g., Tsotsos et al., 1995; Itti and Koch, 2001). The mean visual response of SEF neurons was significantly reduced during search relative to detection (Figure 6.9A-B; mean difference: 2.9 ± 0.7 sp/s; $P < 0.001$, Wilcoxon sign-rank test). Similarly, the mean visual polarization of SEF LFP was significantly reduced during search relative to detection (Figure 6.9C-D; 2.1 ± 0.4 μV; $P < 0.001$). Thus, both FEF and SEF neurons and LFP show evidence of lateral inhibition.

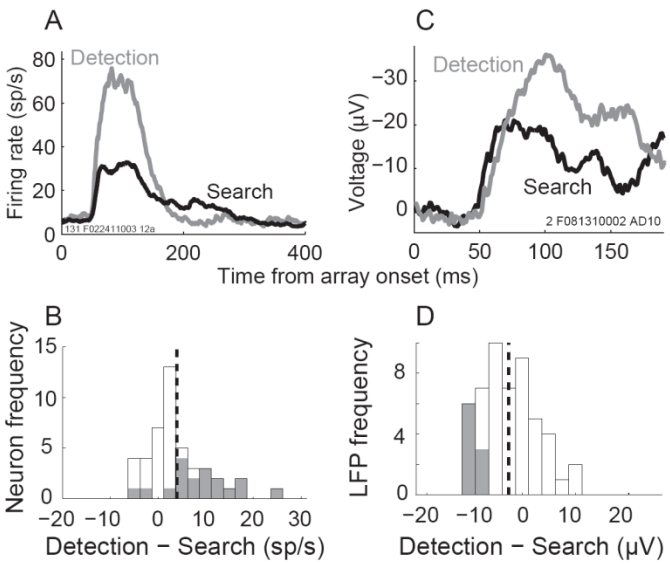

Figure 6.9 Representative SEF neuron (**A**) and LFP (**C**) during detection (gray) and visual search tasks (black) when the target fell inside the RF. Distribution of differences between the mean discharge rate 50 ms to 150 ms after array onset for the population of visually responsive neurons (**B**) and LFP (**D**) during detection and visual search. Shaded bars indicate neurons that attained individual statistical significant (Wilcoxon sign-rank test, $P < 0.05$). Dashed vertical line indicates population mean.

6.4.4 Absence of cognitive control in SEF during priming of pop-out

Medial frontal areas, including SEF, are thought to be involved in overcoming habitual actions in response to changing environmental demands (Schlag-Rey et al., 1997; Rushworth et al., 2002; Nakamura et al., 2005; Isoda and Hikosaka, 2007; Schall and Boucher, 2007; Sumner et al., 2007). We used a priming of pop-out manipulation in which the target and distractor color were swapped randomly after several trials (Figure 6.10A) to test whether SEF contributed to overcoming the primed tendency to look to the previous target color on trials in which target identity switched. Following target switches, both humans and monkeys are slower and more error prone, but performance improves over the next several trials (Maljkovic and Nakayama, 1994; McPeek and Keller, 2001; Bichot and Schall, 2002). FEF neurons show robust modulation with changes in performance with priming of pop-out (Bichot and Schall, 2002), but nothing is known about SEF neurons. Therefore, we also tested whether SEF contributed to improvements in performance in the trials following the switch.

Both monkeys exhibited clear behavioral evidence of priming (Figure 6.10B-C). The mean saccade response time was significantly longer on switch trials relative to non-switch trials (Wilcoxon sign-rank test; monkey F, 16 ms, $P < 0.001$; monkey Z, 22 ms, $P < 0.001$) and percent correct was significantly lower (monkey F, 27%, $P < 0.001$; monkey Z, 28%, $P < 0.001$). We tested for significant improvements in performance following the target switch by fitting a least squares regression line to saccade response time and percent correct as a function of the first five trials since the target switch. Response times declined at an average rate of 4.4 ms/trial following the switch ($P < 0.001$) and percent correct increased an average of 6% per trial ($P < 0.001$), though the largest improvements in performance followed the first trial since the switch. Thus, the monkeys exhibited clear and robust evidence of priming.

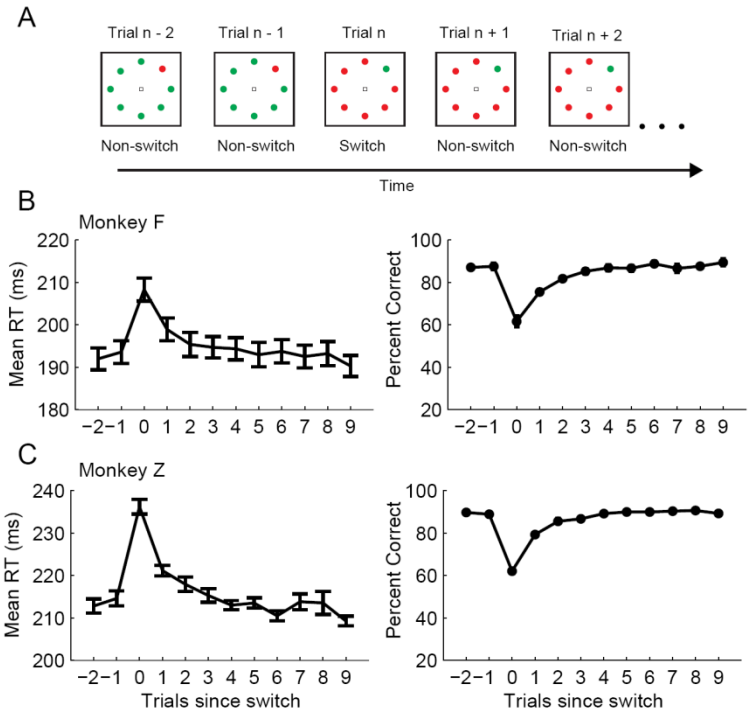

Figure 6.10. Priming of pop-out task and behavior. **A**, The color of the target and distractors switched randomly every 8-16 trials (uniform distribution). **B-C**, mean response time (left) and percent correct (right) as a function of the number of trials since the switch in target identity.

We recorded 91 neurons (29 from monkey F; 62 from monkey Z) that exhibited significant task-related modulation around the time of saccade or following stimulus presentation during

priming of pop-out. These analyses included all task-related neurons, not only visually-responsive neurons. If SEF is involved in overcoming priming, then we would expect changes in discharge rate on switch trials relative to non-switch trials prior to the saccade (Isoda and Hikosaka, 2007). Figure 6.11A illustrates the activity of a representative neuron recorded during priming of popout. The neuron's response was invariant whether or not the target color switched across trials ($P > 0.05$, Wilcoxon rank-sum test). Across the population of neurons, the difference in discharge rate across switch and non-switch trials was indistinguishable (Figure 6.12B; $P = 0.26$). This was true regardless of whether the target (Figure 6.11C; $P = 0.63$) or distractors (Figure 6.11D; $P = 0.39$) fell within the RF of the cell. The same pattern was evident in SEF LFP (all $P > 0.05$). Clearly, SEF neurons do not exhibit appropriate modulation to have controlled changes in performance following target switches.

Behavioral performance improves in the trials following a target switch. If SEF is involved in performance improvements, then we would expect systematic changes in the discharge rate of SEF neurons throughout the trial. Figure 6.12 illustrates the discharge rate of the same representative neuron as a function of the number of trials since the target switch. In contrast to FEF neurons (Bichot and Schall, 2002), there is no monotonic change in discharge rate as performance improves in the trials following the target switch. We fit a least squares regression line to the discharge rate as a function of the first five trials since the target switch to test for co-variation of discharge rate with improvements in performance. The slope of the regression line was not significant for this neuron regardless of whether the target or distractors were inside the neuron's RF (Figure 6.12B). Across the population of neurons, the distribution of slopes was not significantly different from zero regardless of the stimulus in the neuron's RF (all $P > 0.05$) and only chance percentages of neurons attained individual significance (Figure 6.12C). The results were qualitatively similar if discharge rate was directly correlated with saccade response time or percentage correct as a function of trials since the switch. The same pattern was evident in SEF

LFP (all $P > 0.05$). Thus, SEF does not control performance adjustments observed during priming of pop-out.

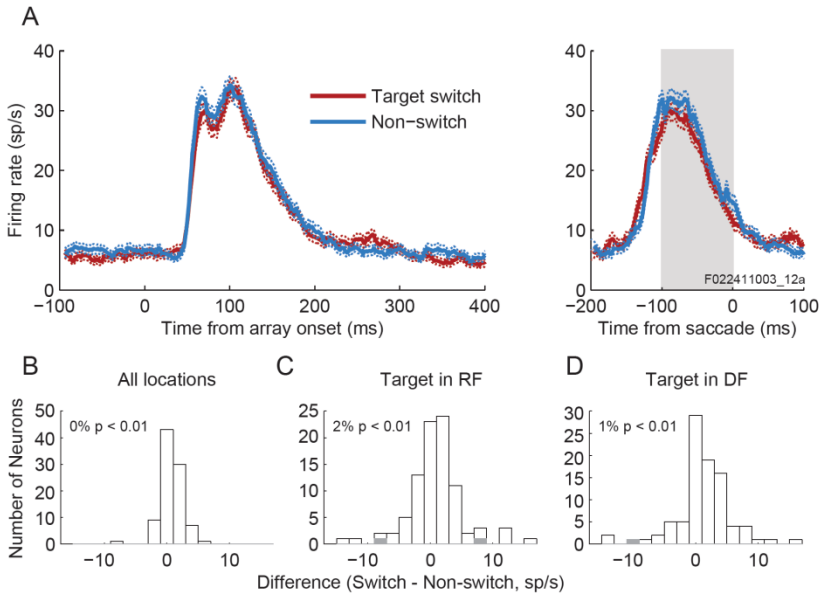

Figure 6.11. **A**, Mean discharge rate of a representative neuron recorded during the priming of pop-out task when the target. At no point does the response of the neuron depend on whether the target identity switched or remained constant from the previous trial. (**B-D**) histograms illustrate the population difference in discharge rate between switch and non-switch trials -100 to 0 ms relative to saccade onset when any stimulus (**B**), the target (**C**), or distractors (**D**) were in the neuron's RF. Shaded bars indicate neurons that attained individual significance (Wilcoxon rank-sum test, $P < 0.01$).

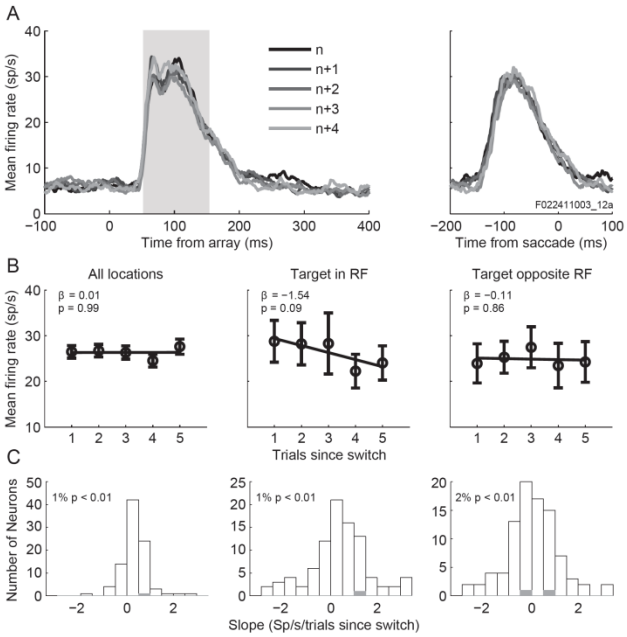

Figure 6.12. **A**, The mean discharge rate of the same representative neuron shown in Figure 6.11 with discharge rate divided by the number of trials since the target switch (n). **B**, the mean discharge rate of the neuron in the interval 50 to 150 ms following array onset and least squares regression line. **C**, the distribution of slopes of least squares regression lines fitted to discharge rate as a function of trials since target switch for the population of neurons when any stimulus (left), the target (middle), or distractor (right) were within the RF of the cell.

6.4.5 Performance monitoring in SEF during visual search

We found that SEF neurons and LFP do not signal the location of salient saccade targets and do not modulate with changes in behavior during priming of pop-out. Does SEF contribute at all to search performance? SEF neurons and LFP signal the occurrence of errors during saccade countermanding (Stuphorn et al., 2000; Emeric et al., 2010), which is thought to produce error-related potentials observed extracranially (Godlove et al., 2011b). However, this observation has never been replicated in another task. Therefore, we asked whether SEF neurons or LFP signal the occurrence of an error when the monkeys incorrectly shifted gaze to a distractor location during visual search

We tested for error-related responses in the 91 neurons recorded during the priming of pop-out manipulation which provided sufficient numbers of error trials. Figure 6.13A shows the response of a representative error-related SEF neuron. Following a brief peri-saccadic

suppression, activity remained at baseline for correct trials to the target, but exhibited a brisk discharge approximately 100-200 ms after erroneous saccades to a distractor. Across the population of neurons, 24/91 (26%) exhibited significant error-related modulations. This is only slightly higher than previous estimates during saccade countermanding (Stuphorn et al., 2000). Figure 6.13B shows the response of a representative LFP site with error-related modulation. Following the saccade, a brief positive-going polarization was followed by a significant negative polarization following erroneous but not correct saccades. Across the population of LFP sites, 17/107 (16%) exhibited significant error-related modulation. This is slightly lower than previous estimates (Emeric et al., 2010). Importantly, these effects cannot be due to the shift of gaze because we matched the distribution of saccade directions across all analyzed correct and error trials. These effects cannot be due to second saccades (e.g., corrective saccades to the target) because trials in which the eyes moved <400 ms after the initial saccade were excluded. Thus, we conclude that SEF neurons are signaling the occurrence of an error during visual search.

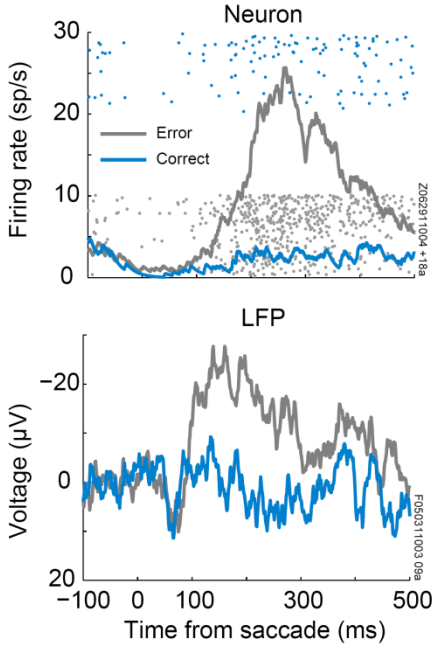

Figure 6.13. Representative error-related neuron during detection and search. **A.** Average spike density function (lines) and raster (dots) for trials in which a saccade was correctly made to the target (blue) or erroneously made to a distractor (gray). **B.** Average voltage for correct and error trials. Conventions as in **A**.

6.5 Discussion

SEF is embedded anatomically within a network of structures that represent visual salience (physical conspicuousness and behavioral relevance). We found that SEF neurons and LFP do not represent visual salience. We also found that SEF is not involved in overcoming priming during pop-out, but did signal the occurrence of search errors.

6.5.1 Absence of salience in SEF

Anatomical connections with cortical and subcortical areas known to encode salience suggested that SEF would represent another node in this network (Figure 6.1). Previous single-unit recording studies in SEF also suggest that it may represent salience. When presented with foveal cues, some SEF neurons fire selectively before saccades to targets (Chen and Wise, 1995a, b, 1996; Olson and Tremblay, 2000). Other populations of SEF neurons signify the target of an upcoming saccade on the basis of reward contingencies (Coe et al., 2002; Seo and Lee, 2009; So and Stuphorn, 2010, 2012) or by virtue of its position in a sequence of saccades (Lu et al., 2002; Berdyyeva and Olson, 2009, 2010). Human imaging studies suggest that SEF may be active during deployment of covert attention (Kastner et al., 1999). These factors can be viewed as 'top-down' salience, but we showed that SEF neurons and LFP do not discriminate the target from distractors during visual search. This is consistent with the relatively limited deficits in target selection observed following lesions of contralateral SEF relative to FEF lesions (Schiller and Chou, 1998, 2000) and the absence of fMRI signal in monkeys presented with pop-out arrays (Wardak et al., 2010).

Our finding that salience is absent in SEF parallels a recent report showing that saccade-related SEF neurons do not directly control saccade initiation (Stuphorn et al., 2010). Many FEF, SC, and SEF neurons show elevated discharge rates before saccades of particular directions (Schlag and Schlag-Rey, 1987), which has been suggested to indicate a similar role in saccade generation (Schall, 1991b; Russo and Bruce, 2000). FEF and SC neurons modulate early enough

to control saccade initiation (Hanes et al., 1998; Pare and Hanes, 2003), but SEF neurons modulated too late to control saccade initiation (Stuphorn et al., 2010). Similarly, we found that although both SEF and FEF neurons have selective visual responses, SEF neurons do not encode salience. SEF may be less important for ongoing decisions about where to move the eyes (Yang et al., 2010), but may play a larger role in monitoring the outcome of prior decisions (Boucher et al., 2007).

6.5.2 Does salience require ventral stream innervation?

The lack of target selectivity and priming effects in SEF neurons is most likely due to an absence of necessary visual afferents (Figure 6.1). FEF, LIP, and SC all receive topographically organized input from visual areas V4, TEO, TE, MT, and MST representing features of objects on which search can be performed such as color, shape, texture, motion, and depth (Blatt et al., 1990; Lui et al., 1995; Schall et al., 1995a; Bullier et al., 1996). In contrast, SEF receives cortical visual input only from areas LIP, 7a, FEF, MST, and the superior temporal polysensory area (Huerta and Kaas, 1990; Schall et al., 1995a). Thus, the absence of a salience representation in SEF can be understood from the lack of visual afferents originating in areas representing stimulus features. Interestingly, our result is also consistent with a recent study which found that FEF neurons projecting to MT are targeted by SEF neurons, but not FEF neurons projecting to V4 (Ninomiya et al., 2012).

We ruled out several alternative explanations for the absence of visual salience in SEF. It could be explained by an absence of topographic visual inputs. However, many SEF neurons and LFP sites exhibited well localized RFs. Furthermore, SEF neuron and LFP tuning widths were, on average, only slightly broader than FEF (see also Bruce and Goldberg, 1985; Schall et al., 1995b; Schall et al., 2004; Monosov et al., 2008). Thus, the absence of topographic visual inputs cannot explain the absence of salience.

Alternatively, the absence of salience could be explained by an absence of lateral inhibition. Several computational models propose that salience is shaped by suppression of distractor inputs (Tsotsos et al., 1995; Itti and Koch, 2001) and lateral inhibition is observed throughout the visual system including FEF (Schall et al., 1995b), SC (McPeek and Keller, 2002), and LIP (Falkner et al., 2010). We found that the response of most SEF neurons and LFP were significantly inhibited by the addition of distractor stimuli in the visual field. This could be due to lateral connections intrinsic to SEF or could reflect competitive interactions taking place in afferent areas. Regardless, an absence of lateral inhibition cannot explain the absence of salience in SEF.

The absence of a salience representation in SEF has implications for the functional connectivity between SEF and other areas in the salience network. Visually-responsive neurons in the superficial layers of FEF encode a representation of salience (Thompson et al., 1996) and project to areas of extrastriate visual cortex (Huerta et al., 1987; Barone et al., 2000; Pouget et al., 2009; Anderson et al., 2011), which are thought to contribute to covert spatial attention (Moore and Armstrong, 2003; Cohen et al., 2009b; Purcell et al., 2010). Given that collateralization of intracortical projections is so limited, the absence of a salience signal in SEF suggests that the neurons in LIP and FEF that encode salience do not project to SEF. Alternatively, the absence of salience in SEF could be due to active cancellation via local-circuit connections. However, the small proportion of neurons and LFP sites that exhibited significant salience signals indicates that these input signals must be suppressed very early in the network, which makes it of limited use for subsequent computations.

6.5.3 Absence of priming effects in SEF neurons

Dorsomedial frontal areas, including SEF, have been implicated in the control processes necessary to overcome a habitual action in response to changing context (Rushworth et al., 2002; Isoda and Hikosaka, 2007; Sumner et al., 2007; Isoda and Hikosaka, 2011). The priming of pop-out task requires the animal to overcome the primed tendency to respond to an old target color.

Our monkeys showed clear evidence of priming; target color switches lead to increased response times and error rates. However, we found no modulation in pre-saccadic discharge rates when the target color switched across our entire sample of SEF neurons or LFP. This suggests that SEF is not necessary to overcome priming of pop-out.

We do not believe that the absence of SEF modulation during priming of pop-out can be explained by an absence of control signals in SEF. Pre-SMA is strongly interconnected with SEF (Huerta and Kaas, 1990; Luppino et al., 1993) and neurons in this area are strongly modulated on trials in which a primed response must be suppressed (Isoda and Hikosaka, 2007). Humans with lesions of SEF show an absence of priming effects in oculomotor tasks (Sumner et al., 2007). Furthermore, SEF neurons fire vigorously during tasks that encourage mutually incompatible responses including anti-saccade (Schlag-Rey et al., 1997), countermanding (Stuphorn et al., 2000; Stuphorn et al., 2010), and flanker tasks (Nakamura et al., 2005). Thus, the absence of priming effects during pop-out does not rule out a role for SEF as a source of control control during tasks in which competing responses to be actively suppressed.

Instead, the absence of modulation in SEF neurons can be explained if delays in early perceptual processes completely account for pop-out priming. Consistent with this account, priming effects cannot be eliminated by voluntary control or expectation (Maljkovic and Nakayama, 1994). Priming effects correlate with reductions in BOLD activity in extrastriate visual areas (Kristjansson et al., 2007). Transcranial magnetic stimulation applied to visual area MT in humans disrupts motion priming (Campana et al., 2006). Finally, lesions of TEO and V4 in monkeys lead to an abolished priming effect (Walsh et al., 2000), but lesions of dorsolateral prefrontal cortex do not eliminate priming (Rossi et al., 2007). SEF does not receive input from these visual areas and cognitive control is not necessary for perceptual priming, and therefore priming effects are not apparent in this area. Thus, our results add to converging evidence that priming of pop-out can be entirely accounted for by changes at the level of early feature representations (Wolfe et al., 2003; Lee et al., 2009). We speculate that other tasks (e.g.,

countermanding) elicited control responses in SEF because those tasks, unlike priming of pop-out, encouraged early preparation of saccade responses that required active suppression by SEF.

6.5.4 Performance-monitoring signals in SEF during visual search

We have ruled out two of the most plausible ways in which SEF could contribute to visual search performance, but what role, if any, does SEF play during visual search? SEF neurons and LFP modulate following errors during saccade countermanding (Stuphorn et al., 2000; Emeric et al., 2010), which is one likely source of error-related potentials recorded extracranially (Godlove et al., 2011b). We found that SEF neurons signaled visual search errors when monkeys incorrectly made saccades to a distractor. Modulation followed saccade initiation and therefore could not play a role in representing salience to guide current search behavior. Rather, these observations can be understood in the context of a performance monitoring framework (Schall and Boucher, 2007). Although SEF does not appear to be actively engaged in modifying ongoing visual search performance, it may play a role in monitoring performance and relaying outcome information to other cortical areas for subsequent behavioral adjustments.

CHAPTER VII:

GENERAL DISCUSSION

7.1 Summary of results

The preceding studies were guided by the assumption that perceptual decisions are performed by integrating a representation of perceptual evidence to a response threshold. Based on that framework, I asked whether I could identify how the evidence representation and evidence accumulation might be implemented in distinct neuronal populations within and across brain areas.

First, these studies inform our understanding of the neural representation of perceptual evidence. In Chapter III, I used the firing rates of visually-responsive FEF neurons to drive a network of stochastic accumulators that predicted search behavior. This demonstrates that the response properties of these neurons are sufficient to serve as a representation of perceptual evidence that drives response accumulators. Chapter IV showed that this evidence is encoded primarily through changes in mean firing rate and not changes in across-trial variability. Chapter V showed that the same pattern of modulation that was observed in FEF visual neurons was also evident in the modulation of extracranial event-related potentials that reflect neuronal activity across many centimeters of posterior visual cortex. This result is consistent with existing neurophysiological and anatomical data suggesting that the representation of perceptual evidence is not isolated in FEF, but is likely distributed across a broad network of brain areas. However, this representation is not everywhere. In particular, Chapter VI showed that the extent of this representation does not include all sensorimotor areas, as it is not evident in the firing rates of SEF neurons in medial frontal cortex.

Second, these studies inform our understanding of the potential neural mechanisms of evidence accumulation. Following the methodology established in Chapter II, Chapter III directly compared the predicted dynamics of stochastic accumulator models fit to visual search

behavior to the response dynamics of FEF movement neurons. The observed pattern of movement neuron activity was consistent with the pattern of modulation observed both in both standard (Chapter II) and neurally-driven (Chapter III) accumulator models, consistent with the idea that these neurons integrate the perceptual evidence encoded by visual neurons. In addition, Chapter IV showed that the pattern of response variability in saccade-related FEF neurons was consistent with the pattern of response variability predicted by stochastic accumulator models. Movement neurons with very similar response properties are also located in superior colliculus (Ratcliff et al., 2003), but SEF neurons do not modulate in a manner consistent with accumulation to a fixed threshold (Stuphorn et al., 2010).

Altogether, these results demonstrate the utility of cognitive models for understanding how the activity of different neuronal populations can influence decision-making behavior. These models provided a framework that allowed us to identify how common computations might be implemented by neuronal populations distributed across many cortical and subcortical areas, and also how different computations might be implemented by distinct populations of neurons within a single brain area. However, despite the advances in our understanding of simple perceptual decisions, these results also raise several open questions concerning the neural mechanisms of perceptual decision-making. In the final sections, I will address several critical questions that remain to be addressed.

7.2 Open questions and future directions

7.2.1 Linking propositions

I have demonstrated how the identification of visually-responsive FEF, SC, and LIP neurons with perceptual evidence and FEF and SC movement neurons with evidence accumulation account for a wide range of neurophysiological and behavioral observations. However, a different line of work has identified perceptual evidence with the firing rates of motion direction selective neurons in MT and evidence accumulation with visually-responsive

neurons in LIP during a motion direction discrimination task. The major findings supporting this mapping are the stimulus-dependent rate of rise in LIP neurons (Roitman and Shadlen, 2002; Churchland et al., 2008), the effects of MT stimulation and LIP stimulation on performance (Salzman et al., 1990; Salzman et al., 1992; Ditterich et al., 2003; Hanks et al., 2006), and the effect of motion pulse simtuli on behavior and LIP activity (Huk and Shadlen, 2005). How can it be that these different populations of neurons each seem to be well explained by a mechanism of stochastic accumulation to threshold, although the models assume only a single evidence accumulation process?

The apparent discrepancy across studies can be somewhat reconciled by appreciating that temporal integration and threshold evaluation are likely common mechanisms implemented by different neuronal populations for different functions. For example, tonic neurons in the brainstem are thought to temporally integrate a velocity to compute position (Cannon and Robinson, 1987). More recently, neurons in anterior cingulated cortex have been proposed to compare firing rates to a threshold to determine whether to leave an environment (Hayden et al., 2011). Thus, it seems likely that temporal integration of signals from extrastriate neurons is used to generate the representation of perceptual evidence that is observed in FEF, LIP, and SC visual neurons and that temporal integration is also used to translate visual neuron firing rates to a saccade command via FEF and SC movement neurons.

Likewise, threshold detection may play a role in the read-out of both visual neuron activity and movement neuron activity. Indeed, the gating inhibition proposed in Chapter III implements a form of threshold on visual neuron activity. However, it is important to appreciate the distinct function role of the threshold on each population. Visual neurons do not project directly to the brainstem saccade generator, and therefore saccades cannot be generated without first relaying a signal through SC or FEF movement neurons. Thus, visual neurons do not reflect the irrevocable decision to act, but may instead reflect the categorical decision that a stimulus is present. The framework proposed in Chapter III reflects the fact that these two decisions may be

independent, but often are inherently linked. Other groups have proposed two-layer accumulator models that are consistent with this idea (Shea-Brown et al., 2008; Carpenter et al., 2009). Simultaneous recordings from LIP and FEF or SC during perceptual decision-making tasks could provide the key data to test this hypothesis.

7.2.2 Modeling at multiple levels

The preceding section reveals a fundamental limitation of using higher-level cognitive models to understand neurobiological mechanisms: The biological machinery needed to implement the processes is necessarily more complex than the simple processes assumed by cognitive models. This problem becomes apparent when one considers that several hundred thousand neurons are necessary to initiate a single eye movement (Brown et al., 2008), but eye movement behavior can be explained by models that assume only a single stochastic accumulator (Reddi and Carpenter, 2000). In order to bridge this gap more completely, we need to develop models at an intermediate level that explain how networks of interacting neurons can implement the proposed model process (Wang, 2002; Zandbelt et al., 2012). However, note that this does not negate the need for higher-level models; rather, the relationship is reciprocal. Higher-level models allow us to efficiently reject hypotheses that narrow down the potential ways in which a behavior could be performed. Lower-level models explain the biological mechanisms by which the computations could be implemented. Thus, a more complete understanding of behavior can be gained through modeling at multiple levels.

7.2.3 On the role of feed-back in perceptual decision-making

According to the standard accumulator model framework, perceptual decisions proceed in an entirely feed-forward manner: perceptual evidence is first generated, and then accumulated over time to a threshold. However, Chapter V found that a representation of perceptual evidence can be detected at the population level via extracranial potentials, and that this representation is

likely due to feedback from frontal and parietal areas that encode perceptual evidence. However, no current stochastic accumulator explains the role of this feedback in the accumulation process. These results suggest that a new generation of models should be developed to understand how feedback from the accumulator could modulate the representation of perceptual evidence and what consequences this might have for predicted behavior and neurophysiological signals.

7.2.4 Performance monitoring during perceptual decisions

Chapter VI found that the firing rates of SEF neurons did not correspond to any component of the stochastic accumulator model framework. Instead, a subpopulation of SEF neurons were shown to fire exclusively after monkeys made erroneous saccades to distractors during visual search. This error detection signal is often proposed to be involved in performance adjustments on subsequent trials, but how these adjustments take place is still an open question. One hypothesis is that these signals represent a reward prediction error signal (Seo and Lee, 2009; So and Stuphorn, 2012). This signal is a critical component of reinforcement learning models that is used to adjust the anticipated value associated with particular stimuli or actions (Sutton and Barto, 1998). However, the relationship between reinforcement learning and accumulator models of perceptual decision-making is poorly understood. Thus, an important goal for future work is to understand the relationship between these two modeling frameworks.

A second important question concerns the specific neuronal mechanisms by which the error signals in SEF could influence decision-making. Imaging evidence suggests that these adjustments might involve interactions among medial prefrontal cortex and other areas involved in perceptual and motor aspects of decision-making (e.g., Danielmeier et al., 2011; Kerns et al., 2004; Carter & van Veen, 2007). Thus, SEF could influence FEF and SC through direct projections or could affect behavior via direct projections to the oculomotor brainstem. Alternatively, SEF could influence behavior via direct projections to the brainstem. Simultaneous recordings across multiple cortical areas will be necessary to tease apart the functional roles of

these different areas.

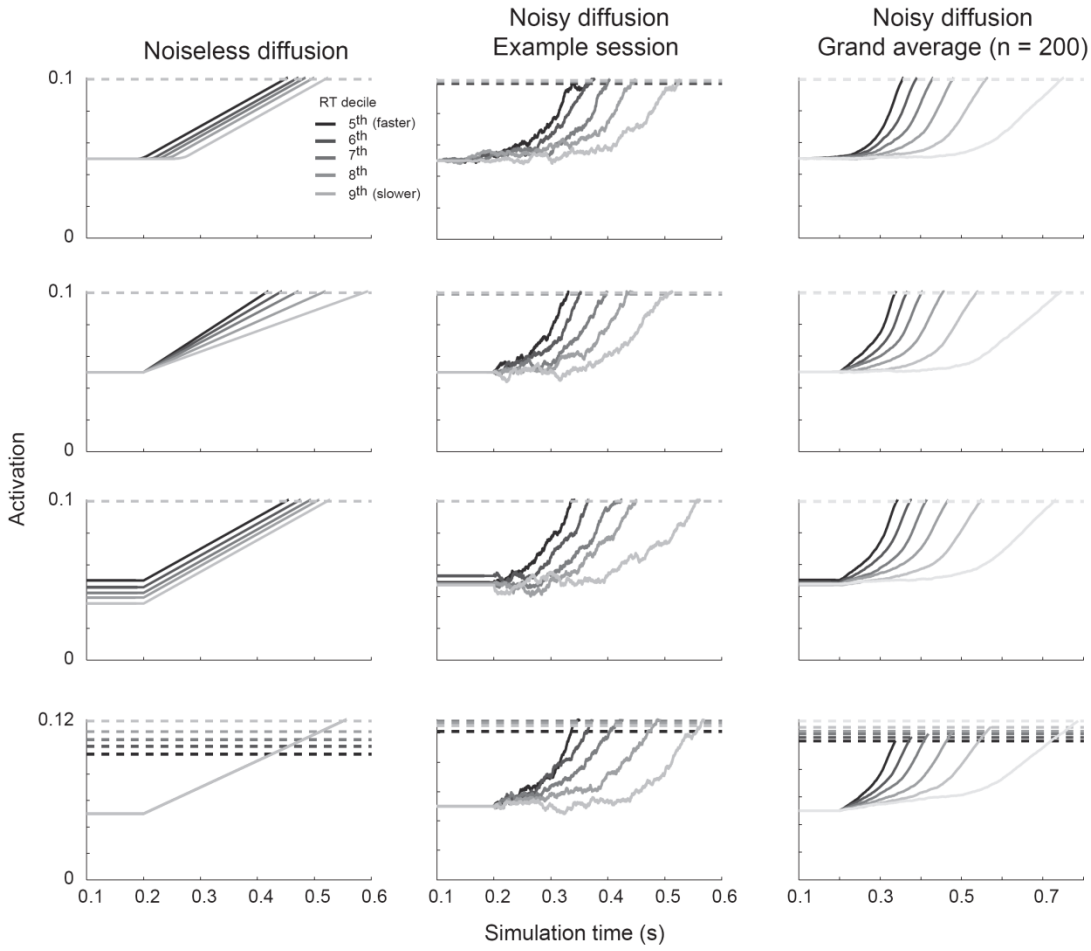

Figure A.1 Diffusion model dynamics. Plotted trajectories are averages from RT deciles. For clarity, only the 5th – 10th decile is plotted. Horizontal dashed lines indicate measured threshold. All simulations used the following primary parameters: $D = 0.2$, $v = 0.2$, $z = 0.05$, $a = 0.1$. The left column of panels show simulated trajectories from a single simulated session (200 trials) of a noiseless independent race model ($s = 0$). Rows differ according to the source of across trial variability (across-trial variability in encoding delay: $st = 0.2$, $\eta = 0$, $sz = 0$, $sa = 0$; across-trial variability in drift rate: $st = 0$, $\eta = 0.1$, $sz = 0$, $sa = 0$; across-trial variability in starting point: $st = 0$, $\eta = 0$, $sz = 0.04$, $sa = 0$; across-trial variability in threshold: $st = 0$, $\eta = 0$, $sz = 0$, $sa = 0.02$). The middle column of panels shows the simulated trajectories for a diffusion model with the same parameters as the left column, but with the addition of noise ($s = 0.1$). All other parameters are identical across rows. The last column of panels shows the grand average trajectories for 200 simulated sessions using the same parameters as the middle column panels.

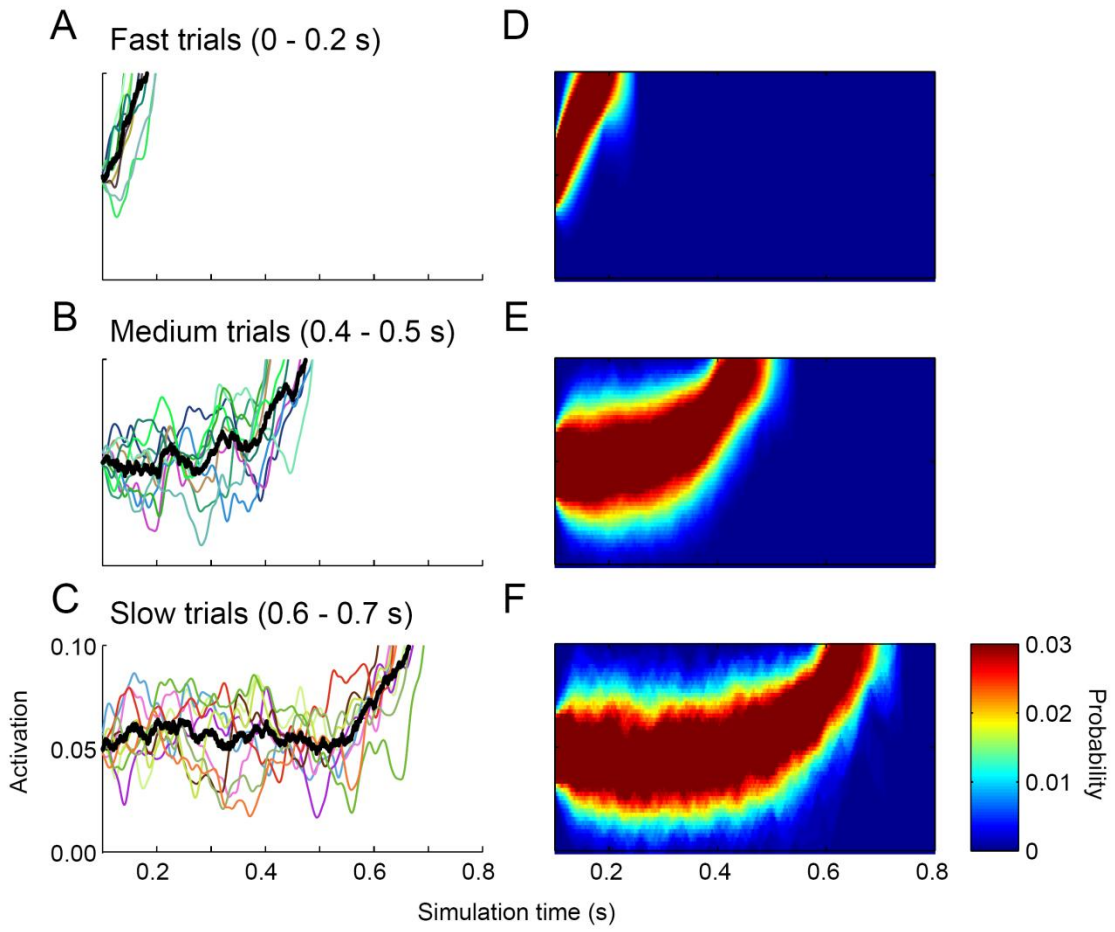

Figure A.2 The impact of noise (s = 0.1) on diffusion model dynamics for simulations resulting in fast (top; RT < 0.2 s), medium (middle; 0.3 s < RT < 0.4 s) and slow (bottom; 0.4 s < RT < 0.5 s) responses. All simulations used the same primary parameters as Figure A.1 (D = 0.2, v = 0.2, z = 0.05, a = 0.1), but with no sources of across-trial variability other than noise ($st = \eta = sz = sa = 0$). **A-C**: Simulated trajectories for 10 individual trials (colored lines) and their average (black). Here, individual trails have been low-pass filtered for illustrative purposes only. All other figures and analyses used unfiltered model trajectories. **D-F**: The conditional probability that the model trajectory was at an activation level at each time step given that the simulation produced a correct fast, medium, or slow RTs.

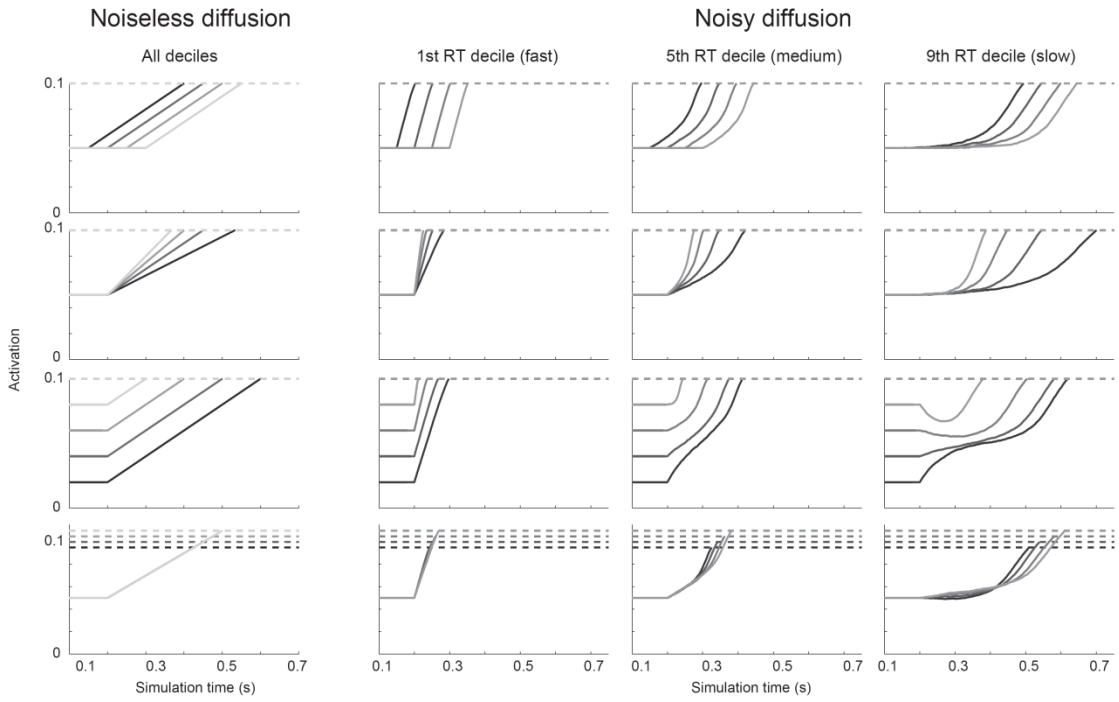

Figure A.3 Across-condition changes in diffusion model dynamics. The left panels show predicted model dynamics for a noiseless diffusion model (left column; $s = 0$). All other panels show predicted model dynamics for a noisy diffusion model at the 1st, 5th, or 9th RT decile, but with the addition of noise ($s = 0.1$). For each row, we selectively manipulated one parameter (delay, *D;* drift, *v;* starting point, *z;* **or** model threshold, *a)* and all other parameters were fixed at default values ($D = 0.2$, $v = 0.2$, $z = 0.018$, $a = 0.5$). All parameters determining across-trial variability were set to 0 ($st = \eta = sz = sa = 0$). Each plot shows the grand average trajectory across 200 simulated sessions for a single RT decile (9th decile).

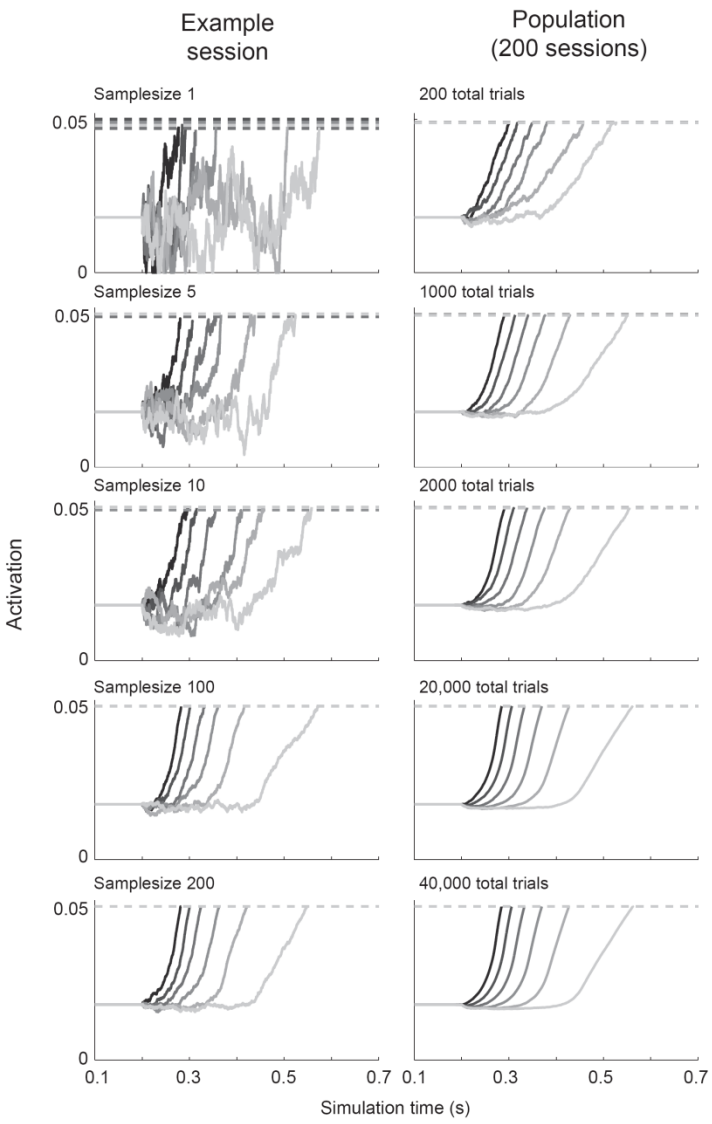

Figure A.4 The effects of varying sample size on the noisy independent race model dynamics. The left column shows trajectories for five RT deciles from example sessions with 1, 5, 10, 100, and 200 simulated trials per sessions. The right column shows grand averages across 200 simulated sessions using the sample sizes given by the left column. In other words, for each row, the left column panel was computed by averaging 200 time the sample size given in the right column panel. Even with sample size as low as five, the measures onset still appears to increase with RT.

REFERENCES

Afshar A, Santhanam G, Yu BM, Ryu SI, Sahani M, Shenoy KV (2011) Single-trial neural correlates of arm movement preparation. Neuron 71:555-564.

Albrecht DG, Hamilton DB (1982) Striate cortex of monkey and cat: Contrast response function. J Neurophysiol.

Amit DJ, Tsodyks MV (1991) Quantitative study of attractor neural network retrieving at low spike rates: I. Substrate-spikes, rates and neuronal gain. Network: Computation in neural systems 2:259-273.

An A, Sun M, Wang Y, Wang F, Ding Y, Song Y (2012) The N2pc Is Increased by Perceptual Learning but Is Unnecessary for the Transfer of Learning. PLoS One 7:e34826.

Andersen RA, Asanuma C, Essick G, Siegel RM (1990) Corticocortical connections of anatomically and physiologically defined subdivisions within the inferior parietal lobule. J Comp Neurol 296:65-113.

Anderson EJ, Mannan SK, Husain M, Rees G, Sumner P, Mort DJ, McRobbie D, Kennard C (2007) Involvement of prefrontal cortex in visual search. Exp Brain Res 180:289-302.

Anderson JC, Kennedy H, Martin KAC (2011) Pathways of attention: synaptic relationships of frontal eye field to V4, lateral intraparietal cortex, and Area 46 in macaque monkey. J Neurosci 31:10872.

Arcizet F, Mirpour K, Bisley JW (2011) A pure salience response in posterior parietal cortex. Cereb Cortex.

Asanuma C, Andersen RA, Cowan WM (2004) The thalamic relations of the caudal inferior parietal lobule and the lateral prefrontal cortex in monkeys: divergent cortical projections from cell clusters in the medial pulvinar nucleus. J Comp Neurol 241:357-381.

Ashby FG (2000) A stochastic version of general recognition theory. J Math Psychol 44:310-329.

Ashby FG, Townsend JT (1986) Varieties of perceptual independence. Psychol Rev 93:154.

Balan PF, Oristaglio J, Schneider DM, Gottlieb J (2008) Neuronal correlates of the set-size effect in monkey lateral intraparietal area. PLoS Biol 6:158.

Barone P, Batardiere A, Knoblauch K, Kennedy H (2000) Laminar distribution of neurons in extrastriate areas projecting to visual areas V1 and V4 correlates with the hierarchical rank and indicates the operation of a distance rule. J Neurosci 20:3263-3281.

Basso MA, Wurtz RH (1998) Modulation of neuronal activity in superior colliculus by changes in target probability. J Neurosci 18:7519-7534.

Basso MA, Wurtz RH (2002) Neuronal activity in substantia nigra pars reticulata during target selection. J Neurosci 22:1883-1894.

Batschelet E (1981) Circular statistics in biology. Academic Press, 111 Fifth Ave, New York, NY 10003, 1981, 388.

Beck JM, Ma WJ, Kiani R, Hanks T, Churchland AK, Roitman J, Shadlen MN, Latham PE, Pouget A (2008) Probabilistic population codes for Bayesian decision making. Neuron 60:1142-1152.

Benevento LA, Standage GP (2004) The organization of projections of the retinorecipient and nonretinorecipient nuclei of the pretectal complex and layers of the superior colliculus to the lateral pulvinar and medial pulvinar in the macaque monkey. J Comp Neurol 217:307-336.

Berdyyeva TK, Olson CR (2009) Monkey supplementary eye field neurons signal the ordinal position of both actions and objects. J Neurosci 29:591.

Berdyyeva TK, Olson CR (2010) Rank signals in four areas of macaque frontal cortex during selection of actions and objects in serial order. J Neurophysiol 104:141.

Bichot NP, Schall JD (1999a) Effects of similarity and history on neural mechanisms of visual selection. Nat Neurosci 2:549-554.

Bichot NP, Schall JD (1999b) Saccade target selection in macaque during feature and conjunction visual search. Visual Neurosci 16:81-89.

Bichot NP, Schall JD (2002) Priming in macaque frontal cortex during popout visual search: feature-based facilitation and location-based inhibition of return. J Neurosci 22:4675.

Bichot NP, Schall JD, Thompson KG (1996) Visual feature selectivity in frontal eye fields induced by experience in mature macaques.

Bichot NP, Rao SC, Schall JD (2001a) Continuous processing in macaque frontal cortex during visual search. Neuropsychologia 39:972-982.

Bichot NP, Thompson KG, Rao SC, Schall JD (2001b) Reliability of macaque frontal eye field neurons signaling saccade targets during visual search. J Neurosci 21:713-725.

Bisley JW, Goldberg ME (2003) Neuronal activity in the lateral intraparietal area and spatial attention. Science 299:81.

Bisley JW, Goldberg ME (2010) Attention, intention, and priority in the parietal lobe. Annu Rev Neurosci 33:1-21.

Blatt GJ, Andersen RA, Stoner GR (1990) Visual receptive field organization and cortico-cortical connections of the lateral intraparietal area(area LIP) in the macaque. J Comp Neurol 299:421-445.

Boehler CN, Tsotsos JK, Schoenfeld MA, Heinze HJ, Hopf JM (2011) Neural Mechanisms of Surround Attenuation and Distractor Competition in Visual Search. J Neurosci 31:5213-5224.

Bogacz R, Brown E, Moehlis J, Holmes P, Cohen JD (2006) The physics of optimal decision making: a formal analysis of models of performance in two-alternative forced-choice tasks. Psychol Rev 113:700-765.

Boucher L, Palmeri TJ, Logan GD, Schall JD (2007) Inhibitory control in mind and brain: An interactive race model of countermanding saccades. Psychol Rev 114:376.

Bozdogan H (2000) Akaike's information criterion and recent developments in information complexity. J Math Psychol 44:62-91.

Britten KH, Shadlen MN, Newsome WT, Movshon JA (1992) The analysis of visual motion: a comparison of neuronal and psychophysical performance. J Neurosci 12:4745-4765.

Brown JW, Bullock D, Grossberg S (2004) How laminar frontal cortex and basal ganglia circuits interact to control planned and reactive saccades. Neural Networks 17:471-510.

Brown JW, Hanes DP, Schall JD, Stuphorn V (2008) Relation of frontal eye field activity to saccade initiation during a countermanding task. Exp Brain Res 190:135-151.

Brown S, Heathcote A (2005) A ballistic model of choice response time. Psychol Rev 112:117-128.

Brown SD, Heathcote A (2008) The simplest complete model of choice response time: Linear ballistic accumulation. Cognitive Psychol 57:153-178.

Bruce CJ, Goldberg ME (1985) Primate frontal eye fields. I. Single neurons discharging before saccades. J Neurophysiol 53:603-635.

Bruce CJ, Goldberg ME, Bushnell MC, Stanton GB (1985) Primate frontal eye fields. II. Physiological and anatomical correlates of electrically evoked eye movements. J Neurophysiol 54:714.

Bullier J, Schall JD, Morel A (1996) Functional streams in occipito-frontal connections in the monkey. Behav Brain Res 76:89-97.

Bundesen C, Habekost T, Kyllingsbæk S (2005) A neural theory of visual attention: Bridging cognition and neurophysiology. Psychol Rev 112:291-328.

Burrows BE, Moore T (2009) Influence and limitations of popout in the selection of salient visual stimuli by area V4 neurons. J Neurosci 29:15169.

Buschman TJ, Miller EK (2007) Top-down versus bottom-up control of attention in the prefrontal and posterior parietal cortices. Science 315:1860.

Buschman TJ, Miller EK (2009) Serial, covert shifts of attention during visual search are reflected by the frontal eye fields and correlated with population oscillations. Neuron 63:386-396.

Busemeyer JR, Townsend JT (1993) Decision field theory: a dynamic-cognitive approach to decision making in an uncertain environment. Psychol Rev 100:432.

Busemeyer JR, Diederich A (2009) Cognitive modeling: Sage Publications, Incorporated.

Campana G, Cowey A, Walsh V (2006) Visual area V5/MT remembers what but not where. Cereb Cortex 16:1766.

Campos M, Breznen B, Andersen RA (2009) Separate representations of target and timing cue locations in the supplementary eye fields. J Neurophysiol 101:448.

Cannon SC, Robinson DA (1987) Loss of the neural integrator of the oculomotor system from brain stem lesions in monkey. J Neurophysiol 57:1383-1409.

Carpenter RHS (2004) Contrast, probability, and saccadic latency: Evidence for independence of detection and decision. Curr Biol 14:1576-1580.

Carpenter RHS, Williams MLL (1995) Neural computation of log likelihood in control of saccadic eye movements. Nature 377:59-62.

Carpenter RHS, Reddi BAJ, Anderson AJ (2009) A simple two stage model predicts response time distributions. The Journal of Physiology 587:4051-4062.

Chang MH, Armstrong KM, Moore T (2012) Dissociation of Response Variability from Firing Rate Effects in Frontal Eye Field Neurons during Visual Stimulation, Working Memory, and Attention. J Neurosci 32:2204-2216.

Chen LL, Wise SP (1995a) Supplementary eye field contrasted with the frontal eye field during acquisition of conditional oculomotor associations. J Neurophysiol 73:1122.

Chen LL, Wise SP (1995b) Neuronal activity in the supplementary eye field during acquisition of conditional oculomotor associations. J Neurophysiol 73:1101.

Chen LL, Wise SP (1996) Evolution of directional preferences in the supplementary eye field during acquisition of conditional oculomotor associations. J Neurosci 16:3067.

Churchland AK, Kiani R, Shadlen MN (2008) Decision-making with multiple alternatives. Nat Neurosci 11:693-702.

Churchland AK, Kiani R, Chaudhuri R, Wang XJ, Pouget A, Shadlen MN (2011) Variance as a signature of neural computations during decision making. Neuron 69:818-831.

Churchland MM, Byron MY, Ryu SI, Santhanam G, Shenoy KV (2006) Neural variability in premotor cortex provides a signature of motor preparation. J Neurosci 26:3697-3712.

Churchland MM, Byron MY, Cunningham JP, Sugrue LP, Cohen MR, Corrado GS, Newsome WT, Clark AM, Hosseini P, Scott BB (2010) Stimulus onset quenches neural variability: a widespread cortical phenomenon. Nat Neurosci 13:369-378.

Cisek P (2006) Integrated neural processes for defining potential actions and deciding between them: a computational model. J Neurosci 26:9761.

Cisek P, Puskas GA, El-Murr S (2009) Decisions in changing conditions: the urgency-gating model. J Neurosci 29:11560.

Coe B, Tomihara K, Matsuzawa M, Hikosaka O (2002) Visual and anticipatory bias in three cortical eye fields of the monkey during an adaptive decision-making task. J Neurosci 22:5081.

Cohen JY, Heitz RP, Schall JD, Woodman GF (2009a) On the origin of event-related potentials indexing covert attentional selection during visual search. J Neurophysiol 102:2375.

Cohen JY, Heitz RP, Woodman GF, Schall JD (2009b) Neural basis of the set-size effect in frontal eye field: timing of attention during visual search. J Neurophysiol 101:1699-1704.

Cohen JY, Crowder EA, Heitz RP, Subraveti CR, Thompson KG, Woodman GF, Schall JD (2010) Cooperation and competition among frontal eye field neurons during visual target selection. J Neurosci 30:3227-3238.

Cohen MR, Newsome WT (2008) Context-dependent changes in functional circuitry in visual area MT. Neuron 60:162-173.

Cohen MR, Maunsell JHR (2009) Attention improves performance primarily by reducing interneuronal correlations. Nat Neurosci 12:1594-1600.

Compte A, Brunel N, Goldman-Rakic PS, Wang XJ (2000) Synaptic mechanisms and network dynamics underlying spatial working memory in a cortical network model. Cereb Cortex 10:910-923.

Constantinidis C, Steinmetz MA (2001) Neuronal responses in area 7a to multiple-stimulus displays: I. Neurons encode the location of the salient stimulus. Cereb Cortex 11:581.

Constantinidis C, Steinmetz MA (2005) Posterior parietal cortex automatically encodes the location of salient stimuli. J Neurosci 25:233.

Cook EP, Maunsell JHR (2002) Dynamics of neuronal responses in macaque MT and VIP during motion detection. Nat Neurosci 5:985-994.

Corbetta M (1998) Frontoparietal cortical networks for directing attention and the eye to visual locations: Identical, independent, or overlapping neural systems? P Natl Acad Sci 95:831.

De Jong R, Coles MG, Logan GD, Gratton G (1990) In search of the point of no return: the control of response processes. J Exp Psychol Human 16:164.

Dean AF (1981) The variability of discharge of simple cells in the cat striate cortex. Exp Brain Res 44:437-440.

Desimone R, Duncan J (1995) Neural mechanisms of selective visual attention. Annu Rev Neurosci 18:193-222.

Ding L, Hikosaka O (2006) Comparison of reward modulation in the frontal eye field and caudate of the macaque. J Neurosci 26:6695.

Ding L, Gold JI (2011) Neural Correlates of Perceptual Decision Making before, during, and after Decision Commitment in Monkey Frontal Eye Field. Cereb Cortex Jul 17 [Epub ahead of print].

Ding L, Gold JI (2012) Neural Correlates of Perceptual Decision Making before, during, and after Decision Commitment in Monkey Frontal Eye Field. Cereb Cortex.

Ditterich J (2006) Stochastic models of decisions about motion direction: behavior and physiology. Neural Networks 19:981-1012.

Ditterich J (2010) A Comparison between Mechanisms of Multi-Alternative Perceptual Decision Making: Ability to Explain Human Behavior, Predictions for Neurophysiology, and Relationship with Decision Theory. Front Decis Neurosci 4.

Ditterich J, Mazurek ME, Shadlen MN (2003) Microstimulation of visual cortex affects the speed of perceptual decisions. Nat Neurosci 6:891-898.

Donders FC (1969) On the speed of mental processes. Acta Psychol 30:412.

Donkin C, Brown S, Heathcote A (2009) The over-constraint of response time models. Psychol Rev.

Donkin C, Brown S, Heathcote A, Wagenmakers E-J (2011) Diffusion versus linear ballistic accumulation: different models but the same conclusions about psychological processes? Psychon B Rev 18:61-69.

Dorris MC, Munoz DP (1998) Saccadic probability influences motor preparation signals and time to saccadic initiation. J Neurosci 18:7015-7026.

Dorris MC, Pare M, Munoz DP (1997) Neuronal activity in monkey superior colliculus related to the initiation of saccadic eye movements. J Neurosci 17:8566-8579.

Dorris MC, Olivier E, Munoz DP (2007) Competitive integration of visual and preparatory signals in the superior colliculus during saccadic programming. J Neurosci 27:5053-5062.

Duncan J, Humphreys GW (1989) Visual search and stimulus similarity. Psychol Rev 96:433.

Efron B, Tibshirani R (1993) An introduction to the bootstrap: Chapman & Hall/CRC.

Eimer M (1996) The N2pc component as an indicator of attentional selectivity. Electroencephalography and clinical neurophysiology 99:225-234.

Eimer M, Kiss M (2010) The top-down control of visual selection and how it is linked to the N2pc component. Acta Psychol 135:100.

Eimer M, Kiss M, Cheung T (2010) Priming of pop-out modulates attentional target selection in visual search: Behavioural and electrophysiological evidence. Vision Res 50:1353-1361.

Eimer M, Kiss M, Press C, Sauter D (2009) The roles of feature-specific task set and bottom-up salience in attentional capture: An ERP study. Journal of Experimental Psychology: Human Perception and Performance; Journal of Experimental Psychology: Human Perception and Performance 35:1316.

Ekstrom LB, Roelfsema PR, Arsenault JT, Bonmassar G, Vanduffel W (2008) Bottom-up dependent gating of frontal signals in early visual cortex. Science 321:414.

Emeric EE, Leslie M, Pouget P, Schall JD (2010) Performance monitoring local field potentials in the medial frontal cortex of primates: Supplementary eye field. J Neurophysiol 104:1523.

Everling S, Munoz DP (2000) Neuronal correlates for preparatory set associated with pro-saccades and anti-saccades in the primate frontal eye field. J Neurosci 20:387-400.

Everling S, Paré M, Dorris MC, Munoz DP (1998) Comparison of the discharge characteristics of brain stem omnipause neurons and superior colliculus fixation neurons in monkey: implications for control of fixation and saccade behavior. J Neurophysiol 79:511.

Everling S, Dorris MC, Klein RM, Munoz DP (1999) Role of primate superior colliculus in preparation and execution of anti-saccades and pro-saccades. J Neurosci 19:2740-2754.

Faisal AA, Selen LPJ, Wolpert DM (2008) Noise in the nervous system. Nat Rev Neurosci 9:292-303.

Falkner AL, Krishna BS, Goldberg ME (2010) Surround suppression sharpens the priority map in the lateral intraparietal area. J Neurosci 30:12787.

Farrell S, Lewandowsky S (2010) Computational modeling in cognition: Principles and practice: Sage Publications, Incorporated.

Fecteau JH, Munoz DP (2006) Salience, relevance, and firing: a priority map for target selection. Trends Cogn Sci 10:382-390.

Findlay JM, Walker R (1999) A model of saccade generation based on parallel processing and competitive inhibition. Behav Brain Sci 22:661-674.

Forstmann BU, Wagenmakers EJ, Eichele T, Brown S, Serences JT (2011) Reciprocal relations between cognitive neuroscience and formal cognitive models: opposites attract? Trends Cogn Sci 15:272-279.

Forstmann BU, Dutilh G, Brown S, Neumann J, Von Cramon DY, Ridderinkhof KR, Wagenmakers EJ (2008) Striatum and pre-SMA facilitate decision-making under time pressure. P Natl Acad Sci 105:17538-17542.

Frank MJ (2006) Hold your horses: a dynamic computational role for the subthalamic nucleus in decision making. Neural Networks 19:1120-1136.

Fries W (2004) Cortical projections to the superior colliculus in the macaque monkey: a retrograde study using horseradish peroxidase. J Comp Neurol 230:55-76.

Fuchs AF, Luschei ES (1970) Firing patterns of abducens neurons of alert monkeys in relationship to horizontal eye movement. J Neurophysiol 33:382-392.

Furman M, Wang XJ (2008) Similarity effect and optimal control of multiple-choice decision making. Neuron 60:1153-1168.

Gawne TJ, Kjaer TW, Richmond BJ (1996) Latency: another potential code for feature binding in striate cortex. J Neurophysiol 76:1356-1360.

Georgopoulos AP, Kettner RE, Schwartz AB (1988) Primate motor cortex and free arm movements to visual targets in three-dimensional space. II. Coding of the direction of movement by a neuronal population. J Neurosci 8:2928.

Gnadt JW, Andersen RA (1988) Memory related motor planning activity in posterior parietal cortex of macaque. Exp Brain Res 70:216-220.

Godlove DC, Garr AK, Woodman GF, Schall JD (2011a) Measurement of the extraocular spike potential during saccade countermanding. J Neurophysiol 106:104.

Godlove DC, Emeric EE, Segovis CM, Young MS, Schall JD, Woodman GF (2011b) Event-Related Potentials Elicited by Errors during the Stop-Signal Task. I. Macaque Monkeys. J Neurosci 31:15640-15649.

Gold JI, Shadlen MN (2001) Neural computations that underlie decisions about sensory stimuli. Trends Cogn Sci 5:10-16.

Gold JI, Shadlen MN (2002) Banburismus and the Brain: Decoding the Relationship between Sensory Stimuli, Decisions, and Reward. Neuron 36:299-308.

Gold JI, Shadlen MN (2007) The neural basis of decision making. Neuroscience 30:535-574.

Goldberg DE (1989) Genetic algorithms in search, optimization, and machine learning.

Gottlieb J (2007) From thought to action: the parietal cortex as a bridge between perception, action, and cognition. Neuron 53:9-16.

Gottlieb J, Goldberg ME (1999) Activity of neurons in the lateral intraparietal area of the monkey during an antisaccade task. Nat Neurosci 2:906-912.

Gottlieb J, Kusunoki M, Goldberg ME (2005) Simultaneous representation of saccade targets and visual onsets in monkey lateral intraparietal area. Cereb Cortex 15:1198-1206.

Gottlieb JP, Kusunoki M, Goldberg ME (1998) The representation of visual salience in monkey parietal cortex. Nature 391:481-484.

Gratton G, Coles MGH, Sirevaag EJ, Eriksen CW, Donchin E (1988) Pre-and poststimulus activation of response channels: a psychophysiological analysis. J Exp Psychol Human 14:331.

Green DM, Swets JA (1966) Signal detection theory and psychophysics: Wiley New York.

Gregoriou GG, Gotts SJ, Desimone R (2012) Cell-Type-Specific Synchronization of Neural Activity in FEF with V4 during Attention. Neuron 73:581-594.

Grice GR (1968) Stimulus intensity and response evocation. Psychol Rev 75:359.

Grossberg S (1976) Adaptive pattern classification and universal recoding: I. Parallel development and coding of neural feature detectors. Biological cybernetics 23:121-134.

Hanes DP, Schall JD (1996) Neural control of voluntary movement initiation. Science 274:427-430.

Hanes DP, Patterson WF, Schall JD (1998) Role of frontal eye fields in countermanding saccades: visual, movement, and fixation activity. J Neurophysiol 79:817-834.

Hanks TD, Ditterich J, Shadlen MN (2006) Microstimulation of macaque area LIP affects decision-making in a motion discrimination task. Nat Neurosci 9:682-689.

Hanks TD, Mazurek ME, Kiani R, Hopp E, Shadlen MN (2011) Elapsed decision time affects the weighting of prior probability in a perceptual decision task. J Neurosci 31:6339-6352.

Hardy SGP, Lynch JC (1992) The spatial distribution of pulvinar neurons that project to two subregions of the inferior parietal lobule in the macaque. Cereb Cortex 2:217-230.

Hartveit E, Heggelund P (1994) Response variability of single cells in the dorsal lateral geniculate nucleus of the cat. Comparison with retinal input and effect of brain stem stimulation. J Neurophysiol 72:1278-1289.

Harvey CD, Coen P, Tank DW (2012) Choice-specific sequences in parietal cortex during a virtual-navigation decision task. Nature 484:62-68.

Hasegawa RP, Matsumoto M, Mikami A (2000) Search target selection in monkey prefrontal cortex. J Neurophysiol 84:1692.

Hayden BY, Pearson JM, Platt ML (2011) Neuronal basis of sequential foraging decisions in a patchy environment. Nat Neurosci 14:933-939.

Heekeren HR, Marrett S, Bandettini PA, Ungerleider LG (2004) A general mechanism for perceptual decision-making in the human brain. Nature 431:859-862.

Heitz R, Schall J (2012) Neural mechanisms of speed-accuracy tradeoff. Neuron.

Heitz RP, Cohen JY, Woodman GF, Schall JD (2010) Neural correlates of correct and errant attentional selection revealed through N2pc and frontal eye field activity. J Neurophysiol 104:2433-2441.

Helmholtz H (1853) Ueber einige Gesetze der Vertheilung elektrischer Ströme in körperlichen Leitern mit Anwendung auf die thierisch-elektrischen Versuche. Annalen der Physik 165:211-233.

Hikosaka O, Wurtz RH (1983) Visual and oculomotor functions of monkey substantia nigra pars reticulata. IV. Relation of substantia nigra to superior colliculus. J Neurophysiol 49:1285-1301.

Hikosaka O, Takikawa Y, Kawagoe R (2000) Role of the basal ganglia in the control of purposive saccadic eye movements. Physiol Rev 80:953-978.

Hopf JM, Boelmans K, Schoenfeld AM, Heinze HJ, Luck SJ (2002) How does attention attenuate target-distractor interference in vision?:: Evidence from magnetoencephalographic recordings. Cognitive Brain Research 15:17-29.

Hopf JM, Boelmans K, Schoenfeld MA, Luck SJ, Heinze HJ (2004) Attention to features precedes attention to locations in visual search: Evidence from electromagnetic brain responses in humans. J Neurosci 24:1822-1832.

Hopf JM, Luck SJ, Girelli M, Hagner T, Mangun GR, Scheich H, Heinze HJ (2000) Neural sources of focused attention in visual search. Cereb Cortex 10:1233.

Huerta MF, Kaas JH (1990) Supplementary eye field as defined by intracortical microstimulation: connections in macaques. J Comp Neurol 293:299-330.

Huerta MF, Krubitzer LA, Kaas JH (1987) Frontal eye field as defined by intracortical microstimulation in squirrel monkeys, owl monkeys, and macaque monkeys II. Cortical connections. J Comp Neurol 265:332-361.

Huk AC, Shadlen MN (2005) Neural activity in macaque parietal cortex reflects temporal integration of visual motion signals during perceptual decision making. J Neurosci 25:10420-10436.

Hussar C, Pasternak T (2010) Trial-to-trial variability of the prefrontal neurons reveals the nature of their engagement in a motion discrimination task. P Natl Acad Sci 107:21842-21847.

Ipata AE, Gee AL, Goldberg ME, Bisley JW (2006) Activity in the lateral intraparietal area predicts the goal and latency of saccades in a free-viewing visual search task. J Neurosci 26:3656-3661.

Isoda M, Hikosaka O (2007) Switching from automatic to controlled action by monkey medial frontal cortex. Nat Neurosci 10:240-248.

Isoda M, Hikosaka O (2011) Cortico-basal ganglia mechanisms for overcoming innate, habitual and motivational behaviors. Eur J Neurosci 33:2058-2069.

Itti L, Koch C (2001) Computational modelling of visual attention. Nat Rev Neurosci 2:194-203.

Joseph JS, Chun MM, Nakayama K (1997) Attentional requirements in a'preattentive'feature search task. Nature 387:805-807.

Kamogawa H, Ohki Y, Shimazu H, Suzuki I, Yamashita M (1996) Inhibitory input to pause neurons from pontine burst neuron area in the cat. Neuroscience letters 203:163-166.

Kara P, Reinagel P, Reid RC (2000) Low response variability in simultaneously recorded retinal, thalamic, and cortical neurons. Neuron 27:635-646.

Kastner S, Pinsk MA, De Weerd P, Desimone R, Ungerleider LG (1999) Increased activity in human visual cortex during directed attention in the absence of visual stimulation. Neuron 22:751-761.

Katsuki F, Constantinidis C (2011) Early involvement of prefrontal cortex in bottom-up visual attention: comparison of neural response times in monkey prefrontal and posterior parietal cortex. J Vis 11:169-169.

Katsuki F, Constantinidis C (2012) Early involvement of prefrontal cortex in visual bottom-up attention. Nat Neurosci 15:1160-1166.

Katzner S, Nauhaus I, Benucci A, Bonin V, Ringach DL, Carandini M (2009) Local origin of field potentials in visual cortex. Neuron 61:35-41.

Kepecs A, Uchida N, Zariwala HA, Mainen ZF (2008) Neural correlates, computation and behavioural impact of decision confidence. Nature 455:227-231.

Kiani R, Hanks TD, Shadlen MN (2008) Bounded integration in parietal cortex underlies decisions even when viewing duration is dictated by the environment. J Neurosci 28:3017-3029.

Kiss M, Driver J, Eimer M (2009) Reward priority of visual target singletons modulates event-related potential signatures of attentional selection. Psychol Sci 20:245-251.

Kristjansson A, Vuilleumier P, Schwartz S, Macaluso E, Driver J (2007) Neural basis for priming of pop-out during visual search revealed with fMRI. Cereb Cortex 17:1612.

Lamberts K (2000) Information-accumulation theory of speeded categorization. Psychol Rev 107:227.

Laming DRJ (1968) Information theory of choice-reaction times.

Lee H, Mozer MC, Vecera SP (2009) Mechanisms of priming of pop-out: Stored representations or feature-gain modulations? Atten Percept Psycho 71:1059-1071.

Leichnetz GR, Gonzalo-Ruiz A (1996) Prearcuate cortex in the Cebus monkey has cortical and subcortical connections like the macaque frontal eye field and projects to fastigial-recipient oculomotor-related brainstem nuclei. Brain research bulletin 41:1-29.

Leichnetz GR, Spencer RF, Hardy SGP, Astruc J (1981) The prefrontal corticotectal projection in the monkey; an anterograde and retrograde horseradish peroxidase study. Neuroscience 6:1023-1041.

Leite FP, Ratcliff R (2010) Modeling reaction time and accuracy of multiple-alternative decisions. Atten Percept Psycho 72:246-273.

Leonards U, Sunaert S, Van Hecke P, Orban GA (2000) Attention mechanisms in visual search-an fMRI study. J Cognitive Neurosci 12:61-75.

Link SW, Heath RA (1975) A sequential theory of psychological discrimination. Psychometrika 40:77-105.

Lo CC, Wang XJ (2006) Cortico–basal ganglia circuit mechanism for a decision threshold in reaction time tasks. Nat Neurosci 9:956-963.

Logan GD (2002) An instance theory of attention and memory. Psychol Rev 109:376.

Logothetis NK, Wandell BA (2004) Interpreting the BOLD signal. Annu Rev Physiol 66:735-769.

Lu X, Matsuzawa M, Hikosaka O (2002) A neural correlate of oculomotor sequences in supplementary eye field. Neuron 34:317-325.

Luce RD (1991) Response times: Their role in inferring elementary mental organization: Oxford University Press, USA.

Luck SJ (2005) An introduction to the event-related potential technique. Cambridge: MIT Press.

Luck SJ, Hillyard SA (1990) Electrophysiological evidence for parallel and serial processing during visual search. Atten Percept Psycho 48:603-617.

Luck SJ, Hillyard SA (1994a) Spatial filtering during visual search: Evidence from human electrophysiology. J Exp Psychol Human 20:1000.

Luck SJ, Hillyard SA (1994b) Electrophysiological correlates of feature analysis during visual search. Psychophysiology 31:291-308.

Luck SJ, Girelli M, McDermott MT, Ford MA (1997a) Bridging the gap between monkey neurophysiology and human perception: An ambiguity resolution theory of visual selective attention. Cognitive Psychol 33:64-87.

Luck SJ, Chelazzi L, Hillyard SA, Desimone R (1997b) Neural mechanisms of spatial selective attention in areas V1, V2, and V4 of macaque visual cortex. J Neurophysiol 77:24.

Ludwig CJH, Gilchrist ID, McSorley E, Baddeley RJ (2005) The temporal impulse response underlying saccadic decisions. J Neurosci 25:9907-9912.

Lui F, Gregory KM, Blanks RHI, Giolli RA (1995) Projections from visual areas of the cerebral cortex to pretectal nuclear complex, terminal accessory optic nuclei, and superior colliculus in macaque monkey. J Comp Neurol 363:439-460.

Luppino G, Matelli M, Camarda R, Rizzolatti G (1993) Corticocortical connections of area F3 (SMA proper) and area F6 (pre-SMA) in the macaque monkey. J Comp Neurol 338:114-140.

Luppino G, Matelli M, Camarda RM, Gallese V, Rizzolatti G (1991) Multiple representations of body movements in mesial area 6 and the adjacent cingulate cortex: an intracortical microstimulation study in the macaque monkey. J Comp Neurol 311:463-482.

Luschei ES, Fuchs AF (1972) Activity of brain stem neurons during eye movements of alert monkeys. J Neurophysiol.

Lynch JC, Hoover JE, Strick PL (1994) Input to the primate frontal eye field from the substantia nigra, superior colliculus, and dentate nucleus demonstrated by transneuronal transport. Exp Brain Res 100:181-186.

Lyon DC, Nassi JJ, Callaway EM (2010) A disynaptic relay from superior colliculus to dorsal stream visual cortex in macaque monkey. Neuron 65:270-279.

Maimon G, Assad JA (2006) A cognitive signal for the proactive timing of action in macaque LIP. Nat Neurosci 9:948-955.

Maljkovic V, Nakayama K (1994) Priming of pop-out: I. Role of features. Mem Cognition 22:657-672.

Markram H, Toledo-Rodriguez M, Wang Y, Gupta A, Silberberg G, Wu C (2004) Interneurons of the neocortical inhibitory system. Nat Rev Neurosci 5:793-807.

Marr D (1982) Vision: A computational investigation into the human representation and processing of visual information, Henry Holt and Co. Inc, New York, NY.

Matelli M, Luppino G, Rizzolatti G (1991) Architecture of superior and mesial area 6 and the adjacent cingulate cortex in the macaque monkey. J Comp Neurol 311:445-462.

Matzke D, Wagenmakers E-J (2009) Psychological interpretation of the ex-Gaussian and shifted Wald parameters: A diffusion model analysis. Psychon B Rev 16:798-817.

Maunsell JHR, Ghose GM, Assad JA, McAdams CJ, Boudreau CE, Noerager BD (1999) Visual response latencies of magnocellular and parvocellular LGN neurons in macaque monkeys. Visual Neurosci 16:1-14.

May JG, Andersen RA (1986) Different patterns of corticopontine projections from separate cortical fields within the inferior parietal lobule and dorsal prelunate gyrus of the macaque. Exp Brain Res 63:265-278.

Mazurek ME, Roitman JD, Ditterich J, Shadlen MN (2003) A role for neural integrators in perceptual decision making. Cereb Cortex 13:1257-1269.

McMillen T, Holmes P (2006) The dynamics of choice among multiple alternatives. J Math Psychol 50:30-57.

McPeek RM, Keller EL (2001) Short-term priming, concurrent processing, and saccade curvature during a target selection task in the monkey. Vision Res 41:785-800.

McPeek RM, Keller EL (2002) Saccade target selection in the superior colliculus during a visual search task. J Neurophysiol 88:2019-2034.

Meyer DE, Osman AM, Irwin DE, Yantis S (1988) Modern mental chronometry. Biological psychology 26:3-67.

Miller J (1998) Effects of stimulusâ€“response probability on choice reaction time: Evidence from the lateralized readiness potential. J Exp Psychol Human 24:1521.

Mitchell JF, Sundberg KA, Reynolds JH (2007) Differential attention-dependent response modulation across cell classes in macaque visual area V4. Neuron 55:131-141.

Mitchell JF, Sundberg KA, Reynolds JH (2009) Spatial attention decorrelates intrinsic activity fluctuations in macaque area V4. Neuron 63:879-888.

Mitz AR, Wise SP (1987) The somatotopic organization of the supplementary motor area: intracortical microstimulation mapping. J Neurosci 7:1010.

Mitzdorf U (1985) Current source-density method and application in cat cerebral cortex: investigation of evoked potentials and EEG phenomena. Physiol Rev 65:37.

Monosov IE, Thompson KG (2009) Frontal eye field activity enhances object identification during covert visual search. J Neurophysiol 102:3656-3672.

Monosov IE, Trageser JC, Thompson KG (2008) Measurements of simultaneously recorded spiking activity and local field potentials suggest that spatial selection emerges in the frontal eye field. Neuron 57:614-625.

Monosov IE, Sheinberg DL, Thompson KG (2010) Paired neuron recordings in the prefrontal and inferotemporal cortices reveal that spatial selection precedes object identification during visual search. P Natl Acad Sci 107:13105-13110.

Monosov IE, Sheinberg DL, Thompson KG (2011) The Effects of Prefrontal Cortex Inactivation on Object Responses of Single Neurons in the Inferotemporal Cortex during Visual Search. J Neurosci 31:15956-15961.

Moore T, Armstrong KM (2003) Selective gating of visual signals by microstimulation of frontal cortex. Nature 421:370-373.

Moran J, Desimone R (1985) Selective attention gates visual processing in the extrastriate cortex. Frontiers in cognitive neuroscienceÃŽ 229:342-345ÃŽ.

Moschovakis AK, Karabelas AB, Highstein SM (1988) Structure-function relationships in the primate superior colliculus. II. Morphological identity of presaccadic neurons. J Neurophysiol 60:263.

Muggleton NG, Juan CH, Cowey A, Walsh V (2003) Human frontal eye fields and visual search. J Neurophysiol 89:3340-3343.

Mulder MJ, Wagenmakers E-J, Ratcliff R, Boekel W, Forstmann BU (2012) Bias in the brain: a diffusion model analysis of prior probability and potential payoff. J Neurosci 32:2335-2343.

Munoz DP, Wurtz RH (1993) Fixation cells in monkey superior colliculus. I. Characteristics of cell discharge. J Neurophysiol 70:559.

Munoz DP, Wurtz RH (1995) Saccade-related activity in monkey superior colliculus. I. Characteristics of burst and buildup cells. J Neurophysiol 73:2313-2333.

Munoz DP, Dorris MC, Pare M, Everling S (2000) On your mark, get set: brainstem circuitry underlying saccadic initiation. Canadian Journal of Physiology and Pharmacology 78:934-944.

Murdock Jr BB (1965) Signal-detection theory and short-term memory. Journal of Experimental Psychology; Journal of Experimental Psychology 70:443.

Murthy A, Thompson KG, Schall JD (2001) Dynamic dissociation of visual selection from saccade programming in frontal eye field. J Neurophysiol 86:2634-2637.

Murthy A, Ray S, Shorter SM, Schall JD, Thompson KG (2009) Neural control of visual search by frontal eye field: effects of unexpected target displacement on visual selection and saccade preparation. J Neurophysiol 101:2485-2506.

Nakahara H, Nakamura K, Hikosaka O (2006) Extended LATER model can account for trial-by-trial variability of both pre-and post-processes. Neural Networks 19:1027-1046.

Nakamura K, Roesch MR, Olson CR (2005) Neuronal activity in macaque SEF and ACC during performance of tasks involving conflict. J Neurophysiol 93:884.

Navalpakkam V, Itti L (2007) Search goal tunes visual features optimally. Neuron 53:605-617.

Nawrot MP, Boucsein C, Rodriguez Molina V, Riehle A, Aertsen A, Rotter S (2008) Measurement of variability dynamics in cortical spike trains. Journal of neuroscience methods 169:374-390.

Nelder JA, Mead R (1965) A simplex method for function minimization. The computer journal 7:308.

Nienborg H, Cumming BG (2009) Decision-related activity in sensory neurons reflects more than a neuronâ€™s causal effect. Nature 459:89-92.

Ninomiya T, Sawamura H, Inoue K, Takada M (2012) Segregated Pathways Carrying Frontally Derived Top-Down Signals to Visual Areas MT and V4 in Macaques. J Neurosci 32:6851-6858.

Nosofsky RM, Palmeri TJ (1997) An exemplar-based random walk model of speeded classification. Psychol Rev 104:266-299.

Noudoost B, Moore T (2011) Control of visual cortical signals by prefrontal dopamine. Nature 474:372-375.

Nunez PL, Srinivasan R (2006) Electric fields of the brain: the neurophysics of EEG: Oxford University Press, USA.

O'Connell RG, Dockree PM, Kelly SP (2012) A supramodal accumulation-to-bound signal that determines perceptual decisions in humans. Nat Neurosci.

Ogawa T, Komatsu H (2004) Target selection in area V4 during a multidimensional visual search task. J Neurosci 24:6371-6382.

Ogawa T, Komatsu H (2009) Condition-dependent and condition-independent target selection in the macaque posterior parietal cortex. J Neurophysiol 101:721-736.

Okun M, Naim A, Lampl I (2010) The subthreshold relation between cortical local field potential and neuronal firing unveiled by intracellular recordings in awake rats. J Neurosci 30:4440.

Olson CR, Tremblay L (2000) Macaque supplementary eye field neurons encode object-centered locations relative to both continuous and discontinuous objects. J Neurophysiol 83:2392.

Oram MW, Xiao D, Dritschel B, Payne KR (2002) The temporal resolution of neural codes: does response latency have a unique role? Philosophical Transactions of the Royal Society of London Series B: Biological Sciences 357:987-1001.

Orban GA (2008) Higher order visual processing in macaque extrastriate cortex. Physiol Rev 88:59-89.

Orban GA, Van Essen D, Vanduffel W (2004) Comparative mapping of higher visual areas in monkeys and humans. Trends Cogn Sci 8:315-324.

Osman A, Lou L, Muller-Gethmann H, Rinkenauer G, Mattes S, Ulrich R (2000) Mechanisms of speed-accuracy tradeoff: evidence from covert motor processes. Biological psychology 51:173-199.

Palmer EM, Horowitz TS, Torralba A, Wolfe JM (2011) What are the shapes of response time distributions in visual search? J Exp Psychol Human 37:58.

Palmer J, Verghese P, Pavel M (2000) The psychophysics of visual search. Vision Res 40:1227-1268.

Palmeri TJ (1997) Exemplar similarity and the development of automaticity. Journal of Experimental Psychology: Learning, Memory, and Cognition 23:324.

Palmeri TJ, Tarr MJ (2008) Visual object perception and long-term memory. Visual memory:163-207.

Pare M, Wurtz RH (2001) Progression in neuronal processing for saccadic eye movements from parietal cortex area lip to superior colliculus. J Neurophysiol 85:2545-2562.

Pare M, Hanes DP (2003) Controlled movement processing: superior colliculus activity associated with countermanded saccades. J Neurosci 23:6480-6489.

Parent A, Hazrati LN (1995) Functional anatomy of the basal ganglia. I. The cortico-basal ganglia-thalamo-cortical loop. Brain Res Rev 20:91-127.

Platt JR (1964) Strong inference. Science 146:347-353.

Platt ML, Glimcher PW (1999) Neural correlates of decision variables in parietal cortex. Nature 400:233-238.

Pouget P, Emeric EE, Stuphorn V, Reis K, Schall JD (2005) Chronometry of visual responses in frontal eye field, supplementary eye field, and anterior cingulate cortex. J Neurophysiol 94:2086.

Pouget P, Logan GD, Palmeri TJ, Boucher L, Paré M, Schall JD (2011) Neural Basis of Adaptive Response Time Adjustment during Saccade Countermanding. J Neurosci 31:12604-12612.

Pouget P, Stepniewska I, Crowder EA, Leslie MW, Emeric EE, Nelson MJ, Schall JD (2009) Visual and motor connectivity and the distribution of calcium-binding proteins in macaque frontal eye field: implications for saccade target selection. Front Neuroanat 3:1-14.

Poulet JFA, Petersen CCH (2008) Internal brain state regulates membrane potential synchrony in barrel cortex of behaving mice. Nature 454:881-885.

Purcell BA, Weigand PK, Schall JD (2012a) Supplementary Eye Field during Visual Search: Salience, Cognitive Control, and Performance Monitoring. J Neurosci 32:10273-10285.

Purcell BA, Schall JD, Woodman GF (2013) On the origin of event-related potentials indexing covert attentional selection during visual search: timing of selection by macaque frontal eye field and event-related potentials during pop-out search. J Neurophysiol 109:557-569.

Purcell BA, Weigand PK, Schall JD (in press) Supplementary eye field during visual search: Salience, cognitive control, and performance monitoring. J Neurosci.

Purcell BA, Schall JD, Logan GD, Palmeri TJ (2012b) From Salience to Saccades: Multiple-Alternative Gated Stochastic Accumulator Model of Visual Search. J Neurosci 32:3433-3446.

Purcell BA, Heitz RP, Cohen JY, Schall JD (2012c) Response Variability of Frontal Eye Field Neurons Modulates with Sensory Input and Saccade Preparation but not Visual Search Salience. J Neurophysiol.

Purcell BA, Heitz RP, Cohen JY, Schall JD, Logan GD, Palmeri TJ (2010) Neurally constrained modeling of perceptual decision making. Psychol Rev 117:1113-1143.

Rao V, DeAngelis GC, Snyder LH (2012) Neural Correlates of Prior Expectations of Motion in the Lateral Intraparietal and Middle Temporal Areas. J Neurosci 32:10063-10074.

Ratcliff R (1978) A theory of memory retrieval. Psychol Rev 85:59.

Ratcliff R (1988) Continuous versus discrete information processing: Modeling accumulation of partial information.

Ratcliff R, Rouder JN (1998) Modeling response times for two-choice decisions. Psychol Sci 9:347-356.

Ratcliff R, Tuerlinckx F (2002) Estimating parameters of the diffusion model: Approaches to dealing with contaminant reaction times and parameter variability. Psychon B Rev 9:438-481.

Ratcliff R, Smith PL (2004) A comparison of sequential sampling models for two-choice reaction time. Psychol Rev 111:333-367.

Ratcliff R, McKoon G (2008) The diffusion decision model: Theory and data for two-choice decision tasks. Neural Comput 20:873-922.

Ratcliff R, Van Zandt T, McKoon G (1999) Connectionist and diffusion models of reaction time. Psychol Rev 106:261.

Ratcliff R, Cherian A, Segraves M (2003) A comparison of macaque behavior and superior colliculus neuronal activity to predictions from models of two-choice decisions. J Neurophysiol 90:1392-1407.

Ratcliff R, Hasegawa YT, Hasegawa RP, Smith PL, Segraves MA (2007) Dual diffusion model for single-cell recording data from the superior colliculus in a brightness-discrimination task. J Neurophysiol 97:17561774.

Ray S, Pouget P, Schall JD (2009) Functional distinction between visuomovement and movement neurons in macaque frontal eye field during saccade countermanding. J Neurophysiol 102:3091.

Reddi BA, Carpenter RH (2000) The influence of urgency on decision time. Nat Neurosci 3:827-830.

Reilly JX, Mars RB (2011) Computational neuroimaging: localising Greek letters? Comment on Forstmann et al. Trends Cogn Sci 15:450.

Reinhart RM, Carlisle NB, Kang MS, Woodman GF (2012a) Event-related potentials elicited by errors during the stop-signal task. II: Human effector specific error responses. J Neurophysiol.

Reinhart RM, Heitz RP, Purcell BA, Weigand PK, Schall JD, Woodman GF (2012b) Homologous mechanisms of visuospatial working memory maintenance in macaque and human: Properties and sources. J Neurosci.

Reynolds JH, Pasternak T, Desimone R (2000) Attention increases sensitivity of V4 neurons. Neuron 26:703-714.

Rinkenauer G, Osman A, Ulrich R, Muller-Gethmann H, Mattes S (2004) On the locus of speed-accuracy trade-off in reaction time: inferences from the lateralized readiness potential. Journal of Experimental Psychology: General; Journal of Experimental Psychology: General 133:261.

Robinson DA (1964) The mechanics of human saccadic eye movement. The Journal of physiology 174:245-264.

Roesch MR, Olson CR (2003) Impact of expected reward on neuronal activity in prefrontal cortex, frontal and supplementary eye fields and premotor cortex. J Neurophysiol 90:1766-1789.

Roitman JD, Shadlen MN (2002) Response of neurons in the lateral intraparietal area during a combined visual discrimination reaction time task. J Neurosci 22:9475-9489.

Rossi AF, Bichot NP, Desimone R, Ungerleider LG (2007) Top-down attentional deficits in macaques with lesions of lateral prefrontal cortex. J Neurosci 27:11306.

Rushworth MFS, Hadland KA, Paus T, Sipila PK (2002) Role of the human medial frontal cortex in task switching: a combined fMRI and TMS study. J Neurophysiol 87:2577.

Russo GS, Bruce CJ (2000) Supplementary eye field: representation of saccades and relationship between neural response fields and elicited eye movements. J Neurophysiol 84:2605.

Sadagopan S, Ferster D (2012) Feedforward Origins of Response Variability Underlying Contrast Invariant Orientation Tuning in Cat Visual Cortex. Neuron 74:911-923.

Salzman CD, Britten KH, Newsome WT (1990) Cortical microstimulation influences perceptual judgements of motion direction. Nature 346:174-177.

Salzman CD, Murasugi CM, Britten KH, Newsome WT (1992) Microstimulation in visual area MT: effects on direction discrimination performance. J Neurosci 12:2331-2355.

Sato T, Murthy A, Thompson KG, Schall JD (2001) Search efficiency but not response interference affects visual selection in frontal eye field. Neuron 30:583-591.

Sato TR, Schall JD (2003) Effects of stimulus-response compatibility on neural selection in frontal eye field. Neuron 38:637-648.

Sato TR, Watanabe K, Thompson KG, Schall JD (2003) Effect of target-distractor similarity on FEF visual selection in the absence of the target. Exp Brain Res 151:356-363.

Schall JD (1991a) Neuronal activity related to visually guided saccadic eye movements in the supplementary motor area of rhesus monkeys. J Neurophysiol 66:530.

Schall JD (1991b) Neuronal activity related to visually guided saccades in the frontal eye fields of rhesus monkeys: comparison with supplementary eye fields. J Neurophysiol 66:559.

Schall JD (2001) Neural basis of deciding, choosing and acting. Nat Rev Neurosci 2:33-42.

Schall JD (2003) Neural correlates of decision processes: neural and mental chronometry. Curr Opin Neurobiol 13:182-186.

Schall JD (2004) On building a bridge between brain and behavior. Psychology 55:23-50.

Schall JD, Hanes DP (1993) Neural basis of saccade target selection in frontal eye field during visual search. Nature 366:467-469.

Schall JD, Thompson KG (1994) Macaque oculomotor thalamus: Saccade target selection. Soc Neurosci Abst 20:145.

Schall JD, Thompson KG (1999) Neural selection and control of visually guided eye movements. Annu Rev Neurosci 22:241-259.

Schall JD, Boucher L (2007) Executive control of gaze by the frontal lobes. Cogn Affect Behav Ne 7:396-412.

Schall JD, Morel A, King DJ, Bullier J (1995a) Topography of visual cortex connections with frontal eye field in macaque: convergence and segregation of processing streams. J Neurosci 15:4464-4487.

Schall JD, Hanes DP, Thompson KG, King DJ (1995b) Saccade target selection in frontal eye field of macaque. I. Visual and premovement activation. J Neurosci 15:6905-6918.

Schall JD, Sato TR, Thompson KG, Vaughn AA, Juan CH (2004) Effects of search efficiency on surround suppression during visual selection in frontal eye field. J Neurophysiol 91:2765-2769.

Schall JD, Purcell BA, Heitz RP, Logan GD, Palmeri TJ (2011) Neural mechanisms of saccade target selection: gated accumulator model of the visualâ€“motor cascade. Eur J Neurosci 33:1991-2002.

Schiller PH, Koerner F (1971) Discharge characteristics of single units in superior colliculus of the alert rhesus monkey. J Neurophysiol 34:920-936.

Schiller PH, Colby CL (1983) The responses of single cells in the lateral geniculate nucleus of the rhesus monkey to color and luminance contrast. Vision Res 23:1631-1641.

Schiller PH, Chou I (1998) The effects of frontal eye field and dorsomedial frontal cortex lesions on visually guided eye movements. Nat Neurosci 1:248-253.

Schiller PH, Chou I (2000) The effects of anterior arcuate and dorsomedial frontal cortex lesions on visually guided eye movements: 2. Paired and multiple targets. Vision Res 40:1627-1638.

Schiller PH, True SD, Conway JL (1979) Effects of frontal eye field and superior colliculus ablations on eye movements. Science 206:590-592.

Schlag-Rey M, Amador N, Sanchez H, Schlag J (1997) Antisaccade performance predicted by neuronal activity in the supplementary eye field. Nature 390:398-400.

Schlag J, Schlag-Rey M (1987) Evidence for a supplementary eye field. J Neurophysiol 57:179.

Schlag J, Dassonville P, Schlag-Rey M (1998) Interaction of the two frontal eye fields before saccade onset. J Neurophysiol 79:64-72.

Schmahmann JD, Pandya DN (1989) Anatomical investigation of projections to the basis pontis from posterior parietal association cortices in rhesus monkey. J Comp Neurol 289:53-73.

Schmahmann JD, Pandya DN (2004) Anatomical investigation of projections from thalamus to posterior parietal cortex in the rhesus monkey: a WGA-HRP and fluorescent tracer study. J Comp Neurol 295:299-326.

Schmolesky MT, Wang Y, Hanes DP, Thompson KG, Leutgeb S, Schall JD, Leventhal AG (1998) Signal timing across the macaque visual system. J Neurophysiol 79:3272.

Schurger A, Sitt JD, Dehaene S (2012) An accumulator model for spontaneous neural activity prior to self-initiated movement. P Natl Acad Sci.

Schwarzenau P, Falkenstein M, Hoormann J, Hohnsbein J (1998) A new method for the estimation of the onset of the lateralized readiness potential (LRP). Behav Res Meth 30:110-117.

Scudder CA, Kaneko C, Fuchs AF (2002) The brainstem burst generator for saccadic eye movements. Exp Brain Res 142:439-462.

Segraves MA (1992) Activity of monkey frontal eye field neurons projecting to oculomotor regions of the pons. J Neurophysiol 68:1967.

Seo H, Lee D (2009) Behavioral and neural changes after gains and losses of conditioned reinforcers. J Neurosci 29:3627-3641.

Shadlen MN, Newsome WT (2001) Neural basis of a perceptual decision in the parietal cortex (area LIP) of the rhesus monkey. J Neurophysiol 86:1916-1936.

Shea-Brown E, Gilzenrat MS, Cohen JD (2008) Optimization of decision making in multilayer networks: The role of locus coeruleus. Neural Comput 20:2863-2894.

Shen K, Paré M (2007) Neuronal activity in superior colliculus signals both stimulus identity and saccade goals during visual conjunction search. J Vis 7:1-13.

Shook BL, Schlag-Rey M, Schlag J (1990) Primate supplementary eye field: I. Comparative aspects of mesencephalic and pontine connections. J Comp Neurol 301:618-642.

Shook BL, Schlag-Rey M, Schlag J (1991) Primate supplementary eye field. II. Comparative aspects of connections with the thalamus, corpus striatum, and related forebrain nuclei. J Comp Neurol 307:562-583.

Simen P, Cohen JD (2009) Explicit melioration by a neural diffusion model. Brain Res 1299:95-117.

Simen P, Cohen JD, Holmes P (2006) Rapid decision threshold modulation by reward rate in a neural network. Neural Networks 19:1013-1026.

Smith PL (1995) Psychophysically principled models of visual simple reaction time. Psychol Rev 102:567.

Smith PL (2010) From Poisson shot noise to the integrated Ornstein-Uhlenbeck process: Neurally principled models of information accumulation in decision-making and response time. J Math Psychol 54:266-283.

Smith PL, Van Zandt T (2000) Time-dependent Poisson counter models of response latency in simple judgment. Brit J Math Stat Psy 53:293-315.

Smith PL, Ratcliff R (2004) Psychology and neurobiology of simple decisions. Trends Neurosci 27:161-168.

Smith PL, Ratcliff R (2009) An integrated theory of attention and decision making in visual signal detection. Psychol Rev 116:283.

Smulders FTY, Kok A, Kenemans JL, Bashore TR (1995) The temporal selectivity of additive factor effects on the reaction process revealed in ERP component latencies. Acta Psychol 90:97-109.

So NY, Stuphorn V (2010) Supplementary eye field encodes option and action value for saccades with variable reward. J Neurophysiol 104:2634.

So NY, Stuphorn V (2012) Supplementary Eye Field Encodes Reward Prediction Error. J Neurosci 32:2950-2963.

Softky WR, Koch C (1993) The highly irregular firing of cortical cells is inconsistent with temporal integration of random EPSPs. J Neurosci 13:334-350.

Sommer MA, Wurtz RH (2000) Composition and topographic organization of signals sent from the frontal eye field to the superior colliculus. J Neurophysiol 83:1979-2001.

Sommer MA, Wurtz RH (2004a) What the brain stem tells the frontal cortex. II. Role of the SC-MD-FEF pathway in corollary discharge. J Neurophysiol 91:1403-1423.

Sommer MA, Wurtz RH (2004b) What the brain stem tells the frontal cortex. I. Oculomotor signals sent from superior colliculus to frontal eye field via mediodorsal thalamus. J Neurophysiol 91:1381-1402.

Somogyi P (1977) A specific 'axo-axonal' interneuron in the visual cortex of the rat. Brain Res 136:345-350.

Sparks DL (1986) Translation of sensory signals into commands for control of saccadic eye movements: role of primate superior colliculus. Physiol Rev 66:118-171.

Sparks DL (2002) The brainstem control of saccadic eye movements. Nat Rev Neurosci 3:952-964.

Stanford TR, Shankar S, Massoglia DP, Costello MG, Salinas E (2010) Perceptual decision making in less than 30 milliseconds. Nat Neurosci 13:379-385.

Stanton GB, Goldberg ME, Bruce CJ (1988) Frontal eye field efferents in the macaque monkey: I. Subcortical pathways and topography of striatal and thalamic terminal fields. J Comp Neurol 271:473-492.

Stanton GB, Deng SY, Goldberg EM, McMullen NT (1989) Cytoarchitectural characteristic of the frontal eye fields in macaque monkeys. J Comp Neurol 282:415-427.

Steinmetz NA, Moore T (2010) Changes in the response rate and response variability of area V4 neurons during the preparation of saccadic eye movements. J Neurophysiol 103:1171-1178.

Sternberg S (2001) Separate modifiability, mental modules, and the use of pure and composite measures to reveal them. Acta Psychol 106:147-246.

Stuphorn V, Schall JD (2006) Executive control of countermanding saccades by the supplementary eye field. Nat Neurosci 9:925-931.

Stuphorn V, Taylor TL, Schall JD (2000) Performance monitoring by the supplementary eye field. Nature 408:857-860.

Stuphorn V, Brown JW, Schall JD (2010) Role of supplementary eye field in saccade initiation: executive, not direct, control. J Neurophysiol 103:801.

Sumner P, Nachev P, Morris P, Peters AM, Jackson SR, Kennard C, Husain M (2007) Human medial frontal cortex mediates unconscious inhibition of voluntary action. Neuron 54:697-711.

Sutton RS, Barto AG (1998) Reinforcement learning: An introduction: Cambridge Univ Press.

Tanaka M (2007) Cognitive signals in the primate motor thalamus predict saccade timing. J Neurosci 27:12109-12118.

Teller DY (1984) Linking propositions. Vision Res 24:1233-1246.

Theeuwes J (2010) Top-down and bottom-up control of visual selection: Reply to commentaries. Acta Psychol 135:133-139.

Thomas NWD, Pare M (2007) Temporal processing of saccade targets in parietal cortex area LIP during visual search. J Neurophysiol 97:942-947.

Thompson KG, Bichot NP (2005) A visual salience map in the primate frontal eye field. Prog Brain Res 147:249-262.

Thompson KG, Bichot NP, Schall JD (1997) Dissociation of visual discrimination from saccade programming in macaque frontal eye field. J Neurophysiol 77:1046-1050.

Thompson KG, Biscoe KL, Sato TR (2005a) Neuronal basis of covert spatial attention in the frontal eye field. J Neurosci 25:9479.

Thompson KG, Bichot NP, Sato TR (2005b) Frontal eye field activity before visual search errors reveals the integration of bottom-up and top-down salience. J Neurophysiol 93:337-351.

Thompson KG, Hanes DP, Bichot NP, Schall JD (1996) Perceptual and motor processing stages identified in the activity of macaque frontal eye field neurons during visual search. J Neurophysiol 76:4040-4055.

Thornton TL, Gilden DL (2007) Parallel and serial processes in visual search. Psychol Rev 114:71.

Tolhurst DJ, Movshon JA, Dean AF (1983) The statistical reliability of signals in single neurons in cat and monkey visual cortex. Vision Res 23:775-785.

Townsend JT, Ashby FG (1984) Stochastic modeling of elementary psychological processes: Cambridge University Press.

Treisman A, Gormican S (1988) Feature analysis in early vision: Evidence from search asymmetries. Psychol Rev 95:15-48.

Treisman A, Sato S (1990) Conjunction search revisited. J Exp Psychol Human 16:459.

Treisman AM, Gelade G (1980) A feature-integration theory of attention. Cognitive Psychol 12:97-136.

Tsotsos JK, Culhane SM, Kei Wai WY, Lai Y, Davis N, Nuflo F (1995) Modeling visual attention via selective tuning. Artif Intell 78:507-545.

Usher M, McClelland JL (2001) The time course of perceptual choice: the leaky, competing accumulator model. Psychol Rev 108:550-592.

Usher M, Olami Z, McClelland JL (2002) Hick's law in a stochastic race model with speed-accuracy tradeoff. J Math Psychol 46:704-715.

van Maanen L, Brown SD, Eichele T, Wagenmakers EJ, Ho T, Serences J, Forstmann BU (2011) Neural correlates of trial-to-trial fluctuations in response caution. J Neurosci 31:17488-17495.

Van Zandt T (2000) How to fit a response time distribution. Psychon B Rev 7:424-465.

Verghese P (2001) Visual search and attention: A signal detection theory approach. Neuron 31:523-535.

Vickers D (1970) Evidence for an accumulator model of psychophysical discrimination. Ergonomics 13:37-58.

Walsh V, Le Mare C, Blaimire A, Cowey A (2000) Normal discrimination performance accompanied by priming deficits in monkeys with V4 or TEO lesions. NeuroReport: For Rapid Communication of Neuroscience Research.

Wang XJ (1999) Synaptic basis of cortical persistent activity: the importance of NMDA receptors to working memory. J Neurosci 19:9587-9603.

Wang XJ (2002) Probabilistic decision making by slow reverberation in cortical circuits. Neuron 36:955-968.

Ward R, McClelland JL (1989) Conjunctive search for one and two identical targets. J Exp Psychol Human 15:664.

Wardak C, Vanduffel W, Orban GA (2010) Searching for a salient target involves frontal regions. Cereb Cortex 20:2464-2477.

Wardak C, Ibos G, Duhamel JR, Olivier E (2006) Contribution of the monkey frontal eye field to covert visual attention. J Neurosci 26:4228-4235.

Wenzlaff H, Bauer M, Maess B, Heekeren HR (2011) Neural Characterization of the Speedâ€“Accuracy Tradeoff in a Perceptual Decision-Making Task. J Neurosci 31:1254-1266.

White BJ, Munoz DP (2011) Separate Visual Signals for Saccade Initiation during Target Selection in the Primate Superior Colliculus. J Neurosci 31:1570.

Wichmann FA, Hill NJ (2001) The psychometric function: II. Bootstrap-based confidence intervals and sampling. Perception & psychophysics 63:1314.

Wolfe JM (1994) Guided search 2.0 A revised model of visual search. Psychon B Rev 1:202-238.

Wolfe JM (1998) What can 1 million trials tell us about visual search? Psychol Sci 9:33-39.

Wolfe JM (2007) Guided Search 4.0: Current Progress with a model of visual search. In: Integrated models of cognitive systems (W. G, ed), pp 99-119. New York: Oxford.

Wolfe JM, Palmer EM, Horowitz TS (2010) Reaction time distributions constrain models of visual search. Vision Res 50:1304-1311.

Wolfe JM, Butcher SJ, Lee C, Hyle M (2003) Changing your mind: on the contributions of top-down and bottom-up guidance in visual search for feature singletons. J Exp Psychol Human 29:483.

Woodman GF (2011) Homologues of human ERP components in nonhuman primates. In: The Oxford Handbook of ERP Components. New York: Oxford University Press.

Woodman GF, Luck SJ (1999) Electrophysiological measurement of rapid shifts of attention during visual search. Nature 400:867-869.

Woodman GF, Luck SJ (2003) Serial deployment of attention during visual search. J Exp Psychol Human 29:121.

Woodman GF, Kang MS, Rossi AF, Schall JD (2007) Nonhuman primate event-related potentials indexing covert shifts of attention. P Natl Acad Sci 104:15111.

Woodman GF, Kang MS, Thompson K, Schall JD (2008) The effect of visual search efficiency on response preparation. Psychol Sci 19:128-136.

Wyder MT, Massoglia DP, Stanford TR (2004) Contextual modulation of central thalamic delay-period activity: representation of visual and saccadic goals. J Neurophysiol 91:2628-2648.

Yang S, Hwang H, Ford J, Heinen S (2010) Supplementary eye field activity reflects a decision rule governing smooth pursuit but not the decision. J Neurophysiol 103:2458-2469.

Young MH, Heitz R, Purcell B, Schall J, Woodman G (2011) Source localization of an event-related potential indexing covert shifts of attention in macaques. J Vis 11:194-194.

Zandbelt BB, Purcell BA, Palmeri TJ, Logan GD, Schall JD (2012) E pluribus unam: out of many accumulators one response time. In: Society for Neuroscience. New Orleans, LA: 2012 Neuroscience Meeting Planner.

Zeki SM (1971) Cortical projections from two prestriate areas in the monkey. Brain Res 34:19.

Zenon A, Krauzlis RJ (2012) Attention deficits without cortical neuronal deficits. Nature.

Zhang K, Guo JZ, Peng Y, Xi W, Guo A (2007) Dopamine-mushroom body circuit regulates saliency-based decision-making in Drosophila. Science Signalling 316:1901.

Zhou H, Desimone R (2010) Feature-based attention in the frontal eye field and area V4 during visual search. Neuron 70:1205-1217.